Studies on the synthesis, characterization, mechanism of peroxidase-like activity, and the application potential of carbon dots prepared from L-glutamic acid and D-(+)-glucose

A Thesis Submitted in Partial Fulfilment for the award of the degree of

Doctor of Philosophy

by

Smita Das

DEPARTMENT OF BIOSCIENCES AND BIOENGINEERING

INDIAN INSTITUTE OF TECHNOLOGY GUWAHATI

GUWAHATI-781039, ASSAM, INDIA

MAY, 2022

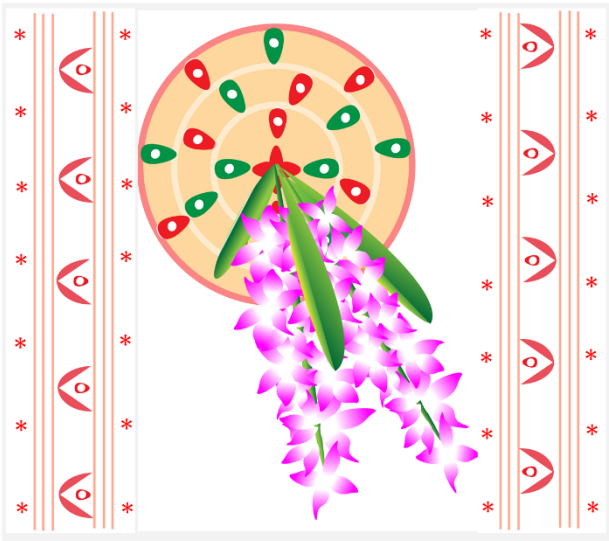

Dedicated to my family, supervisor, and friends

INDIAN INSTITUTE OF TECHNOLOGY GUWAHATI
Department of Biosciences and Bioengineering
Guwahati: 781039

STATEMENT

I do hereby declare that the matter embodied in this thesis entitled "**Studies on the synthesis, characterization, mechanism of peroxidase-like activity, and the application potential of carbon dots prepared from L-glutamic acid and D-(+)-glucose**", is the result of investigations carried out by me in the Department of Biosciences and Bioengineering, Indian Institute of Technology Guwahati, Assam, India, under the guidance of Prof. Pranab Goswami.

In keeping with the general practice of reporting scientific observations, due acknowledgements have been made wherever the work described is based on the findings of other investigators.

May, 2022

Smita Das

Smita Das

INDIAN INSTITUTE OF TECHNOLOGY GUWAHATI
Department of Biosciences and Bioengineering
Guwahati: 781039

CERTIFICATE

It is certified that the work described in this thesis, entitled "**Studies on the synthesis, characterization, mechanism of peroxidase-like activity, and the application potential of carbon dots prepared from L-glutamic acid and D-(+)-glucose"**, done by Smita Das for the award of degree of Doctor of Philosophy is an authentic record of the results obtained from the research work carried out under my supervision in the Department of Biosciences and Bioengineering, Indian Institute of Technology Guwahati, India.

The results embodied in this thesis have not been submitted to any other University or Institute for the award of any degree.

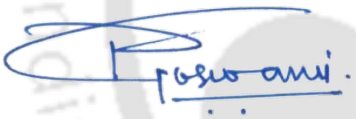

Dr. Pranab Goswami

Professor (Higher Academic Grade)

(Thesis Supervisor)

Acknowledgement

"We must find time to stop and thank the people who make a difference in our lives."

- *John F. Kennedy*

The work presented herein was carried out in the Biosensors and Biofuel Cell Lab at the Indian Institute of Technology (IIT) Guwahati. The challenging yet the exciting PhD journey would not have been feasible without the intellectual, technical, and emotional support from numerous individuals who I am indebted to. Therefore, here is the chance to shower my gratitude to all of them.

First and foremost, I express my profound gratitude to my supervisor, Prof. Pranab Goswami, for providing me the opportunity to work under his guidance. His ceaseless thirst to explore the unconventional domains has greatly inspired me and shaped my perceptivity of scientific research. Besides, his robust technical expertise and ability to visualize the pros and cons of an experimental plan have assisted me during my research. I sincerely appreciate his constant support, time, ideas, and above all, providing a state-of-the-art laboratory to carry out my research work. My heartfelt gratitude goes to him for supporting me emotionally and teaching me not to lose my patience during the time of multiple paper rejections. Thank you, Sir, for everything from teaching me to think like a researcher to many vital life lessons in general that have molded me into a better person.

Next, I would like to acknowledge my doctoral committee members Prof. Siddhartha Sankar Ghosh (Chairman), Prof. Anil Kumar Saikia, and

Dr. Priyadarshi Satpati, for their critical comments, insightful suggestions, and encouragement that lifted me towards the accomplishment of my research objectives. I offer my sincere thanks to all the staff members of Department of Biosciences and Bioengineering, IIT Guwahati, for their limitless help and technical assistance in handling the various instruments. I would also like to acknowledge the Central Instruments Facility (CIF), Centre of Excellence (CoE) of the Department of Biosciences and Bioengineering, and Department of Chemistry, IIT Guwahati, for providing access to various instrumental facilities without which the work would not have been complete. I am thankful to Prof. Ajaikumar B Kunnumakkara for allowing me to use the fluorescence spectroscopy at his lab and his students Uzini and Sosmitha for helping me. Further, I am tremendously grateful to IIT Guwahati, Ministry of Human Resource and Development, India and Department of Biotechnology, Government of India, for their financial assistance and funding, respectively, towards my research work.

I greatly believe that a positive work environment always expedites one's personal growth. Hence, I am thankful to all the past and present lab members of Biosensors and Biofuel Cell lab- Dr. Santhosh, Dr. Ankana, Dr. Priyamvada, Dr. Babina, Dr. Sharbani, Dr. Mrinal, Dr. Priyanki, Dr. Naveen, Dr. Lightson, Dr. Sudarshan, Phurpa, Abdul, Vinay, Pooja, Caraline, Priya, Arup, Rashmi, Aparupa, Malaya, Nabajyoti, Kangkana, Khadija, Kundan, Roshika, Hritushree, Dr. Rofiqul, Dr. Bhaskar, and Dr. Rupinder. Thank you all for your support and cheering me up every time my experiment failed. The fond memories in the lab are endless, from the discussion of recent research updates to diagnose a failed experiment to sharing each of us our day-to-day updates to playing the secret Santa during Christmas. Additionally, I express my special thanks to Roshika (M Tech

project student) and Hritushree (B Tech project student) for their zealous effort in assisting me in the research work.

True friends are a blessing, and hence from the bottom of my heart, I thank each one of them for standing beside me throughout the ups and downs of the PhD journey. A special thanks to my dear friends- Dhritiman, Preeti, Pallavi, Kanchan, for their incredible support, advice, encouragement, and belief in my capabilities despite staying so far away from me. I would also like to thank Dr. Vivek, Dr. Shweta, Roshika, Dr. Ruchika, Dr. Debika, and Dr. Gaurav for all the help and fun that made my stay at the campus more memorable. I am thankful to my adorable juniors, Musfica, Ayushi, and Parama, for keeping the child inside me alive. Further, I owe a debt of gratitude to Musfica for taking care of me when I was unwell.

I extend my deepest gratitude to my parents and my brother for their unconditional love, blessings, and constant encouragement in every step of the PhD journey. No amount of words can perhaps substantiate my acknowledgement to them for their endless sacrifices and their teachings to be determined, strong, and to never lose hope.

Last but not least, I humbly thank the Almighty for bestowing me the strength to keep moving forward despite several challenges.

- **Smita Das**

May, 2022

Table of Contents

Abstract

The advent of nanomaterials as enzyme mimics has drawn significant attention, owing to their high stability, robustness, low cost, and easy synthesis protocol. Carbon dots (CDs) with attractive intrinsic characteristics are a propitious candidate for peroxidase mimic. The present investigation is designed to focus and systematically realize the peroxidase-like activity of CDs synthesized from a widely available organic compound in nature, L-glutamic acid. The compound was selected based on a systematic investigation following a theoretical-cum-experimental approach, which led to identify the -COOH group as a highly active moiety for strongly binding and degrading H_2O_2 in the presence of a reducing equivalent, i.e., ABTS. We explored the influence of different functional groups and identified the -NH_2 group present near the -COOH group exerting the highest peroxidase-like activity as validated by the compound, L-glutamic acid. Following a pyrolysis method, the L-glutamic acid was transformed into CDs having a diameter of 3.18 ± 0.53 nm with its core made of pyroglutamic acid. The CD exhibited thermostability (~90 °C) and higher peroxidase-like activity than the L-glutamic acid. The higher activity of the CD was attributed to its binding affinity with ABTS (2, 2'-azino-bis(3 ethylbenzothiazoline-6-sulfonic acid) and H_2O_2. The K_m and K_{cat} of the CD for H_2O_2 were 5.85 mM and 0.011 s^{-1}, respectively. Based on spectroscopic investigations, we confirmed that the peroxidase-like activity is a surface phenomenon that did not have a significant link to the photophysical property of the CD. Based on the above facts and spectroscopic analysis, one of the critical issues concerning the obscure mechanism of the peroxidase-like activity of the CDs has been addressed. We also highlighted the application potential of the synthesized CDs for the colorimetric detection of peroxide. The colorimetric reaction could be reproduced on a paper platform, confirming the application potential of the CD for developing a low-cost peroxide sensor.

As the application potential of CDs for clinical diagnosis has not been adequately explored, we examined the suitability of pyroglutamate (PGA) CDs for detecting glucose, cholesterol, and alcohol in blood serum through their peroxidative activity in the respective enzyme-catalysed reactions following fluorimetric and colorimetric

approaches. In buffer, the CD's fluorescence intensity ($\lambda_{ex\ 354\ nm}$) enhanced over 115 % after interaction with the enzyme proteins due to different lifetime components on its surface. The enhancement was also linked to FRET with the proteins ($\lambda_{ex\ 274\ nm}$ for TRP/TYR). As revealed from zeta potential study, the electrostatic interactions generated binding energy (ΔG, kcal/mol) in the range of -5.8 to -6.3 and significantly shifted the protein's secondary structure to *β*-strands contents. The CD's fluorescence in the blood serum medium was also enhanced where serum's particulate components contributed to the emission. All these subvert fluorescence emissions could be substantially cleaned for detection of peroxide generated in the enzymatic reaction by filtering the serum particulates and redox proteins prior addition of CDs to the reaction systems. The CD, however, could complement well in ABTS-based (absorbance at $\lambda_{max\ 414\ nm}$) colorimetric reaction in blood serum without introducing protein or particle separation steps for sensitive detection of peroxide. The limit of detection, dynamic range, and sensitivity discerned for peroxide in glucose oxidase catalysed reaction system were 183 μM, 0.02 mM-0.10 mM (R^2 = 0.98), and 0.2482 AU mM^{-1}, respectively. Overall, these findings will stand as guidance for clinical application of the peroxidative CDs to detect various analytes in blood serum following fluorescence and colorimetric-based principles.

To further increase the efficiency of CDs as peroxidase-mimic, it is also desirable to understand the modification of CD's geometry during the catalytic reaction. We concentrated on the change in material property of the CDs upon their reaction with H_2O_2 during the peroxidase reaction. For this, we utilized D-(+)-glucose to synthesize of chiroptical CDs bearing peroxidase-like activity, which could detect H_2O_2 with a limit of detection of 630 μM. Further investigation revealed that the addition of H_2O_2 to the CDs results in its increased molecular orderliness leading to the introduction of polycrystallinity without affecting its peroxidase-like activity.

List of Abbreviations

2-NP	2-Nitrophenol
4-NP	4-Nitrophenol
AA	Acetic Acid
ABPA	3-aminophenylboronic acid
ABTS	2, 2'-azino-bis(3 ethylbenzothiazoline-6-sulfonic acid
AC	Ammonium Citrate
ACQ	Aggregation-induCed emission Quenching
AFM	Atomic Force Microscopy
AIEE	Aggregation-Induced Emission Enhancement
ANOVA	ANalysis Of Variance
AOx	Alcohol Oxidase
Aphen	5-amino-1,10-phenanthroline
Asp	Aspartic acid
Au NRs	Gold Nanorods
B.E.	Binding Energy
BILI	Bilirubin
C_3	*Tris*-malonic acid
C_{60}	Fullerene
CA	Citric Acid
CDs	Carbon Dots
Chol	Cholesterol

ChOx	Cholesterol Oxidase
CL	ChemiLuminescence
CN	Carbon Nitride
CND	Carbon NanoDots
CNF	Cellulose NanoFibrils
CNQD	Carbon Nitride Quantum Dots
CPL	Circularly Polarized Luminescence
CQD	Carbon Quantum Dots
CTC	ChloroTetraCycline
CuN	Copper Nitrate
CV	Cyclic Voltammetry
DAN	DiAminoNaphthalene
DEASA	4-(diethylamino)salicylaldehyde
DFT	Density Functional Theory
DMAC	DiMethylACetamide
DMF	DiMethylFormamide
DMPO	5,5-dimethyl-1-pyrroline N-oxide
DOTA	1,4,7,10-tetraazacyclononane
EA	EthanolAmine
ECL	ElectroChemiLuminescence
EDA	Ethylene DiAmine
EDS	Energy-Dispersive X-ray Spectroscopy
ESI-Q-TOF-MS	ElectroSpray Ionization Quadrupole Time-Of-Flight Tandem Mass Spectrometry
EPA	3-ethoxypropylamine

ESR	Electron Spin Resonance
EtOH	Ethanol
FRET	Fluorescence/Förster Resonance Energy Transfer
FETEM	Field Emission Transmission Electron Microscope
FH	Fluorescein
FTIR	Fourier Transform Infrared Spectroscopy
GCE	Glassy Carbon Electrode
GOx	Glucose Oxidase
Glu	Glutamic acid
GQD	Graphene Quantum Dots
HH	Hydrazine Hydrate
HPPT	4-hydroxy-1H-pyrrole[3,4-c]pyridine-1,3,6(2H,5H)-trione
HRP	HorseRadish Peroxidase
HRTEM	High-Resolution Transmission Electron Microscopy
HSA	Human Serum Albumin
ICP-MS	Inductively Coupled Plasma-Mass Spectrometry
ICT	Intersystem Charge Transfer
IPCA	5-oxo-1,2,3,5-tetrahydroimidazo-[1,2-α]-pyridine-7-carboxylic acid
KBr	Potassium Bromide
LoD	Limit of Detection
m-PD	m-PhenyleneDiamine
MALDI-TOF-MS	Matrix-Assisted Laser Desorption/Ionization Time-Of-Flight Mass Spectrometry
MS	Mass Spectrometry

MeOH	Methanol
NA	Not Available
NBD	Nano Biomass Dots
NIR-CDs	Near-Infrared Region Carbon Dots
NMR	Nuclear Magnetic Resonance Spectroscopy
OPD	*O*-PhenyleneDiamine
ORR	Oxygen Reduction Reactions
OTC	OxyteTraCycline
p-PDA	p-PhenyleneDiAmine
PAA	Poly(Acrylic Acid)
PCM	Phase Change Materials
PD	Polymer Dots/ PhenyleneDiamine
PDA	PolyDopAmine
PEG	Poly(Ethylene Glycol)
PEI	Poly(EthyleneImine)
PGA	PyroGlutAmate
pH	Potential of Hydrogen
PL	PhotoLuminescence
PPi	PyroPhosphate
PTCA	PeryleneTetraCarboxylic Acid
PVP	PolyVinylPyrrolidone
QCE	Quantum Confinement Effect
QD	Quantum Dots
QR	Quinaldine Red

QY	Quantum Yield
RCSB	Research Collaboratory for Structural Bioinformatics
rGO	Reduced Graphene Oxide
Rh6G	Rhodamine 6G
ROS	Reactive Oxygen Species
RT	Room-Temperature
RTP	Room-Temperature Phosphorescence
SA	Stearic Acid
SAED	Selected Area Electron Diffraction
SEM	Scanning Electron Microscopy
SHE	Standard Hydrogen Electrode
SOD	SuperOxide Dismutase
TA	Trimellitic Acid
TCSPC	Time-Correlated Single-Photon Counting
TEM	Transmission Electron Microscopy
TMA	TriMetallic Acid
TMB	3, 3', 5, 5'-tetramethylbenzine
TMPDPA	4-(2,4,6-trimethoxyphenyl)-pyridine-2,6-dicarboxylic acid
TSCDH	TriSodium Citrate DiHydrate
UCPL	UpConversion PhotoLuminescence
UV-Vis	UltraViolet-Visible
WLEDs	White Light-Emitting Diodes
XPS	X-ray Photoelectron Spectroscopy
XRD	X-Ray Diffraction

List of Symbols

°C	Degree Celsius
~	Approximately
ζ	Zeta potential
%	Percent
>	Greater than
2D	Two dimensional
3D	Three dimensional
θ	Theta
µL	Microlitre
µM	Micromolar
µmol	Micromole
µm	Micrometre
λ	Wavelength
λ_{ex}	Excitation wavelength
λ_{em}	Emission wavelength
α	Optical absorption coefficient
π	Pi
σ	Standard deviation
δ	Delta
A	Absorbance
Å	Angstrom
Ai	Amplitude
A_1	Absorbance of the sample
A_2	Maximum absorbance
AgCl	Silver chloride
atm	Standard atmosphere
AU	Absorbance/Arbitrary units
B	Proportionality constant
C	Concentration of the substrate
cm	Centimeter
d	Thickness
D-(+)	Dextrorotatory
D_2O	Heavy water
ε	Molar absorption coefficient
eV	Electronvolt
E_g	Band gap energy
f	Fractional weight
fg	Femtogram
fs	Femtosecond

F	Fluorescence intensity in the presence of the quencher
F_0	Fluorescence intensity in the absence of the quencher
Fe_3O_4	Iron(II, III) oxide
g	Gram
ΔG	Change in free energy
GPa	Gigapascal
h	Hour
H_2O_2	Hydrogen peroxide
H_3PO_4	Phosphoric acid
HSO_3^-	Hydrosulfite
hv	Energy of the incident photons
K_2HPO_4	Dipotassium hydrogen phosphate
KH_2PO_4	Potassium dihydrogen phosphate
kcal	Kilocalorie
K_{cat}	Turnover numbers
K_D	Stern-Volmer quenching constant
kDa	Kilodalton
K_m	Michaelis-Menten constant
kV	Kilovolt
kW	Kilowatt
L	Litre
l	Optical path length
m	Slope of the calibration curve
M	Molarity
MΩ	Mega ohm
MHz	Megahertz
mg	Milligram
min	Minute
mL	Millilitre
mM	Millimolar
mm	Millimetre
mol	Mole
mV	Millivolt
mW	Milliwatt
Na_2HPO_4	Disodium hydrogen phosphate
NaH_2PO_4	Sodium dihydrogen phosphate
NaOH	Sodium hydroxide
nm	Nanometer
nM	Nanomolar
nmol	Nanomole

ns	Nanosecond	**$\cdot SO_3^-$**	Sulphite anionic radical
$\cdot O_2^-$	Superoxide radical	***τ***	Fluorescence lifetime
$^1O_2$	Singlet oxygen	**V**	Volt
$\cdot OH$	Hydroxyl radical	***v***	initial velocity
Q	Quencher	**V_m**	Maximum velocity
r	Empirical exponent constant	**W**	Watt
		w/v	Weight/Volume
R^2	Regression coefficient	**xg**	Centrifugation speed in RCF
s	Second		
[*S*]	Substrate concentration		
SO_2	Sulfur dioxide		

List of Figures

List of Tables

"There's plenty of room at the bottom"

- Richard Phillips Feynman

Chapter 1

Introduction and Literature Review

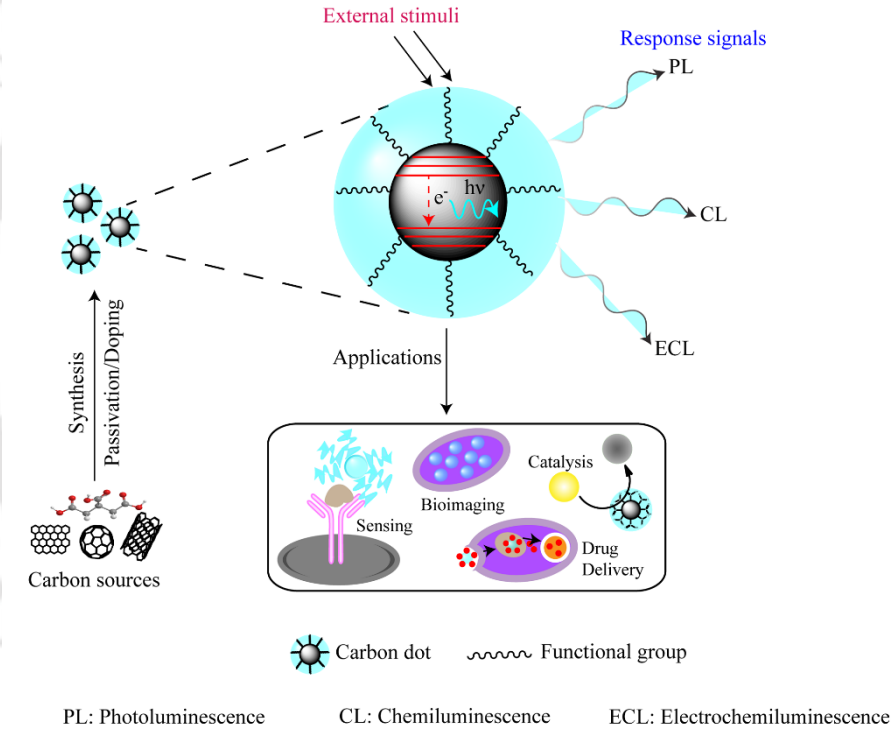

1.1 Introduction

Enzymes have been extensively studied since their discovery and have found applications in different fields such as medicine, food processing, cosmetics, brewing, cleaning (detergents), pulp, and paper industry. However, despite the high catalytic activity, and substrate specificity, the natural protein-based enzymes possess some inherent drawbacks, that hampers their commercial applications. Adverse environmental conditions, denaturants, and digestion hinder the stability as well as the catalytic activity of enzymes. Also, the large-scale production and purification of enzymes are often challenging and expensive. All these bottlenecks led to the discovery of artificial enzymes or enzyme mimetics, which intends to imitate the properties of natural enzymes. In 1970, Professor Ronald Breslow at Columbia University coined the term "artificial enzymes" for natural enzyme alternatives (Wei and Wang, 2013). In his book entitled *Artificial Enzymes*, he mentioned how cyclodextrins (cyclic oligosaccharides with a hydrophilic outer surface and lipophilic cavity) could bind to hydrophobic substrates imitating enzyme-substrate complex. However, some artificial enzymes, such as DNAzymes, hemin, porphyrin, are biomolecules that are susceptible to activity loss due to fluctuations in temperature and pH. These led researchers to explore better alternatives of enzyme mimics.

Over the past few years, it has been established that some nanomaterials can be a potential candidate for enzyme mimics (nanozymes) due to their various advantageous properties. In contrast to natural enzymes, nanozymes are highly stable, easily synthesized, robust, low cost, and can be stored for an extended period. The presence of high surface area to volume ratio and size-dependent tuneable catalytic property further enhances the enzymatic efficiency. These nanomaterials-based artificial enzymes have found profound applications in the field of biosensing, bioimaging, environmental protection, and therapeutics (Figure 1.1) (Wu *et al*., 2019). In most cases, the performance of nanozyme action is mainly dependent on its ability to generate or consume reactive oxygen species (ROS) (He *et al*., 2014).

The concept of nanozyme first came into view in the year 1996 with the introduction of two hydroxyl derivatives of buckminsterfullerene (C_{60}) in cortical neuron culture, for its free radical scavenging property in neuronal injury and apoptotic

death (Dugan *et al*., 1996). Dugan *et al.* observed that both the fullerene derivatives could effectively scavenge hydroxyl radicals generated from the decomposition of hydrogen peroxide, which resulted in reduced neuronal apoptotic death. Eight years later, Ali *et al.* introduced another fullerene (C_{60}) derivative (*tris*-malonic acid (C3)) with potential superoxide dismutase (SOD)-like activity (Ali *et al*., 2004). Superoxide, an anionic radical, and a common toxic by-product in biochemical reactions are dismutated by superoxide dismutase in our body. However, the high-level activity of superoxide dismutase can cause tissue damage, neural injury, and also inflammation. To overcome this, the introduction of SOD mimic *in vivo* was essential. *Tris*-malonic acid (C_3) was found to be capable of eliminating superoxide radicals. The reaction between superoxide and C_3 released the same product H_2O_2 (hydrogen peroxide) and regenerated oxygen, as is found in the case of SOD-based catalysis. Also, structurally there was no modification of C_3 after the reaction, which further indicated that C_3 has enzymatic properties. However, compared to superoxide dismutase, the rate of reaction of C_3 was slow.

The discovery of gold nanoparticles with glucose oxidase-like activity was a breakthrough in the field of nanozymes. In 2004, Comotti *et al*. synthesized naked gold nanoparticles with an average size of 3.6 nm, which mimicked glucose oxidase catalysing glucose in the presence of oxygen to gluconic acid and H_2O_2 (Comotti *et al*., 2004). Another milestone in the history of nanozyme came in 2007 with the discovery of peroxidase-like activity of iron oxide magnetic nanoparticles by Gao and his co-workers. Fe_3O_4 magnetic nanoparticle of different sizes was able to catalyse the oxidation of the peroxidase substrates, i.e., TMB, DAB, and OPD in the presence of H_2O_2 (Gao *et al*., 2007). The Fe_3O_4 magnetic nanoparticle with peroxidase-like activity was later used in the immunoassay for the detection of antigen.

So far, nanozymes have been most commonly reported to exhibit oxidase-like, catalase-like, superoxide dismutase-like, and peroxidase-like activity, with their applications principally in the field of biosensors, environmental remediation, and therapeutics. This expeditious growth of the nanozyme research has been possible mainly because of its advantageous properties mentioned above.

Currently, a great deal of the nanozyme research is focused on mimicking peroxidases. The peroxidase enzyme catalyses the reduction of peroxides such as

hydrogen peroxide (H_2O_2), lipid peroxide, and at the same time, causes oxidation of a redox substrate. The 1st stage of the reaction mechanism of peroxidase involves the binding of an H_2O_2 molecule to the heme (Fe (III)) cofactor resulting in the heterolytic cleavage of the oxygen-oxygen bond in peroxide. Two electron oxidations of the heme results in the formation of an intermediate form of the enzyme (compound I), which can be converted back to the resting enzyme via two successive single-electron oxidations of a redox substrate (SH_2).

$$SH_2 + H_2O_2 \rightarrow S + 2H_2O$$

The horseradish peroxidase (HRP) enzymes are the comprehensively utilized class of peroxidase enzymes in analytical applications, especially in colorimetric biosensors by virtue of their simplicity, practicality, and affordability. In clinical applications, generally, the HRP is utilized to catalyse the H_2O_2 liberated during the oxidation of clinically significant bioactive molecules involving oxidase enzymes. The H_2O_2 is converted to free radicals by HRP, which reacts with a chromogen and generates a coloured reaction product. Accordingly, the intensity of the colour promotes the indirect quantification of the clinically significant bioactive molecule. Fundamentally, using multiple enzymes in a single detection platform leads to increased complexity and cost of the biosensor. In this regard, replacing the HRP enzyme with peroxidase-based nanozymes can substantially simplify the detection processes.

Carbon dots (CDs), a zero-dimensional carbon nanomaterial have received much attention in recent years due to their attractive intrinsic properties. The CDs display fascinating optical and electronic properties that make them a promising candidate for peroxidase mimic. In light of this fact, the present study aims to exploit an in-depth understanding of the enzymatic activity of the CDs, especially the peroxidase-like activity. The investigation intends to decipher the mechanism of the peroxidase-like activity of CDs, the evolution of its material property during the reaction with peroxide, and finally, its potentiality as a signal probe in clinical applications.

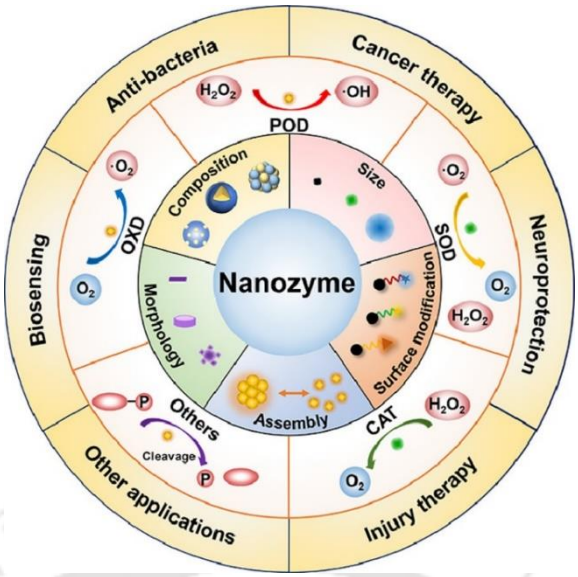

Figure 1.1. Graphical representation of nanozyme characteristics, their enzyme-like properties, and applications. Reprinted with permission from ref. (Wei *et al*., 2021).

1.2 CDs as an Emerging Nanomaterial

Since the fortuitous discovery of CDs in 2004, the interest in these luminescent nanomaterials has been increasing exponentially (Hu *et al*., 2019; Semeniuk *et al*., 2019). The CDs are zero-dimensional carbon nanoparticles with a size of less than 10 nm. Compared to the different types of carbon nanomaterials, the CDs have gained enormous attention due to their advantages such as inexpensive and easy synthesis, facile surface functionalization, low toxicity, biocompatibility, high water-solubility, tunable luminescence property, and stability at room temperature (Li *et al*., 2019). Consequently, their applications are explored in bioimaging, drug delivery, and chemical/biological sensing (Devi *et al*., 2019). Additionally, carbon dot's enzyme-like activity has also attracted wide interest because of their potential to replace the naturally occurring enzymes, as the latter is ordinarily unstable, expensive, and challenging to synthesize on a large scale (Das and Goswami, 2020).

1.2.1 Synthesis of CDs

CDs being the rising star of fluorescent carbon nanoparticles have captivated the interest of the researchers for their application in various fields. Depending on the structure, CDs are classified as graphene quantum dots (GQDs), carbon nanodots

(CNDs), and polymer dots (PDs). GQDs have graphene layer/s that can be connected with functional groups. CNDs are spherical shaped, and they can be further divided into carbon nanoparticles and carbon quantum dots based on the crystal lattice. PDs are formed due to aggregation or cross-linking of polymers (Zhu *et al*., 2015). Therefore, different CDs may be devised and engineered to obtain the desired property by various synthetic routes.

Diverse methods for the synthesis of CDs are known. Typically, the synthesis process can be grouped into two: top-down and bottom-up (Anwar *et al*., 2019). The top-down approach usually follows breaking-down/cleaving larger carbon molecules to smaller molecular structures, whereas the bottom-up approach involves building-up/step-wise chemical fusion of small carbon molecules by pyrolysis or carbonization. Some known top-down approaches include electrochemical/chemical oxidation, laser ablation, and ultrasonic treatment, whereas the bottom-up approaches include hydrothermal/solvothermal, microwave-assisted, thermal decomposition, carbonization, pyrolysis, and ultrasonic treatment. Some prominent reports on the synthesis of CDs via these two routes are mentioned in Table 1.1.

Table 1.1. Synthesis of CDs following top-down and bottom-up approaches.

Precursors	**Synthesis route/Temp/ Time**	**Types of CDs**	**Size(nm)/QY (%)**		**References**
QR, NaOH	Ultrasonic/ RT/6 h	CDs	2.99/27.7		(Gao *et al*., 2019)
CA, PEG	Ultrasonic/ RT/1 h	CDs	2.38/NA		(He *et al*., 2019)
Soybean	Ultrasonic/ NA/2 h	NBDs	24/16.7		(Zhao *et al*., 2019)
Graphite, ethanol	Laser Ablation 800 nm, 150 fs	CDs	F_s	1.4/NA	(Nguyen *et al*., 2020)
			$2F_s$	2/NA	
			F_d-2	1.1/NA	
			F_d-10	1.5/NA	
DEASA, H_3PO_4	Hydrothermal/ 200 °C/2 h	CDs	4.69/19.4		(Chen *et al.*, 2019)
Jeera	Hydrothermal/ 250 °C/6 h	CDs	6-9/5.33		(V. *et al*., 2019)

Tobacco	Hydrothermal/ 300 °C/3 h	CDs	2.14±0.3/27.9	(Miao *et al*., 2018)
Cryptococcus	Hydrothermal/ 160 °C/1 h	CDs	4-9/14.13	(Lu *et al*., 2019)
TMA	Hydrothermal/ 260 °C/12 h	CDs	4.3/13.4	(Jiang *et al*., 2020)
Agaricus bisporus	Hydrothermal/ 160 °C/12 h	CDs	NA/4.2	(Chandra and Singh, 2017)
Chitosan, AA	Hydrothermal/ 180 °C/12 h	CQDs	5/NA	(Sun *et al*., 2018)
CA, EA	Hydrothermal/ 180 °C/8 h	CDs	4/NA	(He *et al*., 2019)
Folic acid, Glucose	Hydrothermal/ 210 °C/12 h	CDs1	1.6/23.5	(Huo *et al*., 2019)
		CDs2	2.6/42.8	
Xylose, H_3PO_4, m-PD	Microwave/ 220 °C/10 min	CDs1	6.80/73.6	(Yang *et al*., 2019)
Xylose, H_3PO_4, m-PD	Microwave/ 200 °C/10 min	CDs2	7.23/56.1	
Xylose, H_3PO_4, m-PD	Microwave/ 180 °C/10 min	CDs3	6.80/40.9	
Xylose, m-PD HNO_3	Microwave/ 220 °C/10 min	CDs4	9.88/65.3	
Xylose, m-PD CH_3COOH	Microwave/ 220 °C/10 min	CDs5	8.83/49.5	
Xylose, m-PD	Microwave/ 220 °C/10 min	CDs6	6.87/42.8	
Xylose, m-PD, Na_3PO_4	Microwave/ 220 °C/10 min	CDs7	16.37/8	
Xylose, m-PD, NaOH	Microwave/ 220 °C/10 min	CDs8	10.70/6.8	
CA, EDA	Microwave/ 720 W/2 min	CDs	4/24	(Xu *et al*., 2018)
CA, urea	Microwave/ 750 W/5 min	CDs	NA/NA	(Asadzadeh-Khaneghah *et al*., 2019)
Anthracite coal, H_2SO_4, HNO_3	Pyrolysis in oil bath/ 120 °C/24 h	CDs	3.5/NA	(Pandey and Balachandran, 2019)
CA, Glu, Asp, lysine	Thermal Pyrolysis/ 200 °C/30 min	CDs	4/8.8	(Pan *et al*., 2019)

CA, acrylamide	Solvothermal/ 200 °C/4 h	CDs	9.5/NA	(Gao *et al*., 2018)
CA	Oven/ 200 °C/1 h	CDs	3/NA	(Liu *et al*., 2019)

F_s: single-pulse ablation (F_{single}=50 Jcm^{-2}); $2F_s$: single-pulse ablation ($2F_{single}$); F_d-2: double-pulse ablation (τ_{delay}=2ps); F_d-10: double-pulse ablation (τ_{delay}=10ps).

The different physicochemical properties like the degree of carbonization, crystallinity, size, morphology, and photoluminescence properties are attained depending on the type of synthesis method and the precursor molecule. For instance, the hydrothermal method is less harsh than the pyrolytic method, but the former generally yields incomplete carbonization, molecular fluorophores, amorphous CDs, whereas the latter predominantly yields graphitic core structures. The functional groups like amine, carboxyl, and hydroxyl on the surface of carbon dot can modify the physicochemical properties, biocompatibility, and stability, thus influencing the selectivity, and sensitivity of the CDs in the analytical applications. Additionally, the molecular precursor used for the synthesis of CD influences the degradation process and other environmental behaviour (Frank *et al*., 2020).

As stated before, various ranges of CD materials with different properties could be achieved by different synthesis conditions. It has been recently observed that if bottom-up synthetic approaches are followed, high PL quantum yield (QY) results. Due to the harsh conditions being applied in the bottom-up synthesis approach, multiple side-products may be produced along with the CDs. Citrazinic acid and other small fluorophore derivatives are produced while synthesizing the nitrogen-doped CDs from citric acid, contributing to the emission in the blue spectral range. Such molecular species and polymerized nanoparticles may attach to the CDs to enhance the optical properties (Schneider *et al*., 2017; Zhu *et al*., 2016).

1.2.1.1 *Heteroatoms Doped-CD Synthesis*

The inherent properties of the CDs can be modulated by doping with heteroatoms such as nitrogen (N), phosphorus (P), sulfur (S), boron (B), and fluorine (F), individually or in various combinations during the synthesis. The introduction of the heteroatoms further adds new electronic, chemical, and optical functionalities to the CD, thereby broadening its application. Depending on the type of element, doping is categorized into non-metal and metal doping.

1.2.1.1.1 Non-Metal Doping

Nitrogen-doped (N-doped) CDs are the most commonly explored type of non-metal doping because of the closer electronic structure with that of carbon. The N-doped CDs are fabricated by introducing the nitrogen element to the dot's core. For the first time in a study, multicolour emissive CDs were synthesized using inorganic ammonium salt via a solvothermal method. The synthesized CDs with increased nitrogen content resulted in a high quantum yield of ~4 % and led to the introduction of new functional groups like cyano. However, because of the multicolour emissive property, these CDs have also opened up various applications for sensing and antibacterial activity (Ju *et al*., 2018). The N-doped CDs developed by using *Lantana camara* berries via a simple green approach exhibited a good quantum yield (QY) of 33.15 %, high stability, high biocompatibility. Additionally, the N-CDs could also detect Pb^{2+} with high sensitivity and selectivity (Bandi *et al*., 2018). Red emissive N-doped CDs were synthesised from citric acid and ethylenediamine through a microwave-assisted pyrolysis method. During the synthesis, the effect of the molar ratio of ethylenediamine to citric acid, pyrolysis time, and the concentration of the reactants was taken into consideration. The optimized molar ratio between amine/acid was found to be 0.75 with an exposure time of 88 s in 1100 W microwave power. The fabricated N-doped CDs displayed remarkable biocompatibility, and can further be used in bioimaging applications (Karakoçak *et al*., 2018). In most instances, the CDs synthesis with co-doping enhances the properties of the nanomaterial. Interestingly, human fingernails as precursor was used to fabricate N, S co-doped CDs through a simple microwave irradiation procedure that exhibited good stability and a QY of 42.8 %. More importantly, the method does not require any passivating agent or a passivation step for the synthesis. The N, S co-doped CDs were employed to detect a synthetic dye, sunset yellow, and in cell imaging (Chatzimitakos *et al*., 2018).

1.2.1.1.2 Metal Doping

Doping CDs with metal ions can modify the charge density and surface properties, thus effectively tuning the optical features of the nanomaterial. For instance, the Cu-doped CDs exhibited enhanced peroxidase-like activity due to the enhancement of the electronic properties and modification of the surface properties after the introduction of the metal ion (Duan *et al*., 2019). In another study, the developed Cu-

doped CDs using ethanediamine and copper chloride dihydrate ($CuCl_2.2H_2O$) as precursors possessed notable photostability for up to 60 mins. Then again, manganese doped CDs (Mn-CDs) displayed excellent fluorescence QY (>54.4 %). By using spectroscopic techniques and DFT-based frontier orbital calculation, it was found that the high QY is due to the change of the oxidation state of Mn from Mn-oxide to Mn-carbonate during the synthesis (Xu *et al*., 2018). Some more examples of metal-doped CDs are given in Table 1.2 for further reference.

Table 1.2 Synthesis of heteroatoms doped CDs following top-down and bottom-up approaches.

Precursors	Synthesis route/ Temp/Time	Types of CDs	Size (nm)/ QY(%)	References
Cryomilled graphite, DMF	Laser Ablation/ 800 °C/3 h	N-CDs	3/4.05	(Novoa-De León *et al*., 2019)
2-aminopyrimidine-5-boronic acid	Laser Ablation/ 170 mW/1014 Wcm^{-1}	N, B-CD	3/58	(Kipnusu *et al*., 2020)
Graphite rods and ammonia hydroxide	Electrochemical and Ultrasonic/ 80 °C/3 h	N-CDs	3-5/NA	(Wu *et al*., 2019)
L-tryptophan, chlorhexidine acetate	Hydrothermal/ 200 °C/12 h	N-CDs	~4.0/NA	(Chu *et al*., 2020)
***P. acidus*, aq. ammonia**	Hydrothermal/ 200 °C/12 h	N-CDs	5/12.5	(Atchudan *et al*., 2019)
PVP	Hydrothermal/ 200 °C/6 h	N-CDs	6.5/6	(Milenkovic *et al*., 2019)
EDA, $CuCl_2.2H_2O$	Hydrothermal/ 180 °C/10 h	Cu-CDs	1.8/7.8	(Fang *et al*., 2019)
Aphen, CA	Hydrothermal/ 200 °C/7 h	AC-CDs	25/52	(T. Zhang *et al*., 2019)
OPD, ABPA	Hydrothermal/ 160 °C/6 h	B,N-CDs	4.09/8.56	(Wang *et al*., 2020)
Mn(III)($C_5H_7O_2$)$_3$	Hydrothermal/ 200 °C/12 h	MnO_x-CDs	5.65±0.30/ 11.3	(Li *et al*., 2020)
Sucrose, nitrobenzene, nitrosobenzene	Hydrothermal/ 180 °C/12 h	CD-NO, and CD-NO_2	gCD 11/21 rCD 13/18	(Srivastava *et al*., 2020)
CA, EDA	Microwave/	N-CDs	~5/95, 11	
CA, EDA, sodium borate		B-CDs	~5/63, 9	

CA, EDA, K_2PO_4	300 W/10 min	P-CDs	~5/63, 6	(Mondal *et al.*, 2019)
p-PDA, EDA	Microwave/ 500 W/20 min	N-CDs	4.8/14	(Ding *et al.*, 2018)
TSCDH, Urea, DMF	Solvothermal/ 160 °C/4 h	$N\text{-}CD_{11}$	4.5/21.6	(Shen *et al.*, 2018)
TSCDH, Urea, DMAC		$N\text{-}CD_{12}$	4.5/18.7	
TSCDH, Urea, DEF		$N\text{-}CD_{21}$	4.5/17.6	
H_2O_2, ethanol, NH_3	Solvothermal/ 180 °C/NA	N-CDs	2.15/56.1	(Zhan *et al.*, 2018)
CA, PD	Solvothermal/ 170 °C/4h	Y-CDs	7.2/24	(Yan *et al.*, 2019b)
CA & DAN	Solvothermal/ 160 °C/6 h	HCP-DB-CDs	2.4/70±10	(Yuan *et al.*, 2020)
PAA, CuN, HH, $(NH_4)_2S_2O_8$	Carbonization/ Polymerization and Pyrolyzation Stirring/24 h & 400 °C/90 min	Cu-CDs	2.8/36	(Wang *et al.*, 2019)
Willow Catkin, Urea & H_2SO_4	Combustion	N,S-CDs	7.3/14.3	(Cheng *et al.*, 2019)
Na_2[Cu(EDTA)] and Ascorbic acid	Thermolysis 250 °C/2 h	Cu-CDs	3.48/9.8	(Mu *et al.*, 2019)

1.2.1.2 *Surface Passivation and Functionalization of CDs*

Apart from doping, the intrinsic properties of the CD can be effectively tuned during their synthesis by tailoring the surface chemistry via surface passivation/functionalization. During the process of surface passivation, functional groups like -OH, -COOH, $-NH_2$, are introduced onto the surface of the CDs, which further enhance the physical property such as solubility and specific chemical reactivity in general as well (Li and Dong, 2018). In a study, Bai *et al*. demonstrated that the polydopamine (PDA) passivated CDs exhibited triple times more QY than the original CDs in the absence of PDA and also displayed 1.5 times enhancement of nucleation site for CD formation (Bai *et al*., 2018).

The surface functionalization of the CDs with different precursors such as L-cysteine (N, S), ethylenediamine (N), and glycine (N, O) resulted in high fluorescence QY and improved selectivity for different metal ion detection due to different binding abilities (Radhakrishnan *et al*., 2019). Understanding the interaction between the CD system and the passivating agents is crucial to tailor the CD's fluorescent properties. For example, the synthesis routes influence the CD-polymer nanoparticle system's interaction that ultimately influencing the photoluminescence property (Momper *et al*., 2018). Ions like Zn^{2+} were also used to develop passivated CDs using zinc gluconate by pyrolysis method of synthesis. The presence of Zn^{2+} during the synthesis prevents aggregation and improves the stability and optical property of the synthesized CD (Yang *et al*., 2018).

The passivation methods and surface functionalization are followed not only to produce better stability and improve the PL intensity but also to enhance other vital characteristics of CDs. Chirality is very important in terms of catalysis, chiral recognition, and even sensing. Recently, Rao and the group developed a strategy using the surface passivation method to prepare chiroptical carbon quantum dots via two steps pyrolytic route. They used tartaric acid and citric acid as carbonaceous sources while producing carbon core, whereas D/L-penicillamine molecules were used to surface passivating agents. In order to retain the chiral information, one of the critical findings of the study was to maintain the reaction temperature lower than the melting point of the ligand in the second pyrolytic step. Interestingly, the strategy did not depend on the chirality of the carbon source (Rao *et al*., 2019). The effects of surface functionalities of CD during cellular uptakes is another interesting study. Here, the CDs which were passivated with two chemical moieties, 3-ethoxypropylamine (EPA-CDs) and poly(ethyleneimine) (PEI-CDs) were considered to evaluate their uptake mechanism, pathways, and effects in HeLa cells (human cervical carcinoma cells). As expected, the internalization pathways of the two CDs were different in the HeLa cells; however, the efficiency of the internalization process with PEI-CDs was higher in comparison to the EPA-CDs. The different moieties present on the surface of CDs could affect the overall behaviours of CDs uptake (Yan *et al*., 2019).

1.2.1.3 *Characterization of CDs*

The unique and typical properties of CDs are exhibited due to their size, shape, chemical skeleton/composition, and structure. So, there have been continuous attempts to explore robust and reliable techniques for their characterization. In this section, some of the updated characterization techniques for CDs are discussed briefly as the characterization of CDs has been discussed more in recent reviews and chapters (Jelinek, 2017; Xu *et al*., 2019; Zhao *et al*., 2020).

1.2.1.3.1 Microscopic and Diffraction Techniques

Non-destructive imaging and microscopic techniques are used to study morphology and different dimension of nanosized particles. Some of the techniques which are being routinely explored for the measurements of CDs are transmission electron microscopy (TEM), scanning electron microscopy (SEM), atomic force microscopy (AFM), X-ray diffraction (XRD).

The morphology, size distribution, or particle size of CDs can be investigated using TEM and SEM. These techniques can be used to determine the agglomeration or dispersion of the prepared particles as well. SEM technique is employed to investigate if the particle size ranges from 1–20 nm, and in case if the measurement exceeds the resolution of SEM, TEM, which could offer better-resolving power, is more advised. Nowadays, high-resolution TEM (HRTEM) is extensively used to study the structure and crystalline nature. To understand dimensional surface images of CDs, AFM is being used to obtain 2D images and 3D information of the surface morphology and topography of CDs. Depending on their diffraction patterns, crystalline materials can be characterized by XRD. Thus, the particle size, crystal structure, and purity of CDs are investigated through this technique. It is a valuable characterization technique to obtain crystallite features, but the technique could also be used to study amorphous CDs (Kang and Lee, 2019; Zhu *et al*., 2015).

1.2.1.3.2 Spectroscopic Techniques

Spectroscopic techniques can characterize the synthetic features of CDs. Some of the commonly used spectroscopic tools are ultraviolet-visible spectroscopy (UV-

Vis), Fourier transform infrared spectroscopy (FTIR), nuclear magnetic resonance spectroscopy (NMR), photoluminescence spectroscopy (PL), and Raman spectroscopy.

FTIR determines and identifies the functional groups such as carbonyl (-C=O), amine/amide (-NH_2/-CN), hydroxyl (-OH), ether/epoxy (-O-), and others that are present on the surface of the CDs. The presence of moieties and heteroatoms in CDs such as boron (B), nitrogen (N), sulphur (S), silicon (Si), and phosphorus (P) could be identified using such technique. The fine structure information of metal-doped CDs such as aluminium (Al), nickel (Ni), or magnesium (Mg) can be further characterized by X-ray photoelectron spectroscopy (Zhao *et al*., 2020).

Another important spectroscopic technique is Raman spectroscopy, a non-destructive and non-invasive method to identify the CDs state. Generally, Raman spectra of CDs have two first-order bands, i.e., D- and G-band. D bands signify the vibration of carbon atoms of disordered graphite or glassy carbon, whereas the G band represents the vibration of sp^2 carbon atoms. The degree of purity or graphitization of CDs could be estimated by the ratio of D band and G band (D/G). A high D/G ratio indicates the amorphous nature, and a high degree of graphitization gives a relatively lower D/G ratio.

NMR usually employs to understand the structural information of CDs further. The presence of sp^2 carbon, sp^3 carbon, functional groups like -C=O, -NH_2, and -OH can be distinguished with the resonance spectroscopy. ^{13}C-NMR could be used to distinguish further and confirm the presence or absence of aliphatic carbon or aromatic carbon on the CDs skeleton. The optical properties of CDs are extensively investigated with the help of UV-Vis and PL spectroscopic techniques. The absorption and the photoluminescence properties of CDs are explained more in the later part of the review.

One of the powerful tools to elucidate the chemical structure of smaller-sized nanoparticles is mass spectrometry (MS). Some of the MS techniques which have been applied and used to characterize CDs are electrospray ionization quadrupole time-of-flight tandem mass spectrometry (ESI-Q-TOF-MS/MS), inductively coupled plasma-mass spectrometry (ICP-MS), and matrix-assisted laser desorption/ionization time-of-flight mass spectrometry (MALDI-TOF-MS) (Tajik *et al*., 2020; Wang *et al*., 2019).

1.2.2 Properties of CDs

CDs are fascinating nanomaterials with remarkable inherent physical and chemical properties that allow their application in diverse fields. Therefore, an in-depth study and understanding of the CD's optical, physical, and chemical properties are essential to further improve its characteristics in order to broaden its applications.

1.2.2.1 Physical property

1.2.2.1.1 Chemical Structure

CDs usually are less than 10 nm with quasi-spherical nanosized carbon particles. However, as mentioned earlier, synthesis routes dictate the various chemical structure of CDs. For instance, GQDs are anisotropic with a crystalline structure of one or more graphene layers. Different analytical techniques such as microscopic, spectroscopic, spectrometric, and diffraction methods are employed to confirm and ascertain the morphology, functional groups, size distribution, and crystalline nature of CDs. For example, the morphology of microstructure CDs-based lubricants following the ultrasonic approach was studied with TEM and HRTEM and found to be 2.38 nm on average and highly crystalline with 0.21 nm lattice spacing and (100) graphene plane (He *et al*., 2019). The structural elucidation of defects and or graphitization could be further confirmed with Raman spectrometry by analysing the G band and D band. By following the pulsed laser ablation synthesis method, nitrogen-doped GQDs were prepared and obtained a 3 nm particle size by Neon and co-workers. The as-prepared N-GQDs exhibited 1565 cm^{-1} as G band and 1311 cm^{-1} as D band in Raman spectrum, confirming the disordered structure (Novoa-De León *et al*., 2019). XRD is a powerful instrument to characterize the physical state of the synthesized CDs. The amorphous character of CDs is observed as a broad hump, which is centred in and around ~2θ = 26° in the XRD profile. Nearly spherical amorphous clusters of ~4–18 nm diameters were observed in the self-passivated CDs from dextrose by following the ultrasonication approach (Siddique *et al*., 2018).

1.2.2.2 Chemical and Optical Property of CDs

1.2.2.2.1 Ultraviolet-Visible Absorption Analysis

The basic chemical structure of CDs can be significantly elucidated by the typical UV-Vis spectral analysis. The presence of π-π* (C=C) and n-π* (C=O, C-N, C-S, etc.) transition of the CDs skeleton indicates the type of surface functional groups, routes of CD synthesis, precursors, and chemical environment. For example, the absorption bands of CDs at around 273 nm and 342 nm may imply sp^2 hybridization of the π and n-π* transition, respectively (Chen *et al*., 2019). Again, the combination of the same carbon but different nitrogen sources also influences the absorption bands position (Khan *et al*., 2018; Yuan *et al*., 2020). The presence of heteroatoms (such as N, O, P, B, S, Se, etc.) in the CD's molecular structure also results in the fluctuations of the UV-Vis peaks. The N, S-CDs fabricated from 3-aminothiophenol via a one-pot hydrothermal method showed two absorption shoulders at 298 nm, and 354 nm attributed to n-π* transition and heteroatoms N and S surface states defect, respectively (Dong *et al*., 2019).

1.2.2.2.2 Photoluminescence Analysis

The most impressive characteristic feature of CDs is the photoluminescent (PL) or the fluorescent property, which has allowed them to expand their field of applications. The PL of CDs is influenced by surface chemistry, quantum size effect, and molecular states of the carbon core. The upconversion photoluminescence (UCPL) in the near-infrared region carbon dots (NIR-CDs) may be because of the thermally activated electron transition from $S_{1\text{-edge}}$ to $S_{1\text{-Int}}$ in the excited state as shown in Figure 1.2 a (Li *et al*., 2019). The various synthetic approaches (as shown in Table 1 and 2) along with different starting materials result in the generation of CDs with unique structures and different luminescent behaviors such as white, blue, green, yellow, red, and deep ultraviolet emission. Since the CDs are fabricated from variable carbon sources via different routes, the PL behavior also depends on the size, solvent, pH, and many more. Generally, due to the diverse electronic transition pathways, the CDs exhibit broad, symmetrical luminescence spectra across the whole wavelength scale. Various energy levels may be created by O-containing groups (named as O-related defect state), P-containing groups (named as P-related defect state), and N-containing

groups (named as N-related defect state) on sp^2 hybridized carbons of the synthesized CDs as shown in Figure 1.2 b (Yang *et al*., 2019). Moreover, compared to the quantum dots and other organic dyes, the CDs usually exhibit large Stokes shifts. The QY of the CDs depends on the surface chemistry and preparation methods. Yellow-emissive CDs from anhydrous citric acid and 2,3-phenanzinediamine were prepared that exhibited large Stokes's shift (188 nm), excellent stability, and 24 % QY (Yan *et al*., 2019b). In another study, multicolour PL emissive CDs were synthesized from m-phenylenediamine (m-PD) and o-phenylenediamine (o-PD) and in the presence and absence of tartaric acid as the starting materials. Tartaric acid played a crucial role in tuning the surface state of CDs, such as the increase in surface oxidation and carboxylation. In the presence of tartaric acid (TA), the CDs from m-PD and o-PD exhibited green colour and red colour respectively whereas, in the absence of TA, CDs from m-PD and o-PD exhibited blue colour and yellow-green colour respectively. In particular, the red-CDs exhibited a high QY of up to 22 %. (Jiang *et al*., 2019). The doping of CD changes the excitation-dependent PL. In a study, the emission of a bare CD that was found to be excitation-independent, showed a large red shift when it was doped with nitrogen. The reason is ascribed to the superimposition of blue (intrinsic molecular centers) and green emission bands (extrinsic molecular centers). In the emission process, the energy is transferred from the electron-hole pair formation at the intrinsic centers of the core to the extrinsic surface centers. Due to the surface defects and hybrid nanostructure in the mesoporous matrix, the contribution of the two bands modified, enhancing the tunability of the emission, thus promoting the green PL from blue emission. Besides, the QY of the CDs was found to vary, for the bare CDs (1.4 %), N-doped CDs (22 %), and purified N-CDs (28 %) (Carbonaro *et al*., 2018). In another study by Kipnusu and co-researchers, nitrogen and boron-doped CDs exhibited enhanced intersystem charge transfer (ICT) due to the presence of donor-acceptor moieties. Due to the ICT, the synthesized CDs produced triple color emission as shown in the Figure 1.2 c (Kipnusu *et al*., 2020). The properties of PL are controlled by the surface functionalization of CDs as well. Recently, surface functionalization was shown to enlarge and narrowed band gap energy. The fluorescence of synthesized CDs could be quenched by tetracycline (TC) due to inner filter effect, whereas by introducing chlorotetracycline (CTC), blue-shift fluorescence was induced which may be due to enlarge energy band gap, and upon introducing oxytetracycline (OTC), fluorescence experienced red shift which could be because of the narrowed band gap as shown in

Figure 1.2 d (Miao *et al*., 2018). In a recent report, the addition of a long-alkyl chain to the CDs promoted the emission of white luminescence under UV light (365 nm), which may be due to the inhibition of the aggregation-caused quenching effect. Additionally, the alkyl chains can effectively interact with the lipophilic fatty residues that can increase the potential applications of the developed white-CDs (Jiang *et al*., 2018). Metal ion-dependent PL quenching of CDs has become a known phenomenon. In a report, the quenching mechanism has been identified as the photoinduced transfer of electrons from amine functional groups of the CDs to the respective metal ions (Mintz *et al*., 2018).

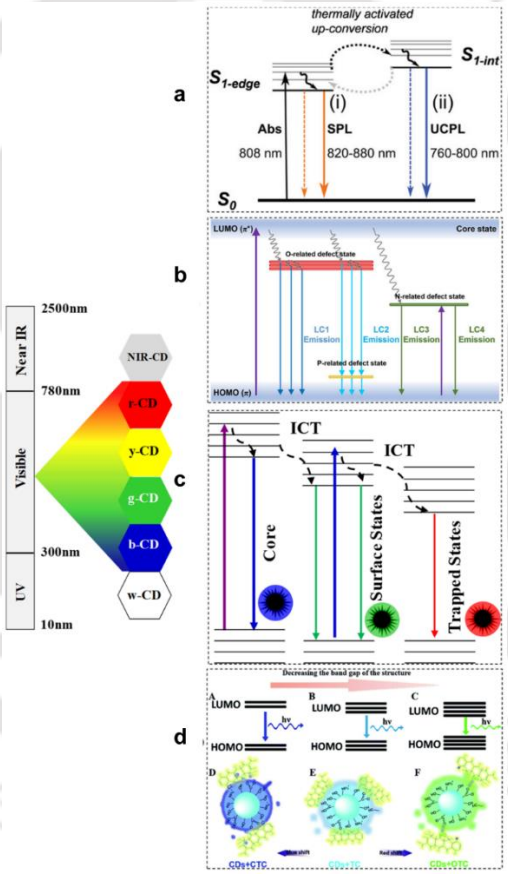

Figure 1.2. The band gap and transition of various colour exhibited by CDs (near infrared CD: NIR-CD, red-CD: r-CD, yellow CD: y-CD, green CD: g-CD, blue CD: b-CD, white CD: w-CD). (i) Proposed mechanism of up-conversion PL in Near IR (NIR) CDs, (ii) Proposed mechanism of CDs with O-defects, P-defects and N-defects states. (iii) Energy diagram of the CDs indicating the role of intersystem, charge transfer. (iv) Band gap transitions of CDs by introducing CTC, TC, and OTC (Das *et al*., 2021b).

1.2.2.2.3 Electron Transfer of CDs

Typically, CDs can act as both an electron acceptor and donor. In an interesting study, considering the exceptional electron mobility property of the CDs at room temperature, CDs functionalized with ionic liquid were fabricated for their application as nanofluid in the field of energy. The nanofluids comprising of organic/inorganic hybrid systems could be used as electrolytes and separators for energy storage. Highly conductive CDs, CDs/[Bmim]Cl/[Tmi][Trif] and CDsCHI/[Bmim]Cl/[Tmi][Trif], could be entrapped in poly(vinyl alcohol) membrane, which exhibited high proton conductivity. Moreover, the nanofluid's features remain constant for four months, even on wetting/drying cycles (Gonçalves *et al*., 2020). One of the most common applications of CDs is in the field of photocatalysis. The photocatalytic performance of the graphitic and amorphous CDs, which were synthesized using fructose, glucose, and citric acid, was investigated. In this study, the type of carbon source and the synthesis route that ultimately determines the potential of the photoelectron transfer determined the CD's structure and optical properties (Emanuele *et al*., 2020). Pure carbonaceous CDs (without dopants) in graphitic form exhibited better photoactivity than the amorphous one, whereas, in the case of nitrogen-doped CDs, the amorphous CDs exhibited better photoredox-activity due to the presence of photo-active molecules. The graphitic defects and the dopant can quench each other, which reduces the photoactivity (Cailotto *et al*., 2018).

Heteroatom doping in carbon materials has long been used to create active catalytic sites and increase oxygen reduction reactions (ORR) in electrocatalysis. The performance of carbon-based catalysts, composites of doped CD and reduced graphene oxide (CD/rGO), and directly doped rGO were studied. In the finding, CD/rGO outperformed in ORR measurement to their corresponding counterparts, and it's noted that N, S-co-doped too performed better than the individual doped N-CDs or S-CDs. Some of the reasons for such behaviour could be the synergistic effects of N, S-co-doping providing four-electron transfer pathways in ORR, active sites of on the CD surfaces and located at the edges/defects in abundant, which may have more accessibility to oxygen molecules. Another reason could be the effective components like graphitic N atoms and C-S-C/S-N species where current density and half-wave potential could be improved (Zhang *et al*., 2019).

1.2.2.2.4 Cytotoxicity and Photostability of CDs

CDs are mostly known for their fascinating biocompatibility and relatively less toxicity, thus fulfilling the required conditions for diverse applications. The cytotoxicity of CDs, both *in vitro* and *in vivo* conditions, are extensively investigated. Moreover, CD's photostability is a crucial characteristic that can be explored for its efficient use as stable fluorescent probes. As the name suggests, photostability here means the labelled cells fluorescence intensity remains stable for a considerable time. With this property, CDs are growingly used in cell imaging. Semi-conductor quantum dots were used in bioimaging methods because of their better photophysical properties than organic chromophores. The use of the conventional metal-based QDs for biomedical applications is limited because of toxicity of the heavy metals like Pb, Cd present in these nanomaterials. Since CDs are free from toxic heavy metals and possess high photostability, these are used in the bioimaging fields and medical diagnosis as well. However, a report of the low toxicity of metal chelated CQD is available. A CQDs from citric acid and polyethylenimine was synthesised and covalently conjugated with 1,4,7,10-tetraazacyclononane (DOTA) to chelate lanthanide ion (Ln = Eu, Tb, Yb, and Gd). The CQDs-DOTA-Ln exhibited low cytotoxicity against Hela cells even at its high concentrations (500 μg mL^{-1}) (Wu *et al*., 2019). However, the synthesis of metal-doped CDs is time-consuming, complicated, involves multiple steps, and requires post-synthetic treatments. In a recent development, ruthenium-containing CDs (Ru-CDs) were fabricated using a simple and efficient strategy. The developed CDs exhibited enhanced red fluorescence compared to the bare CD and Ru-complex and were employed as bioimaging agents for tumour cells and as photodynamic nanoagents for cancer therapy (Yue *et al*., 2020).

1.2.2.2.5 Emerging Property: Chirality of CDs

More recently, efforts have also been made to develop chiral CDs for their application in a myriad of areas ranging from sensing of chirality, separation of chiral molecules, chiral catalysis, bioimaging, and biomedicine. Among the two types of CD synthesis approaches, the “bottom-up” approach usually generates better chiral CDs as the precursor molecules themselves are chiral and therefore do not need the introduction of chiral ligands during the synthesis process (Ru *et al*., 2020). A hybrid CD/CNC (cellulose nanocrystal) nanoparticle synthesized via hydrothermal route showed a

dissymmetry factor of 0.2, which is higher than that of the reported dye/CNC hybrids. Furthermore, the nanoparticle displayed higher left-handed circularly polarized luminescence (CPL) emission than right-handed CPL emission. Based on the significant findings, these hybrids have a promising application to remove autofluorescence drawbacks in bioimaging. The CD/CNC hybrids can also be effectively employed in sensing, drug delivery, and photonic applications as mirror-free cholesteric lasers (Chekini *et al*., 2020b). In another interesting study, using the concept of donor–acceptor complex formation between CDs and porphyrins, the chirality of the carbon nanodots was transferred to the porphyrin. This experimental finding provided the possibility of forming chiral composites for different applications (Đorđević *et al*., 2018). In another approach to enhance the material property for biomedical applications, chiral CDs derived from glutamic acid were doped into gels as the latter display superior biocompatibility. An important aspect of such a doping process is the requirement of chiral match ability between the CD and the gelator, which would otherwise lead to the disintegration of the gel. It was shown that the doping of the chiral CD with the gelator (N,N-bis(octadecyl)-D-aminoglutamic diamide) to form gel resulted in the fluorescence enhancement of the CD. The enhancement was assumed to be the restriction of Brownian motion in the gel system that otherwise is responsible for decreased fluorescence intensity in the liquid system due to collisions between the CDs (Zhou *et al*., 2020). Fluorescence off-on sensors have an enormous demand for the development of smart monitoring systems. Using chiral CD synthesized from citric acid and L-aspartic acid, an on-off and off-on fluorescence sensor was developed to detect both Sn^{2+} ion and L-Lysine enantiomer. While the binding of Sn^{2+} on the surface of the CD resulted in fluorescence quenching (on-off), the addition of L-Lysine to the CD-Sn complex resulted in the enhancement of the fluorescence (off-on) as the L-Lysine preferentially has a stronger binding affinity for Sn^{2+} thereby recovery of the CD's fluorescence (Gao *et al*., 2020).

1.2.3 Photoluminescence (PL) Mechanism of CDs

Even though the research of CDs is thriving, the exact PL mechanism of the CDs is still in debate. Some of the most acceptable PL mechanisms include quantum confinement and surface states-based explanations. In brief, when semiconductors exhibit properties like size-dependent energy and bandgap transition in the nanometer

scale due to the distribution of electrons in the crystal boundary, such behavior of the materials is known as the quantum confinement effect (QCE). The CDs have a band gap that is non-zero, hence exhibiting fluorescence phenomenon under excitation. Additionally, the PL mechanism of CDs could be closely related to surface chemistry, like the presence of functional groups or the surface oxidation states. The diverse surface functional groups such as -C=O, -COOH, -CN, -NH_2, -OH can give rise to distinct fluorophores and energy levels. Besides, the surface defects are directly proportional to the extent of surface oxidation that influences the emission wavelength of the CD.

In a new development, the reported CDs with high QYs (up to 80 %) exhibited green and red reversible switching photoluminescence. The green CDs were synthesized from 3, 4, 9, 10-nitroperylene in an alkaline solution, whereas the red CDs were developed by modifying the surface electronic state of the green CDs by adding alkali. The red emission was due to the narrow band gap, which is further influenced by the surface electronic state, as shown in Figures 1.3 a (Yuan *et al*., 2018). In another interesting study, the PL of CD and ionic liquid were found to be similar. The energetically different associated structures in the ground state of the CD govern the fluorescence response (Roy *et al*., 2018).

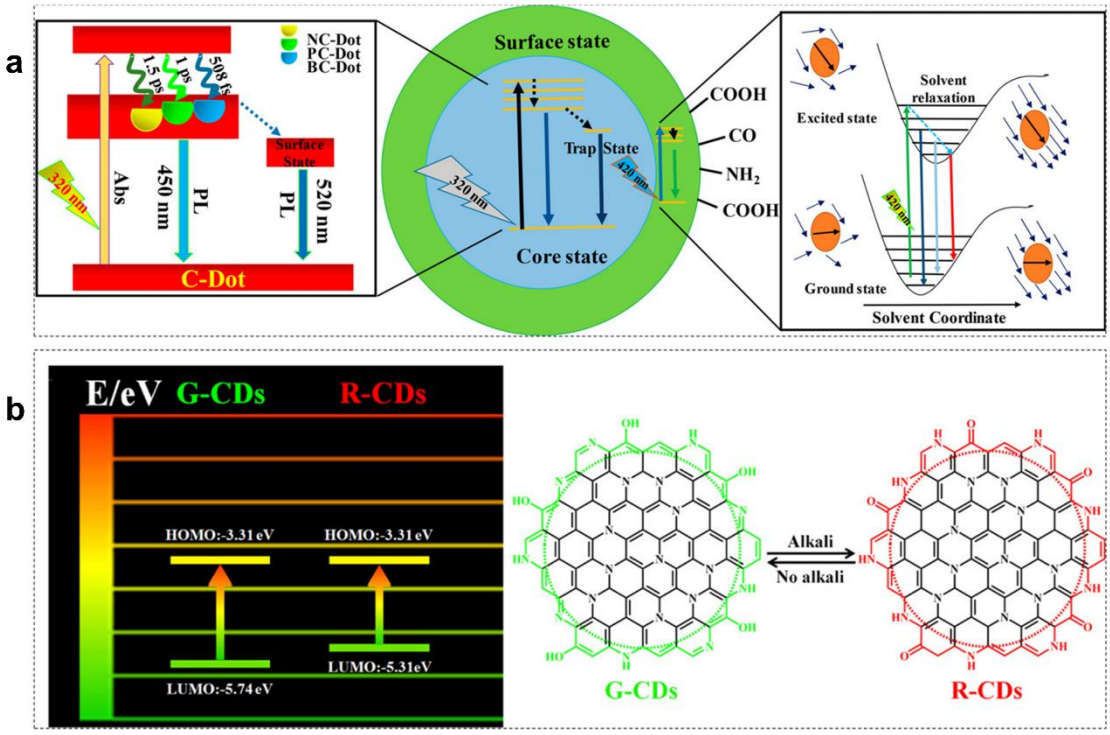

Figure 1.3. (a) Energy levels (HOMO and LUMO) of G-CDs and R-CDs (left side); Luminescence mechanism (right side). (b) Excited-State for Doped C-Dots at Core State and Surface State, (Das *et al*., 2021b).

The surface functional groups on CD play a crucial role in modifying the PL properties. In a report, the CDs from four types of lysine derivatives with different quantities of amino and carboxyl groups were prepared. The CDs with a higher number of functional groups from the precursors resulted in a higher degree of cross-linking, which could lead to fluorescence enhancement and better stability (Yang *et al*., 2020). Besides, the electronic acceptor levels of CDs were influenced by the electronic states of core and ground. The interactions such as hydrogen bonding and affinity behavior of the CDs could be determined by the chemical nature of the surface groups (Ren *et al*., 2019). In another study, the catalytic activity of the CDs was studied with different surface modifications. Two different CDs were synthesized from poly(ethyleneimine) (PEI-CDs) and citric acid (CA-CDs) which were then used to monitor the peroxidase-like activity in the presence of the substrates like 3, 3', 5, 5'-tetramethylbenzine (TMB) and 2, 2'-azino-bis(3 ethylbenzothiazoline-6-sulfonic acid (ABTS). Interestingly, the TMB exhibited a higher affinity to the negatively charges CA-CDs, whereas the ABTS showed a higher affinity to the positively charged PEI-CDs (Shi *et al*., 2019). The surface modification controls the optoelectronic behavior of the CDs like band gap energy, quantum tunnelling, or yield of triplet excitons. Behera *et al*. studied three different surface states of CDs (oxidized CDs, reduced CDs, untreated CDs) that had not much alteration in the physical dimensions. They noticed that the spectral signature of singlet and triplet excited states and the charge transport properties differed from each surface state. Moreover, this study also emphasized the redox-based surface modification as oxidized CDs exhibited a small barrier height compared to the reduced CDs (Behera *et al*., 2019). The influence of CDs bearing different surface amine-derivative ligands on device performance, such as hole transport materials in inverted hybrid LEDs, was studied recently by Paulo-Mirasol's group. They highlighted that the different surface ligands would affect the optical properties and other parameters like device turn-on voltage and luminance. Besides, varying results were also observed for CDs capped with aromatic rings and nonaromatic ligands (Paulo-Mirasol *et al*., 2020).

Doping of CDs with non-metallic ions influences the nanomaterial properties, which further affects the PL mechanism. In a study, the dynamics of the excited-state

with nitrogen-doped, boron-doped, and phosphorus-doped CDs were investigated. It was observed that the relaxation time profoundly depends on the doping type within the core structure. Further, doping also influences the carbon atom's charge delocalization that ultimately affects the solvation time as shown in Fig. 1.3 b. Besides, the N-doped CDs exhibited the highest charge carrying capacity, followed by P-doped and B-doped. The breaking of π-π stacking and formation of defects in the P-doped and B-doped CDs was responsible for low charge carrying capacity (Mondal *et al*., 2019).

Another fascinating new insight of PL is the possible contribution from the small molecular fluorophores. In a recent development, it has been observed that the PL of the CDs could be increased due to the presence of small fluorophore molecules if the bottom-up synthetic route is followed (Xiong *et al*., 2018; Zhu *et al*., 2016). The presence of molecular fluorophores and their aggregates may or may not be CDs and may misguide to understanding the structure-property correlation. Such fluorophores could be embedded in between the polymeric carbon dots and thus exhibit enhanced optical properties in absorption and emission spectra due to the possible synergistic effects (Ehrat *et al*., 2017; Xiong *et al*., 2018). The impact of such molecular fluorophores may be depending on the arrangement and position with CDs. Langer and co-workers reported 5-oxo-1,2,3,5-tetrahydroimidazo-[1,2-α]-pyridine-7-carboxylic acid (IPCA), a molecular fluorophore formed in CDs derived from citric acid and ethylenediamine, showed a tendency to interact and self-assemble into a stacked like system with the CDs. IPCA could also be incorporated and interacted with the core structure of CDs (Langer *et al*., 2020). Some of the moieties or molecular fluorophores not only enhance the optical properties but are also responsible for emission other than the actual CDs emission such as 4-hydroxy-1H-pyrrole[3,4-c]pyridine-1,3,6(2H,5H)-trione (HPPT) (Kasprzyk *et al*., 2018), and hybrid luminescence in the solution (Sendão *et al*., 2019).

1.2.4 CDs in optical-based analytical applications

As evident from the previous sections, the CD's inherent optical properties are remarkably altered in response to one or more external stimuli. Therefore, exploiting the CD's role in a variety of smart applications has become of intense interest.

1.2.4.1 Photoluminescence

One of the most fascinating properties of CDs is photoluminescence or fluorescence. The fluorescence phenomenon occurs when the electronically excited fluorophore relaxes from the singlet state to the ground state. Many recent studies have shown noteworthy advances in the field of fluorescence. CDs are frequently used as fluorescent probes for the detection of bioanalytes, small molecules, and ions.

Most fluorescence-based detection methods use turn-on, and turn-off modes wherein the appearance or disappearance of the colour is sometimes difficult to differentiate. Therefore, to increase the visibility in biosensors, a combination of two fluorophores is often used, wherein only one of the fluorophores is sensitive to the analyte, and the other one is inert. Recently, using CD and rhodamine 6G (Rh6G) fluorophore, a ratiometric fluorescence-based experiment was designed for the detection of glucose in both the aqueous phase and on solid-state hydrogel film by employing glucose oxidase (GOx) and horseradish peroxidase (HRP) enzymes. The developed system resulted in the quenching of the blue-colour emitting CD, whereas the green-colour emitting Rh6G had no response and, therefore, with increasing concentrations of glucose in the CD/Rh6G/GOx/HRP, the colour of the fluorescence changed from blue to green. For the solid film detection, the CD/Rh6G/GOx/HRP was immobilized in a hydrogel film developed by UV curing of 70:30 (w/w) mixture of acrylic acid and diacrylate poly (ethylene glycol). The experimental results indicated that in contrast to the aqueous phase, the solid-state platform was much more selective to glucose, had high stability, and could be reused (Cho and Park, 2019). A ratiometric CD-based fluorescent probe for the detection of lead (Pb^{2+}) and pyrophosphate (PPi) was synthesised. The CDs displayed a three-state "pink-cyan-pink" emission upon the addition of Pb^{2+} and PPi. The Pb^{2+} formed a coordination complex with the amine and porphyrin group on the surface of the CD that resulted in the quenching of the fluorescence. Interestingly, upon the addition of PPi, the CD's fluorescence was

recovered, attributed to the removal of Pb^{2+} from the CD's surface. Based on this, a fast and straightforward paper-based platform for the detection of Pb^{2+} and PPi was designed (Gao *et al*., 2019).

In recent times, CDs have attracted attention for their potential applications in the field of optoelectronics. To this end, various designed strategy has been developed using CD as a fluorescence signal probe. Doping of the CD as an efficient strategy has many reports on the field. For example, nitrogen and sulfur co-doped (N, S) CDs using *O*-Phenylenediamine (OPD) and sulfamide were developed that exhibited excitation-independent properties with bright red fluorescence. A mixture of N, S-CDs along with blue- and green-emitting CDs was used to develop white light-emitting polyvinylpyrrolidone (PVP) film that was subsequently layered on a UV-LED chip to design white light-emitting diodes (WLEDs). The fluorescence intensity of the developed WLEDs remained stable for 20 days and at varying temperatures. The polymer chains in the CDs generated repulsive forces that resulted in the stability of the WLEDs at different temperatures. Further, the fluorescence intensity of the N, S-CDs was quenched in the presence of water, and therefore was employed for the sensitive detection of water in organic solvents (Guan *et al*., 2019). Further, CD/hydrogel composites have also been used to obtain effective sensing platforms. Using cellulose nanofibrils (CNFs) and CDs, a novel fluorescent hydrogel was developed that displayed a high QY of 23.6 %. The CNF's natural skeleton and the amide, hydroxyl, and carboxyl groups on the hydrogel surface allowed the accumulation and adsorption of heavy metal ions. Further, the hydrogel's three-dimensional network generated channels for the diffusion of the ions from the outside to the inside of the adsorption sites, with high adsorption capacity for Fe^{3+}, Ba^{2+}, Pb^{2+}, and Cu^{2+}. Additionally, the hydrogel's fluorescence was rapidly quenched in the presence of Fe^{2+}, and therefore, was applied for the visual optical detection of the ion. The quenching phenomenon is attributed to the constraints of the hydrogel's fluorescence excitation as a result of the adsorption of the Fe^{3+} (Guo *et al*., 2019). In another interesting study, an antibacterial wound dressing was developed from a nano colloidal hydrogel composed of CD/cellulose nanocrystal hybrid nanoparticles and gelatine. The hydrogel displayed high Fe^{3+} ion absorption capacity, limiting the accessibility of these ions required for the pathogenic bacteria's growth at the infection site. As such, the hydrogel absorbed Fe^{3+} ion interacted with the

surface functional group of the CD that resulting in the quenching of the hydrogel's photoluminescence (Chekini *et al*., 2020a).

The CDs are also attracting interest for their application as nanothermometers due to their property to undergo alterations in their fluorescence property in response to temperature stimuli. Mohammed and co-workers reported boron and nitrogen co-doped (B, C) CDs that exhibited variation in the fluorescence intensity at different temperatures (0-90 °C) with a thermo-sensitivity of 1.8 % $°C^{-1}$. Therefore, it can be employed as efficient nanothermometers. The temperature did not influence the CD's surface fluorescent structure as the fluorescence intensity was easily reversed and restored when the temperature was increased and subsequently decreased (Mohammed and Omer, 2020).

The optical-fiber technique in biosensing applications in recent times is highly sought-after. In one such development, a novel optical-fiber glucose biosensor exhibiting high sensitivity and continuous online detection of glucose has been developed. The end face of the optical fiber was immobilized following dip-coating method using carbon quantum dots (CQDs)-glucose oxidase (GOx)-cellulose acetate film, allowing visualization of real-time glucose fluctuations in various concentration ranges including micro-to nano-mole levels (Yu *et al*., 2019).

Surface modification of CDs has emerged as a suitable strategy to facilitate its application in optical-based detection. In a study, a novel thymine functionalized carbon dot (CDs-Thy) was designed to detect Hg^{2+}. In the presence of Hg^{2+}, the thymine moieties on the surface of CD could form T-Hg^{2+}-T structures, allowing photoinduced electron transfer to occur from the excited CDs-Thy to the vacant d orbital of Hg^{2+}. This event resulted in the quenching of the CDs-Thy. In the proposed method, the Hg^{2+} was detected in the linear concentration range of 0-1.0 μmol L^{-1} and a limit of detection (LoD) $3.5x10^{-8}$ mol L^{-1} (Li *et al*., 2018). In another study, for the detection of hypochlorite (ClO^-), a novel dual emission ratiometric probe (FH-GA-CQDs) was synthesized by covalently conjugating fluorescein (FH) derivative (green-colour emission) onto the surface of CDs (CQDs) (blue-colour emission) via the GA linker. In the presence of ClO^-, the xanthene ring of the FH unit opens via oxidative induction, which allows the FRET process to occur from CQD to the FH units resulting in the decrease of the fluorescence intensity of CQD and increase of the fluorescence intensity

of FH units. By using this method, ClO^- as low as 93 nM (LoD) could be detected (Yan *et al*., 2019a). In a recent past, a FRET-based system was developed using CDs as energy donor and gold nanorods (Au NRs) as energy acceptors. By using cysteamine as a bridge, the nanomaterials were covalently connected, hindering the FRET process. Upon the addition of Pb^{2+}, cysteamine interacted with the ion resulting in activation of the fluorescence signal as the FRET process was disturbed. The Pb^{2+} could be detected through this sensor system with high selectivity and sensitivity with 0.05µM as LoD (Liu *et al*., 2019). Table 1.3. Illustrates the various other reports of carbon dot as smart material in PL sensing.

Table 1.3. CD-based photoluminescence detection.

Precursor and Synthesis route	**Size (QY)**	**Application**	**References**
Citric acid, urea, and thiourea **Microwave-assisted**	10 nm (19.2 %)	Mercury (II) and iodide detection	(Tabaraki and Sadeghinejad, 2018)
Succinic acid and glycerol **Hydrothermal**	2.3 nm (11 %) (Blue-CD) 4.6 nm (7 %) (Green-CD)	Fe^{2+}, H_2O_2 detection and bioimaging	(Prathumsuwan *et al*., 2018)
L-glutamate **Pyrolysis**	2 nm-4 nm (34 %)	*Plasmodium falciparum* glutamate dehydrogenase detection	(Singh *et al*., 2018)
Citric acid and ethylenediamine **Microwave-assisted hydrothermal**	3.6nm (NA)	Detection of glucose	(Zhai *et al*., 2018)
Citric acid, formamide, and ethanol (E-CD) **Citric acid, formamide (N-CD)** **Solvothermal**	4.5 nm (15.81 % - water,22.43 %-DMSO, 25.80 %-DMF, 19.42%-methanol) (E-CD) 5.5nm (NA) (N-CD)	Fluorescent pH sensor	(Gao *et al*., 2018)

Sodium citrate and urea **Solvothermal**	3.52 nm (67 %)	Mercury ion detection in living cells and visualization of latent fingerprints	(Ren *et al*., 2018)
Citric acid and ethylenediamine **Hydrothermal**	2 nm (NA)	Doxycycline and MnO_4^- detection	(Fu *et al*., 2018)
Leaf extract of *Bougainvillea* **Microwave-assisted**	10.7 nm (~41 %)	Bioimaging, detection of Cu (II), and as red-emitting fluorescent ink	(Bhati *et al*., 2018)
Pricky pear cactus **Hydrothermal**	5.6 nm (12.7 %)	Arsenic (III) and hypochlorite ion detection in drinking water	(Radhakrishnan and Panneerselvam, 2018)
Citric acid and glycine **Hydrothermal**	2.8 nm (78 %)	Detection of chromium (VI)	(Wang *et al*., 2018)
p-phenylenediamine **Microwave-assisted**	3.8 nm (15 %)	Detection of pH and Fe^{3+}	(Sun *et al*., 2018)
Glycerol and cysteine **Microwave-assisted**	1-6 nm (3.5 %)	Detection of Hg(II)	(Xu *et al*., 2018)

Sodium lignosulfonate and p-phenylenediamine **Solvothermal**	2.02 nm (11.25 % - ethanol, 13.77 % -n-propanol, 11.66 % - isopropanol, 15.07 % - DMF, 14.29 % - DMA), 5.12 % (water), 5.58 % (acetic acid), 5.77 % (propionic acid)	Detection of Fe(III), Ag(I) and as a solvatochromic probe	(Zhu *et al*., 2018)
Glutathione, sodium citrate, (blue-CDs) and 1,2,4-triaminobenzene (yellow-CDs) **Hydrothermal (blue-CDs), Solvothermal (yellow CDs)**	4.0 nm (Blue-CD) 2.4 nm (Yellow-CD) (NA)	Detection of Fe^{3+} and PPi	(Xu *et al*., 2019)
Cellulose-based willow catkin biowaste **Combustion treatment**	7.3 nm (13.3 %)	Detection of Fe^{3+} and bioimaging	(Cheng *et al*., 2019)
Melamine and dithiosalicylic sacid **Solvothermal**	6.5 nm (5.96 %)	Two-switch-mode luminescence ink	(Yang *et al*., 2019)
Glucose and $HAuCl_4$ **Microwave-assisted**	10 nm (0.15 %)	Detection of Pb^{2+}	(Li *et al*., 2020)

Alizarine rmine **Hydrothermal**	2.37±0.23 nm (6.3 %)	Detection of glutathione and cancer cells.	(Li *et al*., 2020)
***o*-phenylenediamine and lysine** **Hydrothermal**	CDs-0-2.51 nm CDs-1-2.55 nm CDs-2-3.35 nm CDs-3-2.95 nm (NA)	Endoplasmic reticulum polarity	(Shuang *et al*., 2020)

1.2.4.1.1 Dual-Mode Detection Systems

CD-based dual-function optical systems are expected to offer confirmed detection along with increased sensitivity for the target. A dual-mode nitrite (NO_2^-) detection method using N-doped CD was synthesized using phenosafranine and citric acid through hydrothermal treatment. The surface-oriented amino group of the N-CD coordinated with the NO_2^- resulting in aggregation of the carbon nanoparticles. This event caused static fluorescence quenching of the orange emitting CD. Additionally, with increasing concentrations of NO_2^-, the colour of the N-CD solution changed ratiometrically from red to purple. The work has potential to detect NO_2^- in A549 cells (Jia *et al*., 2020). In a similar study, smart detection of 2-nitrophenol (2-NP) and 4-nitrophenol (4-NP) using a CD synthesized from EDTA having dual-readout property was demonstrated. Upon the addition of both 2-NP and 4-NP to the CD solution, the fluorescence intensity dropped significantly. The fluorescence quenching of the CD was attributed to the inner filter effect. Besides, the system having CD and 4-NP resulted in the splitting of the corresponding CD peak into two, along with the fluorescence quenching. At the same time, the CD solution turned colourless to yellow in the presence of both 2-NP and 4-NP (Qu *et al*., 2019).

Previously, a red-emitting CD via a hydrothermal route using p-phenylenediamine and phosphoric acid as precursors was synthesised. The CD was employed in an "on-off-on" dual-mode sensing platform for the sequential detection of chromium [Cr(VI)] and cysteine (Cys). The fluorescence of the red-emitting CD was dramatically quenched upon its interaction with Cr(VI) owing to the binding of the later to the surface functional groups that resulted in charge transfer from the excited state

CD to the Cr(VI). The addition of Cys to the CD@Cr(VI) complex restored the fluorescence of the CD, due to the formation of a more stable Cr(VI)@Cys complex. Concurrently, the colour of the CD solution also changed from red to purple to yellow. By integrating the merits of the phenomenon, the nanoprobe was used in cellular imaging and the construction of AND logic gate (Gao *et al*., 2018). Subsequently, a strategy was used to simultaneously detect Cu^{2+} and Al^{3+} using a dual emissive CD synthesized from red tea through a solvothermal treatment. The CD exhibited strong and weak emission peaks corresponding to the red and blue regions, respectively, at an excitation of 410 nm. In the presence of Cu^{2+}, the red emission peak quenched utterly, whereas the intensity of the blue emission peak increased and resulted in a red-shift in the presence of Al^{3+}. This phenomenon is attributed to aggregation-induced emission quenching (ACQ) and aggregation-induced emission enhancement (AIEE) of the CD upon its interaction with Cu^{2+} and Al^{3+}, respectively. Additionally, under the UV light, the fluorescence colour of the CD solution changed from red to orange and then yellow to green in the presence Al^{3+}, which was visible to the naked eye (Song *et al*., 2019). In recent work, pH-sensitive gadolinium (III) (Gd^{3+})-doped CDs were synthesised using citric acid, $GdCl_3$, and urea via a solvothermal route. The CDs displayed excitation-independent bright red fluorescence and a high T1 relaxivity of ~16.0 mM^{-1} s^{-1}. The CDs showed fascinating pH-dependent responses in both fluorescence (FL) and magnetic resonance signals. At acidic pH, the fluorescence of Gd^{3+}-doped CD quenched and exhibited increased brightness of the MR image. However, at alkaline pH, the Gd^{3+}-doped CD displayed bright red fluorescence, and the response of the MR changed from bright to dark. They found that the pH-dependent responses vary reversibly when the pH is switched repeatedly from 10.0 to 1.0. Additionally, based on the Gd^{3+}-doped CD, they also developed an FL/MR dual-readout logic gates, wherein H^+, OH^- and Cu^{2+} acted as input as they stimulate the fluorescence and MR response in a switched manner. Based on this phenomenon, the Gu^{2+}-doped CD was employed in bioimaging *(*Fang *et al*., 2020). Table 1.6 lists some of the other reported CDs with dual-functionality.

Table 1.4. CDs synthesized for dual-mode detections (PL and colorimetric).

Precursor and Synthesis route	Size (QY)	Application	References
2,5-diaminobenzene sulfonic acid, 4-aminophenylboronic acid hydrochloride and Fe^{3+} **Hydrothermal**	NA (0.7 %- in the absence of ascorbic acid, 2.3 %- in the presence of ascorbic acid)	Detection of ascorbic acid	(Liu *et al*., 2018)
Folic acid and p-phenylenediamine **Hydrothermal**	2 nm (8.4 %)	Detection of organophosp-hate pesticide	(Li *et al*., 2018)
Methylene-bis-acrylamide, *p*-phenylenediamine, and trifluoroacetic acid **Hydrothermal**	3.9±0.2 nm (7.5 %)	Detection of Al^{3+}	(Li *et al*., 2018)
m-phenylenediamine and citric acid **Solvothermal**	3-4 nm (65 %)	Detection of Cr(VI)	(Qiao *et al*., 2019)
Citric acid and ethylenediamine Microwave-assisted **Hydrothermal**	NA	Detection of glucose	(Zhai *et al*., 2019)
***N*-(phosphonomethyl)iminodiacetic acid (PMIDA) and branched PEI** **Hydrothermal**	6.71 nm (15.91 %)	Detection of formaldehyde and bioimaging	(Qu *et al*., 2020)

1.2.4.2 Chemiluminescence

Chemiluminescence (CL), a type of luminescence, is the phenomenon of emission of light resulting from a redox chemical reaction between the reagents. Typically, the reaction produces electronically excited intermediates or products, which, when relaxes to the ground state, release energy as photons of light. The

chemiluminescence method is a widely used optical detection method due to its distinctive features such as high sensitivity, no requirement of an external light source for excitation, simple instrumentation, and fast response time. Luminol, potassium permanganate, lucigenin, tris(2,2-bipyridine) ruthenium (II), and peroxyoxalate are the most commonly used classical CL reagents in analytical applications. However, these classical CL reagents are expensive, most are poisonous, have low selectivity, and, most importantly, generate weak CL intensity, which is a major drawback. HCO_4^- and HSO_3^- are some of the green and cheaper CL reagents that are frequently used in combination with various oxidants in CL reaction systems. Nevertheless, these systems also produce weak or ultraweak CL intensity. Therefore, in the past few years, there has been tremendous research on incorporating nanomaterials in CL systems in order to enhance the intensity of CDs, a less/nontoxic and inexpensive fluorophore, have emerged as a suitable candidate for increasing the CL reaction system's applicability. CDs have been growingly employed as enhancers, catalysts, energy acceptors, or emitter in CL studies. In some instances, the carbon nanomaterial is also found to play multiple roles in a single CL reaction system. Hence, it is important to explore the stimuli of CD as well as its application in a CL reaction system. Carbon nitride quantum dots (CNQD) derived from sodium citrate and urea using a solvothermal method found to enhance the CL emission intensity of hydrogen peroxide (H_2O_2) and hydrosulfite (HSO_3^-) reaction system. It was confirmed that in the presence of the CNQD, there was an enhancement of the singlet oxygen ($^1O_2$), superoxide radical ($\cdot O_2^-$), and sulphite anionic radical ($\cdot SO_3^-$), which might be responsible for the increased chemiluminescence intensity of the CNQD-$NaHSO_3$-H_2O_2 reaction system. The study further indicated that the main emitters are SO_2*, $^1O_2$, $(O_2)_2$*, and the excited state CNQD. The CL spectra specified the formation of excited-state CNQD as a result of accepting energy from SO_2*, $^1O_2$, $(O_2)_2$* followed by the subsequent release of the CL. Additionally, it is assumed that the CNQD transferred electrons to the ·OH radical and O_2 that ultimately increased the number of holes in CNQD. This event stimulated the electron-hole annihilation process, which further resulted in enhanced chemiluminescence. Interestingly, the order in which reagents were mixed in the system was found to influence the CL intensity. The presence of ascorbic acid in the reaction system was found to have an inhibitory effect on the CL phenomenon. Therefore, the CNQD-$NaHSO_3$-H_2O_2 system was employed to determine ascorbic acid with an LoD of 8.0×10^{-8} mol L^{-1} (Chen *et al.*, 2018).

In a recent effort, $K_2Cr_2O_7$ was used as an oxidant that oxidized $NaHSO_3$ resulting in the generation of ultraweak chemiluminescence. The synthesized carbon dot (MFCD) acted as an energy acceptor from the excited sulfur dioxide (SO_2*), followed by returning to the ground state with enhanced CL intensity. In this case, ·OH and $\cdot O_2^-$ were the primary intermediate radicals involved in chemiluminescence. Additionally, these oxygen radicals might be responsible for the generation of electron-injected ($MFCD^{\cdot-}$) and hole-injected **(**$MFCD^{\cdot+}$**)** CDs that gave rise to MFCD* by radiative electron-hole annihilation, which further enhanced the CL intensity. Apart from that, it is often observed that the chemiluminescence spectrum of carbon dot is red-shifted compared to its fluorescence spectrum. The shifting to higher wavelength is presumed to be because of the smaller band gap energy of the surface state compared than the core state responsible for fluorescence. Moreover, in the presence of iodide, the chemiluminescence was amplified, and hence the system was used for probing iodide (Li and Han, 2020).

Amjadi *et al*. demonstrated that the chemiluminescence intensity of HCO_3^--H_2O_2 was enhanced to 70-fold in the presence of both silicon-doped CD (Si-CD) and CTAB with a response time of 10 s. This effect has been attributed to the synergistic interaction of Si-CD and the CTAB. The cationic surfactant most probably formed micellar structures on the surface of the carbon dot that attracted the oxygen radicals (·OH and $\cdot O_2^-$). Later, these radicals expedited the process of production of electron-injected and hole-injected CD resulting in enhanced chemiluminescence. The micellar structure also acted as a shield for the excited-state CD to decrease non-radiative deactivation. Based on this phenomenon, a simple and sensitive method was developed for the determination of dopamine, adrenaline, and noradrenaline in biological samples (Amjadi *et al*., 2018).

The presence of nitrogen in CDs have a remarkable effect on the CL signal. Hallaj *et al*. tested different types of luminescent CDs among which carbon nitride quantum dots (CNQDs) were found to dramatically boost the chemiluminescence intensity of the reaction system by a factor of about 75. The nitrogen-containing functional groups on the CNQD stimulated the decomposition of H_2O_2 into oxygen radicals and also caused chelation of Cu^{2+} ions that resulted in generation of redox-active species for reducing H_2O_2 with higher degree. The chemiluminescent system was found to have a linear relationship with increasing concentrations of H_2O_2 and therefore

was employed for the determination of both H_2O_2 (LoD: 10 nM) and glucose (LoD: 100 nM) (Hallaj *et al*., 2017). Transition metal ions such as Fe^{2+} and Cu^{2+} have also been studied to a great extent for enhancing CD-based chemiluminescence. These metal ions can decompose H_2O_2 to hydroxyl radical (·OH) via the Fenton mechanism. Next, the ·OH cause the generation of electrons and holes in the valence and conduction band of CD resulting in the enhancement of chemiluminescent signal. Based on this phenomenon, Shah *et al*. developed a method for the determination of Fe^{2+} using a N-doped CD synthesized from histidine and H_2O_2 as a coreactant (Shah *et al*., 2019).

To further increase the versatility, Duan *et al*. fabricated copper-doped CDs (Cu-CDs) using citric acid via solid-phase synthesis strategy that exhibited excellent peroxidase-like activity. The incorporation of Cu^{2+} to the CDs as a dopant enhanced the electronic properties and surface reactivity. The developed Cu-CD was employed as a chemiluminescent probe for the detection of glucose that displayed a detection limit of 0.32 μM (Duan *et al*., 2019). There are several reports of CDs as a smart material in CL system (Table 1.4).

Table 1.5. CD-based chemiluminescence detection.

Precursor & Synthesis route	Size (QY)	Target of detection	References
Glucose **Ultrasonic**	4 nm (NA)	Gallic acid	(Chen *et al*., 2018)
Ethylene glycol **Solvothermal**	5±1 nm (NA)	Methoxyestradiol	(Zhang *et al*., 2018)
L-cysteine and citric acid **Pyrolysis**	3.1 nm (NA)	Carcinoembryonic antigen	(Cao *et al*., 2019)
Citric acid and 1-3-(3,4-Dihyroxyphenyl) alanine (L-DOPA) **Solid phase thermal**	4.5 nm (NA)	Uric acid	(Shi *et al*., 2019)
Phloroglucinol **Solvothermal**	5.4 nm (NA)	Ascorbic acid	(Zhu *et al*., 2020)
Citric acid, L-cysteine, and heteroatoms **Hydrothermal**	10 nm (80 %)	Oxytetracycline	(Amjadi *et al*., 2020)

1.2.4.3 Electrochemiluminescence

Electrochemiluminescence (ECL), a combination of electrochemistry and luminescence, is the emission of light by an excited-state species originating from high-energy electron transfer reactions at electrodes. Generally, the ECL phenomenon occurs by two pathways: the annihilation pathway and the coreactant pathway (Bachu and Goswami, 2020). In the annihilation pathway, following the applied potential, oxidized and reduced species are formed at the electrode's surface, which subsequently generates the emissive excited state. The coreactant pathway, in contrast, contains an electroactive luminophore as well as a coreactant that is responsible for ECL emission. Compared to the annihilation pathway, the coreactant pathway has more advantages with stronger ECL emission and is suitable for both aqueous and nonaqueous electrolytes. As a new class of the carbon nanomaterial, the CDs due to its high QY, high sensitivity, and low background signal have shown promising applications as an ECL luminophore and a coreactant for the detection of numerous analytes.

Solid ECL platform for the detection of Cu^{2+} ion using phosphorus-doped carbon quantum dots (P-CQDs) with H_2O_2 as a coreactant has been reported. The corresponding QY and the ECL intensity of the P-CQD were 2-fold and 4-fold, higher than the undoped CQD. The increased ECL intensity is because of the phosphorus doping that created emissive traps, and high electron transfer reaction between the electrogenerated P-CQD intermediate ($P\text{-}CQD^{\cdot-}$) and the reduced H_2O_2. The OH radical injects hole into the HOMO level of $P\text{-}CQD^{\cdot-}$ giving rise to the excited P-CQD (P-CQD*) that emits light. Accordingly, the method was employed to detect Cu^{2+}, a Fenton reagent, that results in the generation of more OH radicals from H_2O_2, resulting in enhanced ECL intensity. The developed P-CQD could detect as low as 0.27 nM Cu^{2+} (Venkateswara Raju *et al*., 2020). A sandwich-type novel ECL immunosensor was also fabricated to determine carcinoembryonic antigen (CEA) by using perylenetetracarboxylic acid (PTCA) and CQDs as dual luminophore, graphene as nanocarrier and $S_2O_8^{2-}$ as a coreactant, which exhibited good performance for the detection of CEA in human serum samples. The secondary antibody used to capture the CEA was immobilized on the ECL nanomaterial. Because of the synergistic effect of the luminophores, the sensor displayed a remarkable increase in the ECL intensity. The coreactant reacted with the reduced species of PTCA ($PTCA^{\cdot-}$) and CQDs ($CQDs^{\cdot-}$) to

form the corresponding excited species, which emitted light. The proposed method could detect CEA as low as 0.00026 fg mL^{-1} (Xu *et al*., 2018).

Based on the fact that Hg^{2+} can form T-Hg^{2+}-T complex with two DNA thymine (T) bases, a novel ECL sensor was developed to detect Hg^{2+} by using GQDs-DNA-AuNP as the ECL nanoprobe and poly(5-formylindole)/reduced graphene oxide (P5FIn/erGO) as nanocomposite. A thymine rich ssDNA immobilized on the P5FIn/erGO modified electrode formed the T-Hg^{2+}-T complex in the presence of both Hg^{2+} and the ECL nanoprobe. With increasing Hg^{2+} concentration, the ECL intensity of GQD also increased, and by using this relation, the ECL sensor developed that could detect as low as 2.48 pM Hg^{2+} with good stability, selectivity, and reproducibility. The combination of AuNP, GQD, and P5FIn/erGO in the sensor accelerated the electron transfer rate, an increased loading capacity of ssDNA, and high ECL intensity, ultimately resulting in a lower detection limit (Tang *et al*., 2019).

While carbon nitride quantum dots (GCN QDs) have several advantages, the low ECL efficiency is often a drawback in the analytical applications. To improve the efficiency in ECL assays, a novel luminophore was developed by doping GCN QDs with sulphur (S-GCN QD) that generated element vacancy and also modified the surface state. By using the surface plasmon coupling ECL (SPC-ECL) mode, wherein the ECL intensity can be amplified by surface plasmon coupling effect of AuNP, the S-GCN QDs were used to develop a sandwiched ECL sensor to detect K-RAS gene which is a crucial cancer biomarker (Zhang *et al*., 2019). In a similar study, a novel nitrogen doped hydrazide conjugated CDs was developed that had high quantum efficiency with emission at low excitation potential. The proposed CD was employed to distinguish cancer cells from the normal cells on the basis of more hydrogen peroxide secretion from the former (Chen *et al*., 2020). In Table 1.6, the various other reports of CDs acting as a smart material in ECL systems is shown.

Table 1.6. CD-based electrochemiluminescence detection.

Precursor and Synthesis route	Size (QY)	Application	References
Fullerene (C_{60}) **Hydrothermal**	3.5±1 nm (NA)	Determination of microRNA-21	(Zhang *et al*., 2018)
Citric acid and L-cysteine **Pyrolysis**	NA	Detection of atrazine	(Wu *et al*., 2019)
Melamine **Hydrothermal**	2 nm (NA)	Detection of butein	(Kalaiyarasan *et al*., 2020)

1.2.5 CDs as Smart Materials

The rapid progress in materials science over the past few decades has led to the development of smart materials with attractive physicochemical properties bearing great application potential to design next-generation sensing platforms (Song *et al*., 2011). The smart materials usually include different materials such as metals, nanomaterials, polymers, biomolecules, and even hybrid materials (Cobo *et al*., 2015; Ledin *et al*., 2016). Recently, the carbonaceous materials received increasing attention because of their biocompatibility and non-toxic behaviours. Various carbon-based materials like graphene/graphite and their different derivatives (Angione *et al*., 2011; Jang *et al*., 2020; Scidà *et al*., 2018; Yu *et al*., 2017), carbon nitride (CN) films (Wang *et al*., 2019), carbon fiber tube (Li *et al*., 2018), paper-based bionanocomposites (Naghdi *et al*., 2020) have been studied for diverse applications. Carbon dot or carbon quantum dot is a new addition to this domain of smart materials. These materials are reactive to numerous external stimuli, as discussed below.

1.2.5.1 pH Sensitive

The detection of pH level is crucial in pathological and physiological processes as well as in the natural environment. Recently, CDs have been explored for their applications as a pH probe due to its intense fluorescence property, excellent photostability, and convertible emission colours. Using a one-pot hydrothermal method, AC-CDs were synthesized from 5-amino-1,10-phenanthroline (Aphen) and citric acid (CA). The resulting CDs exhibited an interesting pH-dependent fluorescent tricolour

emission. It is found that Aphen is very sensitive to pH, which may be attributed to the response of the pyridyl group in the presence of H^+ and OH^- medium. The pH-responsive AC-CDs displayed bright green colour at pH 1.0, grayish at pH 1.0 to 8.0 that turned blue to purple from pH 8.0-13.0, and finally to yellow at pH 14.0 (Zhang *et al*., 2019). Heteroatom doped CDs (N, S-CDs) synthesized from o-phenylenediamine, L-cysteine, and ethanol also showed excellent pH-response and reversible fluorescence upon pH change. While the fluorescent intensity of N, S-CDs decreased from pH 1.0-13.0 in the basic condition (NaOH), the fluorescence intensity could be reverted from pH 13.0-1.0 using acidic medium (HCl) (Zhang *et al*., 2019). Yang *et al*. developed different sizes of CDs following a simple green methodology of microwave-assisted pyrolysis using xylose, m-phenylenediamine, and H_3PO_4 as precursors. In this work, green-emitting CDs were selected, followed by adjusting the CD solution's pH from 3.0-11.0 using PBS buffer. No change was observed in the CD's excitation/emission at 442 nm/518 nm upon increasing the pH from 3.0-7.0; however, at pH 8.0, the excitation/emission shifted to 375 nm/500 nm suggesting the pH-dependent PL property of the CD as indicated by green to blue shift performance. The author proposed that the shifting was dominated by the O-related defect state and P-related defect state, respectively (Yang *et al*., 2019). Another interesting study found that when the anticancer drug doxorubicin hydrochloride (Dox) was loaded with the CDs synthesized from citric acid and urea following the microwave-assisted method, the CDs generated white light from pH 12.0-2.0 with reversible photo-switching. The role of FRET was likely to be responsible in the white light generation (Pyne *et al*., 2019). The pH also affects the emission intensity of the CD. The blue emission of the CD was enhanced as the pH of the solution was moved from 7.0-14.0. In contrast, the CD's fluorescence gradually reduced and shifted to longer wavelengths from pH 7.0-1.0. Thus, the as-prepared N-CDs from citric acid and o-phenylenediamine showed promising pH sensing ability (Lu *et al*., 2019).

1.2.5.2 Temperature Sensitive

There are some reports of temperature-responsive CDs in recent times (Lu and Zhou, 2019). With increasing temperature, the fluorescence intensity of the CDs decreased, and vice-versa. The temperature-sensitive property of the synthesized CD was attributed to the dominance of the non-radiative and radiative transitions of the

MnOx-CDs at higher and lower temperatures resulting in decreased or increased emission of photons respectively (Li *et al*., 2020). This feature of the CDs was employed as a thermometer in the HepG2 cancer cell line. The phenomenon was ascribed to thermally activated electronic transitions. Powdered CDs embedded in the trisodium citrate matrix exhibited tunable colour emission from green to yellow. The powdered CD was applied to fabricate white light-emitting devices on blue chips with tunable colour temperature (Shen *et al*., 2018). In another development, the CDs possessing dual-emissive aggregation-induced room-temperature phosphorescence (RTP) behaviour were designed. The CDs were synthesized using trimellitic acid (TA) via a one-pot hydrothermal treatment that emitted white light and yellow light RTP in the solid-state under an on and off UV excitation at 365 nm. While the white light emission was associated with the dual-emissive nature (blue and yellow fluorescence) of the CD, the yellow RTP emission was due to the excited triplet state upon the aggregation of the CD as shown in Figure 1.4 a. The primary goal of the research was to apply the CD in advanced anti-counterfeiting and encryption methodologies (Jiang *et al*., 2020).

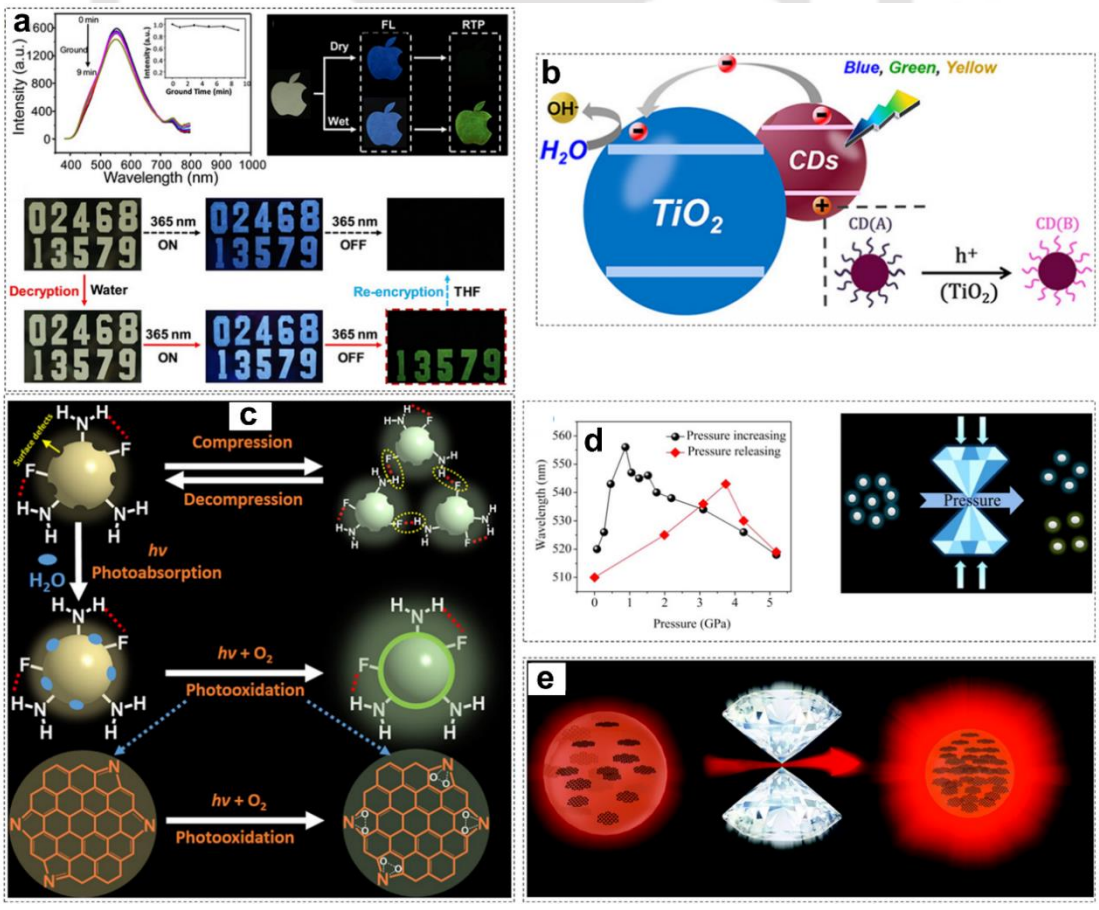

Figure 1.4. (a) Phosphorescent spectra of TA-CDs powder against time, illustration of the CDs with water-stimuli-responsive production, and the encryption and decryption process. (b) The photoenergy transformation in the IA-CDs/TiO_2 nanocomposite system. (c) Proposed mechanism of the pressure triggered fluorescence. (d) PL peaks when pressure is released or increased (left) and proposed mechanism of piezochromic behaviour of N-CDs (right). (e) Illustration of PL enhancement under high pressure (Das *et al*., 2021b).

1.2.5.3 Light Sensitive

Light as a stimulus for CDs to initiate or change various photometric responses is a well-known phenomenon. In a recent report, a bidirectional photochromism via anchoring of CDs to TiO_2 porous films was invented. Under blue light irradiation, the color of the CDs/TiO_2 film obtained by dropping anchoring becomes darker and that obtained by immersion anchoring becomes lighter. The spectral response was intensely dependent on the wavelength and polarization of the exciting light for the photobleaching material system. The findings provide a new dimension for optical information encryption and memory. The mechanism of such behaviour has been attributed to the generation of electron-hole pairs from CDs under visible light excitation, followed by the hole's reaction, which triggered the oxidation reaction with the surface functional group on the CD causing photobleaching as shown in Figure 1.4 b (Wu *et al*., 2020). In another report, the CDs/TiO_2 nanocomposite showed photocatalytic colour switching ability. Upon UV-irradiation, the blue colouration of the methylene blue dyes with the CDs/TiO_2 nanocomposite could be photobleached within one minute to colourless state. With visible light irradiation, the original blue colour was fully recovered within 20 mins (Wang *et al*., 2019).

1.2.5.4 Pressure Sensitive

CDs exhibit piezochromic property wherein an application of 0-22.84 GPa pressure resulted in the change of luminescence colour from yellow to the blue. The pressure-induced change in optical property has been ascribed to the hybridization transition of sp^2 to sp^3 in CD. Additionally, such a phenomenon has also paved the way for a better understanding of the optical properties (Lu *et al*., 2017). Taking advantage of the piezochromic effect, novel N-doped CDs was synthesised that displayed partial

reversible piezochromic luminescence. Upon an application of 0.007-5.18 GPa pressure, the red- and blue-shifted photoluminescence (PL) of the synthesized N-CDs could be observed with blue to the green color of PL, whereas when the pressure was released from 5.18 GPa to 1 atm, the red- and the blue-shifted photoluminescence could be tested as shown in Figure 1.4 d (Zhan *et al*., 2018). Geng *et al*. recognized that in the carbon polymer dots with increasing pressure, the red-shift was because of the increased pi-pi stacking of the pi-conjugated system and the blue-shift resulted due to the hydrogen bonding (Geng *et al*., 2019). In a recent study, a F, N-doped CDs demonstrated a remarkable photoactivated fluorescence enhancement in the presence of continuous UV light and both ambient (1.0 atm) and high pressure (0.1 GPa) as shown in Figure 1.4 c. Besides, the CDs also showed reversible piezochromic behaviour from 1.0 atm to 9.98 GPa pressure with aggregation-induced enhancement (AIE) in the 1.0 atm-0.65 GPa. The AIE behaviour was because of the increased formation of van der Waals forces and hydrogen bonding among the surface -NH_2 and -C-F groups on F, N-doped CDs (Jiang *et al*., 2020). In this direction, the influence of the solvent on the piezochromic behaviour of CD was also identified as with increasing pressure, the CDs displayed red-and blue-shift piezochromism with DMF and water as the pressure transmitting medium. The reason is attributed to the π-π stacking, and protic-solvent-induced surface chemical structure changes for the red-and blue-shift effect, respectively (Jing *et al*., 2018). The stability and enhancement of CD's red fluorescence could be achieved under the influence of external pressure, which may be because of the pressure-triggered aggregation-induced emission. The intensity of the fluorescence decreased when a pressure of above 1.2 GPa was applied, and this phenomenon could be due to the destruction of the molecular structure of R-CDs, as shown in Figure 1.4 e (Wang *et al*., 2019).

1.2.5.5 Multi-Sensitive

A multi-responsive and hybrid white-light-emitting hydrogel network was developed recently by incorporating Eu^{3+}, Tb^{3+}, and CD into polyacrylamide/poly (acrylic acid) hydrogel network. In the network, luminescent lanthanide ions were incorporated with coordination bonding, whereas CDs interacted with radical copolymerization. The white luminescence was achieved by modifying the ratio of blue- light-emitting CD to green- and red-light emitting lanthanide ions. The

photoluminescence study revealed that the mechanism involves energy-transfer from Tb^{3+} to Eu^{3+} and CDs, as shown in Figure 1.5 a-b. The reaction between lanthanide and CDs resulted in the responsiveness of white-light-emitting hydrogel to various stimuli such as pH, vapours, metal ions, and temperature. Additionally, the hybrid network showed thermochromism of green-to-red emission ratios in the 20-70 °C temperature range and a fracture strain stretchability of 400 % (Zhu *et al*., 2018). Recently, a white-light-emitting hydrogel developed by mixing lanthanide (Eu^{3+}), cytidine, fluorescein isothiocyanate, and CDs was found sensitive to pH, Fe^{3+} and temperature (Xue *et al*., 2020). Further, a smart dual-mode sensitive nano-probe based on CDs-Tb-TMPDPA was developed in which Tb^{3+} and CDs were sensitive to temperature and photothermal, respectively, and 4-(2,4,6-trimethoxyphenyl)-pyridine-2,6-dicarboxylic acid (TMPDPA) acted as a two-photon ligand. The developed nano-probe can be ideal for achieving real-time temperature and optical heating simultaneously (Yan *et al*., 2020). Wang and co-workers prepared CDs by polymerizing reaction of citric acid, hyaluronic acid polymers, and ethylenediamine that were smartly utilized as gatekeepers to prevent premature drug release, for targeted drug delivery to tumour cells, IR thermal imaging, and thermo-chemotherapy (Wang *et al*., 2019). The possibility of employing CDs as reversible two switch-mode luminescence ink for advanced anti-counterfeiting and dual encryption was explored. For which CDs were synthesized from melamine and dithiosalicylic acid using a solvothermal method that exhibited blue fluorescence. When mixed with water, the hydrophobic CDs resulted in aggregation leading to red fluorescence as shown in Figure 1.5 ci-ciii. This phenomenon was attributed to the constraints in the intramolecular rotation of disulfide bonds and the interaction of π-π stacking in aggregated structures (Yang *et al*., 2019).

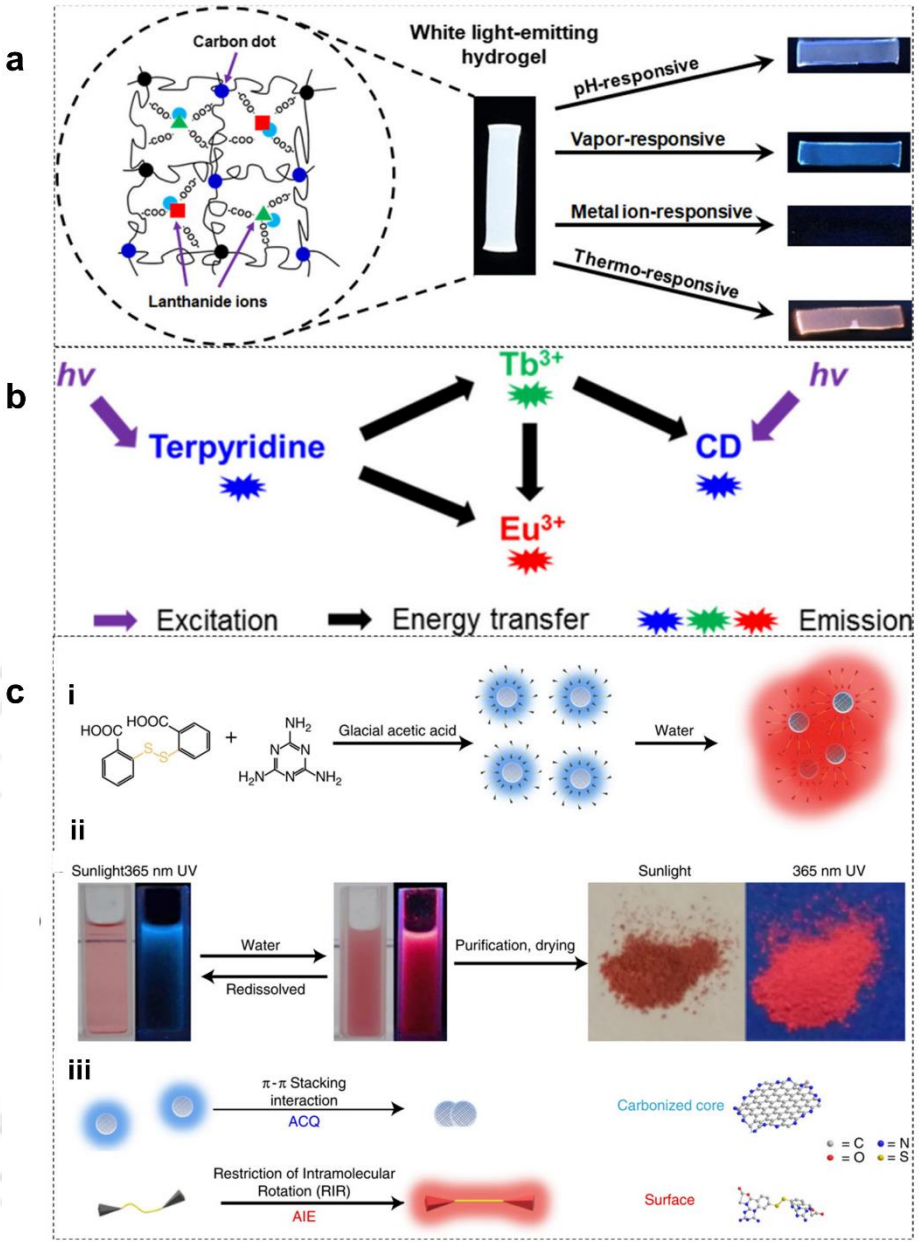

Figure 1.5. (a) Multi-stimuli responsive behaviour of the CDs, (b) Proposed energy-transfer mechanism in white-light-emitting hydrogel. (c-i) Formation of H-CD monomers and their aggregates (the disulphide bond in dithiosalicylic acid molecular is highlighted with yellow). (c-ii**)** Photographs of the H-CD's two-switch-mode luminescence principle. (c-iii) Fluorescence principle and proposed structure of H-CD's core and surface (Das *et al*., 2021b).

1.2.5.6 Phase Sensitive

Photoluminescence-functionalized phase change materials (PCMs) have also attracted attention because of their potential application as smart materials. The PCMs with the property of capturing excess energy and releasing it via phase transition is primarily used in thermal energy management. In a work, a novel MOF-based photoluminescence-functionalized PCMs was developed by incorporating stearic acid (SA) and CQDs that served as a fluorescent guest and thermal energy guest, respectively, into the Cr-MIL-101-NH_2 framework. The nanocomposite possessed remarkable thermal stability, durability, and shape-stabilized ability and prevented conventional aggregation-induced quenching (Chen *et al*., 2019). Smart CDs were also designed wherein CO_2 and N_2 bubbling led to both reversible phase transfer between the organic and aqueous phase of the CDs and simultaneously resulted in reversible luminescence change from blue to cyan-green as shown in Figure 1.6. This phenomenon has been ascribed to the modification of surface chemistry and different emission states that is activated by the CO_2/N_2 bubbling (Xiong *et al*., 2019).

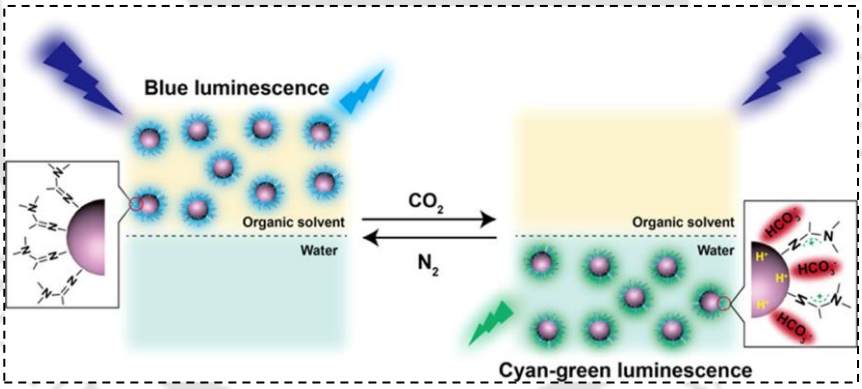

Figure 1.6. The reversible phase transfer of the amidine-modified CDs and the reversible luminescence change between blue and cyan-green luminescence change in the presence of CO_2 and N_2 (Das *et al*., 2021b).

1.2.5.7 Solvent Sensitive

The optical response of CD's is also dependent on the solvent polarity. Li *et al*. developed green- and blue-emitting carbon quantum dots (CQDs) from oxalic acid, citric acid, and urea as precursors. The CQDs exhibited solvent selectivity with the green CQDs soluble in the ethanol, and the blue-CQDs soluble in water. Such an

interesting phenomenon could be because of the structural difference between the two CQDs. The work also demonstrated the reversibility of colour by changing the hydrogen bonding, which is more straightforward than the pressure application for colour reversibility (Li *et al*., 2019). Different hydrochromic CDs were also fabricated from brown sugar following a simple carbonization method that displayed variation in light emission in the presence of water. The synthesized CDs displayed a "structure-hydrochromic property" relationship wherein the CDs with the superior pi character had hydrochromism. The CDs exhibited red shift in the presence of water in aprotic solvents, whereas, in protic solvents, the emission intensity was increased. Therefore, this property of the CD was employed to probe water contamination in different solvents (Senthamizhan *et al*., 2019). Different solvents have different emission wavelengths. Solvent properties such as dehydrating ability, solubility, boiling point, polarity, and (non-) proton influence the particle size and surface state of the synthesized CD (Zhao *et al*., 2019).

1.2.5.8 Sensitivity due to Molecular Interaction

The interaction of CDs with biomolecules such as proteins, enzymes, DNA, etc., has received increased interest in the recent past few years, primarily in the field of drug delivery and biosensing. Notably, the interactions involving proteins and CDs have been most widely studied (Huang *et al*., 2016; Liang *et al*., 2020; Song *et al*., 2020; Xu *et al*., 2016). In general, according to previous reports, the CD quenches the intrinsic fluorescence of the proteins/enzymes (Figure 1.7 a). However, these studies have shown that it is often not the same type of quenching mechanism in all the CDs. Instead, the mechanism is dependent on the type of interaction between the CD and protein/enzyme. While quenching associated with CD-protein complex formation is linked to the static quenching mechanism, the dynamic quenching originates from the collision and energy transfer from protein to the CDs. Nevertheless, these interaction studies have been mostly limited to the human serum albumin protein (HSA) to understand the pharmacokinetic behaviour of the CDs and the associated molecular toxicity. Therefore, an in-depth interaction study with other proteins or enzymes will widen its application potential. Meanwhile, the CD-DNA interactions are mostly investigated in the biosensing field, gene transmission, and delivery (Guo *et al*., 2018; Huang *et al*., 2018; F. Li *et al*., 2019; Loo *et al*., 2016; Qaddare and Salimi, 2017; H.-J. Wang *et al*., 2017;

S. Wang *et al*., 2017), wherein the CDs are utilized for covalently conjugating the nucleic acid molecule (Figure 1.7 b). By using this strategy, CDs have been employed either as a fluorescent signal molecule, quencher or both.

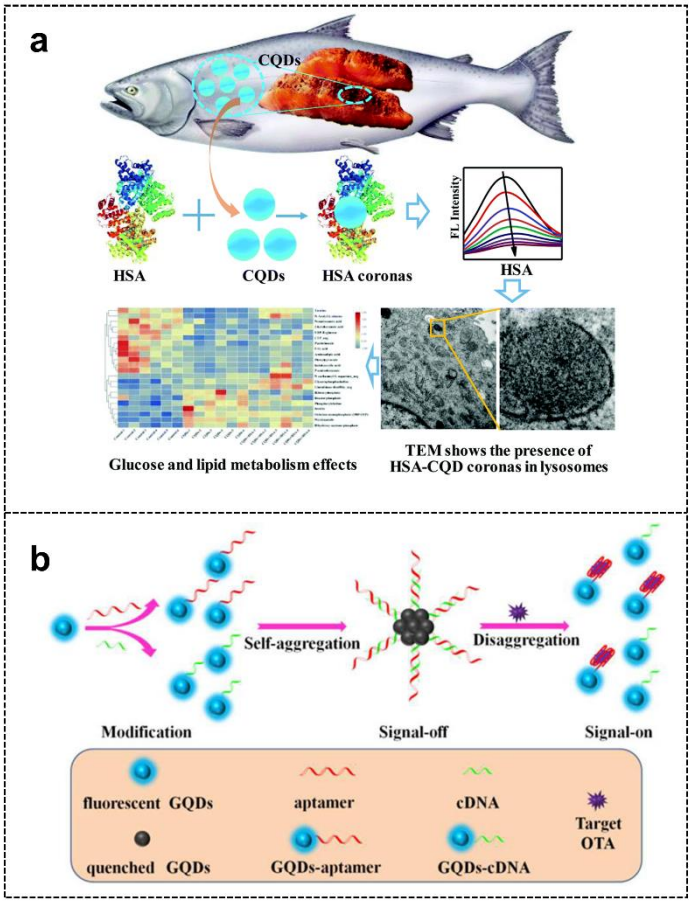

Figure 1.7. (a) Quenching of HSA fluorescence upon interaction with CQD. Reprinted with permission from ref. (Song *et al*., 2020), (b) Sensing mechanism of target DNA using GQD. Reprinted with permission from ref. (Wang *et al*., 2017).

1.3 Significant Gaps in the Research

In spite of the profound research on the utility of CDs as smart material in analytical applications, there are several critical issues that still need to be examined.

- The CDs reported to date have been notably utilized as a peroxidase mimic in diversified research works; however, its mechanism of peroxidase-like activity is still obscure. There is a general agreement that the oxygen-based functional groups on the surface of the CD play a vital role during the peroxidase-like

activity. Nevertheless, the confusion regarding the involvement of the specific oxygen functional group in the catalytic activity still persists.

- The emphasis on the existence of any linkage between the CD's peroxidase-like activity and its photophysical property has not been focussed.

- The literature has well documented the examination of CD's photoluminescence for the detection of bioanalytes in numerous applications. However, its interaction with biomolecules particularly proteins and the consequent photophysical behaviours for bioanalytical applications has not been adequately explored.

- In most of the studies related to the CD's peroxidase-like activity so far, the investigation has been limited to only the determination of kinetic parameters of the peroxidase mimic and the subsequent monitoring of colour development with increasing peroxide concentration. The evolution of CD's geometry during its interaction with the peroxide has not been focussed, which is of key relevance to anticipate the modification of CD's material property during the catalytic activity.

1.4 Objectives of the Study

Considering the above-mentioned gaps in the CDs research, the specific objectives identified for the present study are:

(i) Selection of model compounds to investigate the role of functional groups in the peroxidase-like activity.

(ii) Synthesize and characterization of CDs.

(iii) Insight into the mechanism of the peroxidase-like activity of the synthesized CD.

(iv) Evaluation of CD's potentiality as a fluorescent signal probe in blood serum samples.

(v) To study the modification of the CD's material property upon the interaction with H_2O_2.

1.5 Significance of the Study

The present investigation sheds light on the potentiality of CDs as a promising optical probe in clinical applications, especially peroxide-based detections. To date, there has been a substantial report of CDs acting as peroxidase mimic; however, the studies lack the in-depth and systematic inquiry at the molecular level. In our study, first, we set out to unveil the role of different functional groups on the surface of CD in the peroxidase-like activity. The efficiency of the carboxylic group was found to be maximum in strongly binding to H_2O_2 in the presence of a reducing equivalent. We explored for any linkage between the peroxidase-like activity and the photophysical property of the CD. Secondly, the fluorescence studies suggested the interference from blood serum as a significant challenge in clinical applications employing blue-emitting CDs. Filtering out the serum proteins during the detection will ameliorate the potentiality of the CD in clinical applications. Thirdly, the reaction with H_2O_2 demonstrated the evolution of CD's material property. These findings may decipher to bridge the gap between understanding the biocatalytic phenomenon and the clinical potentiality of the zero-dimensional nanomaterial.

Based on the above, the current work is categorized into four chapters. A section entitled “Conclusion and future outlook” has been included at the end of the chapters.

Chapter 1: Introduction and Literature Review

This chapter highlights the importance of nanomaterials as enzyme mimics, with particular emphasis on CDs. A detailed discussion on the characteristics of CDs, their various routes of synthesis, functionalization, and surface passivation have been included. The physical and chemical properties of CDs like absorption, photoluminescence, electron transfer, cytotoxicity, and photostability are considerably focussed. An effort has also been made to cover the recent development of CD as smart materials that are responsive to external stimuli such as pH, temperature, light, pressure, solvent, phase, and molecular interactions, and the importance of CDs in optical-based analytical applications. Additionally, the chapter discusses the potential gaps in the research, the objectives, and the significance of the present investigation.

Chapter 2: Synthesis of Carbon Dots from L-glutamic acid, their Characterization, and Mechanism of Peroxidase-like Activity

This chapter focuses on the mechanism of the peroxidase-like activity of CDs. A molecular screening protocol was performed on different simple-carbon-containing molecules to determine the role of functional groups in binding to H_2O_2 and its subsequent influence on the peroxidase activity. The synthesis and characterization of CDs were carried out by UV-Vis, fluorescence, FETEM, FTIR, XPS, and NMR. In addition, we unveiled the electron transfer route between CD, H_2O_2, and ABTS during the peroxidase-like activity.

Chapter 3: Multifaceted Interaction Studies between Carbon Dots and Proteins of Clinical Importance for Optical Sensing Signals

This chapter features the prospects of CD as a fluorescent probe for peroxide detection in enzyme-based reaction systems of clinical applications. The investigation was carried out using fluorescence spectroscopy, molecular docking studies, circular dichroism, zeta potential, and FETEM. The performance of the CD was further extended to human blood serum to ascertain for any interference during the detection.

Chapter 4: Analytical Application of H_2O_2-Induced Chiroptical Graphitic Carbon Dots

This chapter discusses the synthesis and characterization of chiroptical CDs synthesized from D-(+)-Glucose. The peroxidase-like activity of the synthesized CD was also exploited. Special emphasis was given to the evolution of the CD's material property during its interaction with H_2O_2

Chapter 2

Synthesis of Carbon Dots from L-glutamic acid, their Characterization, and Mechanism of Peroxidase-like Activity

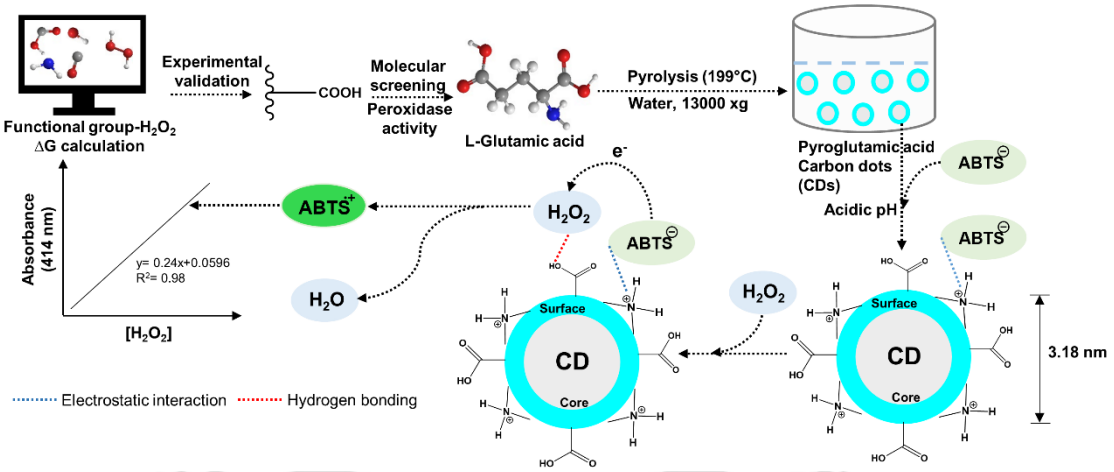

2.1 Overview

Since the discovery of carbon dots (CDs) in 2004, the research on this 0-D carbon nanomaterial has been taken up to address the critical issues related to their preparations, properties, and applications (Xu *et al*., 2004). The primary motivation for this research is the potential advantages of the CDs over the conventional quantum dots such as their biocompatibility, low toxicity, tuneable luminescent properties, high water solubility, and inexpensive synthesis process (Zhang *et al*., 2017). The studies have also demonstrated that many CDs exhibit nanozyme properties (Das and Goswami, 2020). Nanozymes are nanomaterials with intrinsic enzyme-like activity (Gao *et al*., 2007; Liang and Yan, 2019). The interest in nanozymes has been stimulated by their several advantages over the natural protein-based enzymes, such as resistance to proteolysis, high stability, and simple and less expensive production and purification steps (Wei and Wang, 2008).

The research on nanomaterials as peroxidase-mimic is growing impressively (Wang *et al*., 2011). It is worth mentioning that among the various redox enzymes, the peroxidases find significant interest in industrial, environmental, and analytical applications (Lopes *et al*., 2014). The ability of peroxidases to yield chromogenic products at low substrate concentrations makes them well-suited enzymes for various analytical applications. Ever since the discovery of Fe_3O_4 nanoparticles with peroxidase-like activity (Gao *et al*., 2007), considerable effort has been made to find nanomaterials that could replace peroxidase enzymes, such as the widely used horseradish peroxidase (HRP). The HRP catalyses the oxidation of various organic substrates by hydrogen peroxide, which has high importance as a synthetic reagent, biological oxidant, and intermediate in the formation and decay of reactive oxygen species (Winterbourn, 2018).

A significant amount of work on the CDs acting as peroxidase mimics is known. Most of these studies are related to their synthesis (Zhang *et al*., 2017; Zhu *et al*., 2014), and different applications such as detection of glucose (Shi *et al*., 2011), cholesterol (Zhao *et al*., 2019), bioimaging (Wu *et al*., 2013), and immunosorbent assay (Zhu *et al*., 2014). Besides, CDs are also doped or composed of different materials to enhance their peroxidase-like properties (Dong *et al*., 2015; Yang *et al*., 2017). However, a systematic

investigation to understand the detailed mechanism of CD-led peroxidase-like activity is limited. There are some efforts highlighting the mechanism for graphene oxide nanomaterials (Song *et al*., 2010), metal-doped carbon QDs (Dong *et al., 2015;* Zhao *et al*., 2019; Zheng *et al*., 2016), oxygenated carbon nanotubes (Huan Wang *et al*., 2018), and carbon nanodots prepared from candle soots (Shi *et al*., 2011). The identification of the catalytically active and substrate-binding sites on graphene QDs following selective deactivation of the functional groups have also been reported (Sun *et al*., 2015). A broad consensus of oxygen-based functional groups responsible for the CD's peroxidase-like activity is visible from these reports. In contrast, a certain amount of variations among them on the involvement of specific oxygen-containing functional groups for this reaction still exists. Importantly, while the role of these oxygen-containing functional groups for peroxidase-like activity has been recognized, the CD's specific roles and its linked photophysical properties for accelerating these reactions are largely unknown.

Herein, we explored a systematic investigation on the mechanism of peroxidase-like activity of CDs. To this end, we selected simple carbon-containing molecules, each having a distinct functional group, as a model and studied their H_2O_2 binding affinity and peroxidatic activity. Based on these results, we performed additional molecular screening, identified compounds with peroxidase-like activity, and then transformed these into CDs following a simple pyrolysis method. Finally, we identified a CD with high peroxidase-like activity synthesized from L-glutamic acid. Following different spectroscopic and microscopic techniques, we proposed a reaction mechanism on the CD led peroxidase-like reaction and unveiled its relation with the fluorescence-based photophysical phenomena of this organic quantum dot. This study also sheds light on this synthesized CD's application potential for the peroxidase reaction on a paper platform, as detailed in the discussions and conclusion sections.

2.2 Experimental Section

2.2.1 Materials

L-glutamic acid, succinic acid, glycine, D-glucose, glacial acetic acid, ethanol (99.8 %), potassium bromide (KBr), 3,3′,5,5′ -tetramethylbenzidine (TMB) were obtained from HiMedia, India. L-glutamine and acetone were purchased from Sisco Research Laboratories (SRL) Pvt. Ltd., India. 2,2′-azino-bis (3-ethylbenzothiazoline-6-sulfonic acid) (ABTS), 5,5-dimethyl-1-pyrroline N-oxide (DMPO), deuterium oxide or heavy water (D_2O), and aniline were bought from Sigma Aldrich, USA. Citric acid (monohydrate) was purchased from RANKEM, India. Hydrogen peroxide (H_2O_2) solution 50 % w/v was procured from FINAR, India. All other chemicals used in the experiment were of analytical grade. The experiments were performed at room temperature unless mentioned otherwise using ultrapure water (resistivity>18 MΩ.cm). All the reagents and solvents were used as received without further purification.

2.2.2 Microscopy

The size and morphology of the CDs were characterized using a Field Emission Transmission Electron Microscope (FETEM) (JEOL JEM- 2100F) at an accelerating voltage of 200 kV. The samples were diluted to 100-fold in deionized water, followed by drop-casting on a carbon-coated copper grid. The grid was later dried in a vacuum desiccator and then observed under the microscope.

2.2.3 Spectroscopy

The absorption spectra were recorded using a double beam Cary 60 UV–Visible spectrophotometer (Agilent Technologies). Fluorescence measurements were performed on FluoroMax-4 (HORIBA Scientific). All the spectroscopic studies were performed in one mL sample volume in a 1 cm (path length) cuvette. The Stern-Volmer quenching constant was calculated using the following equation (Jain *et al*., 2017), where F_o is the fluorescence intensity in the absence of the quencher, F is the fluorescence intensity in the presence of the quencher, [Q] is the concentration of the quencher and K_D is the Stern-Volmer quenching constant:

$$\frac{F_o}{F} = 1 + K_D[Q] \qquad (2.1)$$

Fourier transformed infrared (FTIR) spectroscopy was carried out on IRAffinity-1S (Shimadzu) using spectroscopic grade KBr pressed disc. Both ^{13}C- and ^{1}H-NMR spectra were collected using a 400 MHz NMR spectrometer (Bruker, ASCEND 400). The experiment was performed using a probe temperature of 300.7 K. The NMR sample was prepared by adding 60 µL of stock CD solution (final 10 mg mL^{-1}), 30 µL of 100 mM H_2O_2 (final 5 mM), 120 µL of 5 mM ABTS (final 1 mM), 60 µL of 100 % D_2O and required amount of ultra-pure water. The solution was then transferred to an NMR tube and measured. Each ^{13}C and ^{1}H NMR was recorded with 100 scans and 32 scans, respectively. For the ^{1}H NMR spectra, we used the zgpr pulse program followed by locking the sample with the D_2O solvent signal. All the spectra were later processed and calibrated using MestreNova software. Electron spin resonance (ESR) measurements were recorded at room temperature on the JEOL (Model: JES-FA200) instrument with conditions: modulation frequency: 100 kHz, power: one mW, amplitude: 50 G. The reaction mixture was put into a capillary glass tube that was transferred to the ESR cavity, followed by a recording of the spectra. The zeta potential measurements were carried out using the Nano Instrument system (Malvern Instruments Limited, UK) in a capillary cell with gold plated beryllium/ copper electrode. The X-ray photoelectron spectroscopy (XPS) study was carried out using PHI 5000 Versa Probe II model.

2.2.4 Synthesis of CDs

The CDs were synthesized by the one-step pyrolysis method with some modifications (Wu *et al*., 2013). Briefly, 400 mg of the compound was heated until the solid powder started melting and turned into pale yellow, indicating the carbonization. The pyrolysis temperatures (°C) used were 199, 185, 184, 153, and 233 for L-glutamic acid, L-glutamine, succinic acid, citric acid, and glycine, respectively. Then 4 mL of water was added under constant stirring for 30 mins to dissolve and to prevent agglomeration of the CDs. The solution was then subjected to 13000 xg for 30 mins to collect the solution containing the CD.

2.2.5 Determination of Band Gap Energy

We determined the band gap energy, E_g, of the synthesized CD by plotting the Tauc's plot between $(\alpha h\nu)^{1/2}$ vs. hν. α is the optical absorption coefficient that can be calculated using absorbance (A) and thickness (d) of the sample ($\alpha = 2.303A/d$) whereas $h\nu$ can be calculated using the relation $h\nu = 1240/\lambda$. The following equation gives the Tauc's relation:

$$\alpha h\nu = B\left(h\nu - E_g\right)^r \qquad (2.2)$$

where B is proportionality constant, and r is the empirical exponent constant. Depending upon the type of transition, the value of r changes. The value of E_g was calculated by extrapolating the linear portion of the curve to intersect at the x-axis at the zero-absorption coefficient value.

2.2.6 Theoretical Studies

The primary tool used in the study was Avogadro, an advanced three-dimensional cross-platform for molecular editing and visualizing design. Using the Gaussian 09 software package, which is an extension of Avogadro, Density Functional Theory (DFT) calculations were carried out for finding the binding energy. Firstly, the geometry of the model molecules, as well as the H_2O_2, were optimized, and their energies were acquired. Later, the interaction was performed by placing the optimized H_2O_2 molecule close to the different functional groups in each of the optimized model molecules. The data presented here are repetition of several experiments. The binding energy (B.E) was calculated using the formula shown below:

$$\begin{aligned}&\text{B. E. } (\Delta G) = (\text{Optimized energy of model molecule}) + \\ &(\text{Optimized energy of } H_2O_2) - \\ &(\text{Optimized energy of interaction between model molecule} - H_2O_2)\end{aligned} \qquad (2.3)$$

2.2.7 Peroxidase-like Activity Assay

In order to examine the peroxidase-like activity of the synthesized CD, the oxidation of ABTS substrate was monitored in the presence of H_2O_2. Oxidized ABTS

has an absorbance maximum at 414 nm along with other peaks at 395 nm, 640 nm, and 737 nm. The influence of different CD concentrations, H_2O_2 concentration, ABTS concentration, time, and temperature on the catalytic activity was investigated. The activity was measured in terms of relative activity (Wang *et al*., 2011).

$$\text{Relative activity (\%)} = \frac{A_1}{A_2} \times 100\% \qquad (2.4)$$

where, A_1 is the absorbance of the sample, and A_2 is the maximum absorbance.

Kinetics study was performed for the reaction by varying the concentration of both H_2O_2 and ABTS. The experiment was carried out by varying the concentration of one substrate while keeping the concentration of the other substrate fixed and subsequently monitoring the absorbance change at 414 nm. The concentration was calculated using the Beer-Lambert Law:

$$C = \frac{A}{\varepsilon l} \qquad (2.5)$$

where C is the concentration of the substrate, A is the absorbance, l is the optical path length, and ε is the molar absorption coefficient (36000 M^{-1} cm^{-1} for the oxidized product of ABTS). The absorbance data was back-calculated to determine the concentration of the oxidized product. The reaction rate at different concentrations of the substrate was determined by calculating the slope of absorbance change. The Michaelis-Menten constant (K_m) and maximum velocity (V_m) were calculated from the Lineweaver-Burk plot of the double reciprocal of the Michaelis-Menten equation:

$$\frac{1}{v} = \frac{K_m}{V_m}\left(\frac{1}{[S]} + \frac{1}{K_m}\right) \qquad (2.6)$$

where v represents initial velocity, K_m is the Michaelis constant, V_m is the maximum velocity, and [S] corresponds to substrate concentration.

2.2.8 Preparation of Paper-Based Platform

We prepared the paper platform using Whatman Grade 1 filter paper. Using a punching machine, we pinched off two 5 mm diameter paper cuts, each for control and test zone. Afterward, the paper cuts were soaked in the stock CD solution (100 mg mL^{-1}) and let it dry for approximately 30 mins in the laminar airflow. Then, 0.5 µL of 1 M

H_2O_2 was added to the test zone followed by addition of 0.5 µL of 1 mM ABTS to both the control and test zones. The progress of the reaction was then monitored from the color change on the paper surface.

2.2.9 Electrochemical Study of the CD

Firstly, a 5 mm diameter glassy carbon electrode (GCE) was cleaned by polishing with a 0.3 µm alumina slurry followed by sonication in ethanol and water for 10 min. The cleaned electrode was dipped into a 10 mg mL^{-1} CD solution (Acetate buffer, pH 3), incubated for 10 h and then performed cyclic voltammetry (CV) in a potential window of -0.50 V to +1.0 V using a scan rate of 50 mV s^{-1}. All electrochemical measurements were performed in a potentiostat (Autolab, PGSTAT 302 N, Netherland) in a three-electrode system using reference Ag/AgCl (197 mV vs. SHE) electrode and the platinum as a counter electrode.

2.3 Results and Discussion

2.3.1 Functional Groups for Peroxidase Activity

In this study, we used acetic acid (CH_3**COOH**), acetone (CH_3**CO**CH_3), ethanol (C_2H_5**OH**), and aniline (C_6H_5**NH**$_2$) as model compounds to comprehend the role of the respective carboxylic group, carbonyl group, hydroxyl group, and amine group in H_2O_2 binding and decomposition studies. The model molecules were allowed to react with the ABTS in the presence of H_2O_2. Results show that acetic acid exhibited the highest peroxidase-like activity (Figure 2.1 a), while the compounds with either hydroxyl (ethanol) or amine (aniline) functional group did not support the reaction. However, we also noted a minor tendency of the acetone to support the reaction. Experiments were then performed to identify the functional group with the best binding to H_2O_2. We carried out Density functional theory (DFT) (B3LYP/631G) calculations using the Gaussian 09 software package. The final optimized stage of the interaction between model molecules and H_2O_2 is shown in Figure 2.2. The binding energy (in eV) of H_2O_2 with acetic acid, acetone, ethanol and, aniline was found to be -35.91, -26.12, -34.89, and -34.01, respectively. As evident, among all the molecules, the acetic acid with the -COOH group displayed the best binding with H_2O_2. Hence, both the theoretical and experimental results confirmed that the carboxylic acid group acts as the substrate

binding and the catalytic site for peroxidase-like activity in CD. A pH-dependent study further threw light on the role of carboxylic (-COOH) and not the carboxylate ($-COO^-$) group, which supports the peroxidase-like activity of acetic acid. With increasing pH, the peroxidase-like activity of the acetic acid decreased and retained the activity only at a pH value below its pK_a value of 4.76 (Figure 2.1 b). The pH study also contradicted a previous report (Sun *et al.*, 2015), where the $-COO^-$ was shown to have a role in the peroxidase-like activity of graphene quantum dots.

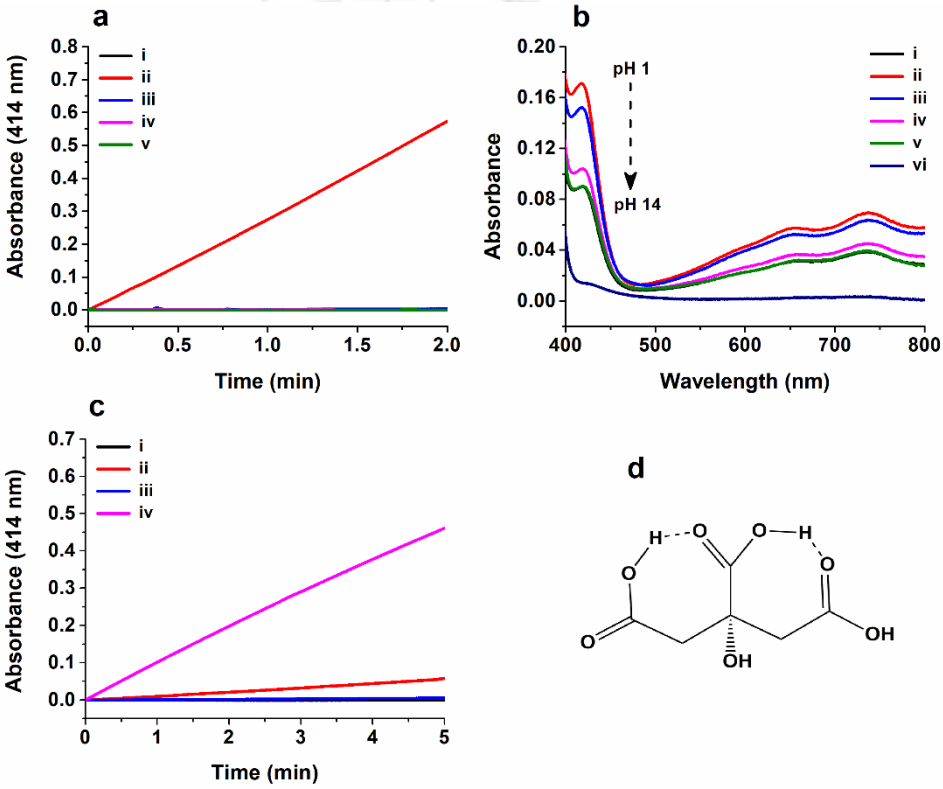

Figure 2.1. (a) Time-dependent peroxidase-like activity of (i) H_2O_2+ABTS (control), (ii) acetic acid, (iii) acetone, (iv) ethanol, and (v) aniline at $\lambda_{414\ nm}$. The experiment was carried out using 100 mM each of acetic acid, acetone, ethanol, and aniline in the presence of 10 mM H_2O_2 and 1 mM ABTS. (b) UV-Vis absorption spectra at varying pH value of acetic acid (100 mM) in the presence of H_2O_2 (10 mM) and ABTS (1 mM), (i-vi) corresponds to pH values of 1.0, 3.0, 5.0, 6.0, and 14.0 respectively. (c) Comparison of peroxidase-like activity of (i) H_2O_2+ABTS (control), (ii) acetic acid, (iii) citric acid, and (iv) succinic acid at pH 1.96. (d) Intramolecular hydrogen bonding in citric acid.

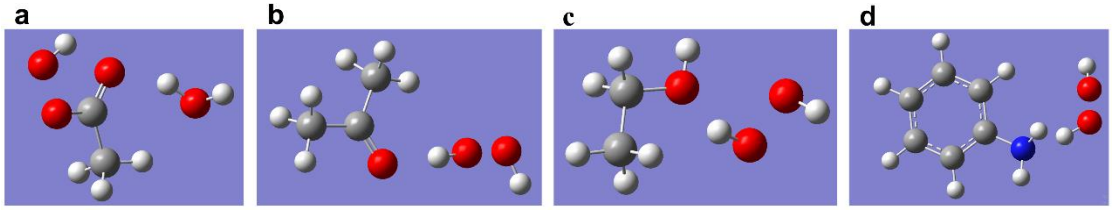

Figure 2.2. Final stages of the optimized interaction between H_2O_2 and (a) acetic acid, (b) acetone, (c) ethanol, (d) aniline.

To understand more about the role of the carboxylic group, we compared the activity among acetic acid (one -COOH), succinic acid (two -COOH) , and citric acid (three -COOH). We observed that succinic acid with two carboxylic acid groups offers 97.4 % higher activity than acetic acid, while the citric acid with three carboxylic functional groups failed to fair well the trend (Figure 2.1 c) (pK_a values in Table 2.1). The occurrence of intramolecular hydrogen bonding between the free carboxylic acid groups (Figure 2.1 d) (Leong, 2010), is the probable reason for the reduced reactivity of citric acid that hinders interaction of the free carboxylic acid groups with the peroxidase substrates. The higher peroxidatic activity of succinic acid than acetic acid has been attributed to the higher number of carboxyl functional groups present in the former molecule.

Table 2.1: Molecular structure and pK_a values of different compounds.

Compound name	Structure	pK_a COOH
L-Glutamic acid	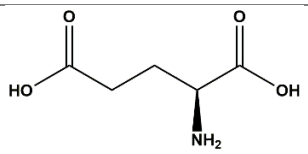	2.19 (main chain) 4.25 (side chain)
L-Glutamine	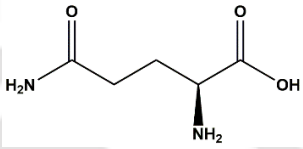	2.17
Succinic acid	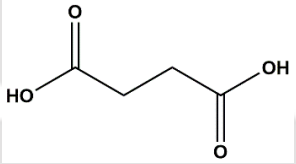	4.21 5.64
Glycine	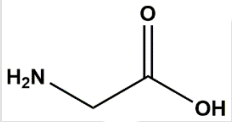	2.31
Citric acid	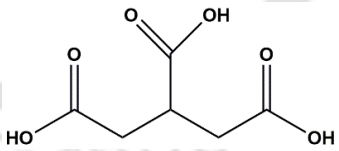	3.1 4.7 6.4
Acetic acid	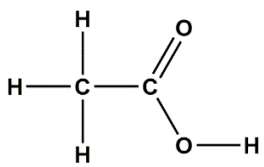	4.76

Since the -COOH group offers better activity than the -COO^- group, a molecule with any functional group that stabilizes this acidic group is expected to confer higher activity. Next, we analysed a range of compounds with a different chemical environment for the -COOH group in each case (Figure 2.3). The peroxidase-like activity significantly varied among the compounds, with the highest activity observed for L-glutamic acid. The activity for L-glutamic acid (1.04×10^{-7} Ms^{-1}) was much higher than the rest of the compounds and 59 % higher than the corresponding succinic acid (4.26×10^{-8} Ms^{-1}) despite the fact that both these compounds have the equal numbers (2 no's) of carboxylic acid groups. Thus, we conclude that the α-amine group to the carboxylic acid is responsible for the higher peroxidatic activity of L-glutamic acid. The reason is attributed to the electron-donating effect of -NH_2 through its lone pair of electrons that stabilises the -COOH group. The closer they are in a carbon backbone, the higher should be the effect. The lower activity of glycine, L-glutamine, and acetic acid than the L-glutamic and succinic acids is evident as they have fewer -COOH groups, as discussed above. Again, between glycine and acetic acid, the activity of glycine (101.1 nmol min^{-1} mL^{-1}) was nearly 30 times higher than acetic acid (3.32 nmol min^{-1} mL^{-1}), which also confirmed the positive effect of the amine group to the stability of the -COOH group.

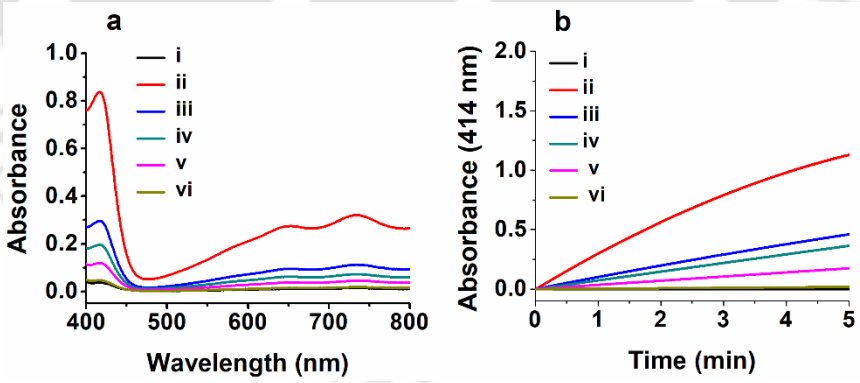

Figure 2.3. (a) UV-Vis absorption spectra of (ii) L-glutamic acid, (iii) succinic acid, (iv) glycine, (v) L-glutamine, and (vi) citric acid in the presence of H_2O_2 and ABTS. (b) Time-dependent absorbance change of (ii) L-glutamic acid, (iii) succinic acid, (iv) glycine, (v) L-glutamine, and (vi) citric acid at 414 nm. Experiment was carried out using 20 mM of each of the compounds, 10 mM of H_2O_2 and 0.5 mM of ABTS. The pH value in the reaction mixtures for the compounds was adjusted to 1.96, which is

below their pK_a values (Table 2.1). (i) in both (a) and (b) corresponds to control (H_2O_2+ABTS).

2.3.2 Synthesis and Characterization of CDs

Motivated by the above results, we synthesized CDs using L-glutamic acid, glycine, succinic acid, citric acid, and L-glutamine to correlate the above findings. We recorded the UV-Vis absorption spectra and the excitation-emission spectra (Figure 2.4-2.8) of the CDs. The fluorescence intensity of CD synthesized from citric acid and succinic acid were either low or not significant. Moreover, the CD derived from succinic acid precipitated rapidly with time. Hence, the fluorescence spectra were recorded only for CDs of L-glutamic acid (Figure 2.8), L-glutamine, and glycine (Figure 2.4 and 2.5). The excitation (λ_{ex}) and emission (λ_{em}) wavelengths for L-glutamic acid ($\lambda_{ex\ 354\ nm}$, $\lambda_{em\ 443\ nm}$, 0.85), L-glutamine ($\lambda_{ex\ 326\ nm}$, $\lambda_{em\ 368\ nm}$, 0.66), and glycine ($\lambda_{ex\ 365\ nm}$, $\lambda_{em\ 435\ nm}$, 0.78) along with their respective λ_{em} to λ_{ex} intensity ratio are shown in the parentheses. The CD derived from glycine turned into a dark brown solution following the pyrolysis process, which interfered with the colorimetric analysis. Similar to the results obtained for the pristine compounds presented above, the CDs obtained from L-glutamic acid (3.18 x 10^{-7} Ms^{-1}) showed the highest peroxidase-like activity, followed by succinic acid (2.40 x 10^{-7} Ms^{-1}), L-glutamine (3.80 x 10^{-8} Ms^{-1}), and citric acid (1.83 x 10^{-8} Ms^{-1}). However, the reaction rate (at λ_{max} 414 nm for oxidized ABTS) with CDs was much higher than their corresponding precursor compounds, as can be exemplified for the L-glutamic acid CD with ~3.1-fold higher than the corresponding reaction rate with free L-glutamic acid. Considering the highest peroxidase-like activity, we pursued further studies with the L-glutamic acid CD (Figure 2.9).

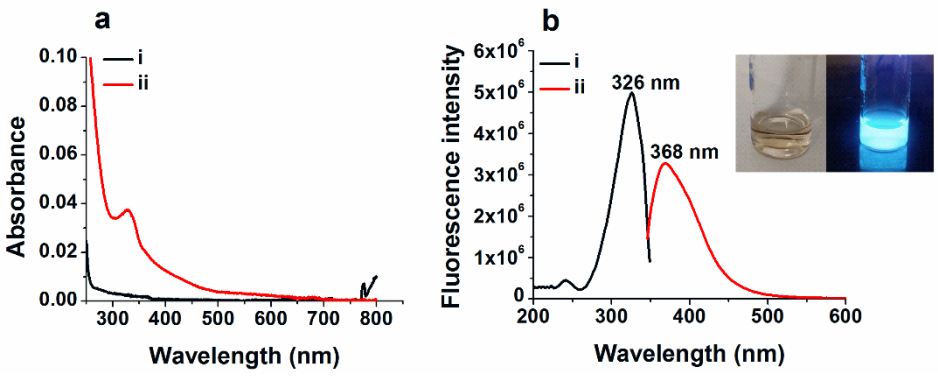

Figure 2.4. (a) UV-Vis absorption spectra of (i) L-glutamine and (ii) CD synthesized from L-glutamine. (b) excitation (i) and emission (ii) spectra of the CD synthesized from L-glutamine. Inset: aqueous CD solution under visible light and UV light.

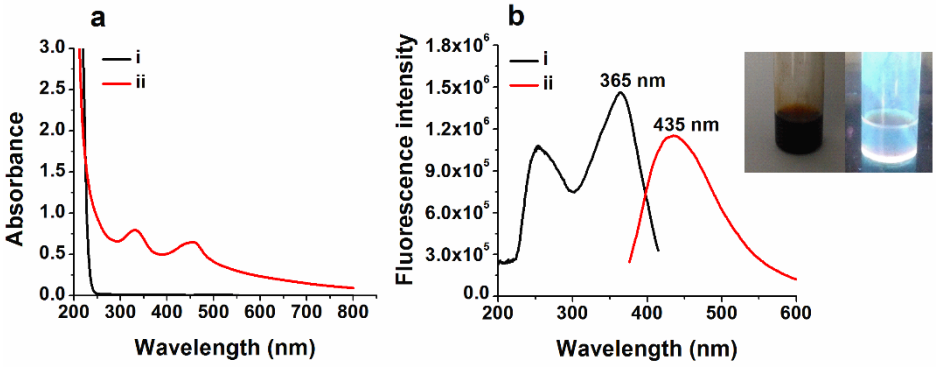

Figure 2.5. (a) UV-Vis absorption spectra of (i) glycine and (ii) CD synthesized from glycine. (b) excitation (i) and emission (ii) spectra of the CD synthesized from glycine. Inset: aqueous CD solution under visible light and UV light.

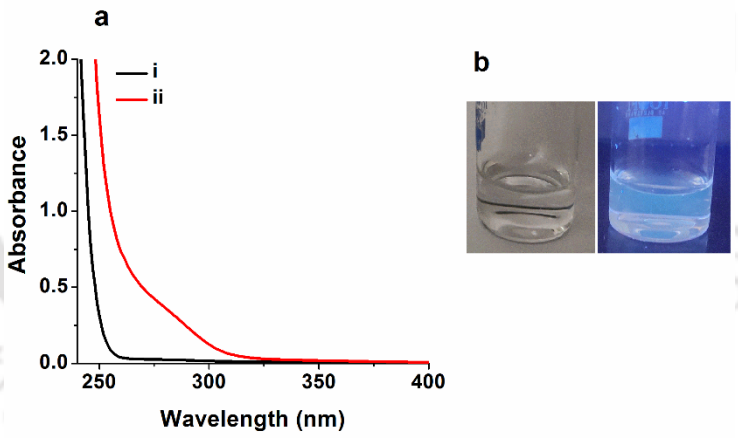

Figure 2.6. (a) UV-Vis absorption spectra of (i) citric acid and (ii) CD synthesized from citric acid. (b) Aqueous CD solution under visible light and UV light.

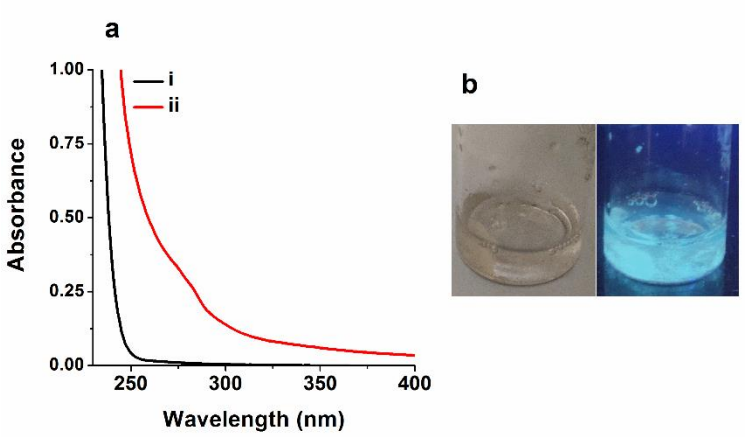

Figure 2.7. (a) UV-Vis absorption spectra of (i) succinic acid and (ii) CD synthesized from succinic acid. (b) Aqueous CD solution under visible light and UV light.

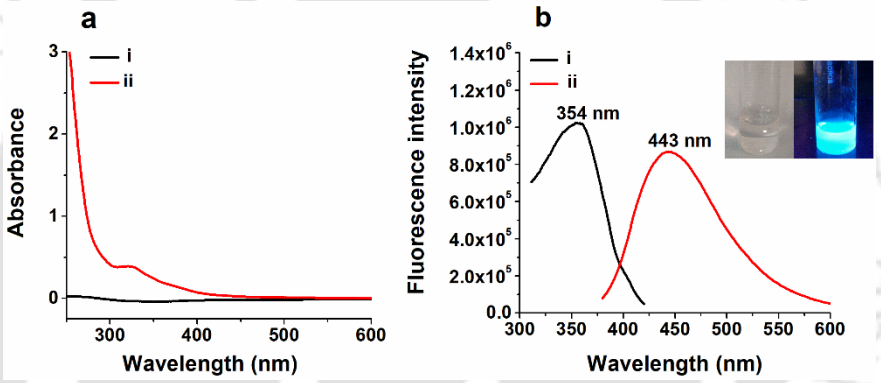

Figure 2.8. (a) UV–vis absorption spectra of L-glutamic acid (i) and CDs (ii) synthesized from L-glutamic acid. (b) Excitation (i) and emission (ii) spectra of the CD synthesized from L-glutamic acid. Inset: aqueous CD solution under visible light and UV light.

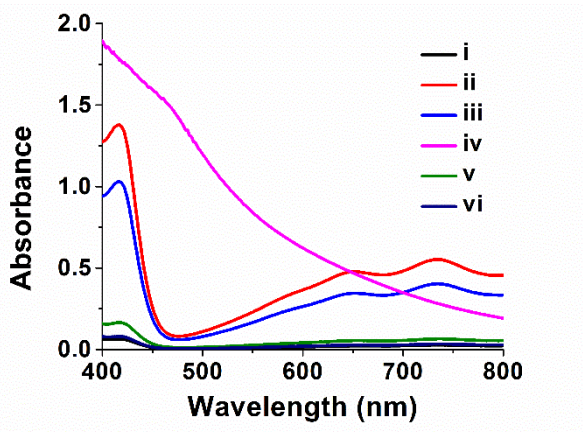

Figure 2.9. Peroxidase-like activity of the CD synthesized from (ii) L-glutamic acid, (iii) succinic acid, (iv) glycine, (v) L-glutamine, and (vi) citric acid. (i) represents control. Experiment was carried out using 20 µL of 100 mg mL^{-1} of CD solution, 10 µL of 1 M H_2O_2 and 100 µL of 5 mM ABTS.

The synthesized L-glutamic acid CDs show a distinct absorption peak at 326 nm (Figure 2.8 a) and an only excitation dependent emission peak at 443nm (Figure 2.8 b). The absorption peak corresponds to the n-π* transition of the C=O/ and heteroatoms N, O (Patir and Gogoi, 2018). The emission peak may be attributed to the surface state energy traps of the synthesized carbon dot. Under UV light, the CD solution appeared blue (inset Figure 2.8 b).

The HRTEM analysis showed that the CDs are spherical nanoparticles, and the Gaussian-fitting curve revealed that their average size is 3.18±0.53 nm (Figure 2.10 b) (Scheme 2.1). The image showed uniformly distributed CDs with a lattice spacing of 0.22 nm (inset Figure 2.10 a). The Selected Area Electron Diffraction pattern (SAED) illustrated the amorphous nature of the synthesized CD (Figure 2.10 c).

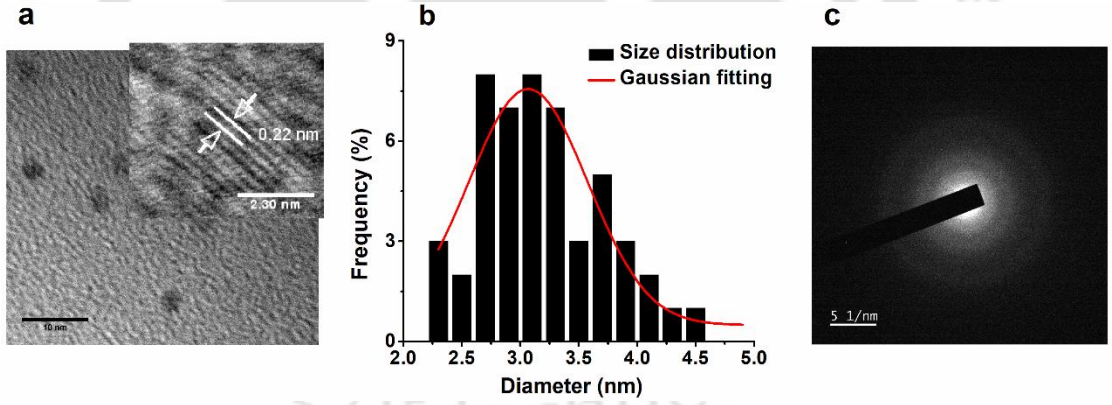

Figure 2.10. (a) FETEM image of the CD synthesized from L-glutamic acid. Inset. Image of a single CD with the lattice spacing. (b) The size distribution of the CDs, (c) SAED pattern.

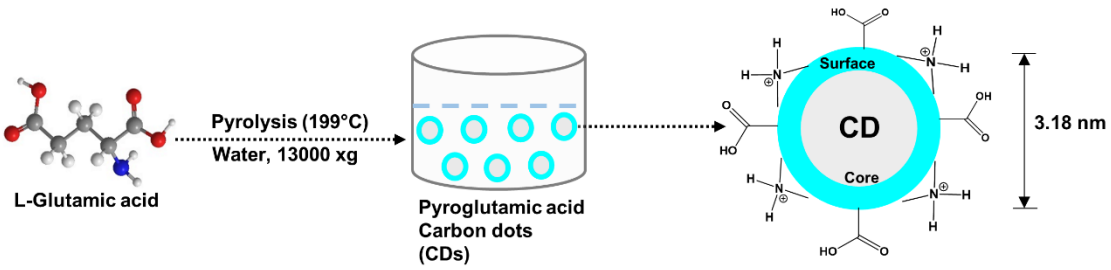

Scheme 2.1. Illustration of the synthesis of CDs from L-glutamic acid.

The surface characteristics of the synthesized CD were analysed. In the FTIR spectrum (Figure 2.11 a), the broad peak at ~3500 cm^{-1} corresponds to O-H and N-H stretching vibrations of the surface hydroxyl group and amine group, respectively, that further reflects the hydrophilic nature of the CD. The peaks between 3000-2500 cm^{-1} are attributed to the C-H stretching vibrations. The band at ~1700 cm^{-1} is because of the C=O stretching vibration of carboxylic acid and amide. The presence of both O-H and C=O stretching vibrations indicates the presence of the carboxylic acid group. C-H scissoring was confirmed with the appearance of 1370-1350 cm^{-1} bands. The band at 1250 cm^{-1} is because of the C-N stretching.

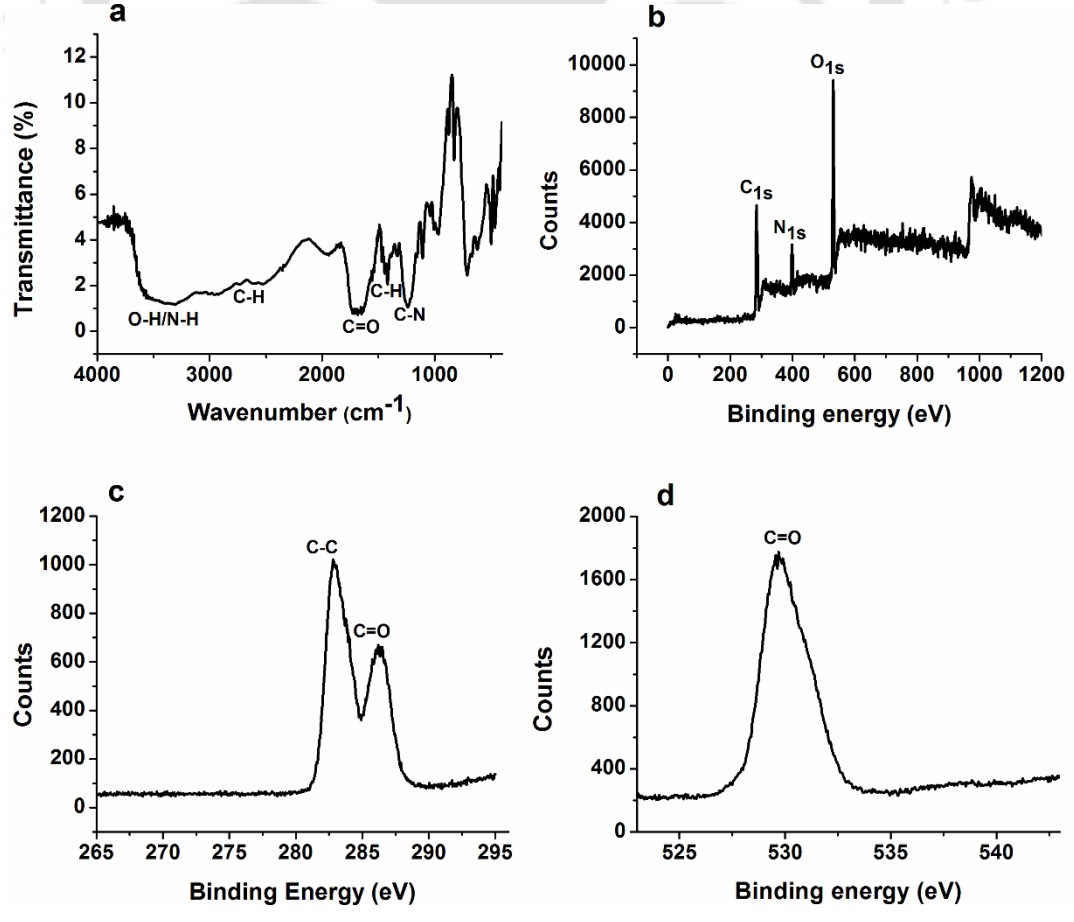

Figure 2.11. (a) FTIR spectrum of the synthesized CD from L-glutamic acid. (b) Wide scan XPS spectrum. (c) C1s XPS spectra. (d) O1s XPS spectra.

The broad scan XPS spectrum (Figure 2.11 b) shows three peaks at 284, 398.4, and 530.4 eV corresponding to C1s, N1s, and O1s, respectively, which confirms the presence of carbon, nitrogen, and oxygen functional groups on the surface of the CD. The deconvolution of high-resolution XPS spectra of C1s shows two peaks at 282.9 and 286.5 eV corresponding to C-C and C=O groups (Figure 2.11). Furthermore, the O1s spectrum shows one peak at 529.7 eV, corresponding to the C=O bond (Figure 2.11 d). Both the FTIR and XPS results showed the presence of hydrophilic functional groups on the CD's surface that is useful for the nanomaterial's stability in aqueous solutions. Notably, the high aqueous stability of the nanoparticles is an essential criterion for their catalytic reactions that involve long operation time. The band gap energy, E_g, we determined for the L-glutamic acid CD was 1.25 eV (Figure 2.12). The small E_g value for the CD is likely to be caused by the presence of carbonyl groups on its surface, which is revealed from the above FTIR studies. The oxygen-containing functional groups are known to lower the band gaps of carbon dots (Figure 2.12) (Liu *et al*., 2019; Yu *et al*., 2018).

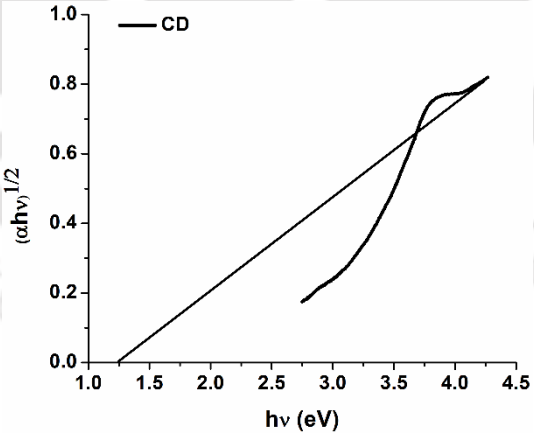

Figure 2.12. Band gap of the CD synthesized from L-glutamic acid.

We utilized both ^{1}H NMR (Figure 2.13 a) and ^{13}C NMR (Figure 2.13 b) spectroscopy and confirmed that the chemical constituent of the CD is only the pyroglutamic acid (IUPAC: 5-oxopyrrolidine-2-carboxylic acid). Notably, the pyrolysis of L-glutamic acid at 300 °C has been reported to produce three products, namely

pyroglutamic acid, pyrrolidinone, and glutarimide (Figure 2.14) (Sharma *et al*., 2004). The result implied that pyrolysis temperature has a significant impact on the chemical constituent of the CDs. A comparatively low pyrolysis temperature used in the present investigation (199 °C) has reduced the chemical complexity by generating a single compound for a homogeneous chemical environment in the CD. We further confirmed the spectra using the ChemDraw software. Except for the hydroxyl proton, all the carbon, as well as the protons were observed in the ^{13}C and ^{1}H NMR spectra, respectively. The hydroxyl proton signal is likely to be suppressed in the NMR spectra because of the proton exchange with the D_2O solvent. Although the water suppression mode was used during the recording, the solvent peak still appeared in the ^{1}H NMR spectra.

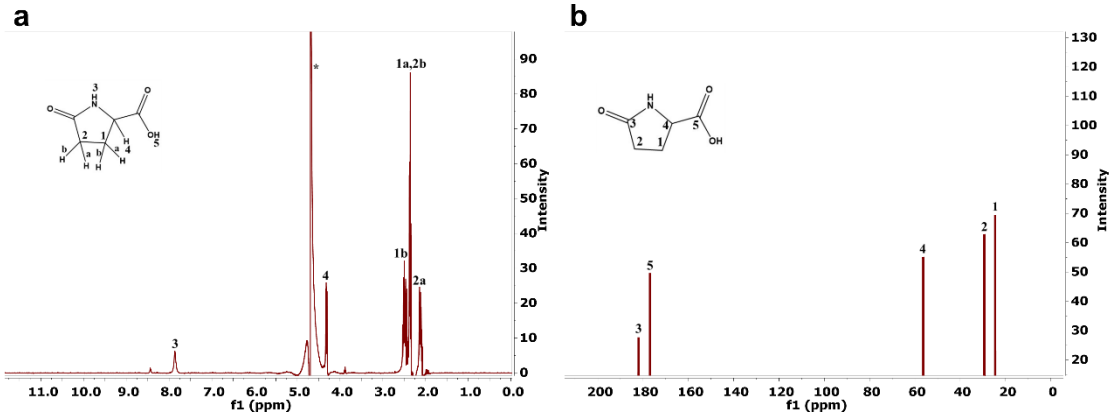

Figure 2.13. (a) ^{1}H-NMR (400 MHz, D_2O) spectra of the synthesized CD: δ (ppm) = 2.14 (-CH, Position 2a), 2.36 (-CH, Position 1a and 2b), 2.50 (-CH, Position 1b), 4.3 (-CH), 7.8 (-NH). The solvent peak is marked with asterisk. (b) ^{13}C-NMR (400 MHz, D_2O) spectra of the synthesized CD: δ (ppm) = 24.5 (C1), 29.3 (C2), 181.9 (C3), 56.3 (C4), and 176.9 (C5).

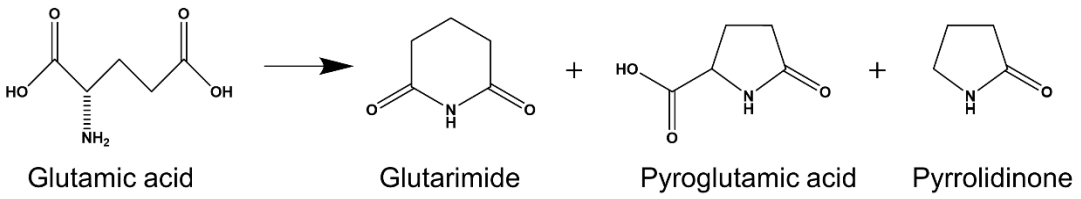

Figure 2.14. Pyrolysis products of L-glutamic acid obtained at 300 °C.

2.3.3 Peroxidase-like Activity of the Synthesized CDs

We observed that the reaction of the peroxidase substrates (H_2O_2 and ABTS) increased (at λ_{max} 414 nm) in the presence of CDs and followed a rate of 1.12 x10^{-6} Ms^{-1} (Figure 2.15 and 2.16). The Michaelis-Menten model was used to discern the kinetic parameters, and from the Lineweaver-Burk plot, the K_m and V_m values were determined (Figure 2.17). The K_m value of the CD with H_2O_2 as the substrate was found to be 5.85 mM (4.53 x 10^{-4} Ms^{-1}), whereas, for ABTS, it was 1.06 mM (6.46 x10^{-3} Ms^{-1}) with V_m values in the brackets. It indicates that the CD has a higher affinity for ABTS compared to H_2O_2. The turnover numbers (K_{cat}) for the CD with H_2O_2 as a substrate was calculated to be 0.011 s^{-1}. All the above results implied that the CDs behave as catalysts, bearing peroxidase-like activity. However, the CD displayed a remarkable performance up to 90 °C (Figure 2.15 c) against the HRP, which only offers a stable activity up to ~40 °C (Figure 2.15 d). Based on the above results, we suggest that the L-glutamic acid CD could be a suitable replacement of the widely used enzyme, HRP, for the peroxidase assay where thermostability is the critical requirement.

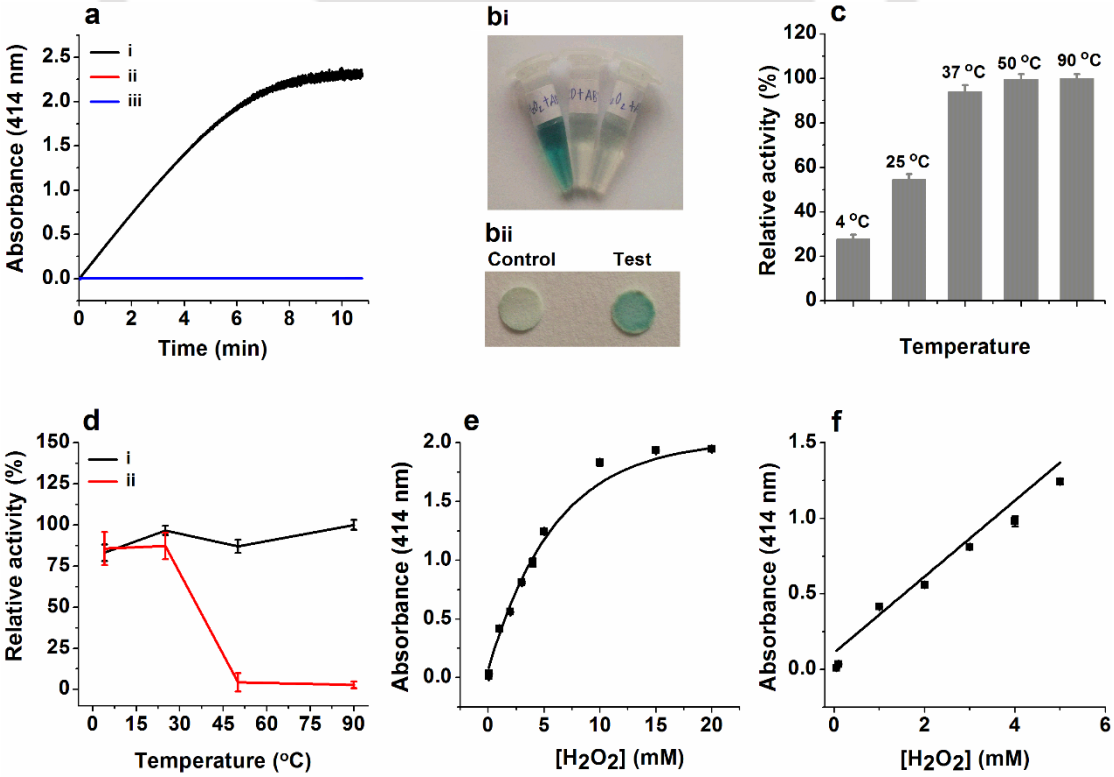

Figure 2.15. (a) Time-dependent absorbance change at 414 nm of ABTS in different reaction systems: (i) ABTS + CD + H_2O_2, (ii) ABTS + CD, and (iii) ABTS + H_2O_2. The

experiment was performed using 10 mg mL^{-1} CD, 1 mM H_2O_2 and 5 mM ABTS. (bi) Photograph of different systems after 2 min of reaction, sequentially from left: ABTS +CD+H_2O_2, ABTS+CD, and ABTS+H_2O_2, (bii) Reaction on the paper platform. Control: CD+ABTS (left panel) and test: CD+H_2O_2+ABTS (right panel). (c) The peroxidase-like activity of CD at different temperatures. (d) Comparison of temperature stability for CD (i) and HRP (ii). (e) Response curve for H_2O_2 using 10 mg mL^{-1} CD, 10 mM ABTS. The error bars represent the standard deviation (n = 3). The experiment was performed using 10 mg mL^{-1} CD and 50 mM ABTS, (f) Linear calibration for H_2O_2 detection.

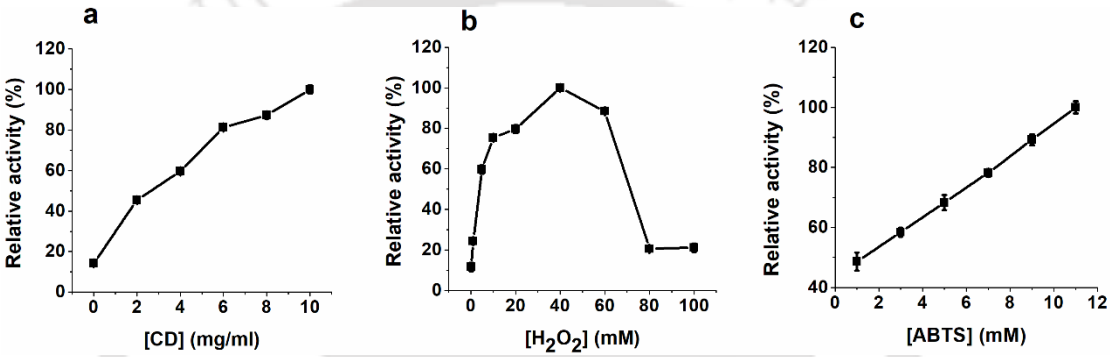

Figure 2.16. The peroxidase-like activity is dependent on the concentrations of (a) CD, (b) H_2O_2, and (c) ABTS.

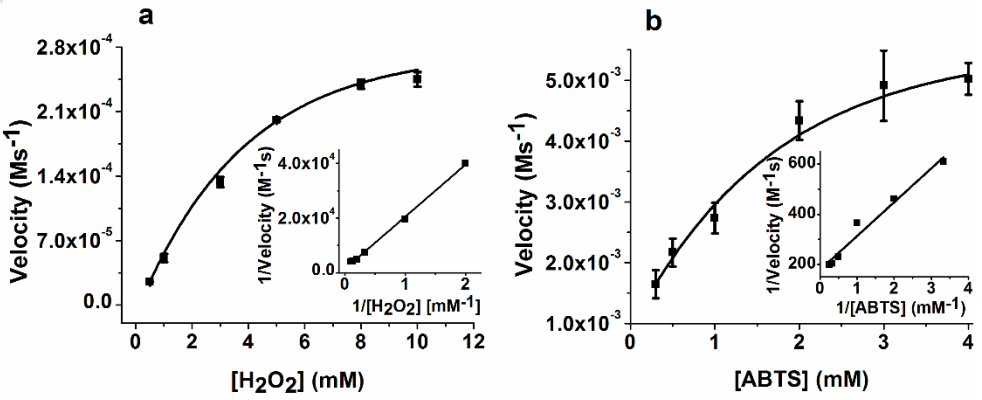

Figure 2.17. Steady state kinetic assay of the CD derived from L-glutamic acid. Experiment was performed using 5 mg mL^{-1} CD at room temperature. (a) The concentration of ABTS was 1mM and the H_2O_2 concentration was varied from 0.1 mM to 10 mM. (b) The concentration of H_2O_2 was 10 mM and the ABTS concentration was varied from 0.1 mM to 4 mM.

Based on the peroxidase-like activity of the CDs, we developed a colorimetric assay for the detection of H_2O_2 by monitoring the absorbance change at λ_{max} 414 nm for the oxidized ABTS (Figure 2.15 e). A dynamic range of 0.05-5 mM with a limit of detection (LoD) of 110 μM for H_2O_2 was identified (Figure 2.15 f). The LoD was calculated using the formula LoD = $3\sigma/m$, where σ is the standard deviation of the absorbance of blank, and m is the slope of the calibration curve. We found that the agglomeration of CDs is a challenge for the assay as described in the next section, and hence conducted a preliminary study of the reaction on a chromatographic paper (Whatman Grade 1) platform (Figure 2.15 bii). The green colour of the oxidized ABTS was formed within a few seconds in the test zone. The result demonstrated that even the paper being a solid material, supports the reaction. Further, this microporous hydrophilic material is likely to prevent the diffusion led aggregation of the nanomaterial caused by the peroxidase substrates.

2.3.4 Characterization of CD Aggregation

The steady-state kinetics of the CD catalysed peroxidase reaction was restricted by the incubation reaction time and higher peroxide concentrations. We found that the reaction did not follow the kinetics rationally beyond the reaction time of approximately two mins, and showed irregularity in response beyond the H_2O_2 concentration of ~10 mM under the standard conditions of the assay. The response (absorbance) waned rapidly, and no change was observed even after the addition of extra ABTS (135 μM) in the reaction (to ensure its concentration beyond the rate-limiting level of 125 μM) (Figure 2.18 ai). The activity, however, abruptly increased (31 %) upon addition of an extra amount (50 % of original) of CD to the reaction (Figure 2.18 aii). The result is intriguing, indicating turnover catalytic power of the CDs used originally has been diminished.

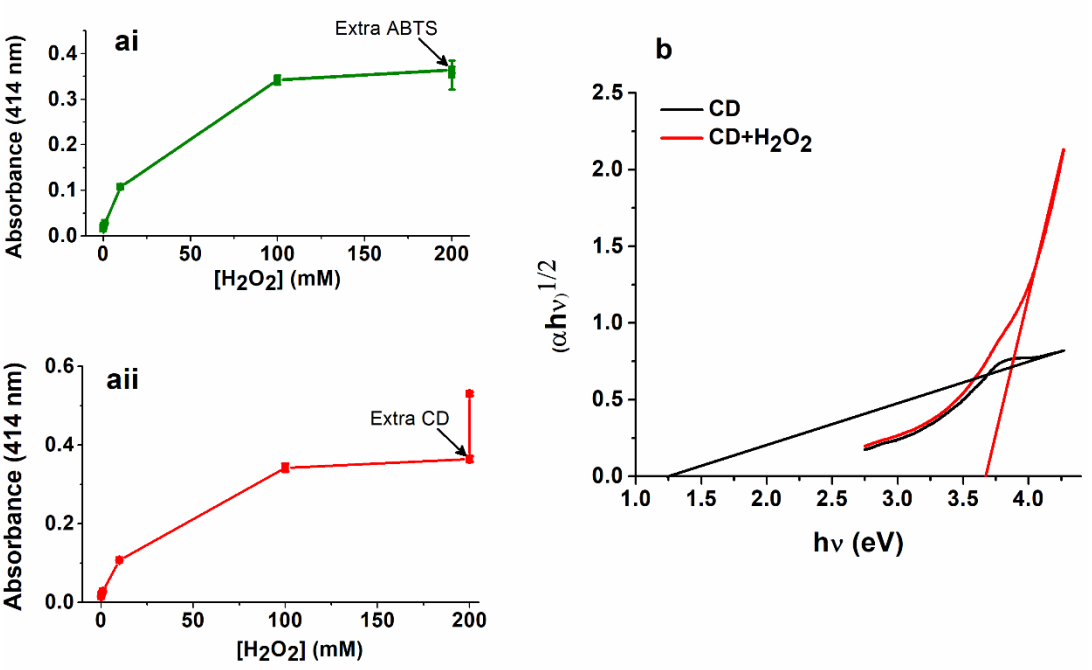

Figure 2.18. Absorbance versus concentration of H_2O_2 at a fixed concentration of CD (5 µg mL^{-1}) and ABTS (125 µM). Response to the absorbance (ai) following the addition of extra ABTS (135 µM) at the saturated H_2O_2 concentration, and (aii) following the addition of extra CD (7.5 µg mL^{-1}) at the saturated H_2O_2 concentration. (b) Comparison of the band gap before and after the reaction of CD with H_2O_2.

We monitored the interaction of the CD with H_2O_2 by UV-Vis spectroscopy following a time lag of two mins. With the increasing concentrations of H_2O_2, a bathochromic shift of the CD spectra occurred (Figure 2.19 a). The wavelength shift occurred with the increasing concentration of H_2O_2 and then slowed down the change (Figure 2.19 b), indicating agglomeration of the nanomaterial. We observed an increase in the band gap of the CD from 1.25 eV to 3.70 eV following its interaction with H_2O_2 (Figure 2.18 b). However, no shift in the fluorescence spectra during the interaction of CD with H_2O_2 was detected following their prolonged incubation. Hence, it is evident that the CD's intrinsic property has not changed, and the observed increase in the band gap is simply because of the agglomeration that affects the absorption of light. This substrate-induced agglomeration phenomenon could be used to explain the observed slowdown of peroxidase reaction and a sudden rise in the reaction (absorbance) upon the addition of an extra amount of CD in the reaction (Figure 2.18 aii).

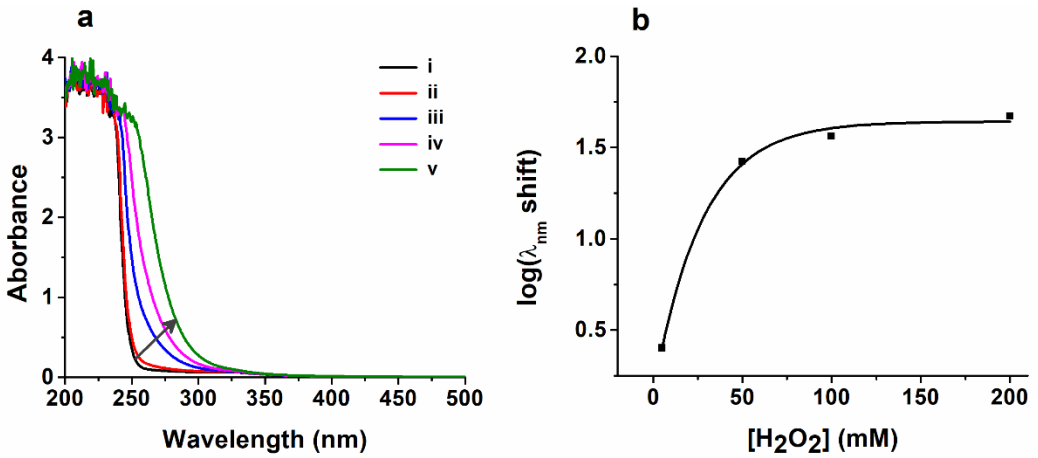

Figure 2.19 (a) UV-Vis absorption spectra of CD at different concentration of H_2O_2. (i–v) Corresponding to CD, CD+5 mM H_2O_2, CD+50 mM H_2O_2, CD+100 mM H_2O_2, and CD+200 mM H_2O_2 respectively. (b) Plot of log (λ_{nm} shift) vs [H_2O_2].

We examined for any changes in the morphology as well as the topography of the CD upon it's prolong reaction with the two-peroxidase substrates. A FETEM study demonstrated that the size of the CD particles increased with increasing concentrations of H_2O_2 and transformed into agglomerated form (Figure 2.20 A). Besides, the agglomeration was also formed when ABTS was introduced into the CD+H_2O_2 system (Figure. 2.20 Ba). Interestingly, the CDs also agglomerated in a solution containing only ABTS (Figure 2.20 Bb). However, the pattern of the agglomerated structures differed in both the cases (i.e., ABTS and H_2O_2), with darker, and hence, denser aggregates are formed with H_2O_2. The carbon-skeleton based ABTS likely to generate less dense and hence lighter agglomerates with CDs reflecting as whitish particles due to lower Brag diffractions. The agglomerates from the mixed substrates (Figure 2.20 Ba) revealed that the size of the agglomerates formed from ABTS is much smaller with uniform sizes than the one formed with H_2O_2. The findings indicate the mechanisms of agglomeration is different for the two substrates that are discussed in the next section. We suggest that this agglomeration of the CDs is responsible for decreased peroxidase activity, as discussed above. The high aggregation is likely to hamper the substrate diffusion to the CD nanoparticles, and thereby significantly reducing the activity. The phenomenon is fascinating, as the general concept of the nanomaterial's inherent tendency to agglomerate (Gosens *et al*., 2010), is not straightway applicable in the

present case, as unlike in the reaction mixture, the unreacted CDs do not aggregate during the tested time scale (Figure 2.20 Aa).

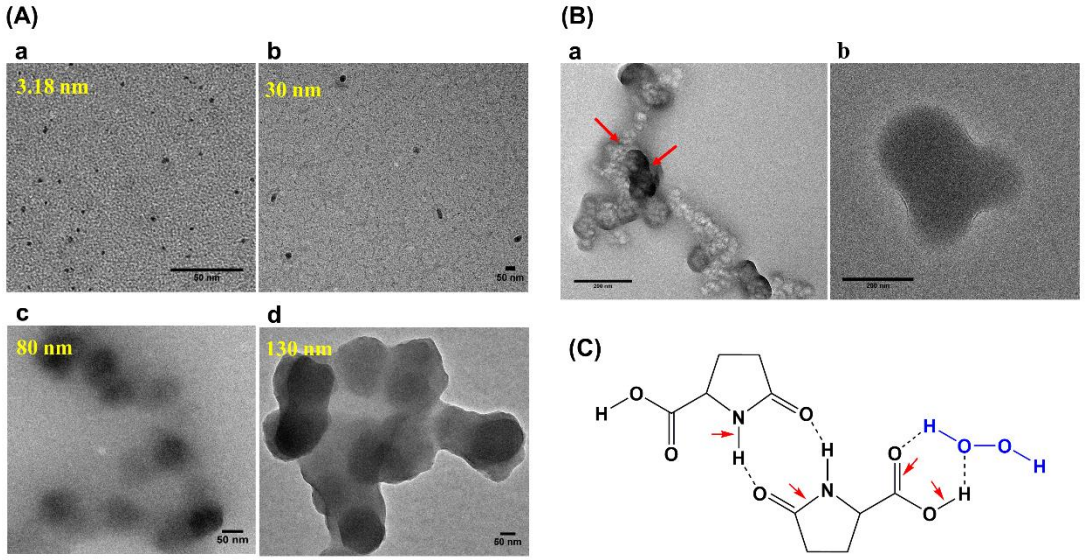

Figure 2.20. FETEM images on the effect of substrates on the morphology of CD. (A) Reaction with H_2O_2 (a) CD (Control: no substrates), (b) CD+25 μM H_2O_2, (c) CD+5 mM H_2O_2, and (d) CD+50 mM H_2O_2. (B): (a) CD+H_2O_2 (5 mM H_2O_2)+ABTS (250 μM) (the denser particles and less dense whitish particles are shown with arrows), and (b) CD+ABTS (250 μM). The experiments were performed using a 2 mg mL^{-1} CD concentration. (C) Schematic illustration of the possible interaction between CD and H_2O_2.The red arrow indicates the possible regions of stretching vibration as a result of the interaction.

Considering the general fact that the agglomeration of nanoparticles is a surface-induced phenomenon (Gosens *et al*., 2010), we examined the zeta (ζ) potential of the native CD and in the presence of its peroxidase substrates (Figure 2.21 a). Upon mixing with H_2O_2, the ζ- potential of the native CD (+2.1 ± 0.10 mV) changed to +1.94 ± 0.15 mV, showing that the surface charge is not significantly affected in the presence of H_2O_2. However, with the addition of ABTS (-2.6 ± 0.05 mV), the ζ- potential of CD changed to +0.1 ± 0.08 mV. Further, the value changed to +0.7 ± 0.1 mV in the presence of both the substrates. The result implies that the interaction between the CD and ABTS is electrostatic, promoting agglomeration of CDs through the surface charge neutralization. However, this initial interaction might also facilitate the transfer of charge from ABTS to CD for the reaction to occur. To crosscheck the fact, instead of

ABTS, we performed the assay with another widely used peroxidase co-substrate, TMB (Figure 2.21 c), which is positively charged. As expected, no reaction was occurred, as indicated by the lack of colour formation with TMB (Figure 2.21 b). Above results also prompted us to conclude that H_2O_2 let agglomeration involves different mechanism, which will be discussed in the next section. As the peroxidase assay was performed in acidic pH, the -COOH group in pyroglutamic acid (pK_a 3.32) is present in the non-dissociated form. Under this acidic condition, the protonated amine group poised the positive zeta potential value to the pyroglutamic acids CD.

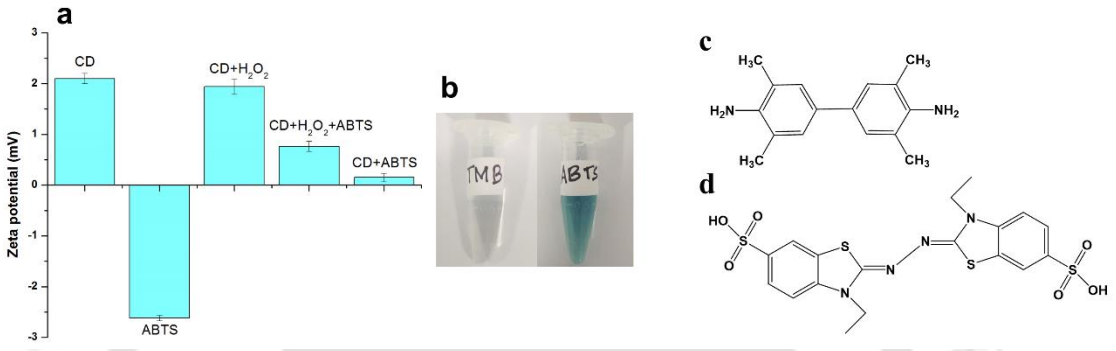

Figure 2.21 (a) Zeta potential of different reaction systems. The concentrations of CD (10 mg mL^{-1}), ABTS (100 μM) and H_2O_2 (1 mM) used in the reaction mixture are shown in the brackets. (b) Comparison of the intensity of colour formation of TMB (1 mM) and ABTS (1 mM) in the presence of CD (10 mg mL^{-1}) and H_2O_2 (10 mM). The final concentrations are shown in the brackets. Structure of (c) TMB, and (d) ABTS.

We performed the ^{13}C NMR (Figure 2.22) and ^{1}H NMR (Figure 2.23) analysis and observed that the skeleton of the CD structure has not changed after its interaction with H_2O_2 and ABTS. However, a negligible peak shift was observed in the ^{1}H NMR spectra for the CD+H_2O_2 and the CD+H_2O_2+ABTS reaction system. While in the CD+H_2O_2 reaction system, an upfield shift, i.e., shielding was observed whereas a downfield shift, i.e., deshielding, was observed in the CD+H_2O_2+ABTS reaction system for the 1st, 2nd, and 4th proton. In the spectra, an inset is shown only for the 4th proton for reference. The negligible shielding and deshielding of the protons at position 1st, 2nd and 4th might be because of the steric hindrance occurring in the agglomerated structures. The D_2O solvent was likely to have a role in the chemical shift.

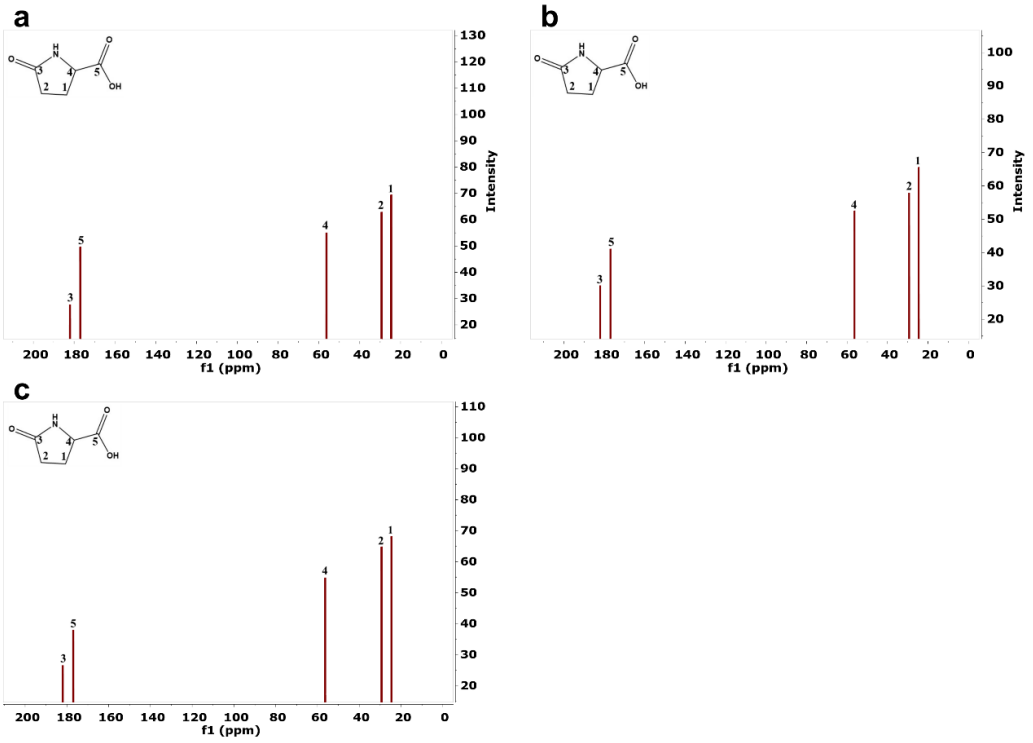

Figure 2.22. ^{13}C NMR spectra of different reaction systems. (a) CD. (b) CD+H_2O_2. (c) CD+H_2O_2+ABTS.

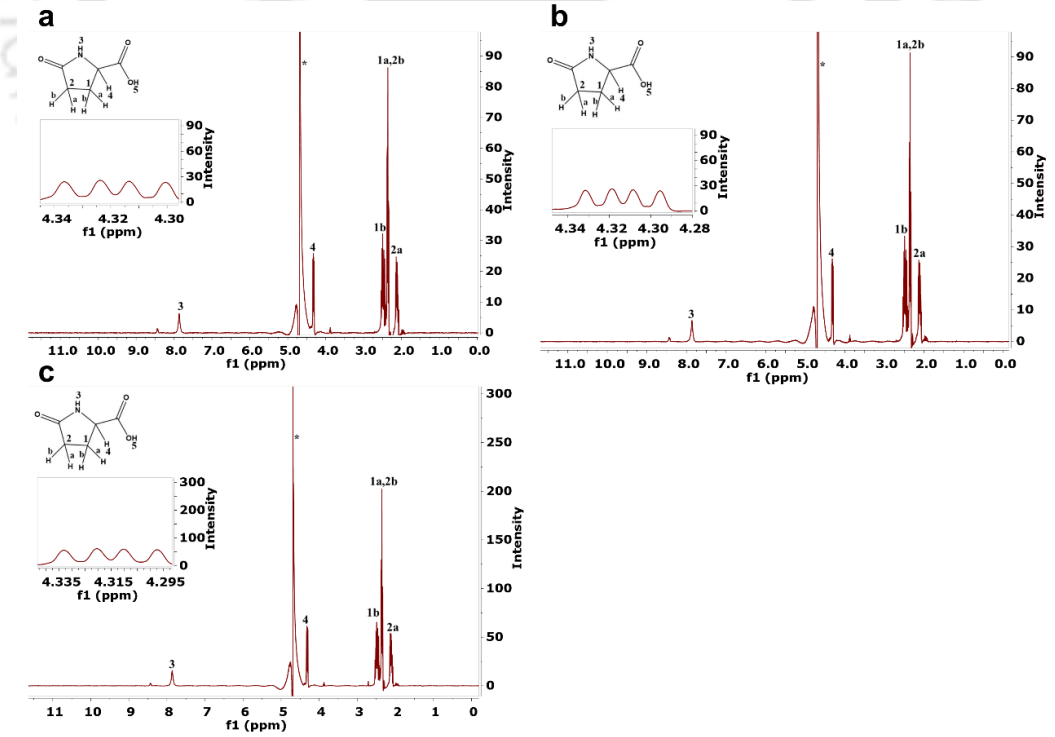

Figure 2.23. ^{1}H NMR spectra of different reaction systems. (a) CD. (b) CD+H_2O_2. (c) CD+H_2O_2+ABTS. Inset: spectra shift. The solvent peak is marked with an asterisk.

An FTIR study was performed to investigate the role of the surface functional groups in the formation of CD agglomerated structures. We visualized the interaction between the CD and H_2O_2, as shown in the scheme (Figure 2.20 C). The H_2O_2 molecule binds with the carboxylic group of the pyroglutamic acid, forming a six-membered ring-like structure that resulted in increased stretching vibration of O-H, N-H, C=O, and C-N groups (Figure 2.24). With the addition of ABTS to the CD+H_2O_2 reaction system, the intensity of the peak at 3500 cm^{-1} decreased to a substantial level. Again, when only ABTS reacted with CD, the peaks within 3500-2500 cm^{-1} were significantly suppressed, indicating the interaction between these entities substantially alters the surface chemical environment of the CDs. We compared the two kinds of aggregations of CD in the backdrops of the above results, and propose that the larger aggregation caused by H_2O_2 is due to its higher intermolecular cross-linking through multiple H-bonding with the CD than the corresponding ABTS. The binding of ABTS with CD is mostly through electrostatic interaction with its available charged groups with the positively charged amino group of the CD.

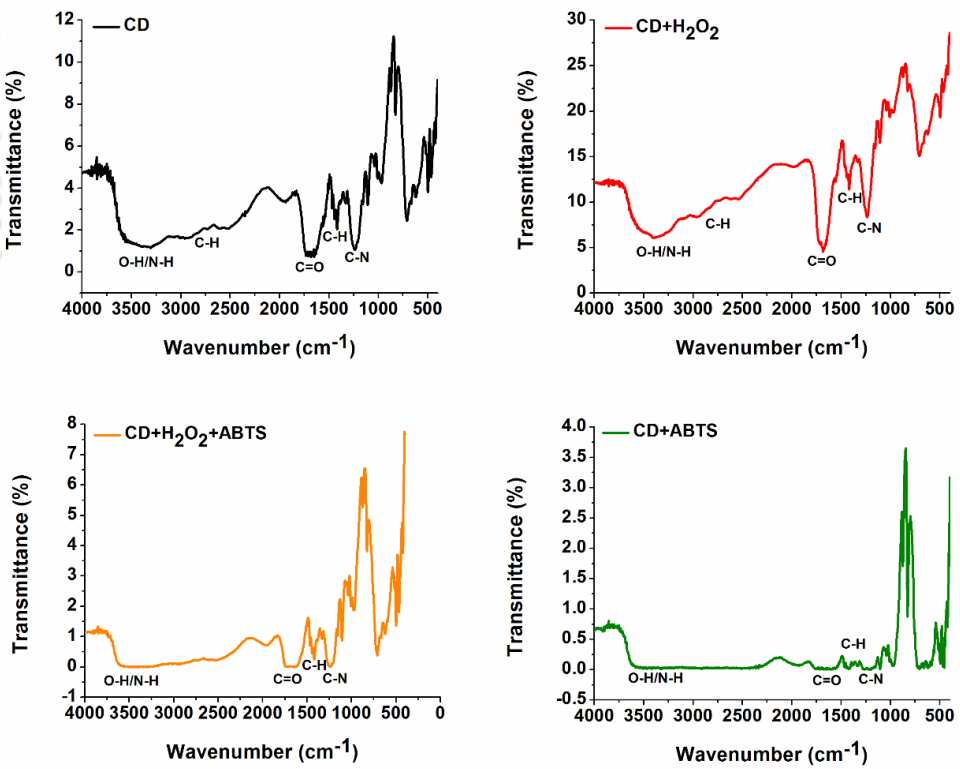

Figure 2.24. Comparison of the FTIR spectra of CD, CD+H_2O_2, CD+H_2O_2+ABTS, and CD+ABTS.

2.3.5 Mechanism of Peroxidase-like Activity of CDs

We examined the electron transfer mechanism of the CD catalysed peroxidase reaction using the ESR technique, followed by UV-Vis and fluorescence spectroscopy. In general, the nanoparticle-based peroxidase reactions are known to undergo Fenton reaction wherein the nanomaterial directly reduces H_2O_2 to $OH\cdot$ (Chen *et al*., 2012)**,** with a few exceptions like Co_3O_4 NPs (Dong *et al*., 2014). Our investigation showed the absence of a typical ESR signal for the hydroxyl radical, indicating that the reaction between CD and H_2O_2 may not follow the Fenton mechanism. We remodelled the experiment (Figure 2.15 a) to a more sensitive scale zone with a variation of CD and fixed ABTS concentrations, and found that even in the absence of H_2O_2, CD oxidises ABTS, albeit at a very low level (Figure 2.25 a). The oxidation was increased with the increasing concentration of CD, as evident from the intensity decreased at λ_{max} 340 nm for ABTS and increased at λ_{max} 414 nm, 640 nm, and 725 nm for the oxidised ABTS. Results indicate that CD acted as an electron trap, capturing electrons from ABTS. Interestingly, in the presence of H_2O_2, the peak for oxidized ABTS (λ_{max} 414 nm, 640 nm, and 725 nm) increased intensely. For example, the intensity at λ_{max} 414 nm for 2 mg mL^{-1} CD and 10 μM of ABTS was increased to 11-fold with the addition of 5 mM of H_2O_2 to the reaction mixture (Figure 2.25 b). The above findings confirmed the CD's catalytic role for the H_2O_2 (+1.776 V) led oxidation of ABTS (+0.69 V) is facilitated by their respective high redox potentials shown in the parentheses under acidic condition.

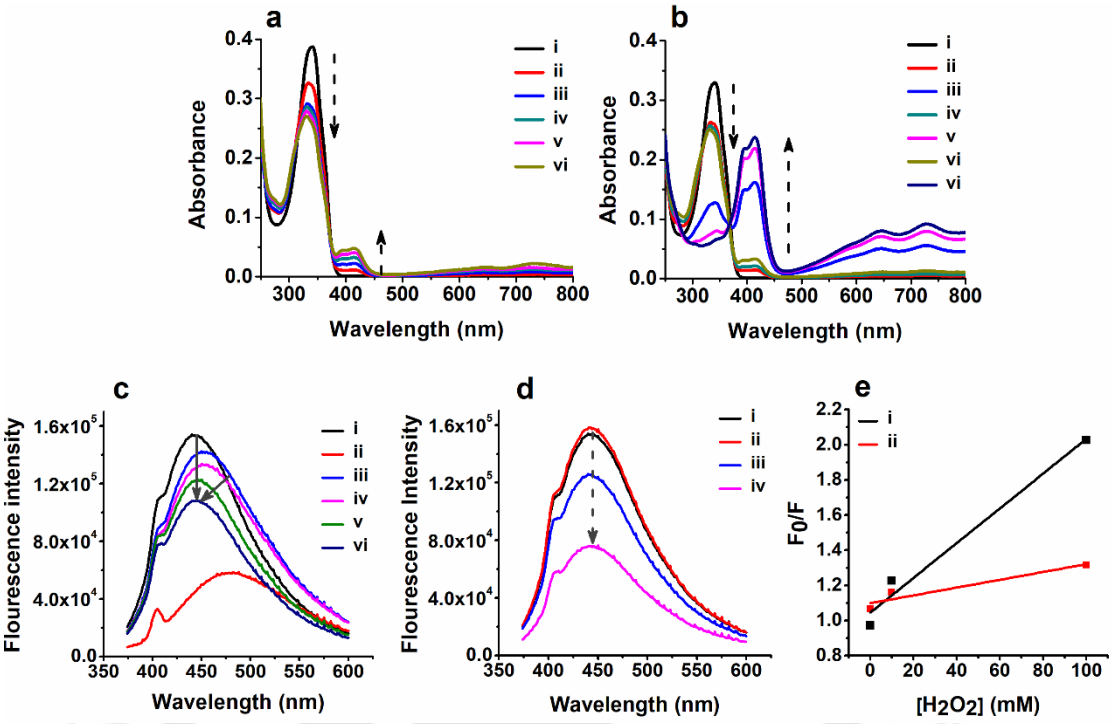

Figure 2.25. (a) Absorption spectra for the reaction between ABTS and increasing concentration of CD, (i-vi) corresponding to 2 mg mL^{-1}, 4 mg mL^{-1}, 6 mg mL^{-1}, 8 mg mL^{-1} and 10 mg mL^{-1} CD concentrations, respectively. (b) Overall reaction among CD, H_2O_2, and ABTS, (i-vi) corresponds to ABTS, ABTS+H_2O_2, 2 mg mL^{-1} CD+ABTS, 2 mg mL^{-1} CD+ H_2O_2+ABTS, 4 mg mL^{-1} CD+ABTS, 4 mg mL^{-1} CD+H_2O_2+ABTS, 6 mg mL^{-1} CD+ABTS, 6 mg mL^{-1} CD+H_2O_2+ABTS, respectively. (c) Fluorescence spectra of different reaction systems: (i) CD, (ii) ABTS, (iii) CD+ABTS, (iv) CD+10 µM H_2O_2+ABTS, (v) CD+10 mM H_2O_2+ABTS, (vi) CD+100 mM H_2O_2+ABTS. (d) CD fluorescence quenching at different concentration of H_2O_2. (i-iv) corresponding to 0 µM, 10 µM, 10 mM, and 100 mM, respectively. (e) Stern-Volmer plot of (i) CD+H_2O_2 and (ii) CD+H_2O_2+ABTS reaction systems. The reaction was performed by mixing suitable quantities of CD and H_2O_2 and incubated for 1 min. Subsequently, a suitable quantity of ABTS was added to the above mixture, followed by incubation for another 1 min. The final concentrations of ABTS in all the reactions was 10 µM, CD in Fig. (c) and (d) was 1 mg mL^{-1}, and H_2O_2 in Fig. (b) was 5 mM. The fluorescence spectra were recorded immediately after the incubation.

We observed that at the λ_{ex} 354 nm of CD, only ABTS without CD and H_2O_2 also exhibits a λ_{em} at ~480 nm. There is considerable overlap between the emission spectra of the CD and ABTS (Figure 2.25 c). Interestingly, the CD, when mixed with

ABTS, a hybrid and only emission peak emerged at λ_{em} 455 nm, which is a 27 nm red shift to the λ_{em} of CD and 25 nm blue shift to the λ_{em} of ABTS. In the presence of H_2O_2, the peak at λ_{em} 455 nm developed a hypsochromic shift, and the shift continues with the increasing concentration of H_2O_2 until the intrinsic λ_{em} 443nm peak for the CD is attained. Further, with increasing H_2O_2 concentrations and a fixed concentration of CD and ABTS, the fluorescence intensities were significantly quenched (Figure 2.25 d) as evident from the Stern-Volmer constant of 2.2 μM^{-1} determined from the plot (Figure 2.25 e). The formation of the hybrid λ_{em} 455 nm peak originated from the ABTS adsorption on the CD surface through electrostatic interactions with their complementary charges and protonation that perturbed the CD's energy. Indeed, protonation of the amino group leads to an increased delocalization of the lowest unoccupied molecular orbital across the whole molecule, which results in a lowering of the excited state energy (Zhang *et al.*, 2013). Additionally, the binding of ABTS to the CD is more like an N-doped phenomenon that resulted in red shift of the spectra (Carolan *et al.*, 2017). The back shifting of the λ_{em} from 455 nm to 443 nm upon addition of H_2O_2 implies gradual desorption of ABTS from the CD surface due to its transformation into the oxidized form because of the peroxidase reaction. All of these findings demonstrated that the electron transfer takes place from ABTS to CD to H_2O_2, the latter is then finally reduced with concomitant regeneration of the original electronic state of CD (Figure 2.26).

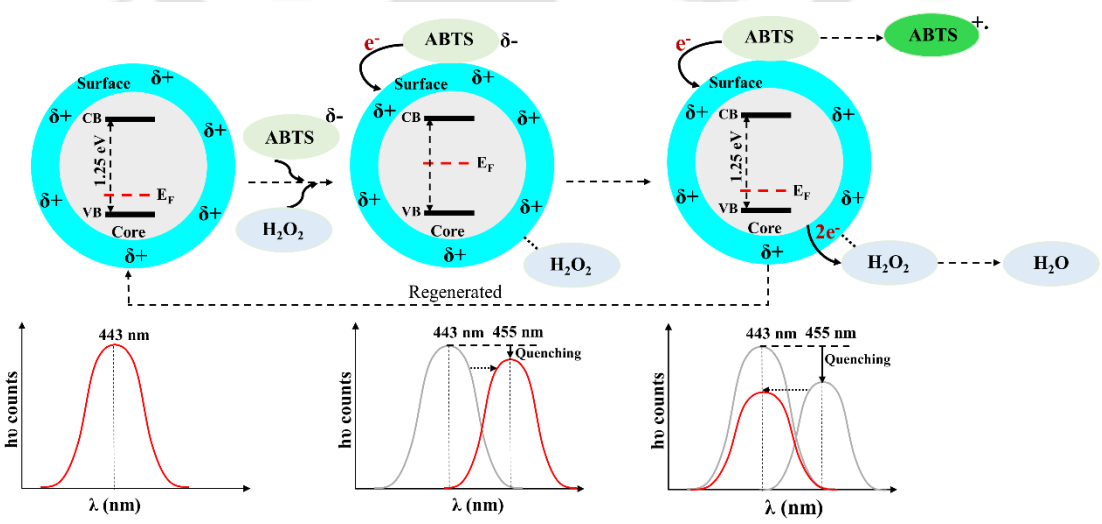

Figure 2.26. Schematic illustration of the electron transfer mechanism.

We find that the H_2O_2 led fluorescence quenching of the CD also occurred in the absence of ABTS. The extent of quenching was determined by using the Stern−Volmer plot (Figure 2.25 e), which is linear for a wide range of H_2O_2 concentrations. The Stern-Volmer constant was determined to be 9.9 μM^{-1}, which is ~4.5 fold higher than the value obtained for the reaction containing ABTS as mentioned above. Expressing in a simplified form, the mixtures containing 10 and 100 mM of H_2O_2 with a fixed ABTS concentration exhibited 5.51 % and 40.46 %, respectively lesser quenching intensity than the corresponding mixtures that void ABTS (Table 2.2). The result implies the depletion of H_2O_2 in the mixture containing both the substrates because of the CD catalysed peroxidase reaction. In a previous study, the electron transfer from the graphene nanomaterial to H_2O_2 has been ascribed to the increased Fermi level electron density that speed up the electron transfer process (Song *et al*., 2010). This non-peroxidase (as no reducing equivalent like ABTS involved) based fluorescence quenching phenomenon could also be exploited to detect H_2O_2 following the similar approach used to detect other compounds and ions (Kong *et al*., 2016; Yarur *et al*., 2019; Zhang *et al*., 2015).

Table 2.2: H_2O_2 led emission quenching of CD with and without ABTS.

H_2O_2 [mM]	**% of quenching (with respect to the CD intensity at λ_{em} 443nm)**	**% of quenching (with respect to the CD+ABTS intensity at shifting λ_{em} from 455 nm to 443nm)**
0.01	-2.92	6.20
10	20.31	14.80
100	67.79	27.33

Based on our critical findings and explanations, we propose here a mechanism on the L-glutamic acid CD-based colorimetric peroxidase reaction, as shown in Figure 2.27 b. Recalling the surface exposed nitrogen and -COOH functional group identified from ^{1}H NMR, ^{13}C NMR, XPS, and FTIR, we depict here the primary point of

electrostatic interaction for ABTS, which is in protonated form (Figure 2.27 a) (Ilyasov *et al*., 2020), is the quaternary amine (under acidic assay condition) exposed on the CD surface. This docking of negatively charged ABTS further stabilizes the -COOH in α-carbon of the pyroglutamic acid, activating the catalytic function and binding affinity of –COOH group to H_2O_2 through H-bonding. We suggest that these interactions and bindings bring the ABTS and H_2O_2 closer to each other in the CD backbone, facilitating hydride transfer from ABTS to the oxygen of the polarized peroxide, leading to the formation of water molecules at the end. The fundamental driving force for this redox process, however, is the favourable redox potentials of ABTS (+0.69 V) and H_2O_2 (+1.776 V), including the redox potential (+0.93 V) of the CD, which is almost in the middle of the redox potential axis between these two peroxidase substrates favouring the transfer of electrons. We identified the redox potential of the CD by cyclic voltammetry (Figure 2.28). Once ABTS is oxidized as a result of the reaction, it detaches from the CD surface due to its electrostatic repulsion from the positively charged amine group of the CD backbone. As a spontaneous event, another ABTS binds to the positively charged amino group of the CD through electrostatic interaction, continues the steady-state reaction process following this linked adsorption, and desorption of ABTS molecules. As a whole, CDs offer docking place for ABTS, -COOH as catalytic and binding sites for H_2O_2, provide interacting distance between these two substrates, and a suitable potential to facilitate the redox reactions.

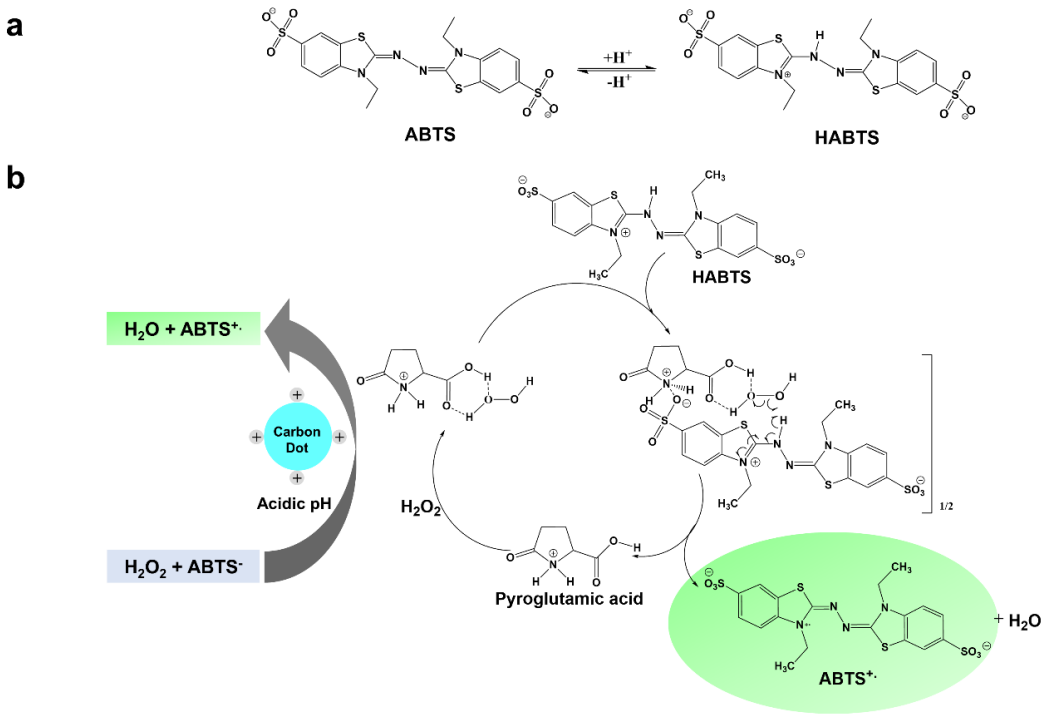

Figure 2.27. (a) Conversion of ABTS to its protonated form at low pH. (b) Mechanism of the CD-based peroxidase-like reaction.

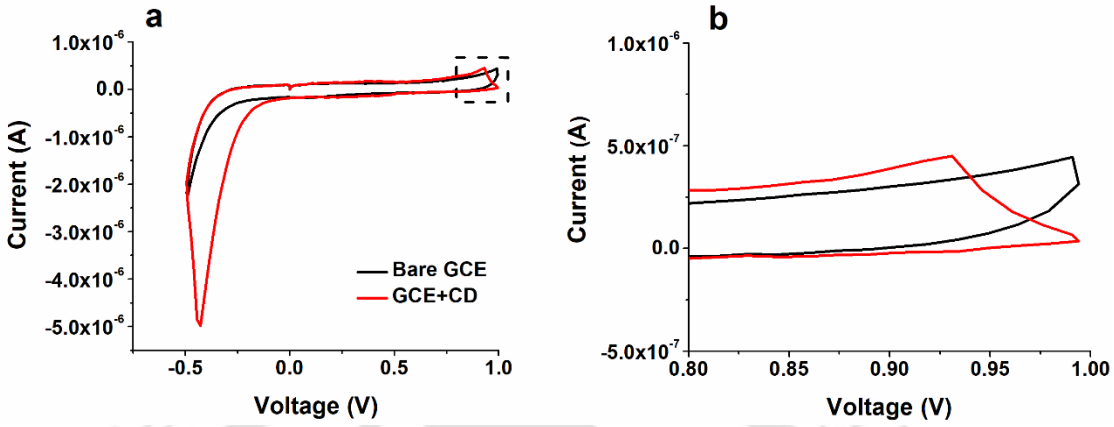

Figure 2.28. (a) Cyclic voltammetry of bare glassy carbon electrode (GCE) and GCE immobilized with CD in 50 mM acetate buffer (pH 3.0) at a scan rate of 50 mV s^{-1} using the Ag/AgCl reference electrode. (b) Expanded redox peak of the CD at +0.93 V.

2.4 Conclusion

This work reports a systematic study on the mechanism of peroxidase-like activity of CD. With the aid of simple carbon-containing molecules as model compounds, we unveiled for the first time that the carboxylic group binds to H_2O_2 with maximum energy and exhibits maximum peroxidase-like activity in contrast to the carbonyl, hydroxyl, and amine group. We also gained a new insight that a compound with an amine group near the carboxyl group exhibits a higher degree of peroxidase-like activity. The strategy of using combined theoretical and experimental studies has identified L-glutamic acid as a suitable compound for peroxidase-like activity. The L-glutamic acid, when carbonized through a simple low-temperature pyrolysis method, a uniformly distributed photoluminescent CD with pyroglutamic acid as the sole core constituent was formed. Interestingly, the CD exhibited much higher peroxidase-like activity than free L-glutamic acid and the CDs prepared from the other compounds including the widely used precursor, citric acid. The amino group of the pyroglutamic acid, along with the conjugated carbonyl system in the ring, is likely to generate the donor/acceptor-environment to bring about the fluorescence phenomenon. The

emission is, however, in a short wavelength region (443nm) owing to a limited π-conjugated system in the CD, as more the π conjugation length longer the λ_{em} reported (Yamaguchi *et al.*, 2008). This study has also confirmed that the CD acts as a peroxidase mimic and interacts electrostatically with ABTS through their complementary charges. Following the reaction with H_2O_2, the oxidized ABTS released from the CD surface, setting its surface free for the next round of reaction. The most plausible interaction of this highly water-soluble nanomaterial with H_2O_2 has been attributed to the H-bonding through its surface-oriented carboxyl functional groups, which are also catalytic and the binding sites for the peroxide as revealed from our studies. These interactions laid the foundation for the charge transfer from ABTS to H_2O_2 through CDs, which behave as a semiconducting electron trap, leading to a substrate-dependent catalytic conversion process. Based on the detailed spectroscopic studies, a reaction mechanism on the peroxidase-like activity of the synthesised CDs was comprehended as a step forward on the subject. Although, the synthesized CD demonstarted low peroxidase-like activity (as evident from high K_m) compared to the previously reported CDs (Dong *et al.*, 2015; Shi *et al.*, 2011; Wu *et al.*, 2013; Yang *et al.*, 2017; Zhao *et al.*, 2019; Zheng *et al.*, 2016; Zhu *et al.*, 2014), the foremost objective of our study was to elucidate the peroxidase-like mechanism of the CD, which would further help to design more efficient peroxidase mimic.

The thermostability of the CD, along with its simple synthesis route through a low-temperature pyrolysis method reported here, may provide ample scope for its application in developing low cost and stable sensor platforms for various peroxide-detections. Further, studies revealed that besides the colorimetric approach, the fluorescence-quenching signal from the CD could also be used for the determination of H_2O_2. The major challenge of using the CDs is their substrate-induced aggregation over time in aqueous reaction medium. To this effect, we suggest solid platforms for the peroxide sensing/assays that are expected to eliminate the diffusion led aggregation of the nanoparticles. From a preliminary study, we find chromatographic paper as a suitable platform for performing the peroxidase reaction of the CDs, where the diffusion led aggregation of the CDs likely to be averted. The understanding from the present investigation may lay the groundwork for developing the CD-based robust analytical platforms to detect H_2O_2 of diverse chemical and biological application.

Chapter 3

Multifaceted Interaction Studies between Carbon Dots and Proteins of Clinical Importance for Optical Sensing Signals

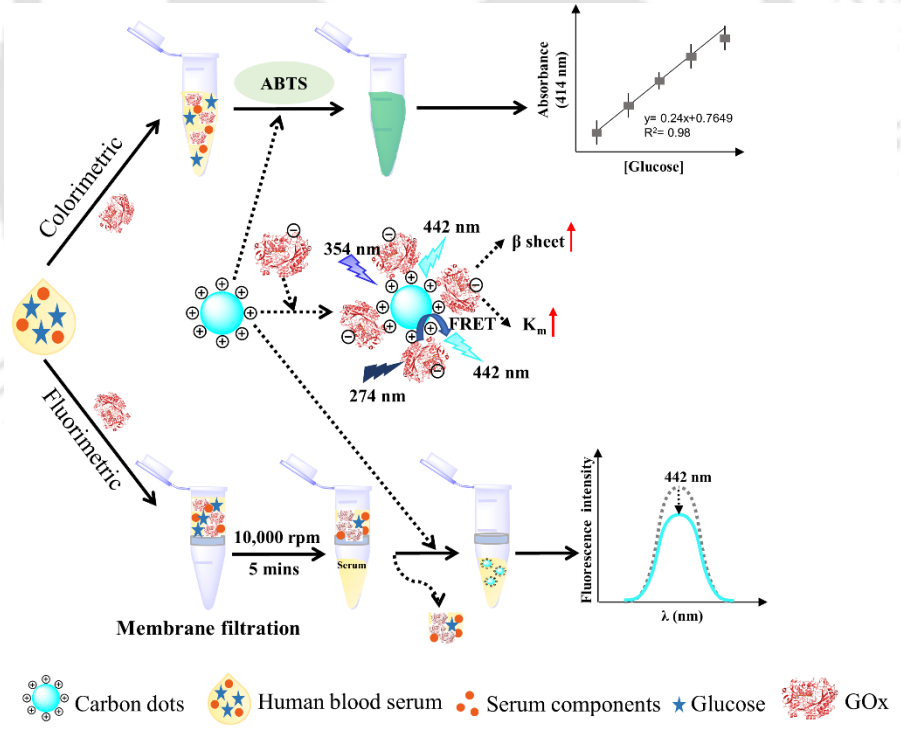

3.1 Overview

Over the last few years, carbon dots (CDs) have received wide attention due to their high-water solubility, good biocompatibility, low toxicity, high optical stability, easy surface functionalization, tuneable fluorescence property, and inexpensive and straightforward synthesis protocols (Das *et al*., 2021b). These properties have prompted the exploration of these zero-dimensional nanomaterials for diverse applications such as bioimaging, sensing, catalysis, dye-sensitized solar cells, drug delivery, and light-emitting devices (Gowthaman *et al*., 2017). Among these applications, CDs have been more aggressively studied in the analytical fields due to their tuneable and stable fluorescence properties and high peroxidative activities (Das *et al*., 2021c; Wang *et al*., 2019; Wang *et al*., 2017). However, these analytical applications urge more in-depth investigations on these sensitive optical materials for their applications in biological samples where a complex cohort of diverse molecular entities is present. Again, within these entities, the molecules and materials bestowed upon with intrinsic fluorescence properties such as proteins need more attention to avoid any fluorescence cross-talk during the analytical applications.

A plethora of reports on the peroxidatic properties of CDs that address both basic as well as application facets of these nanomaterials is available (Das *et al*., 2021c, 2021a; Dong *et al*., 2015; Gul *et al*., 2020; Kitchawengkul *et al*., 2021; Liu *et al*., 2020; Shi *et al*., 2019; Shi *et al*., 2011; Wu *et al*., 2013; Yang *et al*., 2017, 2021; Zhao *et al*., 2019; Zheng *et al*., 2016; Zhu *et al*., 2014). These properties of CDs could provide qualitative or quantitative information on the peroxides present in the sample following both fluorescence and colorimetric principles. These peroxidative functions of CDs could also be coupled with various peroxide-producing enzymatic reactions to indirectly determine the secondary analytes, which is the primary substrate for the redox enzyme catalysis the way peroxidases are used in a bienzyme colorimetric system to extract analytical information for various analytes (Ngo *et al*., 2021; Nirala *et al*., 2015; Shan *et al*., 2014). The current bienzyme systems for detecting these analytes have primarily relied upon horseradish peroxidase (HRP) that catalyses the degradation of H_2O_2. However, using multiple enzymes in a single detection platform increases the cost and complexity of the analytical devices or methods. In order to reduce these

drawbacks, CDs with several unique properties, as discussed above could be a better replacement for HRP (Das and Goswami, 2020).

The studies on CDs as optical signal generating material for clinical diagnosis is not widely known. While replacing peroxidases with CDs in bienzyme reaction systems is inspiring, the risk of interference on the optical signal of these highly sensitive zero-dimensional nanomaterials from the complex milieu of samples, including the coupled redox enzyme proteins, needs to be properly evaluated. There have been a few reports on the interaction between CDs and human serum albumin (HSA) protein (Huang *et al*., 2016; Liang *et al*., 2020; Song *et al*., 2020; Xu *et al*., 2016) However, these reports mainly focuses on the protein fluorescence behaviour occurring during the interaction. Therefore, a detailed study on the multifaceted interactions of the CDs with the coupled enzyme systems of analytical interest and predominant proteins in the samples is essential to comprehend the application scope of these optical nanomaterials as a peroxidase mimic in clinical diagnosis.

Herein, we studied the prospects of pyroglutamate (PGA) CD as a fluorescent probe for peroxide detection in enzyme-based reaction systems of clinical importance. Accordingly, we selected three enzymes, namely, cholesterol oxidase (ChOx), glucose oxidase (GOx), and alcohol oxidase (AOx), the reactions of which are routinely used for the detection of their respective analytes in clinical diagnosis. As a part of the investigation, we first studied the effect of the interactions on the fluorescence signals emanating not only from the quantum CDs but also from the protein for their TRP/TYR residues to understand any optical energy transfer between these two entities that may have any influence on the CD's analytical performance. These interactions encompass CD-enzyme protein and CD-enzyme protein-substrate in both buffer and blood serum mediums. The cause and consequence of the interactions could be divulged by dint of computational, zeta potential, and circular dichroism studies for binding energy, surface charge, and secondary structure of the proteins, respectively. We also extended these interaction studies of CDs to HSA, considering its abundance in blood serum and non-catalytic nature to evaluate its interference in the analytical fluorescence signal. For a comparative account, we also studied the CD as a colorimetric peroxide probe in conjunction with a chromogenic dye (ABTS) and generated analytical information for

the studied enzyme reaction systems. A detailed account of these aspects has been described in this chapter.

3.2 Experimental Section

3.2.1 Materials

Human serum albumin (HSA), glucose oxidase (GOx) from *Aspergillus niger*, cholesterol oxidase (ChOx) from *Streptomyces*, alcohol oxidase (AOx) from *Pichia pastoris*, horseradish peroxidase (HRP), cholesterol (Chol), and 2,2′-azino-bis (3-ethylbenzothiazoline-6-sulfonic acid) (ABTS) were obtained from Sigma Aldrich, USA. Bilirubin (BILI) was purchased from SRL, India. D-(+)-Glucose (GL), ethanol (EtOH) (99.8 %), methanol (MeOH) (99.7 %), sodium dihydrogen phosphate (NaH_2PO_4), disodium hydrogen phosphate (Na_2HPO_4), potassium dihydrogen phosphate (KH_2PO_4), dipotassium hydrogen phosphate (K_2HPO_4), sodium acetate, acetic acid was bought from HiMedia, India. The reagents were of analytical grade and used as received without further purification. All the solutions were prepared using ultrapure water (resistivity>18 MΩ.cm).

3.2.2 Synthesis of CDs

The CDs were synthesized as previously reported by our group (Das *et al*., 2021c). Briefly, 400 mg of L-glutamic acid was heated at 199 °C until it started melting and gradually changed its colour to pale yellow, followed by the addition of 4 mL of water. After stirring the reaction mixture for 30 mins, centrifugation was carried at 13,000 xg for 30 mins. The as-prepared CDs were then dialysed using a semipermeable membrane with a 1 kDa molecular weight cut-off filter. The CDs, which were rigorously characterized in our previous study (Das *et al*., 2021c), exhibits an average diameter of 3.18±0.53 nm, and appears blue under the UV-light.

3.2.3 Fluorescence Measurement

The fluorescence measurements were obtained using FluoroMax-4 (HORIBA Scientific). Each fluorescence spectrum was the average of 3 scans. The fluorescence lifetime was measured by time-correlated single-photon counting (TCSPC) using a Pico Second Time-Resolved Fluorimeter (Make: Edinburg Instruments, Model: Lifespec II) with an excitation at $\lambda_{375\ nm}$. The average lifetime was calculated using the following equation (Shang *et al*., 2014), where *Ai* is the amplitude and τ_i is the lifetime value of the ith lifetime component:

$$\tau_{avg} = \frac{\sum A_i \tau_i^2}{\sum A_i \tau_i} \qquad (3.1)$$

For each enzyme, the fluorescence experiment was performed using 10 µL of 1 mg mL^{-1} stock of each enzyme, 10 µL of stock CD solution (100 mg mL^{-1}), 5 µL of 1M of the substrate (final 5 mM), and the required amount of buffer.

3.2.4 UV-Vis Absorbance and Circular Dichroism Measurements

UV-Vis absorption spectra were recorded by a double beam Cary 60 UV-Visible spectrophotometer (Agilent Technologies). The spectra were measured from $\lambda_{200\ nm}$ to $\lambda_{800\ nm}$ in a 1 cm path length quartz cuvette. The circular Dichroism study was carried out at room temperature on a Jasco J-815 (Japan) spectropolarimeter using a 10 mm path length cuvette. The spectra were recorded in the $\lambda_{185\ nm\text{-}240\ nm}$ range at a 100 nm/min scan rate with continuous scanning. Each spectrum was the average of 3 scans and was corrected by buffer solutions. By using the online DichroWeb server and the SELCON3 analysis program, the secondary structures were predicted.

3.2.5 Zeta Potential Measurements

The zeta potential was studied by the Zetasizer nano series (Malvern Instruments Limited, UK) in a capillary cell with a gold-plated beryllium/copper electrode. All the measurements were carried out at room temperature, and each experiment was repeated three times.

3.2.6 Field Emission Transmission Electron Microscopy (FETEM) Study

FETEM was performed on JEOL JEM- 2100F at an accelerating voltage of 200 kV. The CD samples were diluted, followed by drop-casting on a carbon-coated copper grid, which was dried at room temperature and then visualized under the microscope.

3.2.7 Molecular Docking Investigation

The RCSB Protein Data Bank was used to obtain the crystal structure of ChOx (PDB ID: 1B4V), GOx (PDB ID: 1GAL), and AOx (PDB ID: 5I68). Prior to the docking study, the overall energy of the structures was first minimized using Swiss PDB Viewer, followed by removing of any water molecule and heteroatoms, adding polar hydrogen, and finally charging the enzymes using Kollman and Gasteiger charges. Subsequently, the final structure of the enzyme was utilized for the docking study.

The molecular structure of the synthesized CD is pyroglutamic acid (PGA), as determined from the previous study (Das *et al*., 2021c). The 3D model of the PGA was obtained from PubChem with ID-7405. In addition, the structure of the natural substrates of the respective enzymes, viz. Chol (ID: 5997), GL (ID: 5793), MeOH (ID: 887), was also procured from PubChem. For the docking experiment, energy minimization was carried out for all of these structures using the UCSF Chimera program, followed by the determination of their torsion roots.

The docking study was performed using the AutoDock Vina program. In order to find out the binding mode between the PGA and the enzymes, blind docking was performed, whereas for the substrates, site-specific docking was carried out. The docked structures were visualized by PyMol.

3.2.8 Studies with Blood Serum Samples

In order to demonstrate the practical applicability of CDs as a signal probe, 5 mg mL^{-1} CD was spiked in different dilutions (5-fold, 10-fold, and 50-fold) of the human blood serum sample. The guidelines of the Human Ethics Committee of the Indian Institute of Technology Guwahati, India, were followed for using the blood samples. The

mixture was incubated for 5 mins at room temperature followed by measurement of the fluorescence emission intensity at the CD's excitation wavelength ($\lambda_{ex\ 354\ nm}$). Further, the diluted serum sample with the CD was spiked with 10 µL of 1 mg mL^{-1} stock GOx and 5 µL of 1M of GL (final 5 mM) to test the efficiency.

3.2.9 Statistical Analysis of Data

All the experiments were carried out in triplicates. We used Origin 8.0 software for the statistical analysis of the data. The mean along with the standard deviation is represented as error bars in the manuscript. Statistical significance was determined using one-way analysis of variance (ANOVA) wherein * indicates a *p*-value of < 0.05, ** indicates a *p*-value of < 0.01, *** indicates a *p*-value of < 0.001, and **** indicates a *p*-value of < 0.0001. The limit of detection (LoD) was calculated using the formula $3\sigma/m$, where σ is the standard deviation of the absorbance of the blank sample and m represents the slope of the calibration curve.

3.3 Results and Discussion

3.3.1 Effect of Reaction Components and Media on the Fluorescence of CD

The reaction components considered here constitute different enzyme proteins of analytical importance namely, ChOx, GOx, and AOx, their substrates, the predominant protein in blood serum, namely, HSA, its substrate BILI and blood serum medium.

3.3.1.1 Effect of Enzyme Reaction Components on the Fluorescence of CD:

We studied the effect of ChOx, GOx, and AOx binding on the fluorescence of CD using steady-state fluorescence spectroscopy. Interestingly, the fluorescence intensity of CDs ($\lambda_{ex\ 354\ nm}$) increased significantly upon its interaction with ChOx, GOx, and AOx in buffer solution with the corresponding enhancement level of 122.22 %, 115.64 %, and 123.81 % (considering the intensity of CD as 100 %) (Figure 3.1 a). When their respective substrates were added to the reaction mixtures, the intensity drastically decreased for all the systems, except for AOx, due to the quenching effect

of H_2O_2 generated during the enzymatic reaction. The reason for void quenching in the AOx reaction system has been attributed to the solvatochromic effect of alcohol substrate that surpasses the quenching effect of the peroxide formed in the reaction.

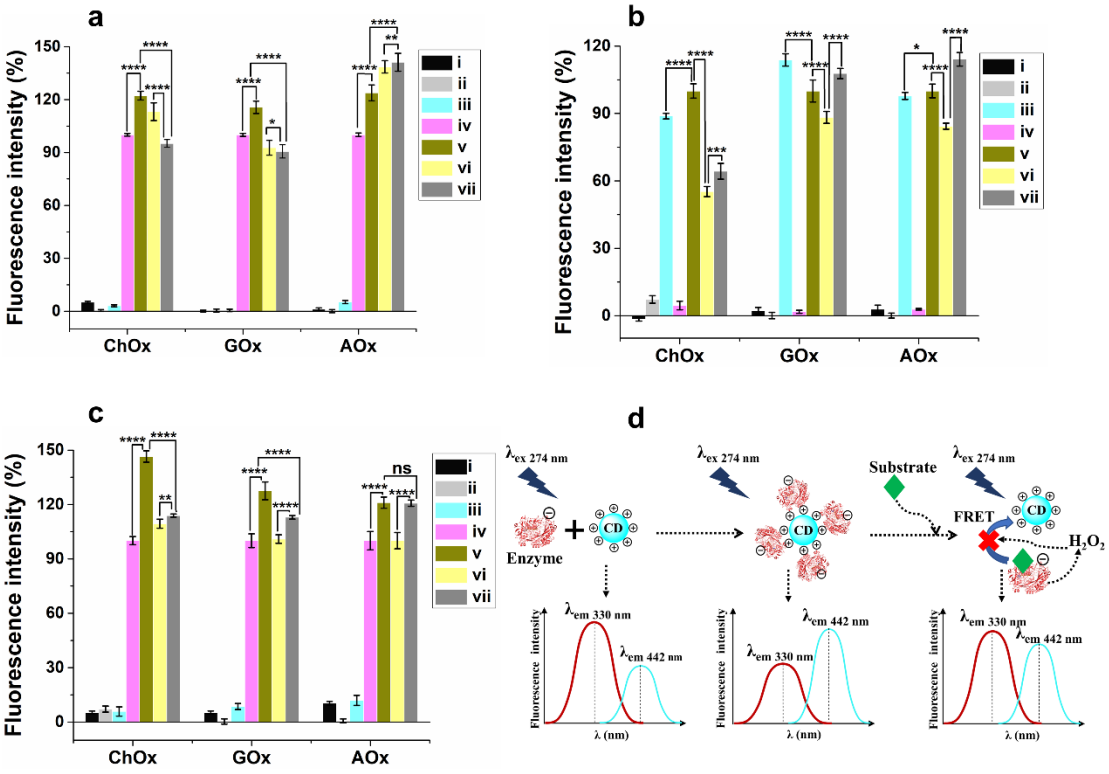

Figure 3.1. (a) Fluorescence intensity ($\lambda_{em\ 442\ nm}$) change of the CD in different reaction systems at $\lambda_{ex\ 354\ nm}$. (i) Enzyme, (ii) Substrate, (iii) Enzyme+Substrate, (iv) CD, (v) CD+Enzyme (after 5 min incubation), (vi) CD+Substrate, and (vii) CD+Enzyme+Substrate. Fluorescence intensity change at $\lambda_{ex\ 274\ nm}$ (for TRP/TYR) in different reaction systems. (b) florescence ($\lambda_{em\ 330\ nm,}$) in (i) CD, (ii) Substrate, (iii) Enzyme+Substrate (iv) CD+Substrate, (v) Enzyme (vi) CD+Enzyme (after 5 mins), (vii) CD+Enzyme+Substrate. (c) fluorescence ($\lambda_{em\ 442\ nm}$) in (i) Enzyme, (ii) Substrate, (iii) Enzyme+Substrate, (iv) CD, (v) CD+Enzyme (after 5 mins), (vi) CD+Substrate, (vii) CD+Enzyme+Substrate. The significance level is set as $p<0.05$ (8), $p<0.01$ (**), $p<0.001$ (***), and $p<0.0001$ (****). No significance (ns).(d) Schematic representation of the interactions.

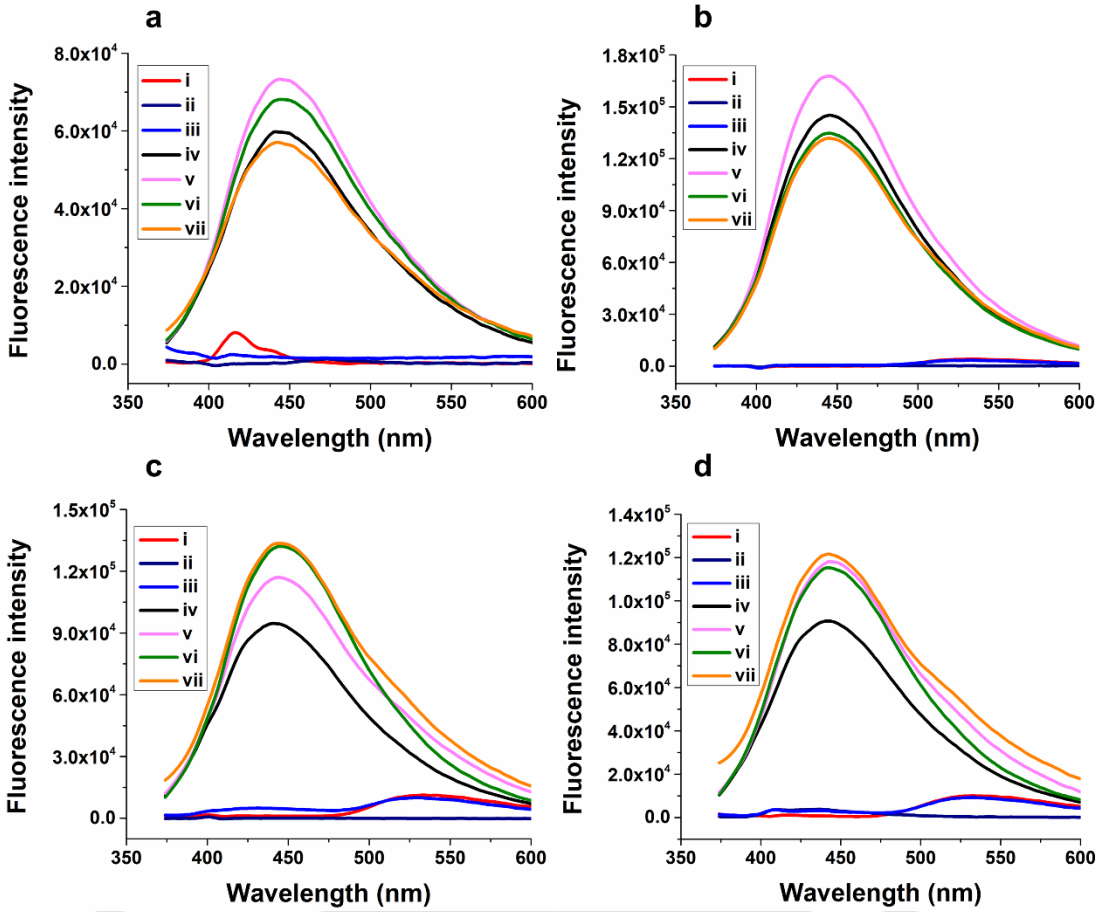

Figure 3.2. (a) Fluorescence change of different reaction systems at the CD excitation wavelength ($\lambda_{354\,nm}$). (i) ChOx, (ii) Chol, (iii) ChOx+Chol, (iv) CD, (v) CD+ChOx (after 5 mins), (vi) CD+Chol, (vii) CD+ChOx+Chol. (b) (i) GOx, (ii) GL, (iii) GOx+GL, (iv) CD, (v) CD+GOx (after 5 mins), (vi) CD+GL, (vii) CD+GOx+GL. (c) (i) AOx, (ii) MeOH, (iii) AOx+MeOH, (iv) CD, (v) CD+AOx (after 5 mins), (vi) CD+MeOH, (vii) CD+AOx+MeOH. (d) (i) AOx , (ii) EtOH, (iii) AOx+EtOH, (iv) CD, (v) CD+AOx (after 5 mins), (vi) CD+EtOH, (vii) CD+AOx+EtOH.

The circular dichroism studies showed that the binding of CD to the enzyme proteins causes a significant shift to the protein's secondary structure (Table 3.1 & Figure 3.3). The shift was mainly towards the *β* contents, at the cost of mostly helix contents of the proteins. A shift of more than 50 % towards beta contents was observed in the case of ChOx and GOx proteins. The shift towards the beta content further increased in the presence of the respective substrates of the enzymes, except for GOx, where a drastic negative trend (> 50 %) was identified. It is likely that a part of the GOx enzyme with *β* sheet turned into α helix.

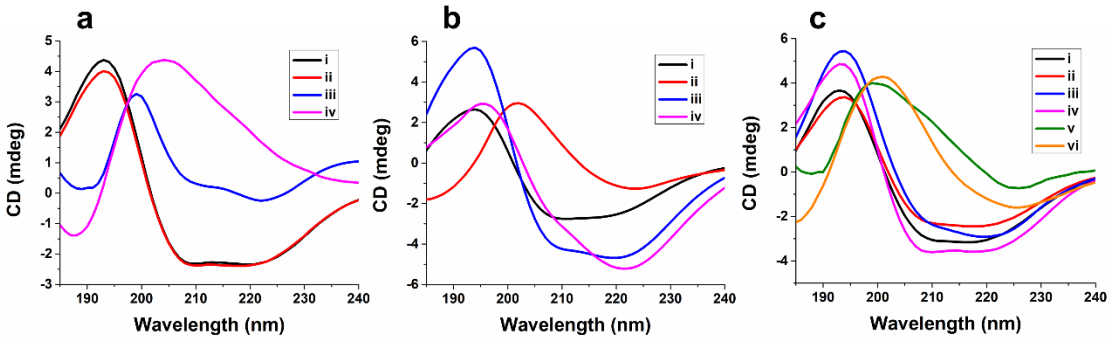

Figure 3.3. (a) Circular dichroism spectra of (i) ChOx, (ii) ChOx+CD, (iii) ChOx+Chol, (iv) ChOx+Chol+CD. (b) Circular dichroism spectra of (i) GOx, (ii) GOx+CD, (iii) GOx+GL, (iv) GOx+GL+CD. (c) Circular dichroism spectra of (i) AOx, (ii) AOx+CD, (iii) AOx+EtOH, (iv) AOx+MeOH, (v) AOx+EtOH+CD, (vi) AOx+MeOH+CD.

Table 3.1: The content of different secondary structures of the enzymes in different reaction systems.

Reaction systems	**α Helix % (% change)**	**β strand % (% change)**	**Turns % (% change)**	**Unordered % (% change)**
ChOx (control)	34.5 (0)	11.0 (0)	23.1 (0)	31.3 (0)
ChOx+CD	30.2 (-12.50) ↓	17.8 **(+61.81)** ↑	22.5 (-2.60)	29.5 (-5.75)
ChOx+Chol	1.9 (-94.50) ↓	43.3 (+293.63) ↑	21.9 (+5.11)	32.9 (+5.11)
ChOx+Chol+CD	9.2 (-73.40) ↓	46 (+318.20) ↑	10.9 (+8.30)	33.9 (+8.30)
GOx (control)	21.5 (0)	31.1 (0)	21.5 (0)	26.8 (0)
GOx+CD	8.3 (-61.40) ↓	47.9 **(+54.01)** ↑	11.9 (-44.65)	33.8 (+26.11)
GOx+GL	39.9 (+85.60) ↑	16.6 (-46.62) ↓	19.6 (-8.83)	25.0 (-6.71)
GOx+GL+CD	38.0 (+76.74) ↑	14.5 (-53.40) ↓	20.8 (-3.25)	31.1 (+16.04)
AOx (control)	16.6 (0)	25.9 (0)	23.8 (0)	33.4 (0)
AOx+CD	15.6 (-6.02) ↓	30.3 **(+16.98)** ↑	18.4 (-22.70)	23.3 (-30.23)
AOx+MeOH	23.5 (+41.56) ↑	22.9 (-11.60) ↓	23.3 (-2.10)	28.0 (-16.16)
AOx+MeOH+CD	9.6 (-42.16) ↓	41.7 (+61.00) ↑	18.7 (-21.42)	30.0 (-10.17)

% change was calculated by considering 100 as the value for the respective secondary structural components for the corresponding proteins being considered as control. Negative and positive symbols imply decrease and increase, respectively. [say, for ChOx helix, 34.5 =100, hence change for ChOx+CD is 12.46 %, so in bracket (-12.46)].

The CD reported here is made up of PGA molecules, the surface of which is covered with carbonyl, carboxyl, and amine functional groups (Das *et al*., 2021c). The docking study showed that the PGA binds with ChOx (ΔG value: -5.8 kcal mol^{-1}), GOx (-6.3 kcal mol^{-1}), and AOx (-5.9 kcal mol^{-1}) with high affinity, as revealed from the corresponding binding energy shown in the parentheses. The binding is facilitated by the electrostatic interaction between the negatively charged enzyme proteins ($pI < 7$) and positively charged CDs, which is revealed from the zeta potential study described in the next section (Figure 3.5). This high binding energy might be responsible for the significant swing of the secondary structure as manifested from the above circular dichroism study.

3.3.1.2 Effect of HSA, BILI, and Serum on the Fluorescence of CD:

HSA, with a molecular mass of 67 kDa, is the most bountiful protein in the human plasma. It plays a vital role as a natural carrier of various substances in the blood. Monitoring the fluorescence response of CD in the presence of HSA will give an insight into the level of interference of blood serum on the CD-based clinical diagnosis of analytes. UV-Vis absorption and fluorescence of CDs upon their interaction with HSA were studied (Figure 3.4). There is a trivial increase in absorbance of the broad absorption band of the CDs at ~325 nm corresponding to n-Π* transition of C=O (Figure. 3.4 a). The florescence intensity of the CD also increased upon its interaction with the HSA, while the magnitude of enhancement (127.85 %) was comparatively higher than those that occurred with the enzyme proteins. Steady-state fluorescence spectroscopy (Figure 3.4 b) indicated a progressive enhancement of the CDs fluorescence in a time scale of 2 to 10 mins upon the binding of HSA. The zeta potential results showed that the CDs and HSA carry opposite charges, and therefore interact electrostatically (Figure 3.5 a). Additionally, surface charge interaction of protein and nanoparticles also plays a pivotal role in the formation of protein corona (Shang *et al*., 2014). The FETEM images of CD+HSA unveiled that the HSA adsorb onto the CD's surface, forming a protein corona (Figure 3.6 a). The average size of the CD+HSA was ~21.76 nm, as estimated from the FETEM study. Consistent with this finding, UV-Vis spectra showed that with increasing HSA concentration, there was progressive shift of the CD spectra indicating increase in the size of the nanomaterial (Figure 3.7).

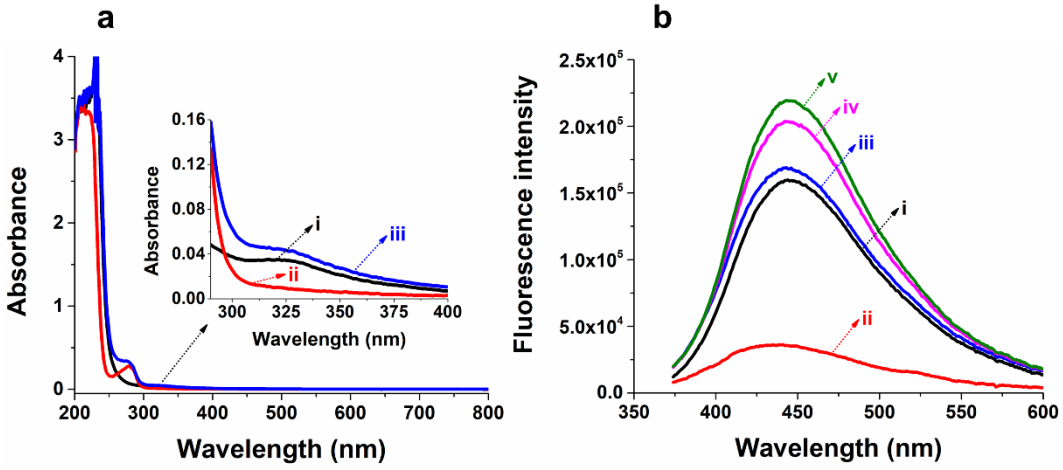

Figure 3.4. (a) Absorbance of different reaction systems: (i) CD, (ii) HSA, and (iii) CD+HSA. (b) Fluorescence emission (i) CD, (ii) HSA, and CD+HSA at (iii) 2 mins, (iv) 6 mins, and (v) 10 mins at excitation of CD (at $\lambda_{ex\ 354\ nm}$) (Inset: Fluorescence intensity of CD+HSA at different time intervals. Experiment was carried out using 50 µL of stock 10.3 mg mL^{-1} HSA and 10 µL of stock CD solution (100 mg mL^{-1}).

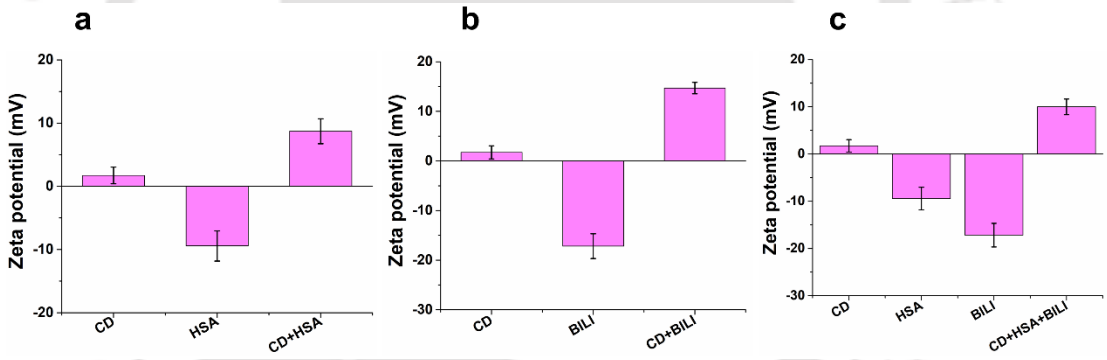

Figure 3.5. Zeta potential of (a) CD, HSA, and CD+HSA, (b) CD, BILI, and CD+BILI, and (c) CD, HSA, BILI, and CD+HSA+BILI. The concentration of CD (1 mg mL^{-1}), HSA (0.52 mg mL^{-1}), and BILI (2 µM) used in the reaction mixture are shown in the bracket.

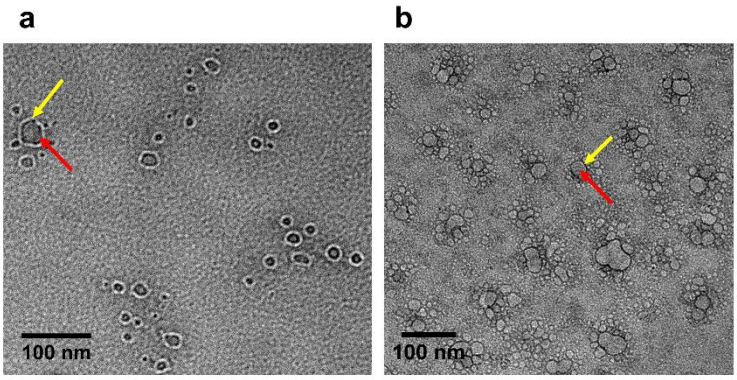

Figure 3.6. FETEM image of the interaction between (a) CD and HSA, and (b) CD+BILI. The respective outer layer of HSA in (a) and BILI in (b) is shown with yellow arrow, and the CD is shown in red in both the cases.

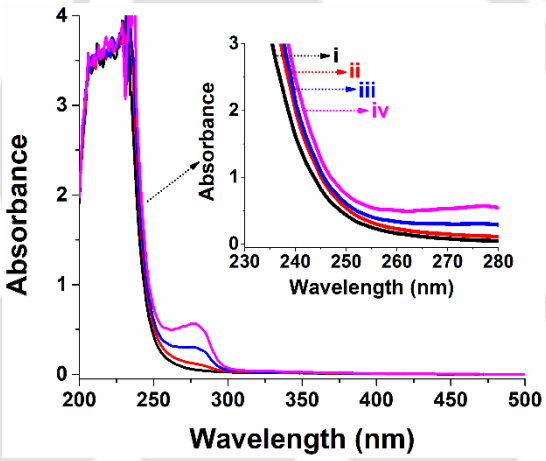

Figure 3.7. UV-Vis spectra of CD and increasing concentrations of HSA. (i) CD, (ii) CD+103 μg mL^{-1} HSA, (iii) CD+515 μg mL^{-1} HSA, (iv) CD+1.03 mg mL^{-1} HSA. The concentration of CD used in the experiment is 1 mg mL^{-1}.

Time-resolved fluorescence lifetime measurement elucidated the fundamental fluorescence enhancement mechanism (Table 3.2, Figure 3.8 a). The interaction of HSA with CD resulted in a slower decay time leading to an average lifetime increasing from 7.68 ns to 8.31 ns (Table 3.2). Analysis revealed that the increased lifetime was due to the longest lifetime component on the CD's surface (1st component); the fractional weight (f) of this component increased from 16.60 % to 29.66 % upon HSA binding. Since HSA is considered a model protein, this finding indicates that the observed fluorescence enhancement in case of ChOx, GOx, and AOx is a consequence

of the interaction between the protein/enzyme and the CD's surface that influenced the fluorescence behaviour of the 1st component.

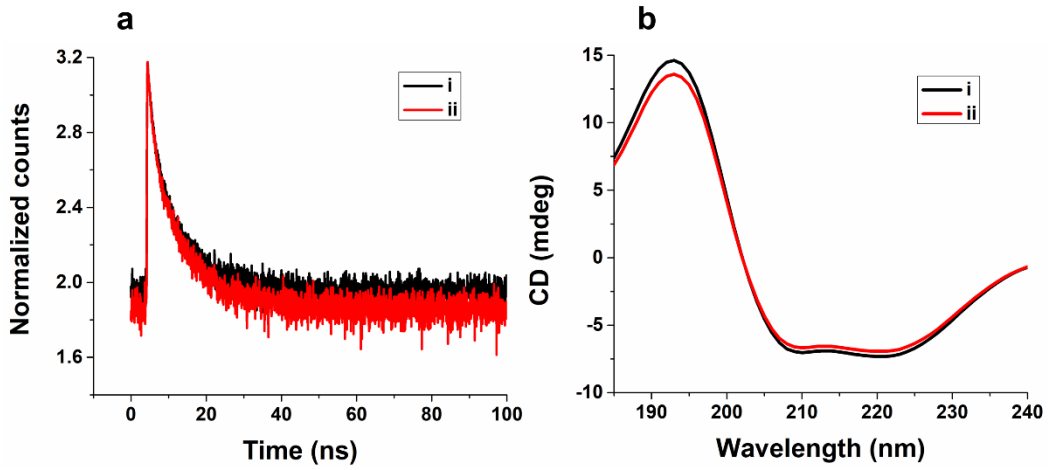

Figure 3.8. (a) Time resolved fluorescence spectra of (i) CD, and (ii) CD+HSA, (b) Circular Dichroism spectra of (i) HSA, (ii) CD+HSA.

Table 3.2: Multi-exponential components for the observed fluorescence decay of CDs in the absence and presence of HSA. The % f shown in parentheses.

Reaction system	**τ_1 (ns) (f_1)**	**τ_2 (ns) (f_2)**	**τ_3 (ns) (f_3)**	**$<\tau>$**
CD	0.665 (16.63 %)	2.575 (39.873 %)	9.19 (43.497 %)	7.68366
CD+HSA	0.947 (29.667 %)	3.671 (39.279 %)	10.902 (31.055 %)	8.313481
CD+BILI	0.54 (14.176 %)	2.326 (40.843 %)	9.229 (44.981 %)	7.834011
CD+HSA+BILI	0.729 (21.407 %)	2.809 (39.149 %)	9.576 (39.445 %)	7.823116

The conformation change of HSA protein upon the interaction with the blue and green-emitting CDs has been reported (Huang *et al*., 2016; Liang *et al*., 2020; Xu *et al*., 2016). According to Liang *et al*., the interaction of CD with the HSA resulted in a notable reduction in the negative ellipticity of the α-helix, illustrating unfolding and increased hydrophilicity of the HSA. In the present investigation, the circular dichroism spectroscopy study showed that the bands at 190 nm, 210 nm, and 220 nm decreased

slightly, suggesting some perturbation of the HSA's secondary structure following the binding of CD (Table 3.3, Figure 3.8 b).

Table 3.3. The content of different secondary structures of HSA in the absence and presence of CD.

Reaction system	α Helix (%)	β strand (%)	Turns (%)	Unordered (%)
HSA	48.1	10.2	17.2	25.1
HSA+CD	48.0	11.4	17.8	25

For a more systematic study, we also chose BILI, a yellowish pigment transported by HSA in serum. The effect of BILI on the CDs was studied both by measuring the absorbance and fluorescence. As shown in Figure 3.9 a, with the addition of BILI to the CDs, the absorbance of the CDs increased, accompanied by a slight blue shift illustrating the interaction between the two. Meanwhile, a shoulder peak around 500 nm was generated at the BILI absorbance band after the interaction of CDs with BILI (Figure 3.9 b). The fluorescence spectra for the CD+BILI reaction system were recorded corresponding to the CDs excitation wavelength ($\lambda_{ex\ 354\ nm}$). The fluorescence of the CDs is gradually increased with increasing BILI concentration (Figure 3.9 c). Zeta potential measurements revealed that the main interacting force between CDs and BILI might be electrostatic (Figure 3.5 b). The FETEM image shows that the BILI form a layer onto the surface of the CDs (Figure 3.6 b). Fluorescence lifetime measurement was performed to understand the contribution of different CD's components in the underlying fluorescence enhancement (Table 3.2, Figure 3.9 d). Upon the interaction of BILI, the fluorescence lifetime of the CD increased from 7.68 ns to 7.83 ns. In contrast to the previous results obtained for HSA, the main contribution to the fluorescence enhancement with BILI was the 2^{nd} and 3^{rd} components. The fractional weight of the 2^{nd} component increased from 39.87 % to 40.84 %, and that of the 3^{rd} component increased from 43.50 % to 45.0 %.

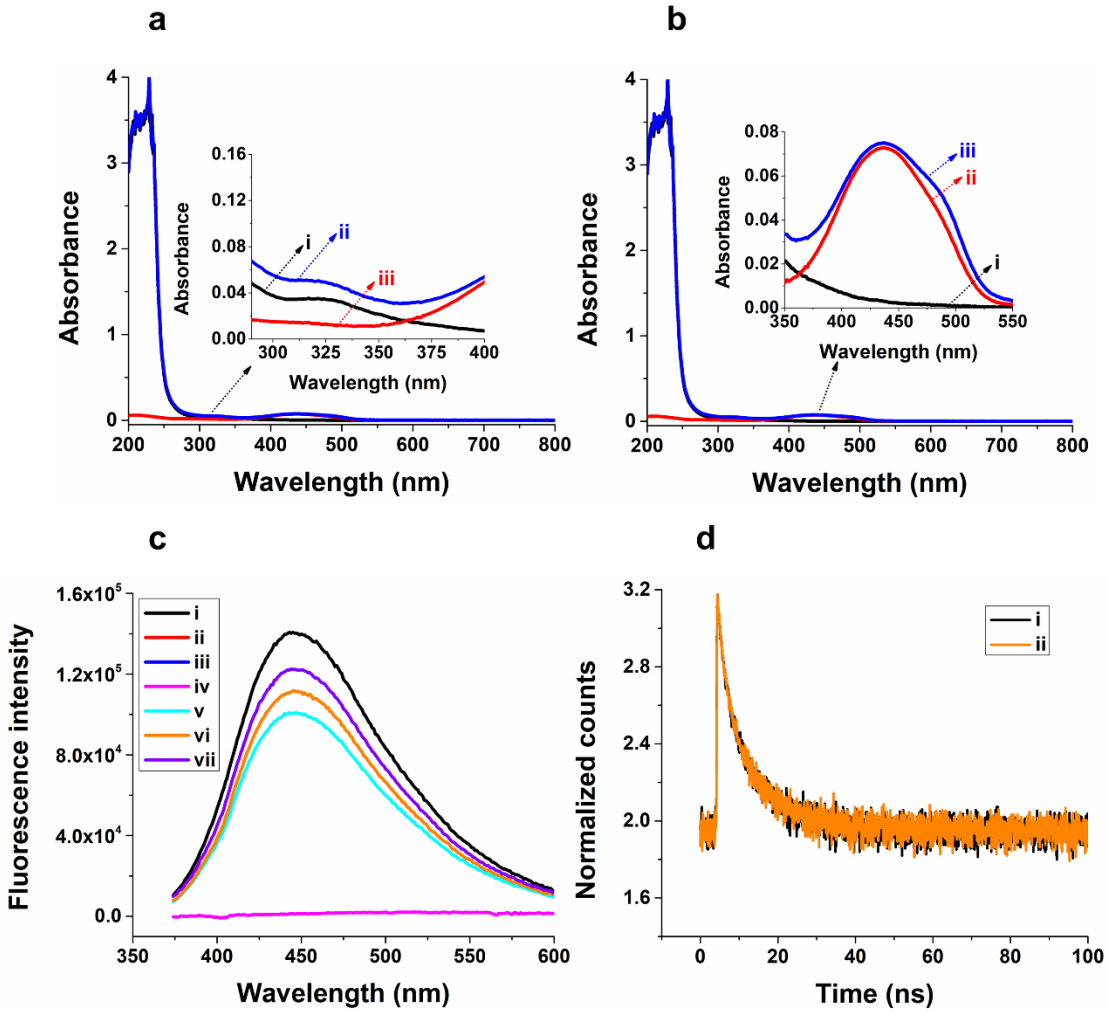

Figure 3.9. (a) Effect of BILI on absorbance of CD. (i) CD, (ii) BILI, and (iii) CD+BILI. (b) Effect of CD on the absorbance of BILI. (i) CD, (ii) BILI, (iii) CD+BILI. (c) Fluorescence of (i) CD, (ii) 0.02 μM BILI, (iii) 0.3 μM BILI, (iv) 2.43 μM BILI, (v) CD+0.02 μM BILI, (vi) CD+0.3 μM BILI, (vii) CD+2.43 μM BILI. (d) Time resolved fluorescence spectra of (i) CD, and (ii) CD+BILI. The concentration of CD used in the experiment is 1 mg mL^{-1}.

BILI has a natural affinity to HSA. Therefore, the molecular interaction of CDs with HSA bound to the BILI was also investigated. We incubated the CDs with HSA in the presence of BILI for 5 mins. The absorbance of HSA and BILI has a similar type of variation as observed in the previous cases when CD interacted with them individually (Figure 3.10 a). At the CD's excitation wavelength, the CD+HSA+BILI system exhibited similar fluorescence enhancement as observed in the case of CD+HSA system (Figure 3.10 c); nevertheless, the maximum emission intensity of the latter was ~12 %

more than that of the former. As displayed in the zeta potential study, the interaction of CD with HSA+BILI is also electrostatic (Figure. 3.5 c). Moreover, the time-resolved fluorescence decay of the CD+HSA+BILI system was calculated as 7.82 ns (Table 3.2, Figure 3.10 d). The results illustrated that the fluorescence enhancement in the CD+HSA+BILI reaction system is due to the 1st component. By utilizing circular dichroism spectroscopy, we enquired for any conformation change of HSA in the presence of both CD and BILI. Like the previous result, the characteristic band at 190 nm, 210 nm, and 220 nm decreased slightly, illustrating some perturbation of the HSA's secondary structure following the binding of CD and BILI (Table 3.4, Figure 3.11).

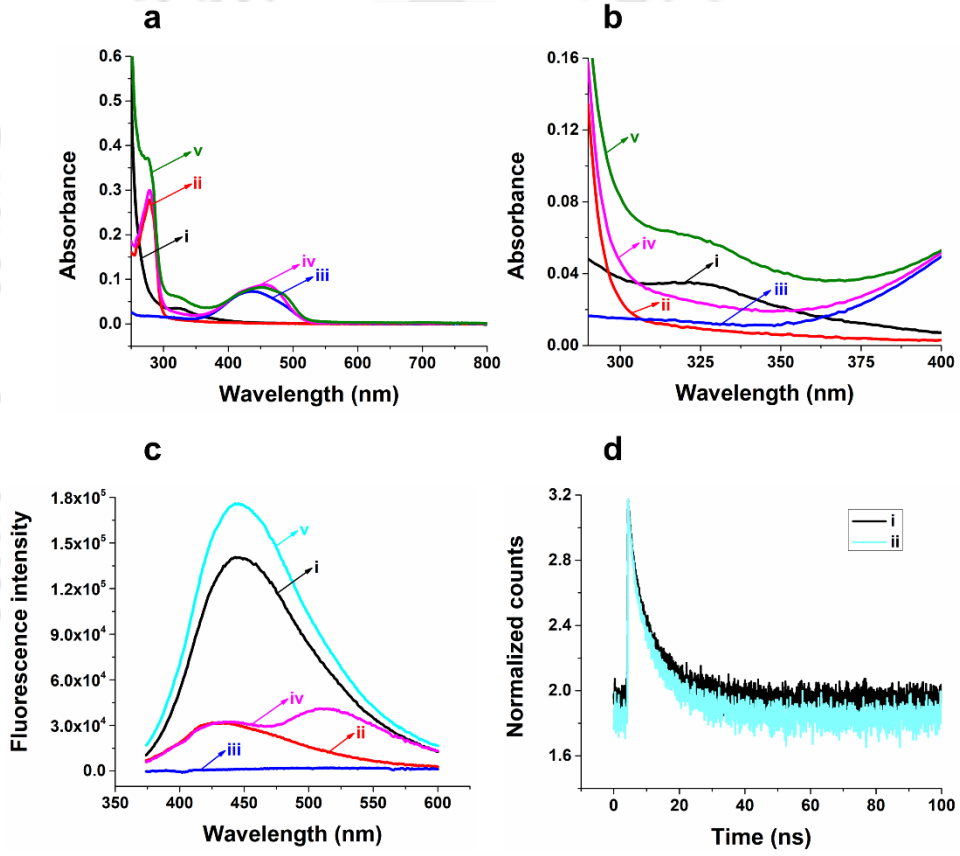

Figure 3.10. (a) Effect of CD on the absorbance of HSA+BILI. (i) CD, (ii) HSA, (iii) BILI, (iv) HSA+BILI, (v) CD+HSA+BILI. (b) Effect of HSA+BILI on the absorbance of CD. (i) CD, (ii) HSA, (iii) BILI, (iv) HSA+BILI, (v) CD+HSA+BILI. (c) Effect of HSA+BILI on the fluorescence of CD (CD excitation wavelength: 354 nm). (i) CD, (ii) HSA, (iii) BILI, (iv) HSA+BILI, (v) CD+HSA+BILI. (d) Time resolved fluorescence spectra of (i) CD, and (ii) CD+HSA+BILI. Experiment was carried out using 50 µL of stock 10.3 mg mL^{-1} HSA, 10 µL of stock CD solution (100 mg mL^{-1}), and 20 µL of stock 100 µM BILI.

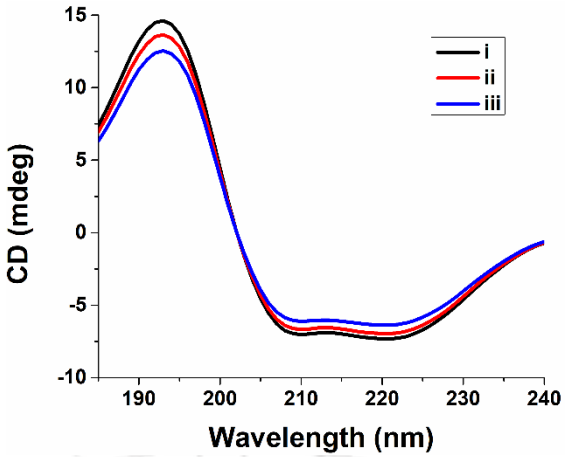

Figure 3.11. Circular Dichroism spectra of (i) HSA, (ii) HSA+BILI, (iii) HSA+BILI+CD.

Table 3.4. The content of different secondary structures of HSA in different reaction systems.

Reaction system	α Helix (%)	β strand (%)	Turns (%)	Unordered (%)
HSA	48.1	10.2	17.2	25.1
HSA+BILI	47.7	12.9	17.5	25.1
HSA+CD+BILI	45.1	13.7	19.7	26.4

To assess the practical applicability, we utilized the blood serum of a healthy individual to check its effect on the optical property of the CDs. Even a 50-fold diluted serum exhibited noticeable fluorescence at the CD's excitation wavelength ($\lambda_{354\ nm}$) (Figure 3.12 a). The autofluorescence of the blood serum at the $\lambda_{ex\ 354\ nm}$ is mainly due to enzyme-bound NAD(P)H (Wolfbeis and Leiner, 1985). When CD was mixed with the blood serum, the fluorescence of the CD significantly increased compared to the CD in the buffer system. The high fluorescence intensity might be due to the interaction between the serum components and the CDs or the synergistic effect between the two.

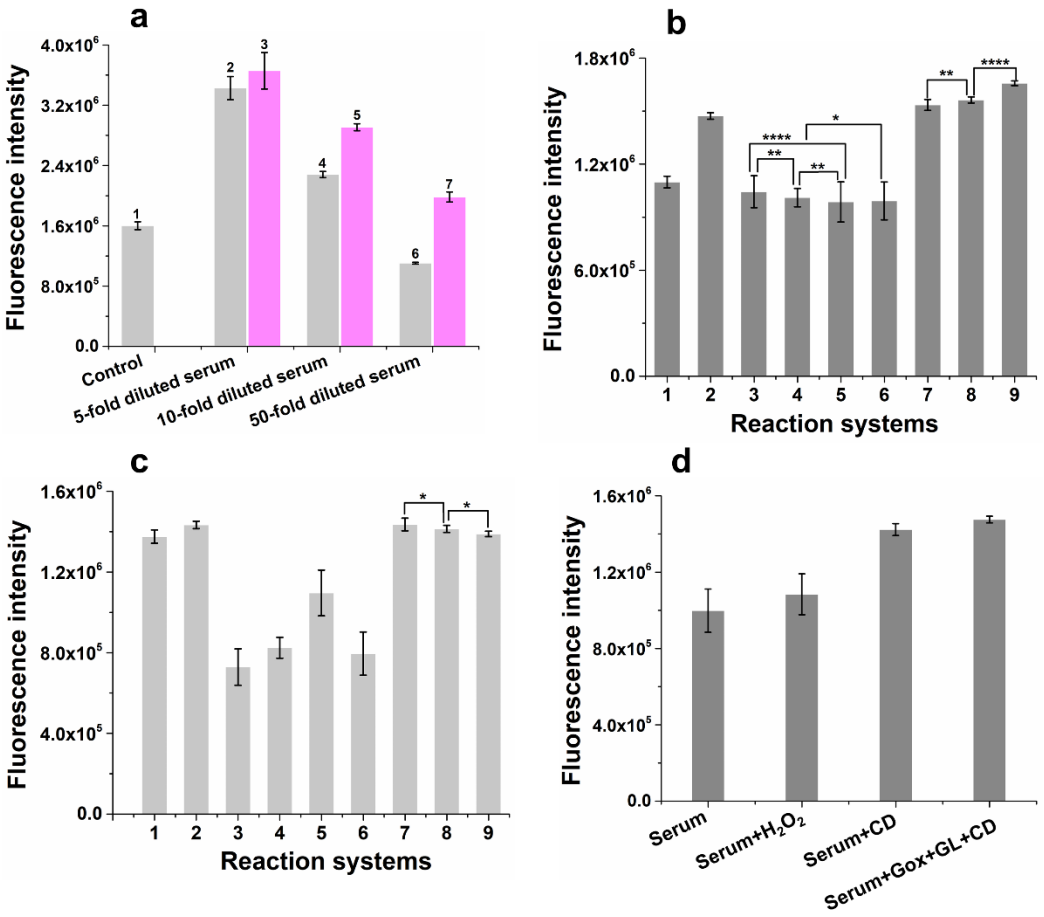

Figure 3.12. (a) Effect of blood serum on the optical property of CD. (1) CD (control), (2) 5-fold diluted serum (control), (3) 5-fold diluted serum+CD, (4) 10-fold diluted serum (control), (5) 10-fold diluted serum+CD, (6) 50-fold diluted serum, (7) 50-fold diluted serum+CD. Comparison of the fluorescence intensity of different reaction systems namely, (1) CD, (2) CD+GOx, (3) serum, (4) serum+GOx, (5) serum+GL, (6) serum+GOx+GL, (7) serum+CD, (8) serum+CD+GOx, (9) serum+CD+GOx+GL: (b) with 50 % diluted serum, and (c) with filtered 50 % diluted serum. (d) Comparison of the fluorescence intensity of different reaction systems using filter residue.

3.3.2 Effect of CD on the Fluorescence of Proteins

At $\lambda_{ex\ 274\ nm}$ (TRP/TYR), the effect of CD on the fluorescence ($\lambda_{em\ 330\ nm}$) of ChOx, GOx, and AOx proteins was studied (Figure 3.1 b). The emission was significantly quenched in all the three proteins, with a slight blue shift for ChOx observed (Figure 3.13 a), indicating that the binding of CD influenced the polarity of the microenvironment surrounding the TRP/TYR residues in the protein. The excitation also changed the intensity of the CDs ($\lambda_{em\ 442\ nm}$) (Figure 3.1 c). In all the three cases,

the intensity of the CD was increased in the presence of the enzyme proteins, suggesting the FRET occurring between TRP/TYR and CD (Figure 3.1 b and 3.1 c). Interestingly, upon the addition of substrate to their respective enzymes+CD reaction systems, an increase in the corresponding protein's fluorescence intensity was detected (Figure 3.1 b) (for substrate EtOH see Figure 3.13), indicating the *in-situ* generated peroxide hampered FRET between enzyme and CD. The interaction of CD and the proteins (*Pf*GDH) that initiates FRET has been previously reported, which was ascribed to protein-induced fluorescence enhancement of CD due to FRET (Singh *et al*., 2018). During the interaction with the protein, the surface state of the CDs might be acting as a trap for electronic energy (Liu *et al*., 2019; Semeniuk *et al*., 2019), which subsequently resulted in the enhancement of its fluorescence.

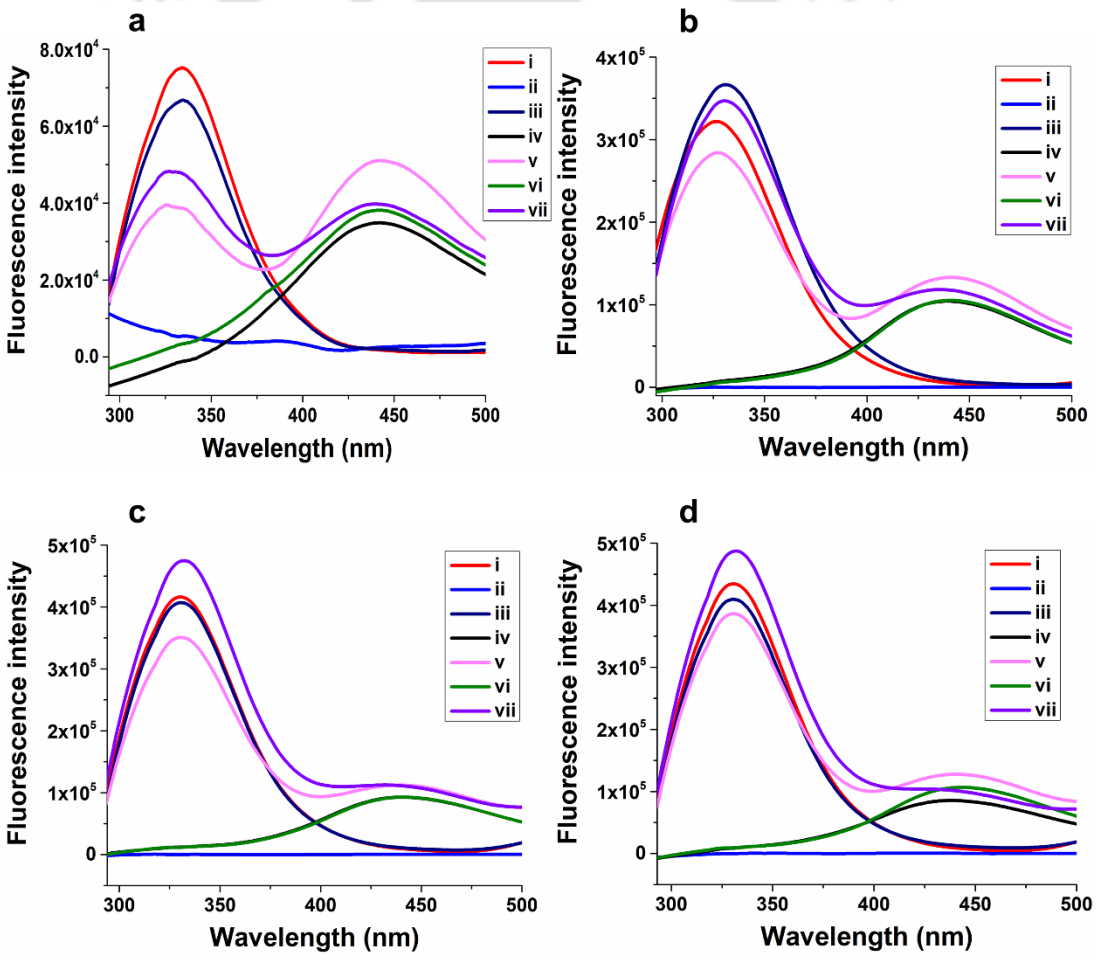

Figure 3.13. (a) Fluorescence change of different reaction systems at the ChOx excitation wavelength ($\lambda_{274\ nm}$). (i) ChOx, (ii) Chol, (iii) ChOx+Chol, (iv) CD, (v) CD+ChOx (after 5 mins), (vi) CD+Chol, (vii) CD+ChOx+Chol. (b) Fluorescence change of different reaction systems at the GOx excitation wavelength ($\lambda_{274\ nm}$): (i)

GOx, (ii) GL, (iii) GOx+GL, (iv) CD, (v) CD+GOx (after 5 mins), (vi) CD+GL, (vii) CD+GOx+GL. (c) Fluorescence change of different reaction systems at the AOx excitation wavelength ($\lambda_{274\ nm}$): (i) AOx , (ii) MeOH, (iii) AOx+MeOH, (iv) CD, (v) CD+AOx (after 5 mins), (vi) CD+MeOH, (vii) CD+AOx+MeOH. (d) Fluorescence change of different reaction systems at the AOx excitation wavelength ($\lambda_{274\ nm}$): (i) AOx , (ii) EtOH, (iii) AOx+EtOH, (iv) CD, (v) CD+AOx (after 5 mins), (vi) CD+EtOH, (vii) CD+AOx+EtOH.

In the case of ChOx, PGA binds in a pocket between the substrate (cholesterol) and the enzyme's cofactor (Figure 3.14). Within the binding pocket, PGA interacts via hydrophobic bonds with nine amino acid residues, viz. TRP67, ARG71, THR72, GLU73, ALA74, PRO75, ASP97, TYR107, TYR219, and hydrogen bonds with SER65, SER66, LYS69, ARG98 residues of the ChOx enzyme (Figure 3.14 c). In agreement with the fluorescence experiment results, the docking studies suggest a favourable interaction of the PGA with the TRP67 amino residue of the ChOx enzyme that might also be responsible for the observed blue shift (Figure 3.13 a). In the case of GOx, the PGA interacts primarily with the TYR68, ASN107, GLY108, GLN347, GLU412, PHE414, TRP426, ASN514, TYR515 amino acid residues via hydrophobic bond, and hydrogen bond with the THR110, HIS516, HIS559 residues (Figure 3.15 c). Whereas, in the case of AOx, the best binding sites for PGA appeared on the enzyme's surface while some sites also overlapped with the active site (Figure 3.16 c). Within the binding pocket, PGA interacts via hydrophobic bond with the PHE282, GLY283, LYS287, LEU288, LEU299, GLY301, VAL302, GLY303, ILE429, HIS430, TRP585 residues and hydrogen bond with the GLN278, ASP284, PRO300, ARG304 residues. In all the cases, the binding of TRP/TYR residues involved. This binding event might expose the TRP/TYR residues in the protein matrix resulting in increased fluorescence intensity. This study also identified the functional groups of the PGA, -C=O, -COOH, and -NH, in the binding with the amino acid residues of the enzymes (Figure 3.17 and Table 3.5).

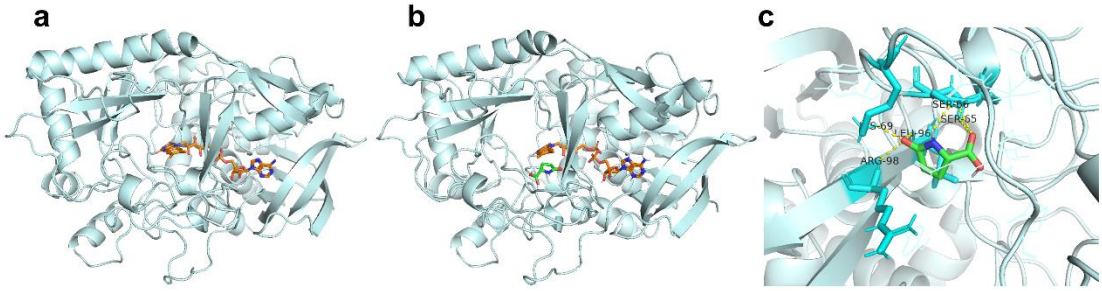

Figure 3.14. (a) Crystallographic structure of ChOx with the FAD (orange). (b) Best binding pose for PGA (green) with ChOx. (c) Amino acid residues in ChOx that form hydrogen bond with PGA.

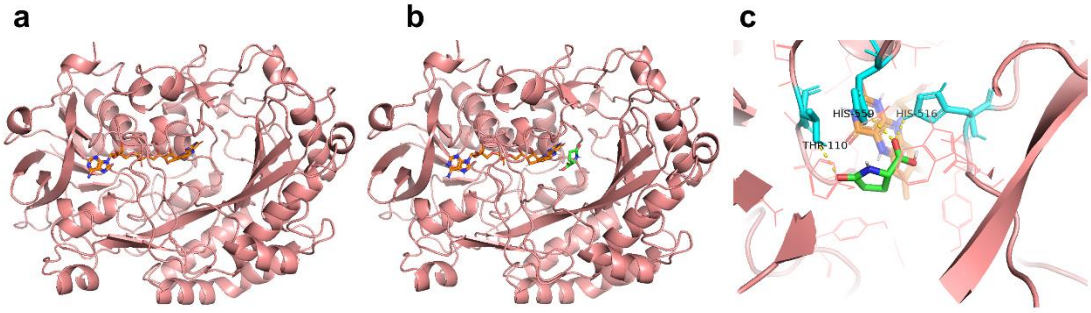

Figure 3.15. (a) Crystallographic structure of GOx with the FAD (orange). (b) Best binding pose for PGA (green) with GOx. (c) Amino acid residues in GOx that form hydrogen bond with PGA.

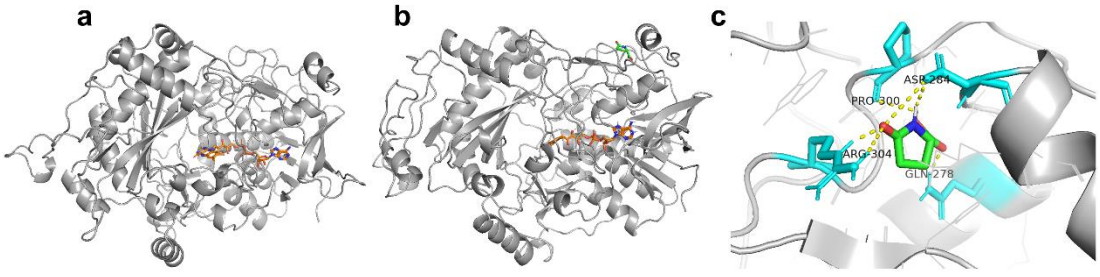

Figure 3.16. (a) Crystallographic structure of AOx with the FAD (orange). (b) Best binding pose for PGA (green) with AOx. (c) Amino acid residues in AOx that form hydrogen bond with PGA.

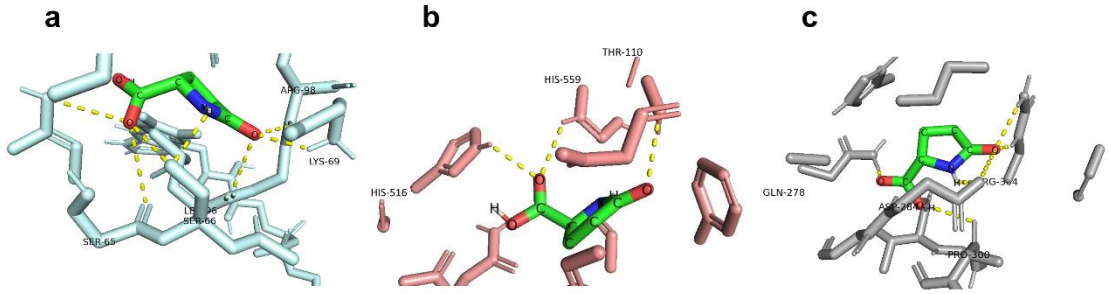

Figure 3.17. Different functional groups of the PGA involved in the binding with amino acids of (a) ChOx, (b) GOx, and (c) AOx.

Table 3.5 Binding of the different functional groups of the PGA to the amino acid residues of the enzymes.

Functional groups	ChOx	GOx	AOx
-C=O	LYS69, LEU96, ARG98	THR110	ARG304, ASP284
-COOH	SER65, SER66, TYR219	HIS516, HIS559	GLN278, PRO300
-NH	SER66	-	ASP284

Through the molecular docking studies, the binding sites of the substrate with the respective enzyme were also analysed (Table 3.6). The distance between PGA and the respective substrates of the enzyme, i.e., Chol, GL, and MeOH, was found to be 8.1 Å, 11.2 Å, and 19.3 Å, respectively (Figure 3.18).

Table 3.6 Binding site of the substrates with their respective enzyme.

Enzyme	Substrate	Interacting amino acids (hydrophobic bond)	Interacting amino acids (hydrogen bond)
Cholesterol oxidase	Chol	ASN70, ARG71, THR72, GLU73, ALA74, PRO75, LEU76, SER78, PHE79, ASN86, ARG98, TYR107, LEU432, PHE433, GLY434	GLY77
Glucose oxidase	GL	TYR80, ILE94, ARG95, SER103, ALA289, GLY290, VAL293, SER294, ASP328, TYR450, TYR515, HIS516, VAL518, ASP548, SER550	SER96, SER291, ALA292, GLY517, GLY549
Alcohol oxidase	MeOH	LYS6, ALA87, GLY269, THR270, ILE271, LYS568	-

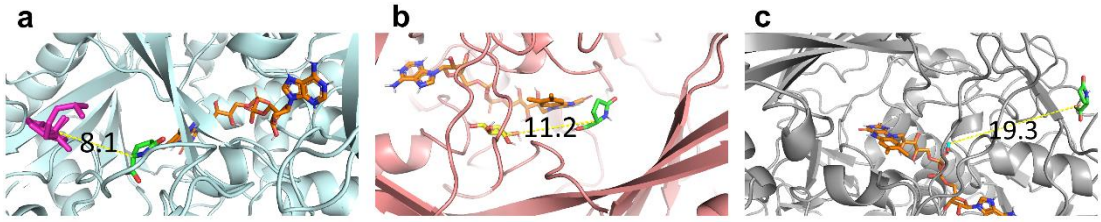

Figure 3.18. Distance between PGA and different substrates of the respective enzyme. (a) ChOx+Chol+CD, (b) GOx+GL+CD, (c) AOx+MeOH+CD. The hydrogen bonding is shown in imaginary yellow lines.

The effect of CD on the optical property of the HSA protein was also studied. Addition of CDs to the HSA resulted in the variation of the HSA's absorbance band, indicating that the CDs interact with the HSA (Figure 3.19 a). A similar blue shift of the HSA's fluorescence, as observed for ChOx, was found upon the binding of the CD (Figure 3.19 b). Meanwhile, with increasing time intervals, the intrinsic fluorescence intensity of the HSA gradually decreased, whereas, for CD, the fluorescence intensity ($\lambda_{em\sim442\ nm}$) increased (Figure 3.19 c). The fluorescence emission wavelength of HSA in the presence of CDs and BILI blue shifted (Figure 3.19 d); however, the maximum fluorescence emission intensity was ~3.24 % less than that of CD+HSA.

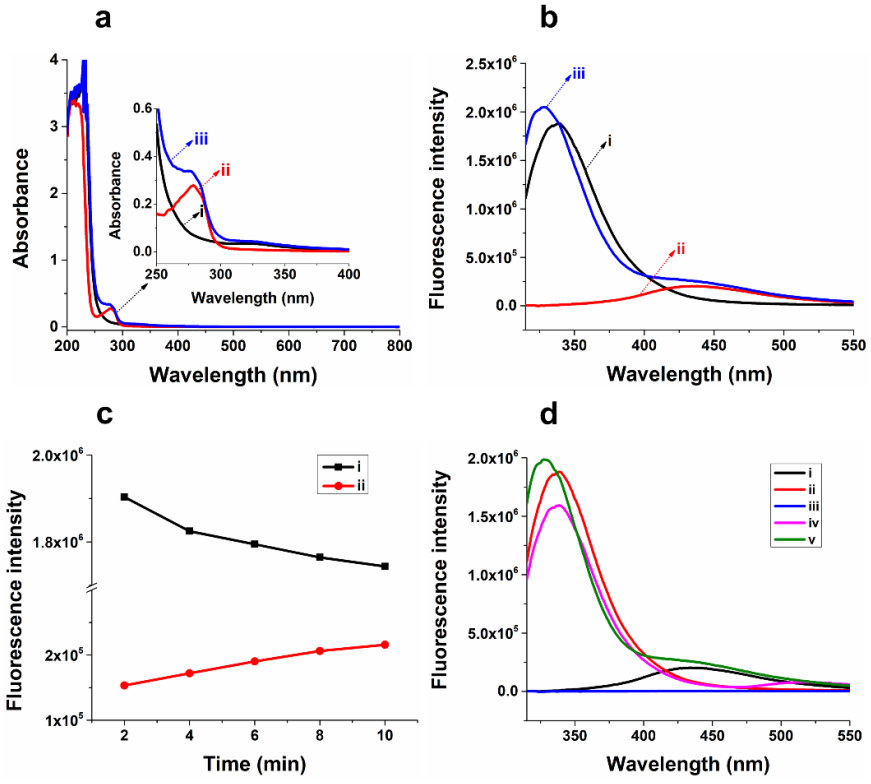

Figure 3.19. (a) Absorbance of different reaction systems: (i) CD, (ii) HSA, and (iii) CD+HSA. (b) Fluorescence of (i) HSA, (ii) CD, and (iii) CD+HSA (after 5 mins) at the HSA excitation wavelength ($\lambda_{ex\ 295\ nm}$). (c) Fluorescence change of (i) HSA and (ii) CD at different incubation time at HSA excitation wavelength ($\lambda_{ex\ 295\ nm}$). (d) Effect of CD on the fluorescence of HSA+BILI (HSA excitation wavelength: 295 nm). (i) CD, (ii) HSA, (iii) BILI, (iv) HSA+BILI, (v) CD+HSA+BILI. Experiment was carried out using 50 µL of stock 10.3 mg mL^{-1} HSA and 10 µL of stock CD solution (100 mg mL^{-1}).

3.3.3 Sample Particle Separation to Minimize the Background Noise

We selected the GOx as a reference enzyme to evaluate the CD's efficiency as a fluorescent signal probe in the enzyme-based detection in the human blood serum (Figure 3.12 b). The GOx and GL had a negligible effect on the serum's autofluorescence. Surprisingly, in the serum system, we did not observe the fluorescence quenching of the CD in the presence of GOx+GL, which contrasts the result observed in Figure 3.1. To scrutinize the role of serum components in the fluorescence enhancement in the GOx+GL+CD reaction system, we performed a similar experiment using filtered serum (Figure 3.12 c). We observed fluorescence quenching of the CD in the presence of GOx+GL. Considering this outcome, we further measured the fluorescence intensity of filtered serum residue with spiked H_2O_2 (Figure 3.12 d). As expected, we observed an increase in fluorescence enhancement, confirming that the generated H_2O_2 during the reaction of GOx+GL reacts with the serum components that ultimately result in fluorescence enhancement (Figure 3.12 b). Under the only buffer condition, the enzyme and the CD are directly exposed to each other; hence, the reaction is not hindered. Therefore, as from the above discussion, while there is obvious fluorescence interference, we propose the filtration of the human serum prior to performing experiments with the CD to avoid the crosstalk fluorescence and the background noise.

3.3.4 Colorimetric Detection of the Substrate

Considering the autofluorescent blood serum components as a major interferents in the fluorescence-based enzyme-linked clinical diagnosis, we investigated the colorimetric-based detection method. In the colorimetric assay, the oxidation of ABTS

is monitored at $\lambda_{max\ 414\ nm}$ in the presence of H_2O_2 and the CD (Das *et al*., 2021c), and indirectly measures the analyte. Meanwhile, we observed that when the CD is added along with the enzyme (GOx) before the addition of substrate, the catalytic activity of the GOx drastically decreased to a level of 93.7 % at the CD concentration of 10 mg mL^{-1} (Figure 3.20). This might be due to modification of the GOx secondary structure upon its binding to the CD. With increasing concentrations of CD, the absorbance corresponding to the oxidized ABTS decreased (Figure 3.20). To avoid inactivation of the enzyme, the CD was added following the reaction between the enzyme and the substrate. Using different concentration of GL, LoD was examined in both the buffer and the blood serum. In case of buffer, a dynamic range of 0.1 mM-0.5 mM (R^2= 0.99)with a LoD of 44 µM was identified, whereas in the blood serum, the dynamic range was found to be 0.02 mM-0.10 mM (R^2= 0.98) with a LoD of 183 µM (Figure 3.21). The sensitivity of the colorimetric assay towards the detection of GL was calculated to be 0.9917 AU mM^{-1} and 0.2482 AU mM^{-1} in the buffer and serum reaction system, respectively.

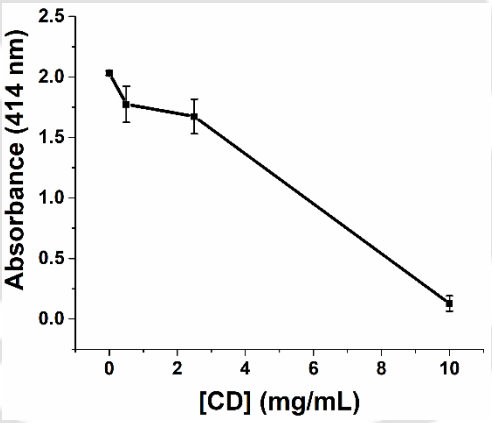

Figure 3.20. Influence of interaction of CD on the catalytic activity of GOx. Experiment was performed using different concentrations (0 mg mL^{-1}, 1 mg mL^{-1}, 2.5 mg mL^{-1}, and 10 mg mL^{-1}) of stock 100 mg mL^{-1} CD solution, 10 µL of 1 mg mL^{-1} stock GOx, 10 mM GL, and 5 mM ABTS.

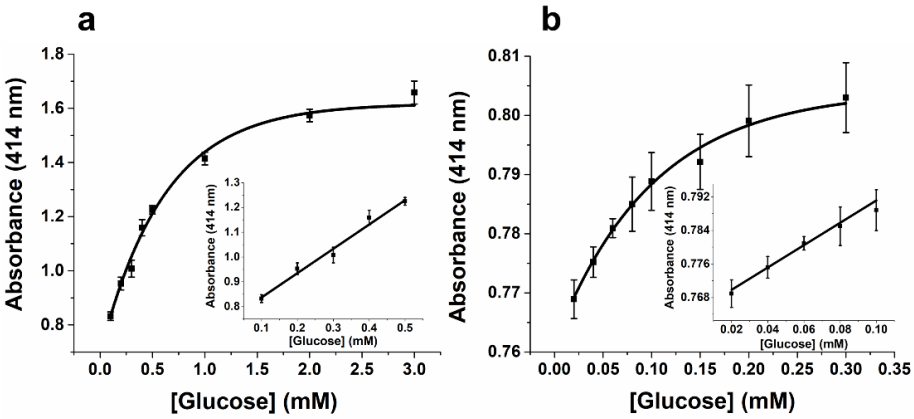

Figure 3.21. (a) Response curve for glucose in the buffer system (Inset: Linear calibration plot for glucose detection). (b) Response curve for glucose in the blood serum system (Inset: Linear calibration plot for glucose detection). The error bars represent the standard deviation (n=3).

3.4 Conclusion

Herein, we demonstrated for the first time that the fluorescence signals of CDs are highly sensitive not only to the surrounding protein environment but also to the blood serum systems. At the same time, we also demonstrated that the CD significantly affects the intrinsic fluorescence signals of enzyme proteins. We concluded the above facts using the enzyme-catalysed reaction systems of clinical importance, commonly exploited to detect glucose, cholesterol, and alcohol in blood serum. The results were also supported by the interaction studies of the CDs with a non-catalytic protein, HSA, which is a predominant protein in blood serum. The reason for fluorescence cross-talk between the CD and proteins has been attributed to the strong interactive electrostatic force that significantly increased the binding energy between these two organic entities. Docking studies indicate that the surface functional groups of CD, viz. -C=O, -COOH, and -NH, are involved in the binding with the amino acids of protein through hydrogen bonding. These avid binding processes shift the secondary structures of the enzyme proteins, mostly to the β strand components, expose their TRP/TYR residues, and initiate FRET with the CDs. The FRET phenomenon between the TRP/TYR residues of the protein/enzyme and CD significantly increases the fluorescence intensity. The time-resolved fluorescence lifetime showed that the existence of the longest lifetime component on the CD's surface is responsible for the fluorescence enhancement. However, with the introduction of the substrate into the reaction system, the *in-*

situ generated peroxide obstructed the FRET phenomenon between the redox enzyme and the CD. We have further shown that while the enzymatic reactions with the CDs were pronounced in the buffer system, there was much interference in the blood serum system. The presence of autofluorescent serum components with emission wavelength same as the CDs interfered with the detection process. The above experimental analysis confirmed that the autofluorescent blood serum components are major interferents in the fluorescence-based enzyme-linked clinical diagnosis.

The interference from blood serum illustrated that the CDs are not a potential signal probe for fluorescence-based direct detections of clinically significant analytes in blood serum samples. We proposed the ABTS dye-based colorimetric detection approach with CD to resolve this conundrum, wherein the blood serum components showed no interference. To circumvent the effect of CD on the secondary structure of enzymes proteins, we suggest the addition of CD following the incubation of the substrate with the enzyme. We recommend this approach based on the additional fact that the CD drastically affects the catalytic function of the enzymes.

The present study provided new insights in interpreting the application potential of zero-dimensional CDs. More prominently, these CDs might be promising for colorimetric-based detections in clinical applications. To the best of our knowledge, this is the first systematic investigation on the fluorescence cross-talk between the CDs and protein/enzymes. The findings of this research have greatly enhanced our understanding of the application potential of the CD in enzyme and blood serum-based clinical diagnosis.

Chapter 4

Analytical Application of H_2O_2-Induced Chiroptical Graphitic Carbon Dots

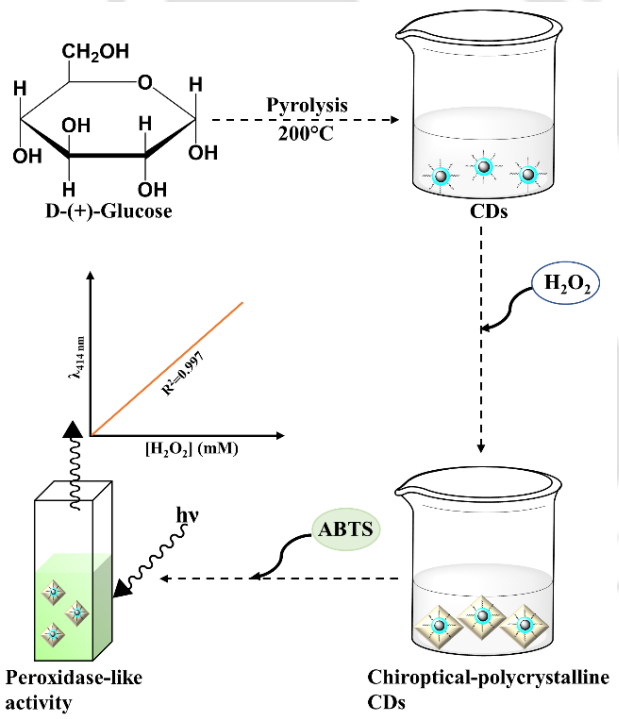

4.1 Overview

The zero-dimensional carbon dots (CDs) have recently attracted much attention because of their interesting optical and other properties, as discussed in the previous chapters (Das *et al*., 2021b). These properties have stimulated its applications in diverse areas, including biochemical sensing, photocatalysis, drug delivery, biolabeling, and optoelectronic devices (Das *et al*., 2021b; Semeniuk *et al*., 2019). Recent studies have also demonstrated the intrinsic peroxidase-like activity of CDs as another promising property (Das *et al*., 2021e; Dong *et al*., 2015; Gul *et al*., 2020; Kitchawengkul *et al*., 2021; Liu *et al*., 2020; Shi *et al*., 2019; Shi *et al*., 2011; Wu *et al*., 2013; Yang *et al*., 2017, 2021; Zhao *et al*., 2019; Zheng *et al*., 2016; Zhu *et al*., 2014). The significant advantage of using CDs as peroxidase mimic is their facile synthesis, low cost, long-term storage, and resistance to proteolysis, unlike the natural peroxidase enzymes (Das and Goswami, 2020). Previous work has demonstrated that the peroxidase-like activity of graphene quantum dots (GQDs) emanates from their ability to decompose H_2O_2 to $OH^{\cdot}$ (Sun *et al*., 2014). Notably, the functional groups on the surface of the CDs play a prominent role in the binding of the H_2O_2 during the catalytic activity (Das *et al*., 2021c; Das *et al*., 2021; Sun *et al*., 2015).

In recent years, CDs are also attracting more interest because of their chiroptical features (Ru *et al*., 2020). Chirality constitutes a vital aspect of optically-active nanostructures and has not been focussed much. With enormous advancement to understand chirality at the molecular scale and its influence on the structural property, it also becomes crucial to study chirality at the nanoscale for its possible applications (Wang *et al*., 2013). The introduction of chirality into CDs can augment remarkable properties to develop prospects for connecting material science, biology, and medicine (Hu *et al*., 2017). The synthesis of chiral CDs involves covalent modification or capping with chiral moieties or synthesis with chiral molecules; the latter has advantages as it does not involve the additional step of functionalization with chiral molecules (Deka and Chowdhury, 2017).

The evolution of CD's geometry during the various interaction processes is a less studied area. Previous studies have reported the importance of agglomeration of the CDs by the substrates during the peroxidase-like reaction (Das *et al*., 2021c). With

distinct geometry and material properties, the CDs can also serve as sensing agents for analytical applications. In this context, an in-depth mechanistic knowledge of the modification of CD's material property during the catalytic activity also becomes essential. Herein, we investigated the synthesis of CDs from D-(+)-glucose using a single-step pyrolysis method. We selected D-(+)-glucose as the precursor for the synthesis of CDs as it is widely available and also to analyse whether the chirality of the D-(+)-glucose is retained in the synthesized CDs. The as-prepared CDs exhibited blue photoluminescence under a single excitation wavelength and demonstrated intrinsic peroxidase-like activity. The results indicated that the structural characteristics of the CD are related to the corresponding H_2O_2 concentration.

4.2 Experimental Section

4.2.1 Materials

D-(+)-Glucose anhydrous was purchased from Himedia, India. 2,2'-azino-bis (3-ethylbenzothiazoline-6-sulfonic acid) (ABTS) was obtained from Sigma Aldrich, USA. Hydrogen peroxide (H_2O_2) solution 50 % w/v was purchased from FINAR, India. Deionized water with a resistivity of >18 MΩ.cm was used throughout the experiment.

4.2.2 Characterization

UV-Visible absorption spectra was monitored using a double beam Cary 60 UV-Visible spectrophotometer (Agilent Technologies). The fluorescence spectra was collected using FluoroMax-4 (HORIBA Scientific). The FETEM images and SAED pattern were observed using JEOL JEM- 2100F with an accelerating voltage of 200 kV. The Energy-Dispersive X-ray Spectroscopy (EDS), which was attached to the JEOL JEM-2100F was utilized to determine the relative content of carbon and oxygen in the synthesized carbon dots.The FTIR measurements were obtained by PerkinElmer FTIR spectrometer at room temperature using spectroscopic grade KBr pressed disc. The circular dichroism spectra was recorded by Jasco J-815 spectropolarimeter (Japan) at room temperature using 10 mm path length cuvette. The spectra was measured between 170 nm to 300 nm in continuous scanning mode with 10 nm bandwidth and a scanning speed of 100 nm min^{-1}. X-ray diffraction (XRD) was performed on Rigaku

Technologies powder X-ray diffractometer (Japan) with Cu Kα radiation operating at 90 kW.

4.2.3 Synthesis of CDs

The CDs were synthesized by pyrolyzing D-(+)- glucose. Briefly, 1 g of D-(+)-glucose was heated at 200 °C until it melted and gradually turned the colorless liquid to a dark yellow solution. Then, 5 mL of water was added and kept under constant stirring for 30 mins. After that, the solution was centrifuged at 13000 xg for 30 mins. The supernatant was further collected after centrifugation followed by dialysis with 1 kDa cut-off filter for 3 hours. Finally, the dialysed solution was used for the experiment.

4.2.4 Peroxidase-like Activity Assay

The peroxidase-like activity of the CDs synthesized from D-(+)-glucose was tested for the catalytic oxidation of ABTS in the presence of H_2O_2. Typically, the experiment was performed by mixing 2 mg mL^{-1} CD, 10 mM H_2O_2, and 4 mM ABTS in a reaction volume of 1 mL. The reaction mixture was incubated for 5 mins and then was monitored by recording the absorbance at λ= 414 nm that corresponds to the oxidation product of ABTS.

4.3 Results and Discussion

4.3.1 Synthesis and Characterization of CDs

The chiral CDs were synthesized by pyrolyzing D-(+)-glucose at 200 °C (Scheme 4.1). During the pyrolysis process, the glucose molecules probably have undergone nucleation followed by growth and subsequently transformed into CDs similar to the previous report (Tang *et al*., 2012). Unlike the microwave-assisted, ultrasonic, and hydrothermal synthesis methods (Egorova *et al*., 2018; Ma *et al*., 2012; Tang *et al*., 2012; Zheng *et al*., 2016), the CDs synthesised by us involved a simple single-step low temperature (200 °C) pyrolysis process. The resulting CDs with a pH of approximately 5.0 were well dispersed in an aqueous solution. The synthesized CDs showed two UV absorption bands almost analogous to the earlier reports (Figure 4.1 a) (Tang *et al*., 2012). Compared to the starting material, the high energy absorption band at 230 nm corresponds to Π to Π* electronic transition is due to C=C and is only found

in case of the CD, while the low energy absorption band at 282 nm assigned to n to Π* electronic transitions due to C=O is observed in both the cases. Subsequently, the photoluminescence property of the CD was investigated (Figure 4.1 b). Under the UV lamp, the CD solution appeared blue. As shown in Figure 4.1 b, a broad emission peak centered around 424 nm is observed on excitation at 329 nm.

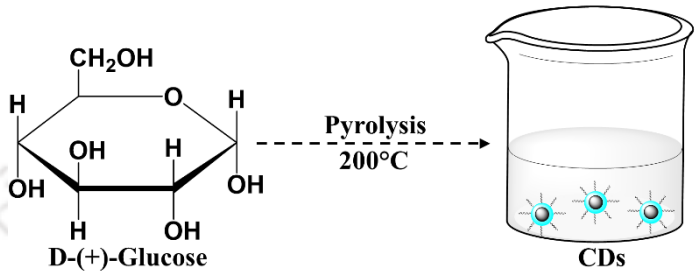

Scheme 4.1. Illustration of the synthesis of CDs from D-(+)-glucose.

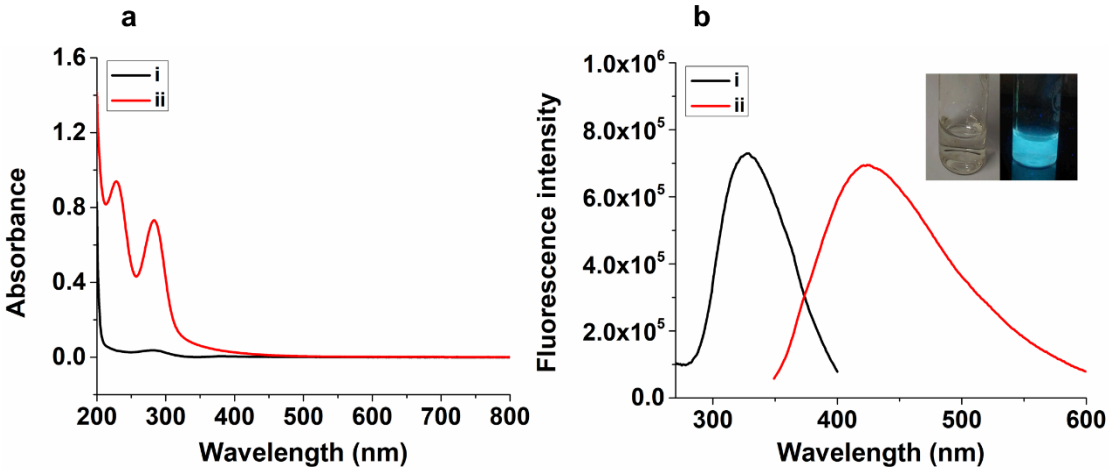

Figure 4.1. (a) UV-Vis absorption spectra of (i) D-(+)-glucose and (ii) the synthesized CD. (b) (i) excitation, and (ii) emission spectra of the CD synthesized from D-(+)-glucose. Inset: Photograph of aqueous CD solution under visible light and UV light.

The transmission electron microscope (TEM) studies showed that the as-prepared CDs are quasi-spherical in morphology and have good monodispersity (Figure 4.2 a). The Gaussian fitting curve showed that the CDs have an average size of 3.14±0.4 nm (Figure 4.2 b). The HRTEM image of the CDs showed two distinct lattice parameters of 0.20 nm and 0.24 nm, corresponding to (101) facet of graphitic structure and (1120) lattice fringes of graphene (Figure 4.2 a) (Peng *et al.*, 2012). The selected

area electron diffraction (SAED) pattern revealed two-electron diffraction rings (Figure 4.2 c). The d-spacing of the rings corresponds to the hkl (reciprocal lattice perpendicular plane) values (101) and (112). The elemental content of the synthesized CD was determined by EDS. The relative atomic percentage was found to be 92.33 % for carbon (C), and 7.67 % for oxygen (O) (Figure 4.3). Circular dichroism was used to investigate the chiroptical property of the CDs (Figure 4.4 a). For D-(+)-glucose, the circular dichroism spectra display a peak at 184.6 nm due to its chirality. Upon pyrolysis and the transformation of the D-(+)-glucose to CDs, the peak was still observed, suggesting that the chirality property was intact. Notably, despite dialysis, chirality was present in the synthesized CDs, albeit there was a slight decrease in the intensity. The surface functional groups of the CD were monitored by Fourier Transform Infrared (FTIR) spectroscopy. The peak at 3250 cm^{-1} is due to the -OH stretching vibrations that show the CD's hydrophilic nature. In addition, the peaks corresponding to C=O (1740 cm^{-1}), C=C (1647 cm^{-1}), C-O (1014 cm^{-1}) and C-H (2930 cm^{-1}, 1365 cm^{-1}) are also observed (Figure 4.4 b). The typical powder X-ray diffraction profile of the synthesized CD is shown in Figure 4.5. The CDs exhibit a broad peak centered around 23.06°, corresponding to an interlayer distance of 0.38 nm (002), broader than that of bulk graphite (0.364 nm). The broad peak is due to the small size of the synthesized CDs, whereas the high value of the interlayer distance is attributed to the oxygen functional groups that resulted in a turbostratic structure (Puvvada *et al*., 2012; Shi *et al*., 2015). Besides, the XRD spectra also show a hump around 44.35°, corresponding to an interlayer spacing of 0.20 nm, which may be associated with the (101) planes (JCPDS card no. 00-001-0640).

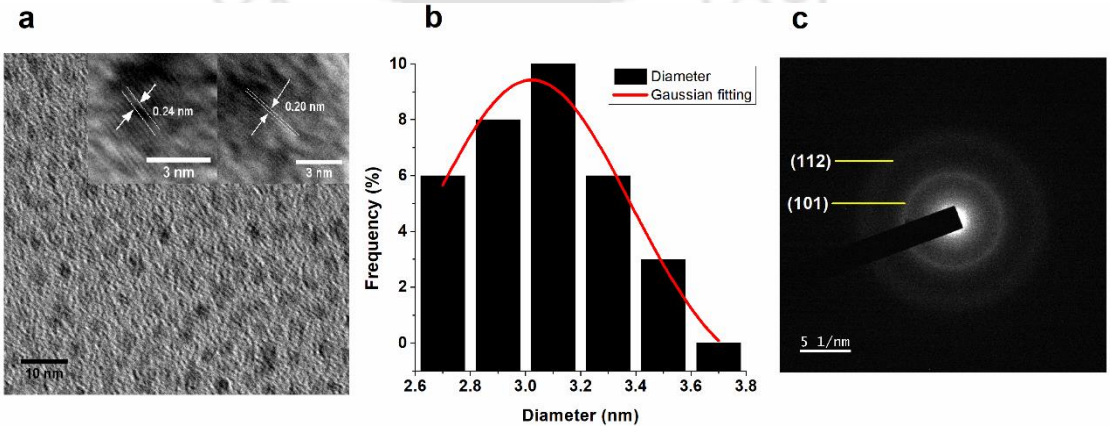

Figure 4.2. (a) FETEM image of the CD with a scale bar of 10 nm. Inset: lattice planes of an individual CD. (b) Particle size distribution of the synthesized CD. (c) SAED pattern of the CDs.

a

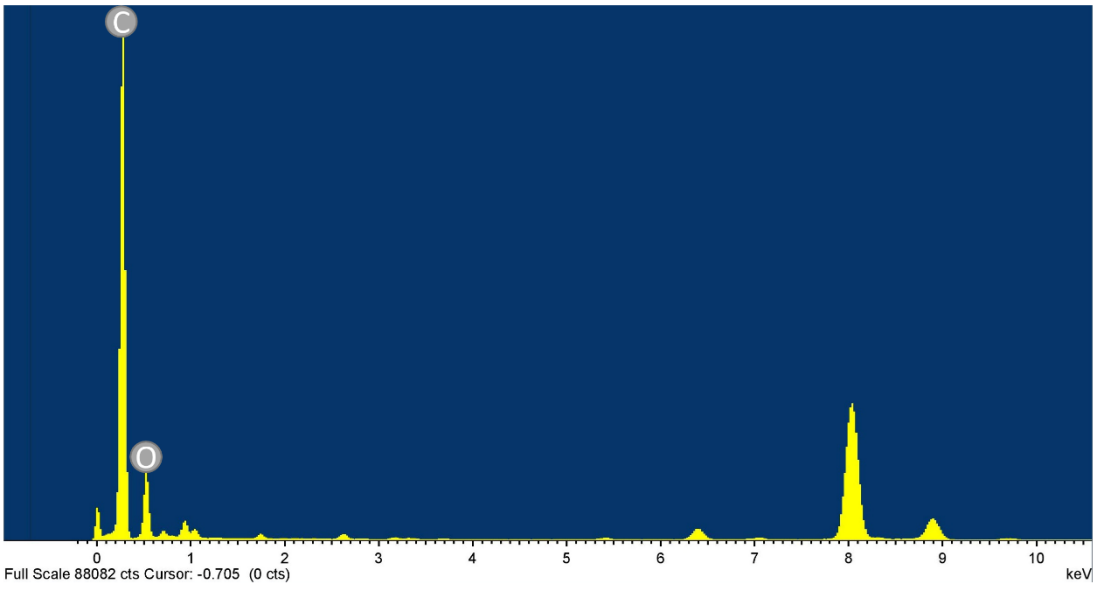

b

C K (Atomic %)	O K (Atomic %)
92.33%	7.67

Figure 4.3. (a) EDS spectra of the synthesized CD. (b) Relative atomic percentage of the synthesized CD.

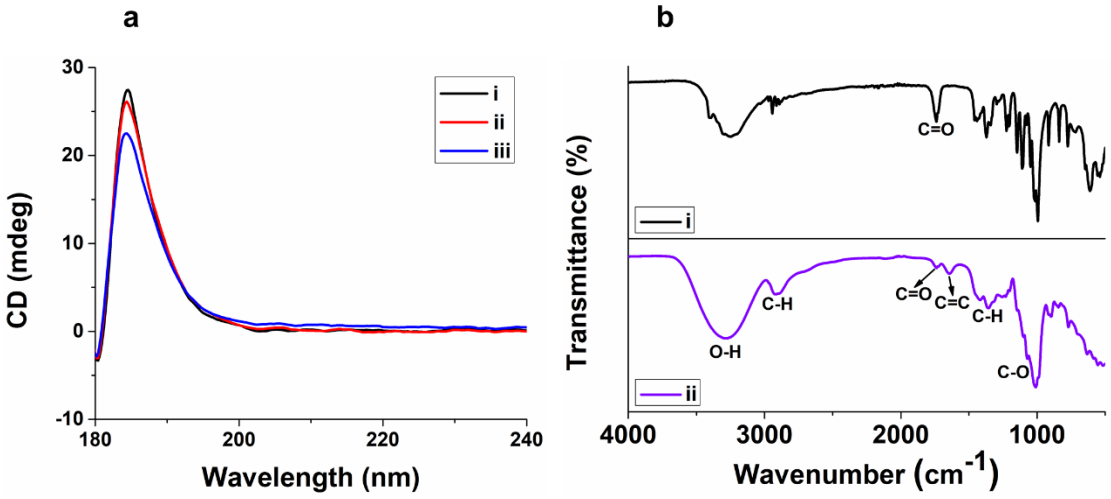

Figure 4.4. (a) Circular dichroism spectra of (i) D-(+)-glucose, (ii) the synthesized CD (undialysed), and (iii) the synthesized CD (dialysed). (b) FTIR spectra of (i) D-(+)-glucose, and (ii) the synthesized CD.

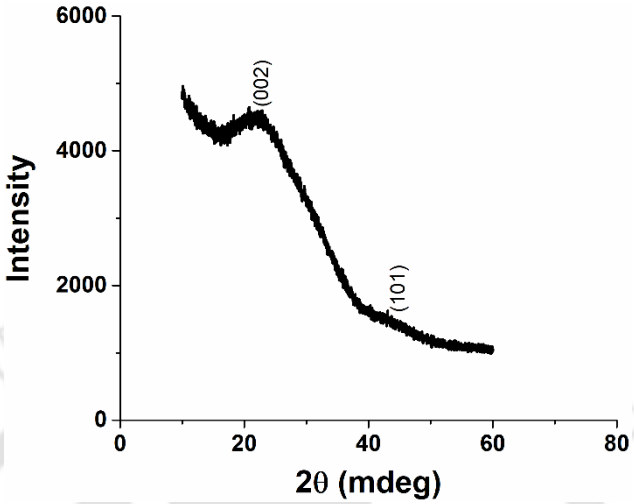

Figure 4.5. XRD pattern of the synthesized CD.

4.3.2 Peroxidase-like Activity of the Synthesized CDs

To the best of our knowledge, CDs synthesized from D-(+)-glucose is not yet explored for peroxidase-like activity. Therefore, we evaluated the intrinsic peroxidase-like activity of the CDs in the presence of H_2O_2 and ABTS. With the addition of H_2O_2, the CDs can catalyse the oxidation of ABTS to generate a green coloured product, which suggests that the CDs possess peroxidase-like activity (Figure 4.6 a). The reaction system with CDs or H_2O_2 alone does not result in a notable colour change. The absorbance peak of the oxidized ABTS is at 414 nm. The as-prepared CD also exhibits pH-dependent peroxidase-like behaviour, with higher activity at lower pH conditions (Figure 4.6 b). Considering the higher peroxidase-like activity at lower pH conditions, the CD's material property was screened at pH 1.0 and pH 5.0 in the absence of H_2O_2 using UV-Vis spectroscopy. At pH 1.0, the absorption peak corresponding to C=C at 252 nm decreased, whereas the absorption peak corresponding to C=O (282 nm) increased compared to the CDs at pH 5.0 (Figure 4.7 a). FTIR spectroscopy was used to explore the effect on the CD's surface functional groups at different pH levels. It is worth noting from the spectra that at pH 1.0, an increase in the intensity of stretching vibration corresponding to C=O at 1740 cm^{-1} and C=C at 1647 cm^{-1} was observed

(Figure 4.7 b). By integrating the results from Figure 4.7 a, and 4.7 b, we suggest that the C=O functional group has a vital role in the peroxidase-like activity of the CDs derived from D-(+)-glucose. Furthermore, the fluorescence intensity at pH 1.0 was lesser than at pH 5.0 (Figure 4.7 c). The phenomenon reported to be caused by the surface states C=C bonds of CDs (Tang *et al*., 2012), which is also in agreement with the UV-Vis spectra (Figure 4.7 a), wherein there is a decrease in the intensity of the absorbance peak for the C=C band. Interestingly, the stretching vibration intensity of C=O further increased upon CD's interaction with H_2O_2 (Figure 4.7 d). This may be due to the binding of H_2O_2 to the C=O functional group that resulted in increased vibration intensity. Additionally, it can also be assumed that in the pyrolyzed glucose structure, one of the carbons bonded to the oxygen of the H_2O_2, which resulted in the formation of C=O, thus causing an increase in the number of C=O groups and linked increased intensity. Therefore, the UV-Vis and FTIR spectroscopy study demonstrated that the C=O groups play an important role in the CD's peroxidase-like behaviour, similar to some previous reports (Sun *et al*., 2015).

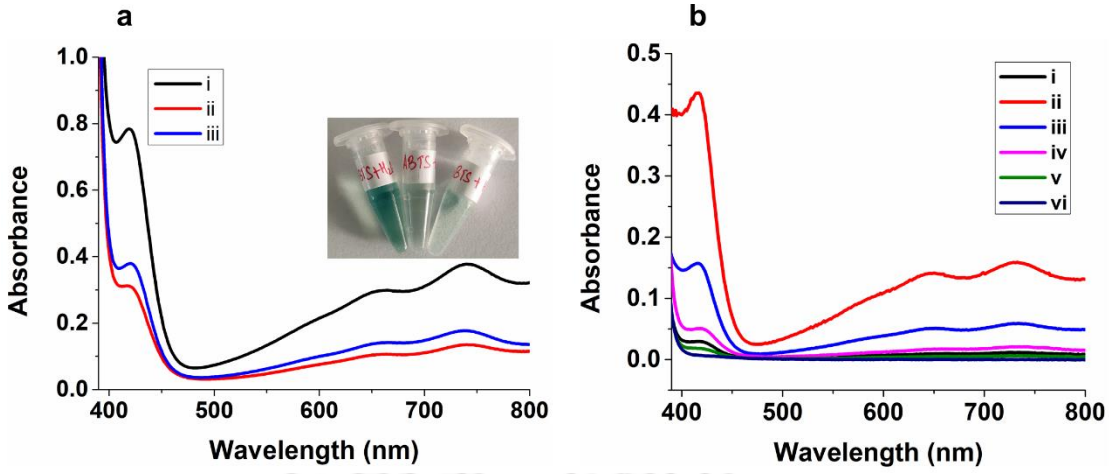

Figure 4.6. (a) UV-Vis absorption spectra of different reaction systems. (i) ABTS+H_2O_2+CD, (ii) ABTS+H_2O_2, and (iii) ABTS+CD. (b) pH-dependent peroxidase-like activity of the CD synthesized from D-(+)-glucose. (i) ABTS+H_2O_2 (Control), (ii) pH 1.0, (iii) pH 3.0, (iv) pH 5.0, (v) pH 7.0, and (vi) pH 10.0.

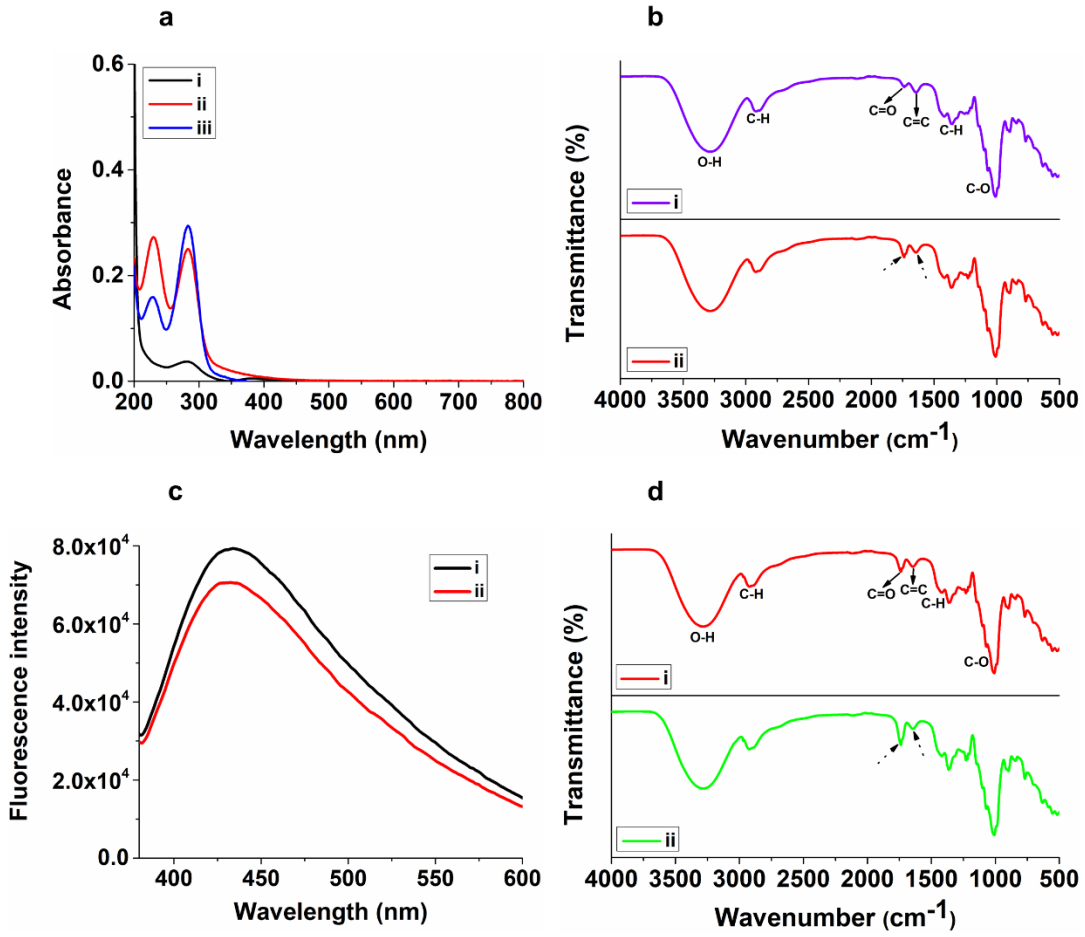

Figure 4.7. (a) UV-Vis spectra of (i) D-(+)-glucose, and CD at pH (ii) 5.0 and (iii) 1.0. (b) Comparison of the FTIR spectra of CD at pH (i) 5.0 and (ii) 1.0. (c) Comparison of the fluorescence spectra of CD at pH (i) 5.0 and (ii) 1.0. (d) Comparison of the FTIR spectra of (i) CD (pH 1.0), and (ii) CD (pH 1.0+H_2O_2).

Since the peroxidase-like activity of the CDs is H_2O_2 concentration-dependent, we used the CD synthesized from D-(+)-glucose for the label-free H_2O_2 detection. The typical H_2O_2 concentration-dependent response curve (y = 0.0696x+0.15644) with a linear range from 0.01 mM to 20 mM and a LoD of 630 μM (Figure 4.8). The LoD was calculated using the formula LoD = $3\sigma/m$, where σ is the standard deviation of the absorbance of blank, and m is the slope of the calibration curve.

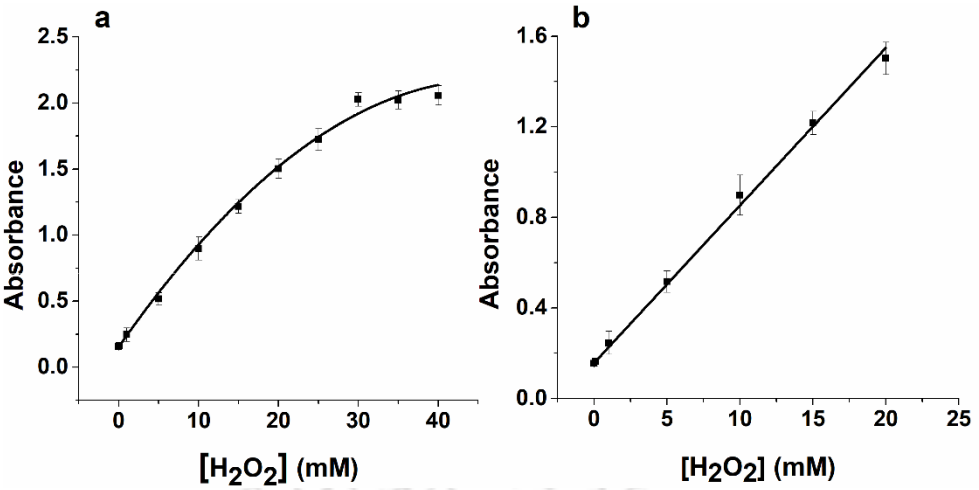

Figure 4.8. (a) The response curve of H_2O_2 using 10 mg mL^{-1} CD and 4 mM ABTS. The error bars represent the standard deviation (n =3). The experiment was performed using 10 mg mL^{-1} CD and 50 mM ABTS. (b) Linear calibration for H_2O_2 detection in the range 0.01 mM to 20 mM.

4.3.2 Characterization of CD Agglomeration

To investigate the geometry of the CDs during the interaction with H_2O_2, we measured the UV-Vis absorption, FETEM, XRD, and circular dichroism spectra. With increasing H_2O_2 concentrations, the C=C absorbance peak disappeared, along with a slight hyperchromic shift of the C=O peak (Figure 4.9 a). By TEM, we observed that the addition of H_2O_2 to the CDs (pH 1.0) resulted in its agglomeration (Figure 4.9 b), similar to the previous report (Das et al., 2021c). Figure 4.10 shows the XRD profiles for CD and CD+H_2O_2. The XRD peak position for CD+H_2O_2 is shifted to a lower degree (20°) than the CD's peak at 23.06°. The shifting originated due to the introduction of more oxygen-containing groups in the CD upon interaction with H_2O_2 (Peng *et al.*, 2012). Further, the increased intensity of the hump at 44.35° is due to the increased molecular orderliness within the agglomerated structures. Besides, the increase in the size of the CDs due to agglomeration is supposed to be responsible for the narrow peaks in contrast to the broad peaks of the synthesized CD (Londoño-Restrepo *et al.*, 2019). Consequently, the selected area electron diffraction (SAED) pattern of the CD+H_2O_2 displayed small spots making up the ring (Figure 4.11 b). The spots indicate the introduction of polycrystallinity in the CDs. Besides, compared to the pure CD, the CD+H_2O_2 also demonstrated a new diffraction ring with spots corresponding to the

(116) plane of the graphite (JCPDS card no. 00-001-0640). Considering these observations, it confirms that H_2O_2 induces some crystallinity in the CD+H_2O_2 agglomerated structures. Based on these observations, we assume that at the beginning, as a result of H_2O_2 addition, the CDs drew closer to one another in a proper orientation to form agglomerates. As the reaction progresses, well-organized CD+H_2O_2 moieties form a separate polycrystalline phase. The circular dichroism spectra obtained for CDs with different concentrations of H_2O_2 reflected the change in CD's chiroptical properties as a result of agglomeration (Figure 4.12). The synthesized CD at pH 1.0 shows a peak around 194 nm. With increasing H_2O_2 concentrations, the peak at 194 nm gradually red-shifted. This observation proved the formation of a CD-H_2O_2 hybrid accompanied by an increase in the size of the CDs.

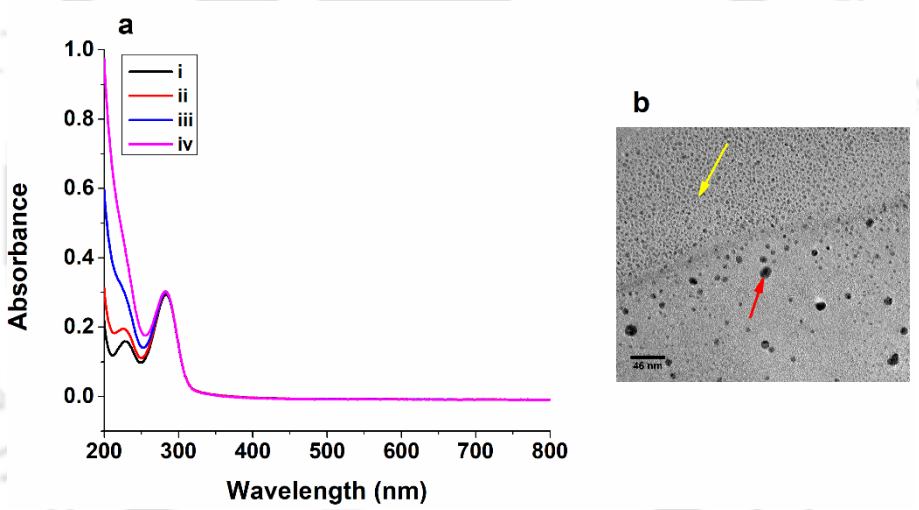

Figure 4.9. (a) UV-Vis absorption spectra of CD (pH 1.0) at different H_2O_2 concentrations. (i) CD (control), (ii) CD+1 mM H_2O_2, (iii) CD+5 mM H_2O_2, and (iv) CD+10 mM H_2O_2. (b) FETEM image of the effect of H_2O_2 on the morphology of CD. Only CD is shown with yellow arrow and CD+25 µM H_2O_2 is shown with red arrow.

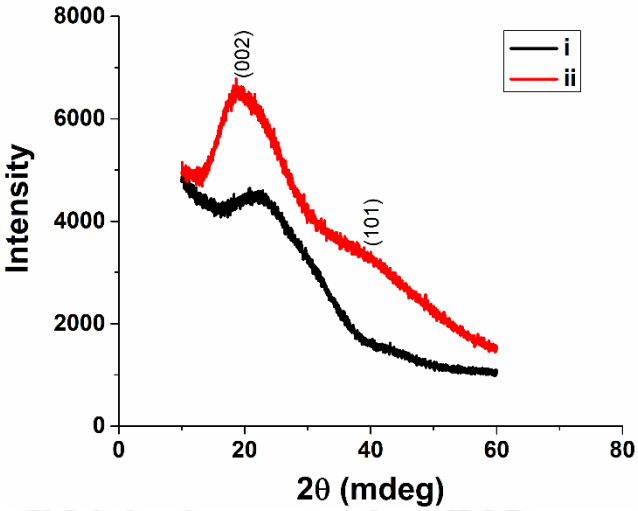

Figure 4.10. XRD pattern of (i) CD, and (ii) CD+H_2O_2.

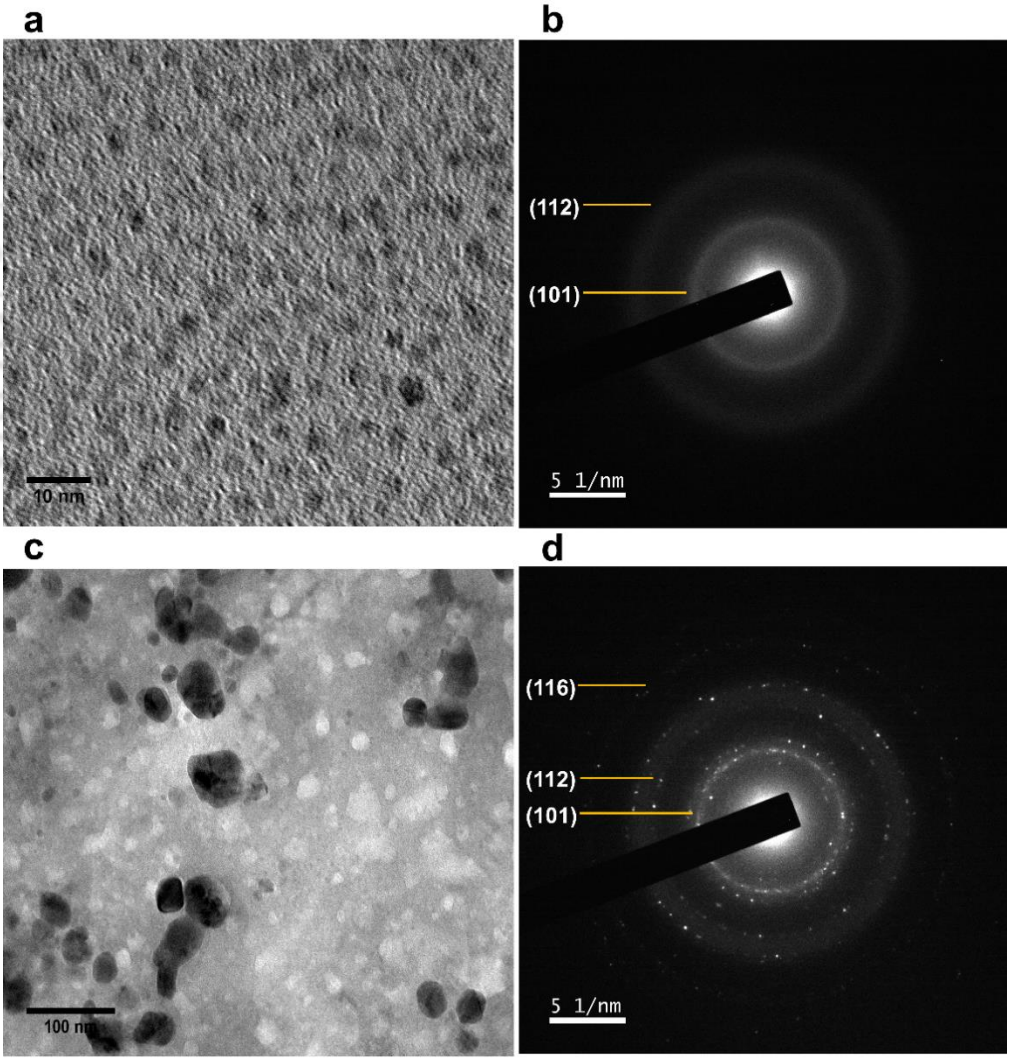

Figure 4.11. (a,c) FETEM images, and (b,d) corresponding SAED pattern of CD and CD+25 μM H_2O_2, respectively.

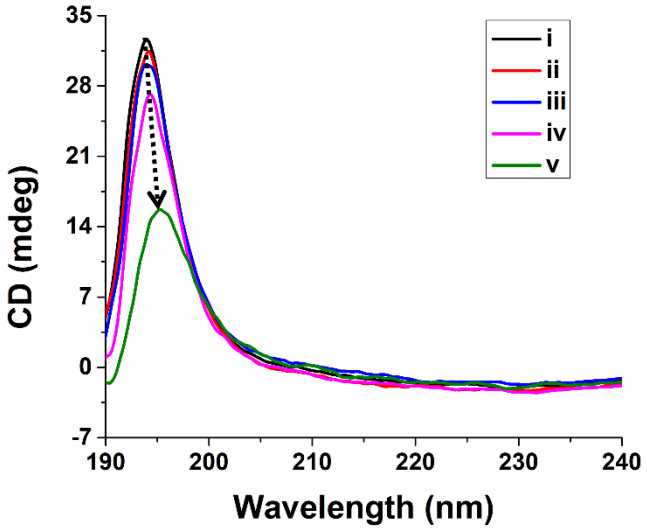

Figure 4.12. Circular dichroism spectra of CD (8 mg mL^{-1}) with different concentrations of H_2O_2: (i) CD, (ii) CD+0.025 mM H_2O_2, (iii) CD+5 mM H_2O_2, (iv) CD+10 mM H_2O_2, (v) CD+50 mM H_2O_2.

4.4 Conclusion

In summary, we have synthesized chiral CDs from D-(+)-glucose through a simple single-step pyrolysis method and demonstrated that the nanostructure could be utilized as an efficient peroxidase-mimic. However, compared to the L-glutamic acid-derived CD, the peroxidase-like activity of the D-(+)-glucose CD was far lower. With no carboxylic group in the D-(+)-glucose structure, the -C=O functional group of the CD plays a vital role in the peroxidase process. We established for the first time that the CDs undergo a structural transition upon their interaction with H_2O_2. Interestingly, we also observed that the concentration of H_2O_2 significantly affects the chiroptical property of the CD. These transitions, however, did not affect the catalytic property of the synthesised CD. The H_2O_2-induced chiroptical nanocrystal CDs can have great prospects, especially in drug delivery and clinical applications. This research validates the importance of exploring in-depth material modification of CD during the interactions for recognition of novel properties.

Conclusion and Future Outlook

The replacement of the natural horseradish peroxidase enzyme with CD-based peroxidase mimic has attracted enormous attention in diversified fields due to its favourable properties. In the present thesis, the primary objective comprised of elucidating the mechanism of the peroxidase-like activity of CDs and their application potential in clinical diagnosis. In this regard, firstly, simple carbon-containing molecules as model compounds were examined to understand the role of the carboxylic group, carbonyl group, hydroxyl group, and amine group in H_2O_2 binding and their decomposition. From both theoretical and experimental investigations, we demonstrated for the first time that the carboxylic group binds to H_2O_2 with maximum energy and exhibits maximum peroxidase-like activity in contrast to the carbonyl, hydroxyl, and amine group. A detailed analysis revealed that the presence of the amine group near the carboxyl group resulted in a higher degree of peroxidase-like activity. Accordingly, we identified L-glutamic acid as a potential candidate to synthesize CDs. Subsequently, an in-depth investigation was carried out to determine its mechanism of peroxidase-like activity. Our study confirmed that the synthesized CD interacts electrostatically with the ABTS and via hydrogen bonding with the H_2O_2 through the surface-bound carboxylic group. The interaction resulted in charge transfer from ABTS through CD to H_2O_2, wherein the CD acted as a semiconducting electron trap. The LoD of H_2O_2 achieved through the colorimetric-based peroxidase assay was determined to be 110 μM. Besides, substrate-induced aggregation of the CDs over time in the aqueous medium was one of the crucial challenges noticed in the current investigation. Therefore, to eliminate the aforementioned phenomenon, we suggested solid platforms such as paper platforms as a suitable medium for peroxide assays. We envision that the findings will provide prospects for establishing improved H_2O_2 detecting platforms.

The next phase of the investigation involved the evaluation of the application potential of the pyroglutamate CD in clinical diagnosis. Multifaceted interaction studies showed that the fluorescence signals of CD are susceptible to the proteins/enzymes, their substrate, and the blood serum medium. Notably, the fluorescence intensity of the CD increased to many folds in the presence of proteins/enzymes. The strong electrostatic

interaction between the CD and the proteins, which further increased the binding energy, is most likely responsible for the observed fluorescence cross-talk. Additionally, we noticed the involvement of the longest lifetime component on the CD's surface in the fluorescence enhancement using time-resolved fluorescence lifetime measurement. The binding event also increased the β strand component in the protein's secondary structure, exposing the TRP/TYR residues, and initiating the FRET phenomenon with the CDs. Nevertheless, the addition of substrate into the reaction system generated the peroxide that obstructed the FRET phenomenon occurring between the CD and the redox enzyme. It was observed that the enzymatic reaction suffered much interference in the blood serum system in contrast to the buffer system. We found that autofluorescent serum components with emission wavelength similar to that of the CDs are the cause of interference in the blood serum medium. In order to reduce the interference, we proposed filtering of serum components before the addition of CD to the reaction system. Besides, we noted that the ABTS dye-based colorimetric detection approach is suitable to resolve the issue, wherein the blood serum components showed no interference. Since the CD drastically affects the catalytic function of the enzymes, we recommend the addition of CD following the incubation of the substrate with the enzyme

Finally, another CD was prepared from D-(+)-glucose using a one-step pyrolysis method. The reason for selecting D-(+)-glucose as the precursor was to analyse whether the chirality of the aforementioned is retained after its transformation to the zero-dimensional CDs. The synthesized CDs preserved the chirality of D-(+)-glucose and displayed as an efficient peroxidase-mimic with a LoD of H_2O_2 calculated to be 630 μM. In this case, the -C=O functional group of the CD played a crucial role during the catalytic activity. Interestingly, in this study, we observed that the synthesized CD undergoes a structural transition upon its reaction with H_2O_2. The molecular orderliness of the CDs increased with the addition of H_2O_2 thereby leading to the introduction of polycrystallinity in the nanostructure. The peroxidase-like activity of the CD was not hampered during the event. However, we noted that the chiroptical property changed with increasing H_2O_2 concentrations. The study as a whole displayed the significance of exploring in-depth nanostructure material modification during interactions to identify novel attributes.

In a nutshell, the present thesis work presented a systematic and in-depth investigation of the CD-based peroxidase mimic. We expect that the investigation would help discover new horizons in the field of nanozyme, thereby increasing its practical applicability in analytical fields.

Future outlook

The findings embodied in this thesis require further exploration to improve the scope of CD-based peroxidase mimics in biosensing applications. On a critical examination of the work, the following are some major challenges that may be addressed in the future:

(i) Peroxide substrate-induced aggregation of CDs, which hampers analytical response.

(ii) Interference (autofluorescence) from the blood serum is a major obstacle for utilizing CD as a fluorescence probe for peroxide detection.

(iii) Improving the catalytic turnover of CD, which is inferior to HRP, for faster reaction and rapid analysis of samples.

(iv) Reusability and suitable immobilization strategy of CD on solid surfaces for developing sensing devices for peroxide detection.

Bibliography

Ali, S.S., Hardt, J.I., Quick, K.L., Sook Kim-Han, J., Erlanger, B.F., Huang, T., Epstein, C.J., Dugan, L.L., A biologically effective fullerene (C60) derivative with superoxide dismutase mimetic properties. Free Radical Biology and Medicine 37, 1191–1202 (2004).

Amjadi, M., Hallaj, T., Manzoori, J.L., Shahbazsaghir, T., An amplified chemiluminescence system based on Si-doped carbon dots for detection of catecholamines. Spectrochimica Acta Part A: Molecular and Biomolecular Spectroscopy 201, 223–228 (2018).

Amjadi, M., Hallaj, T., Mirbirang, F., A chemiluminescence reaction consisting of manganese(IV), sodium sulfite, and sulfur- and nitrogen-doped carbon quantum dots, and its application for the determination of oxytetracycline. Microchim Acta 187, 191 (2020).

Angione, M.D., Pilolli, R., Cotrone, S., Magliulo, M., Mallardi, A., Palazzo, G., Sabbatini, L., Fine, D., Dodabalapur, A., Cioffi, N., Torsi, L., Carbon based materials for electronic bio-sensing. Materials Today 14, 424–433 (2011).

Anwar, S., Ding, H., Xu, M., Hu, X., Li, Z., Wang, J., Liu, L., Jiang, L., Wang, D., Dong, C., Yan, M., Wang, Q., Bi, H., Recent Advances in Synthesis, Optical Properties, and Biomedical Applications of Carbon Dots. ACS Appl. Bio Mater. 2, 2317–2338 (2019).

Asadzadeh-Khaneghah, S., Habibi-Yangjeh, A., Nakata, K., Decoration of carbon dots over hydrogen peroxide treated graphitic carbon nitride: Exceptional photocatalytic performance in removal of different contaminants under visible light. Journal of Photochemistry and Photobiology A: Chemistry 374, 161–172 (2019).

Atchudan, R., Edison, T.N.J.I., Perumal, S., Clament Sagaya Selvam, N., Lee, Y.R., Green synthesized multiple fluorescent nitrogen-doped carbon quantum dots as an efficient label-free optical nanoprobe for *in vivo* live-cell imaging. Journal of Photochemistry and Photobiology A: Chemistry 372, 99–107 (2019).

Bachu, V., Goswami, P., Bioelectrochemiluminescence as an Analytical Signal of Extreme Sensitivity, in: Goswami, P (Ed.), Advanced Materials and Techniques for Biosensors and Bioanalytical Applications. CRC Press (2020), p. 233-250.

Bai, Y., Zhang, B., Chen, L., Lin, Z., Zhang, X., Ge, D., Shi, W., Sun, Y., Facile One-Pot Synthesis of Polydopamine Carbon Dots for Photothermal Therapy. Nanoscale Research Letters 13, 287 (2018).

Bandi, R., Dadigala, R., Gangapuram, B.R., Guttena, V., Green synthesis of highly fluorescent nitrogen – Doped carbon dots from Lantana camara berries for effective detection of lead(II) and bioimaging. Journal of Photochemistry and Photobiology B: Biology 178, 330–338 (2018).

Behera, R.K., Sau, A., Mishra, L., Bera, K., Mallik, S., Nayak, A., Basu, S., Sarangi, M.K., Redox Modifications of Carbon Dots Shape Their Optoelectronics. J. Phys. Chem. C 123, 27937–27944 (2019).

Bhati, A., Anand, S.R., Saini, D., Khare, P., Dubey, P., Sonkar, S.K., Self-doped nontoxic red-emitting Mg–N-embedded carbon dots for imaging, Cu(II) sensing and fluorescent ink. New J. Chem. 42, 19548–19556 (2018).

Cailotto, S., Mazzaro, R., Enrichi, F., Vomiero, A., Selva, M., Cattaruzza, E., Cristofori, D., Amadio, E., Perosa, A., Design of Carbon Dots for Metal-free Photoredox Catalysis. ACS Appl. Mater. Interfaces 10, 40560–40567 (2018).

Cao, J.-T., Zhang, W.-S., Wang, H., Ma, S.-H., Liu, Y.-M., A novel nitrogen and sulfur co-doped carbon dots-H_2O_2 chemiluminescence system for carcinoembryonic antigen detection using functional HRP-Au@Ag for signal amplification. Spectrochimica Acta Part A: Molecular and Biomolecular Spectroscopy 219, 281–287 (2019).

Carbonaro, C.M., Chiriu, D., Stagi, L., Casula, M.F., Thakkar, S.V., Malfatti, L., Suzuki, K., Ricci, P.C., Corpino, R., Carbon Dots in Water and Mesoporous Matrix: Chasing the Origin of their Photoluminescence. J. Phys. Chem. C 122, 25638–25650 (2018).

Carolan, D., Rocks, C., Padmanaban, D.B., Maguire, P., Svrcek, V., Mariotti, D., Environmentally friendly nitrogen-doped carbon quantum dots for next generation solar cells. Sustainable Energy Fuels 1, 1611–1619 (2017).

Chandra, A., Singh, N., Cell Microenvironment pH Sensing in 3D Microgels Using Fluorescent Carbon Dots. ACS Biomater. Sci. Eng. 3, 3620–3627 (2017).

Chatzimitakos, T., Kasouni, A., Sygellou, L., Leonardos, I., Troganis, A., Stalikas, C., Human fingernails as an intriguing precursor for the synthesis of nitrogen and sulfur-doped carbon dots with strong fluorescent properties: Analytical and bioimaging applications. Sensors and Actuators B: Chemical 267, 494–501 (2018).

Chekini, M., Krivoshapkina, E., Shkodenko, L., Koshel, E., Shestovskaya, M., Dukhinova, M., Kheiri, S., Khuu, N., Kumacheva, E., Nanocolloidal Hydrogel with Sensing and Antibacterial Activities Governed by Iron Ion Sequestration. Chem. Mater. 32, 10066–10075 (2020a).

Chekini, M., Prince, E., Zhao, L., Mundoor, H., Smalyukh, I.I., Kumacheva, E., Chiral Carbon Dots Synthesized on Cellulose Nanocrystals. Advanced Optical Materials 8, 1901911 (2020b).

Chen, A., Liang, W., Wang, H., Zhuo, Y., Chai, Y., Yuan, R., Anodic Electrochemiluminescence of Carbon Dots Promoted by Nitrogen Doping and Application to Rapid Cancer Cell Detection. Anal. Chem. 92, 1379–1385 (2020).

Chen, B., Chai, S., Liu, J., Liu, C., Li, Y., He, J., Yu, Z., Yang, T., Feng, C., Huang, C., 2,4,6-Trinitrophenol detection by a new portable sensing gadget using carbon dots as a fluorescent probe. Anal Bioanal Chem 411, 2291–2300 (2019).

Chen, B., Wang, F., Yao, W., Lin, Z., Zhang, X., Luo, S., Zheng, L., Lin, X., Carbon nitride quantum dot-enhanced chemiluminescence of hydrogen peroxide and hydrosulfite and its application in ascorbic acid sensing. Anal. Methods 10, 474–480 (2018).

Chen, X., Gao, H., Yang, M., Xing, L., Dong, W., Li, A., Zheng, H., Wang, G., Smart integration of carbon quantum dots in metal-organic frameworks for fluorescence-functionalized phase change materials. Energy Storage Materials 18, 349–355 (2019).

Chen, X., Zhang, J., Han, S., Liu, H., Du, Y., A carbon quantum dots-enhanced chemiluminescence method for the determination of gallic acid in food samples. Journal of the Chinese Chemical Society 65, 883–887 (2018).

Chen, Z., Yin, J.-J., Zhou, Y.-T., Zhang, Y., Song, L., Song, M., Hu, S., Gu, N., Dual Enzyme-like Activities of Iron Oxide Nanoparticles and Their Implication for Diminishing Cytotoxicity. ACS Nano 6, 4001–4012 (2012).

Cheng, C., Xing, M., Wu, Q., A universal facile synthesis of nitrogen and sulfur co-doped carbon dots from cellulose-based biowaste for fluorescent detection of Fe^{3+} ions and intracellular bioimaging. Materials Science and Engineering: C 99, 611–619 (2019).

Cho, M.-J., Park, S.-Y., Carbon-dot-based ratiometric fluorescence glucose biosensor. Sensors and Actuators B: Chemical 282, 719–729 (2019).

Chu, X., Wu, F., Sun, B., Zhang, M., Song, S., Zhang, P., Wang, Y., Zhang, Q., Zhou, N., Shen, J., Genipin cross-linked carbon dots for antimicrobial, bioimaging and bacterial discrimination. Colloids and Surfaces B: Biointerfaces 190, 110930 (2020).

Cobo, I., Li, M., Sumerlin, B.S., Perrier, S., Smart hybrid materials by conjugation of responsive polymers to biomacromolecules. Nature Mater 14, 143–159 (2015).

Comotti, M., Della Pina, C., Matarrese, R., Rossi, M., The Catalytic Activity of "Naked" Gold Particles. Angewandte Chemie International Edition 43, 5812–5815 (2004).

Das, S., Gogoi, S., Singh, N.K., Goswami, P., Analytical application of H_2O_2 -induced chiroptical graphitic carbon dots. Nano Ex. 2, 040003 (2021a).

Das, S., Goswami, P., Nanozymes as Potential Catalysts for Sensing and Analytical Applications, in: Goswami, P (Ed.), Advanced Materials and Techniques for Biosensors and Bioanalytical Applications. CRC Press (2020), p. 143-161.

Das, S., Ngashangva, L., Goswami, P., Carbon Dots: An Emerging Smart Material for Analytical Applications. Micromachines 12, 84 (2021b).

Das, S., Ngashangva, L., Mog, H., Gogoi, S., Goswami, P., An insight into the mechanism of peroxidase-like activity of carbon dots. Optical Materials 115, 111017 (2021c).

Das, T.K., Remanan, S., Ghosh, S., Ghosh, S.K., Das, N.Ch., Efficient synthesis of catalytic active silver nanoparticles illuminated cerium oxide nanotube: A mussel inspired approach. Environmental Nanotechnology, Monitoring & Management 15, 100411 (2021).

Deka, M.J., Chowdhury, D., Chiral carbon dots and their effect on the optical properties of photosensitizers. RSC Adv. 7, 53057–53063 (2017).

Devi, P., Rajput, P., Thakur, A., Kim, K.-H., Kumar, P., Recent advances in carbon quantum dot-based sensing of heavy metals in water. TrAC Trends in Analytical Chemistry 114, 171–195 (2019).

Ding, Y.-Y., Gong, X.-J., Liu, Y., Lu, W.-J., Gao, Y.-F., Xian, M., Shuang, S.-M., Dong, C., Facile preparation of bright orange fluorescent carbon dots and the constructed biosensing platform for the detection of pH in living cells. Talanta 189, 8–15 (2018).

Dong, J., Song, L., Yin, J.-J., He, W., Wu, Y., Gu, N., Zhang, Y., Co_3O_4 Nanoparticles with Multi-Enzyme Activities and Their Application in Immunohistochemical Assay. ACS Appl. Mater. Interfaces 6, 1959–1970 (2014).

Dong, W., Wang, R., Gong, X., Dong, C., An efficient turn-on fluorescence biosensor for the detection of glutathione based on FRET between N,S dual-doped carbon dots and gold nanoparticles. Anal Bioanal Chem 411, 6687–6695 (2019).

Dong, Y., Zhang, J., Jiang, P., Wang, G., Wu, X., Zhao, H., Zhang, C., Superior peroxidase mimetic activity of carbon dots–Pt nanocomposites relies on synergistic effects. New J. Chem. 39, 4141–4146 (2015).

Đorđević, L., Arcudi, F., D'Urso, A., Cacioppo, M., Micali, N., Bürgi, T., Purrello, R., Prato, M., Design principles of chiral carbon nanodots help convey chirality from molecular to nanoscale level. Nat Commun 9, 3442 (2018).

Duan, Y., Huang, Y., Chen, S., Zuo, W., Shi, B., Cu-Doped Carbon Dots as Catalysts for the Chemiluminescence Detection of Glucose. ACS Omega 4, 9911–9917 (2019).

Dugan, L.L., Gabrielsen, J.K., Yu, S.P., Lin, T.-S., Choi, D.W., Buckminsterfullerenol Free Radical Scavengers Reduce Excitotoxic and Apoptotic Death of Cultured Cortical Neurons. Neurobiology of Disease 3, 129–135 (1996).

Egorova, M.N., Tomskaya, A.E., Kapitonov, A.N., Alekseev, A.A., Smagulova, S.A., Hydrothermal Synthesis of Luminescent Carbon Dots from Glucose and Birch Bark Soot. J Struct Chem 59, 780–785 (2018).

Ehrat, F., Bhattacharyya, S., Schneider, J., Löf, A., Wyrwich, R., Rogach, A.L., Stolarczyk, J.K., Urban, A.S., Feldmann, J., Tracking the Source of Carbon Dot Photoluminescence: Aromatic Domains versus Molecular Fluorophores. Nano Lett. 17, 7710–7716 (2017).

Emanuele, A., Cailotto, S., Campalani, C., Branzi, L., Raviola, C., Ravelli, D., Cattaruzza, E., Trave, E., Benedetti, A., Selva, M., Perosa, A., Precursor-Dependent Photocatalytic Activity of Carbon Dots. Molecules 25, 101 (2020).

Fang, J., Zhuo, S., Zhu, C., Fluorescent sensing platform for the detection of p-nitrophenol based on Cu-doped carbon dots. Optical Materials 97, 109396 (2019).

Fang, Y., Zhou, L., Zhao, J., Zhang, Y., Yang, M., Yi, C., Facile synthesis of pH-responsive gadolinium(III)-doped carbon nanodots with red fluorescence and magnetic resonance properties for dual-readout logic gate operations. Carbon 166, 265–272 (2020).

Frank, B.P., Sigmon, L.R., Deline, A.R., Lankone, R.S., Gallagher, M.J., Zhi, B., Haynes, C.L., Fairbrother, D.H., Photochemical Transformations of Carbon Dots in Aqueous Environments. Environ. Sci. Technol. 54, 4160–4170 (2020).

Fu, X., Lv, R., Su, J., Li, H., Yang, B., Gu, W., Liu, X., A dual-emission nano-rod MOF equipped with carbon dots for visual detection of doxycycline and sensitive sensing of MnO_4^-. RSC Adv. 8, 4766–4772 (2018).

Gao, D., Liu, X., Jiang, D., Zhao, H., Zhu, Y., Chen, X., Luo, H., Fan, H., Zhang, X., Exploring of multicolor emissive carbon dots with novel double emission mechanism. Sensors and Actuators B: Chemical 277, 373–380 (2018).

Gao, L., Zhuang, J., Nie, L., Zhang, J., Zhang, Y., Gu, N., Wang, T., Feng, J., Yang, D., Perrett, S., Yan, X., Intrinsic peroxidase-like activity of ferromagnetic nanoparticles. Nature Nanotech 2, 577–583 (2007).

Gao, P., Xie, Z., Zheng, M., Chiral carbon dots-based nanosensors for Sn(II) detection and lysine enantiomers recognition. Sensors and Actuators B: Chemical 319, 128265 (2020).

Gao, Y., Jiao, Y., Lu, W., Liu, Y., Han, H., Gong, X., Xian, M., Shuang, S., Dong, C., Carbon dots with red emission as a fluorescent and colorimeteric dual-readout probe for the detection of chromium (VI) and cysteine and its logic gate operation. Journal of Materials Chemistry B 6, 6099–6107 (2018).

Gao, Y., Jiao, Y., Zhang, H., Lu, W., Liu, Y., Han, H., Gong, X., Li, L., Shuang, S., Dong, C., One-step synthesis of a dual-emitting carbon dot-based ratiometric fluorescent probe for the visual assay of Pb^{2+} and PPi and development of a paper sensor. J. Mater. Chem. B 7, 5502–5509 (2019).

Gao, Z., Wang, S., Xu, Z., Liu, J., Huang, Y., Hu, S., Ren, X., Synthesis of novel cationic carbon dots and application to quantitative detection of K^+ in human serum samples. New J. Chem. 43, 17937–17940 (2019).

Geng, T., Feng, T., Ma, Z., Cao, Y., Chen, Y., Tao, S., Xiao, G., Lu, S., Yang, B., Zou, B., Insights into supramolecular-interaction-regulated piezochromic carbonized polymer dots. Nanoscale 11, 5072–5079 (2019).

Gosens, I., Post, J.A., de la Fonteyne, L.J., Jansen, E.H., Geus, J.W., Cassee, F.R., de Jong, W.H., Impact of agglomeration state of nano- and submicron sized gold particles on pulmonary inflammation. Particle and Fibre Toxicology 7, 37 (2010).

Gowthaman, N.S.K., Sinduja, B., Karthikeyan, R., Rubini, K., Abraham John, S., Fabrication of nitrogen-doped carbon dots for screening the purine metabolic disorder in human fluids. Biosensors and Bioelectronics 94, 30–38 (2017).

Guan, Q., Su, R., Zhang, M., Zhang, R., Li, W., Wang, D., Xu, M., Fei, L., Xu, Q., Highly fluorescent dual-emission red carbon dots and their applications in optoelectronic devices and water detection. New J. Chem. 43, 3050–3058 (2019).

Gul, U., Kanwal, S., Tabassum, S., Gilani, M.A., Rahim, A., 2020. Microwave-assisted synthesis of carbon dots as reductant and stabilizer for silver nanoparticles with enhanced-peroxidase like activity for colorimetric determination of hydrogen peroxide and glucose. Microchim Acta 187, 135 (2020).

Guo, R., Chen, B., Li, F., Weng, S., Zheng, Z., Chen, M., Wu, W., Lin, X., Yang, C., Positive carbon dots with dual roles of nanoquencher and reference signal for the ratiometric fluorescence sensing of DNA. Sensors and Actuators B: Chemical 264, 193–201 (2018).

Guo, X., Xu, D., Yuan, H., Luo, Q., Tang, S., Liu, L., Wu, Y., A novel fluorescent nanocellulosic hydrogel based on carbon dots for efficient adsorption and sensitive sensing in heavy metals. J. Mater. Chem. A 7, 27081–27088 (2019).

Hallaj, T., Amjadi, M., Song, Z., Bagheri, R., Strong enhancement of the chemiluminescence of the Cu(II)-H_2O_2 system on addition of carbon nitride quantum dots, and its application to the detection of H_2O_2 and glucose. Microchim Acta 185, 67 (2017).

He, C., Peng, L., Lv, L., Cao, Y., Tu, J., Huang, W., Zhang, K., In situ growth of carbon dots on TiO_2 nanotube arrays for PEC enzyme biosensors with visible light response. RSC Advances 9, 15084–15091 (2019).

He, C., Yan, H., Li, X., Wang, X., In situ fabrication of carbon dots-based lubricants using a facile ultrasonic approach. Green Chem. 21, 2279–2285 (2019).

He, W., Liu, Y., Wamer, W.G., Yin, J.-J., Electron spin resonance spectroscopy for the study of nanomaterial-mediated generation of reactive oxygen species. Journal of Food and Drug Analysis, Nanomaterials - Toxicology and Medical Applications 22, 49–63 (2014).

Hu, C., Li, M., Qiu, J., Sun, Y.-P., Design and fabrication of carbon dots for energy conversion and storage. Chem. Soc. Rev. 48, 2315–2337 (2019).

Hu, L., Sun, Y., Zhou, Y., Bai, L., Zhang, Y., Han, M., Huang, H., Liu, Y., Kang, Z., Nitrogen and sulfur co-doped chiral carbon quantum dots with independent photoluminescence and chirality. Inorg. Chem. Front. 4, 946–953 (2017).

Huang, J., Li, F., Guo, R., Chen, Y., Wang, Z., Zhao, C., Zheng, Y., Weng, S., Lin, X., A signal-on ratiometric fluorometric heparin assay based on the direct interaction between amino-modified carbon dots and DNA. Microchim Acta 185, 260 (2018).

Huang, S., Qiu, H., Xie, J., Huang, C., Su, W., Hu, B., Xiao, Q., Systematical investigation of in vitro molecular interaction between fluorescent carbon dots and human serum albumin. RSC Adv. 6, 44531–44542 (2016).

Huo, F., Kang, Z., Zhu, M., Tan, C., Tang, Y., Liu, Y., Zhang, W., Metal-triggered fluorescence enhancement of multicolor carbon dots in sensing and bioimaging. Optical Materials 94, 363–370 (2019).

Ilyasov, I.R., Beloborodov, V.L., Selivanova, I.A., Terekhov, R.P., ABTS/PP Decolorization Assay of Antioxidant Capacity Reaction Pathways. Int J Mol Sci 21, 1131 (2020).

Jain, P., Chakma, B., Patra, S., Goswami, P., Hairpin stabilized fluorescent silver nanoclusters for quantitative detection of NAD^+ and monitoring NAD^+/NADH based enzymatic reactions. Analytica Chimica Acta 956, 48–56 (2017).

Jang, Y., Kim, S.M., Spinks, G.M., Kim, S.J., Carbon Nanotube Yarn for Fiber-Shaped Electrical Sensors, Actuators, and Energy Storage for Smart Systems. Advanced Materials 32, 1902670 (2020).

Jelinek, R., Characterization and Physical Properties of Carbon-Dots, in: Jelinek, R. (Ed.), Carbon Quantum Dots: Synthesis, Properties and Applications, Carbon Nanostructures. Springer International Publishing, Cham, (2017), pp. 29–46.

Jia, J., Lu, W., Li, L., Gao, Y., Jiao, Y., Han, H., Dong, C., Shuang, S., Orange-emitting N-doped carbon dots as fluorescent and colorimetric dual-mode probes for nitrite detection and cellular imaging. J. Mater. Chem. B 8, 2123–2127 (2020).

Jiang, B.-P., Yu, Y.-X., Guo, X.-L., Ding, Z.-Y., Zhou, B., Liang, H., Shen, X.-C., White-emitting carbon dots with long alkyl-chain structure: Effective inhibition

of aggregation caused quenching effect for label-free imaging of latent fingerprint. Carbon 128, 12–20 (2018).

Jiang, K., Feng, X., Gao, X., Wang, Y., Cai, C., Li, Z., Lin, H., Preparation of Multicolor Photoluminescent Carbon Dots by Tuning Surface States. Nanomaterials 9, 529 (2019).

Jiang, K., Gao, X., Feng, X., Wang, Y., Li, Z., Lin, H., Carbon Dots with Dual-Emissive, Robust, and Aggregation-Induced Room-Temperature Phosphorescence Characteristics. Angewandte Chemie International Edition 59, 1263–1269 (2020).

Jiang, L., Ding, H., Lu, S., Geng, T., Xiao, G., Zou, B., Bi, H., Photoactivated Fluorescence Enhancement in F,N-Doped Carbon Dots with Piezochromic Behavior. Angewandte Chemie 132, 10072–10077 (2020).

Jing, P., Han, D., Li, D., Zhou, D., Shen, D., Xiao, G., Zou, B., Qu, S., Surface related intrinsic luminescence from carbon nanodots: solvent dependent piezochromism. Nanoscale Horiz. 4, 175–181 (2018).

Ju, B., Nie, H., Zhang, X., Chen, Q., Guo, X., Xing, Z., Li, M., Zhang, S.X.-A., Inorganic Salt Incorporated Solvothermal Synthesis of Multicolor Carbon Dots, Emission Mechanism, and Antibacterial Study. ACS Appl. Nano Mater. 1, 6131–6138 (2018).

Kalaiyarasan, G., Raju, C.V., Veerapandian, M., Kumar, S.S., Joseph, J., Impact of aminated carbon quantum dots as a novel co-reactant for $Ru(bpy)_3^{2+}$: resolving specific electrochemiluminescence for butein detection. Anal Bioanal Chem 412, 539–546 (2020).

Kang, Z., Lee, S.-T., Carbon dots: advances in nanocarbon applications. Nanoscale 11, 19214–19224 (2019).

Karakoçak, B.B., Liang, J., Kavadiya, S., Berezin, M.Y., Biswas, P., Ravi, N., Optimizing the Synthesis of Red-Emissive Nitrogen-Doped Carbon Dots for Use in Bioimaging. ACS Appl. Nano Mater. 1, 3682–3692 (2018).

Kasprzyk, W., Świergosz, T., Bednarz, S., Walas, K., Bashmakova, N.V., Bogdał, D., Luminescence phenomena of carbon dots derived from citric acid and urea – a molecular insight. Nanoscale 10, 13889–13894 (2018).

Khan, S., Verma, N.C., Chethana, Nandi, C.K., Carbon Dots for Single-Molecule Imaging of the Nucleolus. ACS Appl. Nano Mater. 1, 483–487 (2018).

Kipnusu, W.K., Doñate-Buendía, C., Fernández-Alonso, M., Lancis, J., Mínguez-Vega, G., Nonlinear Optics to Glucose Sensing: Multifunctional Nitrogen and Boron Doped Carbon Dots with Solid-State Fluorescence in Nanoporous Silica Films. Particle & Particle Systems Characterization 37, 2000093 (2020).

Kitchawengkul, N., Prakobkij, A., Anutrasakda, W., Yodsin, N., Jungsuttiwong, S., Chunta, S., Amatatongchai, M., Jarujamrus, P., Mimicking Peroxidase-Like Activity of Nitrogen-Doped Carbon Dots (N-CDs) Coupled with a Laminated Three-Dimensional Microfluidic Paper-Based Analytical Device (Laminated 3D-μPAD) for Smart Sensing of Total Cholesterol from Whole Blood. Anal. Chem. 93, 6989–6999 (2021).

Kong, D., Yan, F., Han, Z., Xu, J., Guo, X., Chen, L., Cobalt(II) ions detection using carbon dots as an sensitive and selective fluorescent probe. RSC Adv. 6, 67481–67487 (2016).

Langer, M., Paloncýová, M., Medved', M., Otyepka, M., 2020. Molecular Fluorophores Self-Organize into C-Dot Seeds and Incorporate into C-Dot Structures. J. Phys. Chem. Lett. 11, 8252–8258 (2020).

Ledin, P.A., Jeon, J.-W., Geldmeier, J.A., Ponder, J.F., Mahmoud, M.A., El-Sayed, M., Reynolds, J.R., Tsukruk, V.V., Design of Hybrid Electrochromic Materials with Large Electrical Modulation of Plasmonic Resonances. ACS Appl. Mater. Interfaces 8, 13064–13075 (2016).

Leong, Y.-K., Role of Molecular Architecture of Citric and Related Polyacids on the Yield Stress of α-Alumina Slurries: Inter- and Intramolecular Forces. Journal of the American Ceramic Society 93, 2598–2605 (2010).

Li, C., Qin, Z., Wang, M., Liu, W., Jiang, H., Wang, X., Manganese oxide doped carbon dots for temperature-responsive biosensing and target bioimaging. Analytica Chimica Acta 1104, 125–131 (2020).

Li, C., Zhao, J., Chen, Y., Wang, X., Sun, X., Pan, W., Yu, G., Yan, Z., Wang, J., A carbon dots/rutin system for colorimetric and fluorimetric dual mode detection of Al^{3+} in aqueous solution. Analyst 143, 5467–5473 (2018).

Li, D., Liang, C., Ushakova, E.V., Sun, M., Huang, X., Zhang, X., Jing, P., Yoo, S.J., Kim, J.-G., Liu, E., Zhang, W., Jing, L., Xing, G., Zheng, W., Tang, Z., Qu, S., Rogach, A.L., Thermally Activated Upconversion Near-Infrared Photoluminescence from Carbon Dots Synthesized via Microwave Assisted Exfoliation. Small 15, 1905050 (2019).

Li, D., Wang, S., Azad, F., Zhao, L., Su, S., A simple method for the preparation of multi-color carbon quantum dots by using reversible regulatory color transformation. Microchim Acta 186, 612 (2019).

Li, D., Yuan, X., Li, C., Luo, Y., Jiang, Z., A novel fluorescence aptamer biosensor for trace Pb(II) based on gold-doped carbon dots and DNAzyme synergetic catalytic amplification. Journal of Luminescence 221, 117056 (2020).

Li, F., Cai, Q., Hao, X., Zhao, C., Huang, Z., Zheng, Y., Lin, X., Weng, S., Insight into the DNA adsorption on nitrogen-doped positive carbon dots. RSC Adv. 9, 12462–12469 (2019).

Li, H., Yan, X., Lu, G., Su, X., Carbon dot-based bioplatform for dual colorimetric and fluorometric sensing of organophosphate pesticides. Sensors and Actuators B: Chemical 260, 563–570 (2018).

Li, J., Wang, B., Zhang, H., Yu, J., Carbon Dots-in-Matrix Boosting Intriguing Luminescence Properties and Applications. Small 15, 1805504 (2019).

Li, L., Dong, T., Photoluminescence tuning in carbon dots: surface passivation or/and functionalization, heteroatom doping. J. Mater. Chem. C 6, 7944–7970 (2018).

Li, L., Shi, L., Jia, J., Eltayeb, O., Lu, W., Tang, Y., Dong, C., Shuang, S., Dual Photoluminescence Emission Carbon Dots for Ratiometric Fluorescent GSH Sensing and Cancer Cell Recognition. ACS Appl. Mater. Interfaces 12, 18250–18257 (2020).

Li, Y., Han, S., Carbon dots-enhanced chemiluminescence method for the sensitive determination of iodide. Microchemical Journal 154, 104638 (2020).

Li, Y., Nie, M., Wang, Q., Facile Fabrication of Electrically Conductive Low-Density Polyethylene/Carbon Fiber Tubes for Novel Smart Materials via Multiaxial Orientation. ACS Appl. Mater. Interfaces 10, 1005–1016 (2018).

Li, Y., Zhang, Z.-Y., Yang, H.-F., Shao, G., Gan, F., Highly selective fluorescent carbon dots probe for mercury(II) based on thymine–mercury(II)–thymine structure. RSC Adv. 8, 3982–3988 (2018).

Liang, C.-Y., Pan, J., Bai, A.-M., Hu, Y.-J., Insights into the interaction of human serum albumin and carbon dots: Hydrothermal synthesis and biophysical study. International Journal of Biological Macromolecules 149, 1118–1129 (2020).

Liang, M., Yan, X., Nanozymes: From New Concepts, Mechanisms, and Standards to Applications. Acc. Chem. Res. 52, 2190–2200 (2019).

Liu, G., Feng, D.-Q., Qian, Y., Wang, W., Zhu, J.-J., Construction of FRET biosensor for off-on detection of lead ions based on carbon dots and gold nanorods. Talanta 201, 90–95 (2019).

Liu, M.L., Chen, B.B., Li, C.M., Huang, C.Z., Carbon dots: synthesis, formation mechanism, fluorescence origin and sensing applications. Green Chem. 21, 449–471 (2019).

Liu, W., Tian, L., Du, J., Wu, J., Liu, Y., Wu, G., Lu, X., Triggered peroxidase-like activity of Au decorated carbon dots for colorimetric monitoring of Hg^{2+} enrichment in Chlorella vulgaris. Analyst 145, 5500–5507 (2020).

Liu, Y., Wei, Z., Duan, W., Ren, C., Wu, J., Liu, D., Chen, H., A dual-mode sensor for colorimetric and "turn-on" fluorescent detection of ascorbic acid. Dyes and Pigments 149, 491–497 (2018).

Londoño-Restrepo, S.M., Jeronimo-Cruz, R., Millán-Malo, B.M., Rivera-Muñoz, E.M., Rodriguez-García, M.E., Effect of the Nano Crystal Size on the X-ray Diffraction Patterns of Biogenic Hydroxyapatite from Human, Bovine, and Porcine Bones. Sci Rep 9, 1–12 (2019).

Loo, A.H., Sofer, Z., Bouša, D., Ulbrich, P., Bonanni, A., Pumera, M., Carboxylic Carbon Quantum Dots as a Fluorescent Sensing Platform for DNA Detection. ACS Appl. Mater. Interfaces 8, 1951–1957 (2016).

Lopes, G.R., Pinto, D.C.G.A., Silva, A.M.S., Horseradish peroxidase (HRP) as a tool in green chemistry. RSC Adv. 4, 37244–37265 (2014).

Lu, C., Liu, J., Gan, L., Yang, X., Employing Cryptococcus-directed carbon dots for differentiating and detecting m-benzenediol and p-benzenediol. Sensors and Actuators B: Chemical 301, 127077 (2019).

Lu, D., Tang, Y., Gao, J., Chen, Y., Wang, Q., Green anhydrous assembly of carbon dots via solar light irradiation and its multi-modal sensing performance. Dyes and Pigments 165, 287–293 (2019).

Lu, M., Zhou, L., One-step sonochemical synthesis of versatile nitrogen-doped carbon quantum dots for sensitive detection of Fe^{2+} ions and temperature in vitro. Materials Science and Engineering: C 101, 352–359 (2019).

Lu, S., Xiao, G., Sui, L., Feng, T., Yong, X., Zhu, S., Li, B., Liu, Z., Zou, B., Jin, M., Tse, J.S., Yan, H., Yang, B., Piezochromic Carbon Dots with Two-photon Fluorescence. Angewandte Chemie 129, 6283–6287 (2017).

M. R. Gonçalves, H., Neves, S.A.F., Duarte, A., de Zea Bermudez, V., Nanofluid Based on Carbon Dots Functionalized with Ionic Liquids for Energy Applications. Energies 13, 649 (2020).

Ma, Z., Ming, H., Huang, H., Liu, Y., Kang, Z., One-step ultrasonic synthesis of fluorescent N-doped carbon dots from glucose and their visible-light sensitive photocatalytic ability. New J. Chem. 36, 861–864 (2012).

Miao, H., Wang, Y., Yang, X., Carbon dots derived from tobacco for visually distinguishing and detecting three kinds of tetracyclines. Nanoscale 10, 8139–8145 (2018).

Milenkovic, I., Algarra, M., Alcoholado, C., Cifuentes, M., Lázaro-Martínez, J.M., Rodríguez-Castellón, E., Mutavdžić, D., Radotić, K., Bandosz, T.J., Fingerprint imaging using N-doped carbon dots. Carbon 144, 791–797 (2019).

Mintz, K.J., Guerrero, B., Leblanc, R.M., Photoinduced Electron Transfer in Carbon Dots with Long-Wavelength Photoluminescence. J. Phys. Chem. C 122, 29507–29515 (2018).

Mohammed, L.J., Omer, K.M., Dual functional highly luminescence B, N Co-doped carbon nanodots as nanothermometer and Fe^{3+}/Fe^{2+} sensor. Sci Rep 10, 3028 (2020).

Momper, R., Steinbrecher, J., Dorn, M., Rörich, I., Bretschneider, S., Tonigold, M., Ramanan, C., Ritz, S., Mailänder, V., Landfester, K., Bannwarth, M.B., Enhanced photoluminescence properties of a carbon dot system through surface interaction with polymeric nanoparticles. Journal of Colloid and Interface Science 518, 11–20 (2018).

Mondal, S., Yucknovsky, A., Akulov, K., Ghorai, N., Schwartz, T., Ghosh, H.N., Amdursky, N., Efficient Photosensitizing Capabilities and Ultrafast Carrier Dynamics of Doped Carbon Dots. J. Am. Chem. Soc. 141, 15413–15422 (2019).

Mu, Z., Hua, J., Feng, S., Yang, Y., A ratiometric fluorescence and light scattering sensing platform based on Cu-doped carbon dots for tryptophan and Fe(III). Spectrochimica Acta Part A: Molecular and Biomolecular Spectroscopy 219, 248–256 (2019).

Naghdi, T., Golmohammadi, H., Yousefi, H., Hosseinifard, M., Kostiv, U., Horák, D., Merkoçi, A., Chitin Nanofiber Paper toward Optical (Bio)sensing Applications. ACS Appl. Mater. Interfaces 12, 15538–15552 (2020).

Ngo, Y.-L.T., Nguyen, P.L., Jana, J., Choi, W.M., Chung, J.S., Hur, S.H., Simple paper-based colorimetric and fluorescent glucose sensor using N-doped carbon dots and metal oxide hybrid structures. Analytica Chimica Acta 1147, 187–198 (2021).

Nguyen, V., Zhao, N., Yan, L., Zhong, P., Nguyen, V.C., Le, P.H., Double-pulse femtosecond laser ablation for synthesis of ultrasmall carbon nanodots. Mater. Res. Express 7, 015606 (2020).

Nirala, N.R., Abraham, S., Kumar, V., Bansal, A., Srivastava, A., Saxena, P.S., Colorimetric detection of cholesterol based on highly efficient peroxidase mimetic activity of graphene quantum dots. Sensors and Actuators B: Chemical 218, 42–50 (2015).

Novoa-De León, I.C., Johny, J., Vázquez-Rodríguez, S., García-Gómez, N., Carranza-Bernal, S., Mendivil, I., Shaji, S., Sepúlveda-Guzmán, S., Tuning the luminescence of nitrogen-doped graphene quantum dots synthesized by pulsed laser ablation in liquid and their use as a selective photoluminescence on–off–on probe for ascorbic acid detection. Carbon 150, 455–464 (2019).

Pan, M., Xu, Z., Jiang, Q., Feng, J., Sun, J., Wang, F., Liu, X., Interfacial engineering of carbon dots with benzenediboronic acid for fluorescent biosensing. Nanoscale Advances 1, 765–771 (2019).

Pandey, M., Balachandran, M., Green Luminescence and Irradiance Properties of Carbon Dots Cross-linked with Polydimethylsiloxane. J. Phys. Chem. C 123, 19835–19843 (2019).

Patir, K., Gogoi, S.K., Facile Synthesis of Photoluminescent Graphitic Carbon Nitride Quantum Dots for Hg^{2+} Detection and Room Temperature Phosphorescence. ACS Sustainable Chem. Eng. 6, 1732–1743 (2018).

Paulo-Mirasol, S., Gené-Marimon, S., Martínez-Ferrero, E., Palomares, E., Inverted Hybrid Light-Emitting Diodes Using Carbon Dots as Selective Contacts: The Effect of Surface Ligands. ACS Appl. Electron. Mater. 2, 1388–1394 (2020).

Peng, J., Gao, W., Gupta, B.K., Liu, Z., Romero-Aburto, R., Ge, L., Song, L., Alemany, L.B., Zhan, X., Gao, G., Vithayathil, S.A., Kaipparettu, B.A., Marti, A.A., Hayashi, T., Zhu, J.-J., Ajayan, P.M., Graphene Quantum Dots Derived from Carbon Fibers. Nano Lett. 12, 844–849 (2012).

Prathumsuwan, T., Jamnongsong, S., Sampattavanich, S., Paoprasert, P., Preparation of carbon dots from succinic acid and glycerol as ferrous ion and hydrogen peroxide dual-mode sensors and for cell imaging. Optical Materials 86, 517–529 (2018).

Puvvada, N., Kumar, B.N.P., Konar, S., Kalita, H., Mandal, M., Pathak, A., 2012. Synthesis of biocompatible multicolor luminescent carbon dots for bioimaging applications. Science and Technology of Advanced Materials 13, 045008.

Pyne, A., Layek, S., Patra, A., Sarkar, N., An easy and smart way to explore the light-emitting responses of carbon dot and doxorubicin hydrochloride assembly: white light generation and pH-dependent reversible photoswitching. J. Mater. Chem. C 7, 6414–6425 (2019).

Qaddare, S.H., Salimi, A., Amplified fluorescent sensing of DNA using luminescent carbon dots and AuNPs/GO as a sensing platform: A novel coupling of FRET and DNA hybridization for homogeneous HIV-1 gene detection at femtomolar level. Biosensors and Bioelectronics 89, 773–780 (2017).

Qiao, G., Lu, D., Tang, Y., Gao, J., Wang, Q., Smart choice of carbon dots as a dual-mode onsite nanoplatform for the trace level detection of $Cr_2O_7^{2-}$. Dyes and Pigments 163, 102–110 (2019).

Qu, J., Zhang, X., Liu, Y., Xie, Y., Cai, J., Zha, G., Jing, S., N, P-co-doped carbon dots as a dual-mode colorimetric/ratiometric fluorescent sensor for formaldehyde and cell imaging via an aminal reaction-induced aggregation process. Microchim Acta 187, 355 (2020).

Qu, Y., Ren, G., Yu, L., Zhu, B., Chai, F., Chen, L., The carbon dots as colorimetric and fluorescent dual-readout probe for 2-nitrophenol and 4-nitrophenol detection. Journal of Luminescence 207, 589–596 (2019).

Radhakrishnan, K., Panneerselvam, P., Green synthesis of surface-passivated carbon dots from the prickly pear cactus as a fluorescent probe for the dual detection of arsenic(III) and hypochlorite ions from drinking water. RSC Adv. 8, 30455–30467 (2018).

Radhakrishnan, K., Panneerselvam, P., Marieeswaran, M., A green synthetic route for the surface-passivation of carbon dots as an effective multifunctional fluorescent sensor for the recognition and detection of toxic metal ions from aqueous solution. Anal. Methods 11, 490–506 (2019).

Rao, X., Yuan, M., Jiang, H., Li, L., Liu, Z., A universal strategy to obtain chiroptical carbon quantum dots through the optically active surface passivation procedure. New J. Chem. 43, 13735–13740 (2019).

Ren, G., Meng, Y., Zhang, Q., Tang, M., Zhu, B., Chai, F., Wang, C., Su, Z., Nitrogen-doped carbon dots for the detection of mercury ions in living cells and visualization of latent fingerprints. New J. Chem. 42, 6824–6830 (2018).

Ren, J., Weber, F., Weigert, F., Wang, Y., Choudhury, S., Xiao, J., Lauermann, I., Resch-Genger, U., Bande, A., Petit, T., Influence of surface chemistry on optical, chemical and electronic properties of blue luminescent carbon dots. Nanoscale 11, 2056–2064 (2019).

Roy, S., Preeyanka, N., Majhi, D., Seth, S., Sarkar, M., Striking Similarities in the Fluorescence Behavior between Carbon Dots and Ionic Liquids: Toward Understanding the Fluorescence Behavior of Carbon Dots. J. Phys. Chem. C 122, 12384–12394 (2018).

Ru, Y., Ai, L., Jia, T., Liu, X., Lu, S., Tang, Z., Yang, B., Recent advances in chiral carbonized polymer dots: From synthesis and properties to applications. Nano Today 34, 100953 (2020).

Schneider, J., Reckmeier, C.J., Xiong, Y., von Seckendorff, M., Susha, A.S., Kasák, P., Rogach, A.L., Molecular Fluorescence in Citric Acid-Based Carbon Dots. J. Phys. Chem. C 121, 2014–2022 (2017).

Scidà, A., Haque, S., Treossi, E., Robinson, A., Smerzi, S., Ravesi, S., Borini, S., Palermo, V., Application of graphene-based flexible antennas in consumer electronic devices. Materials Today 21, 223–230 (2018).

Semeniuk, M., Yi, Z., Poursorkhabi, V., Tjong, J., Jaffer, S., Lu, Z.-H., Sain, M., Future Perspectives and Review on Organic Carbon Dots in Electronic Applications. ACS Nano 13, 6224–6255 (2019).

Sendão, R.M.S., Crista, D.M.A., Afonso, A.C.P., Yuso, M. del V.M. de, Algarra, M., Silva, J.C.G.E. da, Silva, L.P. da, Insight into the hybrid luminescence showed by carbon dots and molecular fluorophores in solution. Phys. Chem. Chem. Phys. 21, 20919–20926 (2019).

Senthamizhan, A., Fragouli, D., Balusamy, B., Patil, B., Palei, M., Sabella, S., Uyar, T., Athanassiou, A., Hydrochromic carbon dots as smart sensors for water sensing in organic solvents. Nanoscale Adv. 1, 4258–4267 (2019).

Shah, S.N.A., Dou, X., Khan, M., Uchiyama, K., Lin, J.-M., N-doped carbon dots/H2O2 chemiluminescence system for selective detection of Fe^{2+} ion in environmental samples. Talanta 196, 370–375 (2019).

Shan, X., Chai, L., Ma, J., Qian, Z., Chen, J., Feng, H., B-doped carbon quantum dots as a sensitive fluorescence probe for hydrogen peroxide and glucose detection. Analyst 139, 2322–2325 (2014).

Shang, L., Brandholt, S., Stockmar, F., Trouillet, V., Bruns, M., Nienhaus, G.U., Effect of Protein Adsorption on the Fluorescence of Ultrasmall Gold Nanoclusters. Small 10, 1667–1667 (2014).

Shang, L., Yang, L., Seiter, J., Heinle, M., Brenner-Weiss, G., Gerthsen, D., Nienhaus, G.U., Nanoparticles Interacting with Proteins and Cells: A Systematic Study of Protein Surface Charge Effects. Advanced Materials Interfaces 1, 1300079 (2014).

Sharma, R.K., Chan, W.G., Wang, J., Waymack, B.E., Wooten, J.B., Seeman, J.I., Hajaligol, M.R., On the role of peptides in the pyrolysis of amino acids. Journal of Analytical and Applied Pyrolysis 72, 153–163 (2004).

Shen, C.-L., Zang, J.-H., Lou, Q., Su, L.-X., Li, Z., Liu, Z.-Y., Dong, L., Shan, C.-X., In-situ embedding of carbon dots in a trisodium citrate crystal matrix for tunable solid-state fluorescence. Carbon 136, 359–368 (2018).

Shi, B., Su, Y., Duan, Y., Chen, S., Zuo, W., A nanocomposite prepared from copper(II) and nitrogen-doped graphene quantum dots with peroxidase mimicking properties for chemiluminescent determination of uric acid. Microchim Acta 186, 397 (2019).

Shi, J., Yin, T., Shen, W., Effect of surface modification on the peroxidase-like behaviors of carbon dots. Colloids and Surfaces B: Biointerfaces 178, 163–169 (2019).

Shi, W., Fan, H., Ai, S., Zhu, L., Preparation of fluorescent graphene quantum dots from humic acid for bioimaging application. New J. Chem. 39, 7054–7059 (2015).

Shi, W., Wang, Q., Long, Y., Cheng, Z., Chen, S., Zheng, H., Huang, Y., Carbon nanodots as peroxidase mimetics and their applications to glucose detection. Chem. Commun. 47, 6695–6697 (2011).

Shuang, E., Mao, Q.-X., Wang, J.-H., Chen, X.-W., Carbon dots with tunable dual emissions: from the mechanism to the specific imaging of endoplasmic reticulum polarity. Nanoscale 12, 6852–6860 (2020).

Siddique, A.B., Pramanick, A.K., Chatterjee, S., Ray, M., Amorphous Carbon Dots and their Remarkable Ability to Detect 2,4,6-Trinitrophenol. Sci Rep 8, 9770 (2018).

Singh, N.K., Chakma, B., Jain, P., Goswami, P., Protein-Induced Fluorescence Enhancement Based Detection of Plasmodium falciparum Glutamate Dehydrogenase Using Carbon Dot Coupled Specific Aptamer. ACS Comb. Sci. 20, 350–357 (2018).

Song, J., Ma, Q., Liu, Y., Guo, Y., Feng, F., Shuang, S., Novel single excitation dual-emission carbon dots for colorimetric and ratiometric fluorescent dual mode detection of Cu^{2+} and Al^{3+} ions. RSC Adv. 9, 38568–38575 (2019).

Song, Y., Qu, K., Zhao, C., Ren, J., Qu, X., Graphene Oxide: Intrinsic Peroxidase Catalytic Activity and Its Application to Glucose Detection. Advanced Materials 22, 2206–2210 (2010).

Song, Y., Wang, H., Zhang, L., Lai, B., Liu, K., Tan, M., Protein corona formation of human serum albumin with carbon quantum dots from roast salmon. Food Funct. 11, 2358–2367 (2020).

Song, Y., Wei, W., Qu, X., Colorimetric Biosensing Using Smart Materials. Advanced Materials 23, 4215–4236 (2011).

Srivastava, I., Misra, S.K., Bangru, S., Boateng, K.A., Soares, J.A.N.T., Schwartz-Duval, A.S., Kalsotra, A., Pan, D., Complementary Oligonucleotide Conjugated Multicolor Carbon Dots for Intracellular Recognition of Biological Events. ACS Appl. Mater. Interfaces 12, 16137–16149 (2020).

Sun, H., Gao, N., Dong, K., Ren, J., Qu, X., Graphene Quantum Dots-Band-Aids Used for Wound Disinfection. ACS Nano 8, 6202–6210 (2014).

Sun, H., Zhao, A., Gao, N., Li, K., Ren, J., Qu, X., Deciphering a Nanocarbon-Based Artificial Peroxidase: Chemical Identification of the Catalytically Active and Substrate-Binding Sites on Graphene Quantum Dots. Angewandte Chemie International Edition 54, 7176–7180 (2015).

Sun, Y., Ding, C., Lin, Y., Sun, W., Liu, H., Zhu, X., Dai, Y., Luo, C., 2018. Highly selective and sensitive chemiluminescence biosensor for adenosine detection based on carbon quantum dots catalyzing luminescence released from aptamers

functionalized graphene@magnetic β-cyclodextrin polymers. Talanta 186, 238–247 (2018).

Sun, Y., Wang, X., Wang, Chan, Tong, D., Wu, Q., Jiang, K., Jiang, Y., Wang, C., Yang, M., Red emitting and highly stable carbon dots with dual response to pH values and ferric ions. Microchim Acta 185, 83 (2018).

Tabaraki, R., Sadeghinejad, N., Microwave assisted synthesis of doped carbon dots and their application as green and simple turn off–on fluorescent sensor for mercury(II) and iodide in environmental samples. Ecotoxicology and Environmental Safety 153, 101–106 (2018).

Tajik, S., Dourandish, Z., Zhang, K., Beitollahi, H., Van Le, Q., Won Jang, H., Shokouhimehr, M., Carbon and graphene quantum dots: a review on syntheses, characterization, biological and sensing applications for neurotransmitter determination. RSC Advances 10, 15406–15429 (2020).

Tang, L., Ji, R., Cao, X., Lin, J., Jiang, H., Li, X., Teng, K.S., Luk, C.M., Zeng, S., Hao, J., Lau, S.P., Deep Ultraviolet Photoluminescence of Water-Soluble Self-Passivated Graphene Quantum Dots. ACS Nano 6, 5102–5110 (2012).

Tang, Y., Li, J., Guo, Q., Nie, G., An ultrasensitive electrochemiluminescence assay for Hg^{2+} through graphene quantum dots and poly(5-formylindole) nanocomposite. Sensors and Actuators B: Chemical 282, 824–830 (2019).

V., R., Gujar, V., Pathan, H., Islam, S., Tawre, M., Pardesi, K., Santra, M.K., Ottoor, D., Bioimaging Applications of Carbon dots (C. dots) and its Cystamine Functionalization for the Sensitive Detection of Cr(VI) in Aqueous Samples. J Fluoresc 29, 1381–1392 (2019).

Venkateswara Raju, C., Kalaiyarasan, G., Paramasivam, S., Joseph, J., Senthil Kumar, S., Phosphorous doped carbon quantum dots as an efficient solid state electrochemiluminescence platform for highly sensitive turn-on detection of Cu^{2+} ions. Electrochimica Acta 331, 135391 (2020).

Wang, A., Xiao, X., Zhou, C., Lyu, F., Fu, L., Wang, C., Ruan, S., Large-scale synthesis of carbon dots/TiO_2 nanocomposites for the photocatalytic color switching system. Nanoscale Adv. 1, 1819–1825 (2019).

Wang, Huan, Li, P., Yu, D., Zhang, Y., Wang, Z., Liu, C., Qiu, H., Liu, Z., Ren, J., Qu, X., Unraveling the Enzymatic Activity of Oxygenated Carbon Nanotubes and Their Application in the Treatment of Bacterial Infections. Nano Lett. 18, 3344–3351 (2018).

Wang, H., Liu, S., Xie, Y., Bi, J., Li, Y., Song, Y., Cheng, S., Li, D., Tan, M., Facile one-step synthesis of highly luminescent N-doped carbon dots as an efficient fluorescent probe for chromium(VI) detection based on the inner filter effect. New J. Chem. 42, 3729–3735 (2018).

Wang, H.-J., He, X., Luo, T.-Y., Zhang, J., Liu, Y.-H., Yu, X.-Q., Amphiphilic carbon dots as versatile vectors for nucleic acid and drug delivery. Nanoscale 9, 5935–5947 (2017).

Wang, J., Xu, M., Wang, D., Li, Z., Primo, F.L., Tedesco, A.C., Bi, H., Copper-Doped Carbon Dots for Optical Bioimaging and Photodynamic Therapy. Inorg. Chem. 58, 13394–13402 (2019).

Wang, N., Wang, M., Yu, Y., Yang, G., Su, X., Label-free fluorescence assay based on near-infrared B,N-doped carbon dots as a fluorescent probe for the detection of sialic acid. New Journal of Chemistry 44, 2350–2356 (2020).

Wang, Q., Zhang, S., Wang, B., Yang, X., Zou, B., Yang, B., Lu, S., Pressure-triggered aggregation-induced emission enhancement in red emissive amorphous carbon dots. Nanoscale Horiz. 4, 1227–1231 (2019).

Wang, S., Zhang, Yajun, Pang, G., Zhang, Yingwei, Guo, S., Tuning the Aggregation/Disaggregation Behavior of Graphene Quantum Dots by Structure-Switching Aptamer for High-Sensitivity Fluorescent Ochratoxin A Sensor. Anal. Chem. 89, 1704–1709 (2017).

Wang, T., Chen, G., Li, L., Wu, Y., Highly Fluorescent Green Carbon Dots as a Fluorescent Probe for Detecting Mineral Water pH. Sensors (Basel) 19, 3801 (2019).

Wang, X., Feng, Y., Dong, P., Huang, J., A Mini Review on Carbon Quantum Dots: Preparation, Properties, and Electrocatalytic Application. Frontiers in Chemistry 7, 671 (2019).

Wang, X., Li, X., Mao, Y., Wang, D., Zhao, Q., Wang, S., Multi-stimuli responsive nanosystem modified by tumor-targeted carbon dots for chemophototherapy synergistic therapy. Journal of Colloid and Interface Science 552, 639–650 (2019).

Wang, X., Qu, K., Xu, B., Ren, J., Qu, X., Multicolor luminescent carbon nanoparticles: Synthesis, supramolecular assembly with porphyrin, intrinsic peroxidase-like catalytic activity and applications. Nano Res. 4, 908–920 (2011).

Wang, X., Zhang, F., Liu, L., Leng, J., Liu, Y., Zhao, X., Zhang, H., A humidity-driven flexible carbon nitride film with multiple deformations. Smart Mater. Struct. 28, 105007 (2019).

Wang, X.-X., Wu, Q., Shan, Z., Huang, Q.-M., BSA-stabilized Au clusters as peroxidase mimetics for use in xanthine detection. Biosensors and Bioelectronics 26, 3614–3619 (2011).

Wang, Y., Zhu, Y., Yu, S., Jiang, C., Fluorescent carbon dots: rational synthesis, tunable optical properties and analytical applications. RSC Adv. 7, 40973–40989 (2017).

Wang, Y., Xu, J., Wang, Yawen, Chen, H., Emerging chirality in nanoscience. Chem. Soc. Rev. 42, 2930–2962 (2013).

Wei, H., Wang, E., Nanomaterials with enzyme-like characteristics (nanozymes): next-generation artificial enzymes. Chem. Soc. Rev. 42, 6060–6093 (2013).

Wei, H., Wang, E., Fe_3O_4 Magnetic Nanoparticles as Peroxidase Mimetics and Their Applications in H_2O_2 and Glucose Detection. Anal. Chem. 80, 2250–2254 (2008).

Wei, M., Lee, J., Xia, F., Lin, P., Hu, X., Li, F., Ling, D., Chemical design of nanozymes for biomedical applications. Acta Biomaterialia 126, 15–30 (2021).

Winterbourn, C.C., Biological Production, Detection, and Fate of Hydrogen Peroxide. Antioxidants & Redox Signaling 29, 541–551 (2018).

Wolfbeis, O.S., Leiner, M., Mapping of the total fluorescence of human blood serum as a new method for its characterization. Analytica Chimica Acta 167, 203–215 (1985).

Wu, F., Yue, L., Yang, L., Wang, K., Liu, G., Luo, X., Zhu, X., Ln(III) chelates-functionalized carbon quantum dots: Synthesis, optical studies and multimodal bioimaging applications. Colloids and Surfaces B: Biointerfaces 175, 272–280 (2019).

Wu, J., Fu, S., Zhang, X., Wu, C., Wang, A., Li, C., Shan, G., Liu, Y., Bidirectional Photochromism via Anchoring of Carbon Dots to TiO_2 Porous Films. ACS Appl. Mater. Interfaces 12, 6262–6267 (2020).

Wu, J., Wang, X., Wang, Q., Lou, Z., Li, S., Zhu, Y., Qin, L., Wei, H., Nanomaterials with enzyme-like characteristics (nanozymes): next-generation artificial enzymes (II). Chem. Soc. Rev. 48, 1004–1076 (2019).

Wu, X., Tian, F., Wang, W., Chen, J., Wu, M., Zhao, J.X., Fabrication of highly fluorescent graphene quantum dots using L-glutamic acid for in vitro/in vivo imaging and sensing. J. Mater. Chem. C 1, 4676–4684 (2013).

Wu, Y., Chen, Y., Zhang, S., Zhang, L., Gong, J., Bifunctional S, N-Codoped carbon dots-based novel electrochemiluminescent bioassay for ultrasensitive detection of atrazine using activated mesoporous biocarbon as enzyme nanocarriers. Analytica Chimica Acta 1073, 45–53 (2019).

Wu, Y., Liu, Y., Yin, J., Li, H., Huang, J., Facile ultrasonic synthesized NH2-carbon quantum dots for ultrasensitive Co^{2+} ion detection and cell imaging. Talanta 205, 120121 (2019).

Xiong, R., Chen, M., Cui, X., Wang, Q., Liu, X., Geng, B., Simultaneous and Reversible Triggering of the Phase Transfer and Luminescence Change of Amidine-Modified Carbon Dots by CO2. ACS Appl. Mater. Interfaces 11, 22851–22857 (2019).

Xiong, Y., Schneider, J., Ushakova, E.V., Rogach, A.L., Influence of molecular fluorophores on the research field of chemically synthesized carbon dots. Nano Today 23, 124–139 (2018).

Xu, L., Zhang, W., Shang, L., Ma, R., Jia, L., Jia, W., Wang, H., Niu, L., Perylenetetracarboxylic acid and carbon quantum dots assembled synergistic electrochemiluminescence nanomaterial for ultra-sensitive carcinoembryonic antigen detection. Biosensors and Bioelectronics 103, 6–11 (2018).

Xu, Q., Li, W., Ding, L., Yang, W., Xiao, H., Ong, W.-J., Function-driven engineering of 1D carbon nanotubes and 0D carbon dots: mechanism, properties and applications. Nanoscale 11, 1475–1504 (2019).

Xu, Q., Su, R., Chen, Y., Theruvakkattil Sreenivasan, S., Li, N., Zheng, X., Zhu, J., Pan, H., Li, W., Xu, C., Xia, Z., Dai, L., Metal Charge Transfer Doped Carbon Dots with Reversibly Switchable, Ultra-High Quantum Yield Photoluminescence. ACS Appl. Nano Mater. 1, 1886–1893 (2018).

Xu, S., Zhang, F., Xu, L., Liu, X., Ma, P., Sun, Y., Wang, X., Song, D., A fluorescence resonance energy transfer biosensor based on carbon dots and gold nanoparticles for the detection of trypsin. Sensors and Actuators B: Chemical 273, 1015–1021 (2018).

Xu, X., Ray, R., Gu, Y., Ploehn, H.J., Gearheart, L., Raker, K., Scrivens, W.A., Electrophoretic Analysis and Purification of Fluorescent Single-Walled Carbon Nanotube Fragments. J. Am. Chem. Soc. 126, 12736–12737 (2004).

Xu, X., Ren, D., Chai, Y., Cheng, X., Mei, J., Bao, J., Wei, F., Xu, G., Hu, Q., Cen, Y., Dual-emission carbon dots-based fluorescent probe for ratiometric sensing of Fe(III) and pyrophosphate in biological samples. Sensors and Actuators B: Chemical 298, 126829 (2019).

Xu, Y., Li, H., Wang, B., Liu, H., Zhao, L., Zhou, T., Liu, M., Huang, N., Li, Y., Ding, L., Chen, Y., Microwave-assisted synthesis of carbon dots for "turn-on" fluorometric determination of Hg(II) via aggregation-induced emission. Microchim Acta 185, 252 (2018).

Xu, Z.-Q., Yang, Q.-Q., Lan, J.-Y., Zhang, J.-Q., Peng, W., Jin, J.-C., Jiang, F.-L., Liu, Y., Interactions between carbon nanodots with human serum albumin and γ-globulins: The effects on the transportation function. Journal of Hazardous Materials 301, 242–249 (2016).

Xue, J., Xu, X., Zhu, Y., Yang, D., Lanthanide based white-light-emitting hydrogel mediated by fluorescein and carbon dots with high quantum yield and multi-stimuli responsiveness. J. Mater. Chem. C 8, 3380–3385 (2020).

Yamaguchi, Y., Matsubara, Y., Ochi, T., Wakamiya, T., Yoshida, Z., How the π Conjugation Length Affects the Fluorescence Emission Efficiency. J. Am. Chem. Soc. 130, 13867–13869 (2008).

Yan, F., Bai, Z., Ma, T., Sun, X., Zu, F., Luo, Y., Chen, L., Surface modification of carbon quantum dots by fluorescein derivative for dual-emission ratiometric fluorescent hypochlorite biosensing and in vivo bioimaging. Sensors and Actuators B: Chemical 296, 126638 (2019a).

Yan, F., Bai, Z., Zu, F., Zhang, Y., Sun, X., Ma, T., Chen, L., Yellow-emissive carbon dots with a large Stokes shift are viable fluorescent probes for detection and cellular imaging of silver ions and glutathione. Microchim Acta 186, 113 (2019b).

Yan, G.-H., Song, Z.-M., Liu, Y.-Y., Su, Q., Liang, W., Cao, A., Sun, Y.-P., Wang, H., Effects of carbon dots surface functionalities on cellular behaviors – Mechanistic exploration for opportunities in manipulating uptake and translocation. Colloids and Surfaces B: Biointerfaces 181, 48–57 (2019).

Yan, H., Ni, H., Yang, Y., Shan, C., Yang, X., Li, X., Cao, J., Wu, W., Liu, W., Tang, Y., Smart nanoprobe based on two-photon sensitized terbium-carbon dots

for dual-mode fluorescence thermometer and antibacterial. Chinese Chemical Letters 31, 1792–1796 (2020).

Yang, H., Liu, Y., Guo, Z., Lei, B., Zhuang, J., Zhang, X., Liu, Z., Hu, C., Hydrophobic carbon dots with blue dispersed emission and red aggregation-induced emission. Nat Commun 10, 1789 (2019).

Yang, M., Tang, Q., Meng, Y., Liu, J., Feng, T., Zhao, X., Zhu, S., Yu, W., Yang, B., Reversible "Off–On" Fluorescence of Zn^{2+}-Passivated Carbon Dots: Mechanism and Potential for the Detection of EDTA and Zn^{2+}. Langmuir 34, 7767–7775 (2018).

Yang, P., Zhu, Z., Zhang, T., Chen, M., Cao, Y., Zhang, W., Wang, X., Zhou, X., Chen, W., Facile synthesis and photoluminescence mechanism of green emitting xylose-derived carbon dots for anti-counterfeit printing. Carbon 146, 636–649 (2019).

Yang, S., Zhang, Y., Xue, Y., Lu, S., Yang, H., Yang, L., Ding, C., Yu, S., Cross-Linked Polyamide Chains Enhanced the Fluorescence of Polymer Carbon Dots. ACS Omega 5, 8219–8229 (2020).

Yang, W., Huang, T., Zhao, M., Luo, F., Weng, W., Wei, Q., Lin, Z., Chen, G., High peroxidase-like activity of iron and nitrogen co-doped carbon dots and its application in immunosorbent assay. Talanta 164, 1–6. (2017)

Yang, Z., Liu, Y., Lu, C., Yue, G., Wang, Y., Rao, H., Zhang, W., Lu, Z., Wang, X., One-pot synthesis of CeO_2-carbon dots with enhanced peroxidase-like activity and carbon dots for ratiometric fluorescence detection of H_2O_2 and cholesterol. Journal of Alloys and Compounds 862, 158323 (2021).

Yarur, F., Macairan, J.-R., Naccache, R., 2019. Ratiometric detection of heavy metal ions using fluorescent carbon dots. Environ. Sci.: Nano 6, 1121–1130 (2019).

Yu, J., Liu, C., Yuan, K., Lu, Z., Cheng, Y., Li, L., Zhang, X., Jin, P., Meng, F., Liu, H., Luminescence Mechanism of Carbon Dots by Tailoring Functional Groups for Sensing Fe^{3+} Ions. Nanomaterials 8, 233 (2018).

Yu, S., Ding, L., Lin, H., Wu, W., Huang, J., A novel optical fiber glucose biosensor based on carbon quantum dots-glucose oxidase/cellulose acetate complex sensitive film. Biosensors and Bioelectronics 146, 111760 (2019).

Yu, X., Cheng, H., Zhang, M., Zhao, Y., Qu, L., Shi, G., 2017. Graphene-based smart materials. Nat Rev Mater 2, 1–13 (2017).

Yuan, B., Guan, S., Sun, X., Li, X., Zeng, H., Xie, Z., Chen, P., Zhou, S., Highly Efficient Carbon Dots with Reversibly Switchable Green–Red Emissions for Trichromatic White Light-Emitting Diodes. ACS Appl. Mater. Interfaces 10, 16005–16014 (2018).

Yuan, F., Wang, Y.-K., Sharma, G., Dong, Y., Zheng, X., Li, P., Johnston, A., Bappi, G., Fan, J.Z., Kung, H., Chen, B., Saidaminov, M.I., Singh, K., Voznyy, O., Bakr, O.M., Lu, Z.-H., Sargent, E.H., Bright high-colour-purity deep-blue carbon dot light-emitting diodes via efficient edge amination. Nat. Photonics 14, 171–176 (2020).

Yue, L., Li, H., Sun, Q., Zhang, J., Luo, X., Wu, F., Zhu, X., Red-Emissive Ruthenium-Containing Carbon Dots for Bioimaging and Photodynamic Cancer Therapy. ACS Appl. Nano Mater. 3, 869–876 (2020).

Zhai, H., Bai, Y., Qin, J., Feng, F., Colorimetric and Ratiometric Fluorescence Dual-Mode Sensing of Glucose Based on Carbon Quantum Dots and Potential UV/Fluorescence of o-Diaminobenzene. Sensors 19, 674 (2019).

Zhai, H., Bai, Y., Wang, H., Qin, J., Liu, H., Feng, F., Development of a novel fluorescence ratiometric glucose sensor based on carbon dots and a potential fluorophore m-dihydroxybenzene. Anal. Methods 10, 5380–5386 (2018).

Zhan, Y., Geng, T., Liu, Y., Hu, C., Zhang, X., Lei, B., Zhuang, J., Wu, X., Huang, D., Xiao, G., Zou, B., Near-Ultraviolet to Near-Infrared Fluorescent Nitrogen-Doped Carbon Dots with Two-Photon and Piezochromic Luminescence. ACS Appl. Mater. Interfaces 10, 27920–27927 (2018).

Zhang, J., Chen, J., Xu, B., Wang, L., Ma, S., Dong, Y., Li, B., Ye, L., Tian, W., 2013. Remarkable fluorescence change based on the protonation–deprotonation control in organic crystals. Chem. Commun. 49, 3878–3880 (2013).

Zhang, M., Jia, Y., Cao, J., Li, G., Ren, H., Li, H., Yao, H., Carbon dots-enhanced luminol chemiluminescence and its application to 2-methoxyestradiol determination. Green Chemistry Letters and Reviews 11, 379–386 (2018).

Zhang, M., Su, R., Zhong, J., Fei, L., Cai, W., Guan, Q., Li, W., Li, N., Chen, Y., Cai, L., Xu, Q., Red/orange dual-emissive carbon dots for pH sensing and cell imaging. Nano Res. 12, 815–821 (2019).

Zhang, P., Wei, J.-S., Chen, X.-B., Xiong, H.-M., Heteroatom-doped carbon dots based catalysts for oxygen reduction reactions. Journal of Colloid and Interface Science 537, 716–724 (2019).

Zhang, Q., Liu, Yuying, Nie, Y., Liu, Yang, Ma, Q., Wavelength-Dependent Surface Plasmon Coupling Electrochemiluminescence Biosensor Based on Sulfur-Doped Carbon Nitride Quantum Dots for K-RAS Gene Detection. Anal. Chem. 91, 13780–13786 (2019).

Zhang, Q., Zhang, C., Li, Z., Ge, J., Li, C., Dong, C., Shuang, S., Nitrogen-doped carbon dots as fluorescent probe for detection of curcumin based on the inner filter effect. RSC Adv. 5, 95054–95060 (2015).

Zhang, R., Chen, A., Yu, Y., Chai, Y., Zhuo, Y., Yuan, R., Electrochemiluminescent carbon dot-based determination of microRNA-21 by using a hemin/G-wire supramolecular nanostructure as co-reaction accelerator. Microchim Acta 185, 432 (2018).

Zhang, T., Dong, S., Zhao, F., Deng, M., Fu, Y., Lü, C., Tricolor emissive carbon dots for ultra-wide range pH test papers and bioimaging. Sensors and Actuators B: Chemical 298, 126869 (2019).

Zhang, X., Lu, J., Li, X., Chai, L., Jiao, Y., Facile heat reflux synthesis of blue luminescent carbon dots as optical nanoprobes for cellular imaging. New J. Chem. 41, 702–708 (2017).

Zhao, D., Liu, X., Zhang, Z., Zhang, R., Liao, L., Xiao, X., Cheng, H., Synthesis of Multicolor Carbon Dots Based on Solvent Control and Its Application in the Detection of Crystal Violet. Nanomaterials (Basel) 9, 1556 (2019).

Zhao, L., Wu, Z., Liu, G., Lu, H., Gao, Y., Liu, F., Wang, C., Cui, J., Lu, G., High-activity Mo, S co-doped carbon quantum dot nanozyme-based cascade colorimetric biosensor for sensitive detection of cholesterol. J. Mater. Chem. B 7, 7042–7051 (2019).

Zhao, Q., Song, W., Zhao, B., Yang, B., Spectroscopic studies of the optical properties of carbon dots: recent advances and future prospects. Materials Chemistry Frontiers 4, 472–488 (2020).

Zhao, W.-B., Liu, K.-K., Song, S.-Y., Zhou, R., Shan, C.-X., Fluorescent Nano-Biomass Dots: Ultrasonic-Assisted Extraction and Their Application as Nanoprobe for Fe^{3+} detection. Nanoscale Research Letters 14, 130 (2019).

Zheng, C., Ke, W., Yin, T., An, X., Intrinsic peroxidase-like activity and the catalytic mechanism of gold@carbon dots nanocomposites. RSC Adv. 6, 35280–35286 (2016).

Zhou, L., Zheng, D., Wu, B., Zhu, Y., Zhu, L., Gel Systems Doped with Chiral Carbon Dots for Optical Combination. ACS Appl. Nano Mater. 3, 946–952 (2020).

Zhu, L., Cui, X., Wu, J., Wang, Z., Wang, P., Hou, Y., Yang, M., Fluorescence immunoassay based on carbon dots as labels for the detection of human immunoglobulin G. Anal. Methods 6, 4430–4436 (2014).

Zhu, Q., Liu, G., Yan, M., Ye, J., Zhu, L., Huang, J., Yang, X., Cu^{2+} enhanced chemiluminescence of carbon dots-H2O2 system in alkaline solution. Talanta 208, 120380 (2020).

Zhu, Q., Zhang, L., Van Vliet, K., Miserez, A., Holten-Andersen, N., White Light-Emitting Multistimuli-Responsive Hydrogels with Lanthanides and Carbon Dots. ACS Appl. Mater. Interfaces 10, 10409–10418 (2018).

Zhu, S., Song, Y., Zhao, X., Shao, J., Zhang, J., Yang, B., The photoluminescence mechanism in carbon dots (graphene quantum dots, carbon nanodots, and polymer dots): current state and future perspective. Nano Res. 8, 355–381 (2015).

Zhu, S., Zhao, X., Song, Y., Lu, S., Yang, B., Beyond bottom-up carbon nanodots: Citric-acid derived organic molecules. Nano Today 11, 128–132 (2016).

Zhu, W., Zhang, J., Jiang, Z., Wang, W., Liu, X., 2014. High-quality carbon dots: synthesis, peroxidase-like activity and their application in the detection of H_2O_2, Ag^{+} and Fe^{3+}. RSC Adv. 4, 17387–17392 (2014).

Zhu, X., Wang, J., Zhu, Y., Jiang, H., Tan, D., Xu, Z., Mei, T., Li, J., Xue, L., Wang, X., Green emitting N,S-co-doped carbon dots for sensitive fluorometric determination of Fe(III) and Ag(I) ions, and as a solvatochromic probe. Microchim Acta 185, 510 (2018).

List of Publications

A. In Peer-Reviewed Journals:

1. **Smita Das,** Roshika Kaushik, Pranab Goswami. Multifaceted Interaction Studies between carbon dots and Proteins of Clinical Importance for Optical Sensing Signal. ***ACS Applied Bio Materials*** 5, 889-896. (Part of Chapter 3)

2. **Smita Das,** Sudarshan Gogoi, Naveen Kumar Singh, Pranab Goswami, 2021. "Analytical Application of H_2O_2-Induced Chiroptical Graphitic Carbon Dots". ***Nano Express*** 2, 040003. (Part of Chapter 4)

3. **Smita Das,** Lightson Ngashangva, Hritushree Mog, Sudarshan Gogoi, Pranab Goswami, 2021. "An Insight into the Mechanism of Peroxidase-like Activity of Carbon Dots". ***Optical Materials*** 115, 111017. (Part of Chapter 2)

4. **Smita Das,** Lightson Ngashangva, Pranab Goswami, 2021. "Carbon Dots: An Emerging Smart Material for Analytical Applications". ***Micromachines*** 12, 84. **(Editor's Choice and Feature Paper)** (Part of Chapter 1)

5. Naveen Kumar Singh, Priyamvada Jain, **Smita Das**, Pranab Goswami, 2019. "Dye-Coupled Aptamer-Captured Enzyme Catalysed Reaction for Detection of Pan Malaria and *P. falciparum* Species in Laboratory Settings and Instrument-Free Paper Based Platform". ***Analytical Chemistry*** 91, 4213-4221.

6. Priyamvada Jain, **Smita Das**, Pranab Goswami, 2016. "Aptamer-Graphene Oxide for Highly Sensitive Dual Electrochemical Detection of *Plasmodium* Lactate Dehydrogenase". ***Analytical Biochemistry,*** 514, 32-37 **(Equal 1st author contribution)**

B. Book Chapter

1. **Smita Das,** Pranab Goswami, 2020. "Nanozymes as Potential Catalysts for Sensing and Analytical Applications", Advanced Materials and Techniques for Biosensors and Bioanalytical Applications. CRC Press, p. 143-161. (Part of Chapter 1)

C. Patents Filed

1. Pranab Goswami, Lightson Ngashangva, **Smita Das,** 2020. Title of Invention: A Paper Platform-Based Methanol Detection Kit. Application No. 202031004522.

D. Abstracts Published in Conferences

1. **Smita Das,** Pranab Goswami, Mechanism of Peroxidase-like Activity of Carbon Dots Synthesized from L-glutamic acid, 7th International Conference on Advanced Nanomaterials and Nanotechnology (ICANN), (2021), held at IIT Guwahati during 14th-17th December.

2. **Smita Das,** Pranab Goswami, A Colorimetric Assay for Rapid Dual Detection of Glucose and Cholesterol, 6th International Conference on Advanced Nanomaterials and Nanotechnology (ICANN), (2019), held at IIT Guwahati during 18th-21st December.

3. **Smita Das,** Pranab Goswami, Carbon Dots as Peroxidase Mimetic Catalyst for Detection of H_2O_2 and Cholesterol, 5^{h} International Conference on Advanced Nanomaterials and Nanotechnology (ICANN), (2017), held at IIT Guwahati during 18th-21st December.

4. **Smita Das,** Pranab Goswami, Development of Aptasensor for the Detection of *Plasmodium* Lactate Dehydrogenase, Research Conclave, (2019), held at IIT Guwahati during 14th-17th March. **(Best Oral Presentation).**

E. Workshops Attended

1. CeNSE DBT Nano-biotechnology Alliance (C-DNA) Familiarization workshop, (2022), organized by Centre for Nanoscience and Engineering, IISc Bangalore during 11th-13th January.

2. Scanning Electron Microscope: Technique and its Applications Online Workshop, (2021), conducted by North East Centre for Biological Sciences and Healthcare Engineering (NECBH), IIT Guwahati during 29th-30th July.

3. Indo-US Workshop on Pain Mechanisms and Therapeutics, (2021), organized by Department of Pharmaceutical Engineering & Technology, IIT BHU during 6th-10th May.

4. CeNSE DBT Nano-biotechnology Alliance (C-DNA) Familiarization workshop, (2021), organized by Centre for Nanoscience and Engineering, IISc Bangalore during 11th-13th January.

5. One Day Workshop on "Biomedical Device Technology", (2017), organized by Centre for Nanotechnology, IIT Guwahati on 18th December.

6. 3D-printing workshop organized by Centre for Nanoscience and Engineering, (2017), conducted by IISc Bangalore on 16th May.

Awards and Achievements

1. 1st prize for the research proposal in Guwahati Biotech Park's Talent Search Contest (6th edition) entitled, "Lab-on-Paper for the Selective Detection of Methanol and Formaldehyde" held on 10th February, 2022 organized by Guwahati Biotech Park, Assam, India.

Front Pages of the Papers Published in International Journals

micromachines

MDPI

Review

Carbon Dots: An Emerging Smart Material for Analytical Applications

Smita Das †, Lightson Ngashangva † and Pranab Goswami *

Department of Biosciences and Bioengineering, Indian Institute of Technology Guwahati, Guwahati 781039, Assam, India; smita@iitg.ac.in (S.D.); ng.lightson@iitg.ac.in (L.N.)
* Correspondence: pgoswami@iitg.ac.in; Tel.: +91-361-258-2202; Fax: +91-361-258-2249
† These authors contribute equally to this manuscript.

Abstract: Carbon dots (CDs) are optically active carbon-based nanomaterials. These nanomaterials can change their light emission properties in response to various external stimuli such as pH, temperature, pressure, and light. The CD's remarkable stimuli-responsive smart material properties have recently stimulated massive research interest for their exploitation to develop various sensor platforms. Herein, an effort has been made to review the major advances made on CDs, focusing mainly on its smart material attributes and linked applications. Since the CD's material properties are largely linked to their synthesis approaches, various synthesis methods, including surface passivation and functionalization of CDs and the mechanisms reported so far in their photophysical properties, are also delineated in this review. Finally, the challenges of using CDs and the scope for their further improvement as an optical signal transducer to expand their application horizon for developing analytical platforms have been discussed.

Keywords: carbon dots; smart materials; photoluminescence; chemiluminescence; electrochemiluminescence; analytical; optical

Citation: Das, S.; Ngashangva, L.; Goswami, P. Carbon Dots: An Emerging Smart Material for Analytical Applications. *Micromachines* **2021**, *12*, 84. https://doi.org/10.3390/mi12010084

Received: 23 December 2020
Accepted: 12 January 2021
Published: 15 January 2021

1. Introduction

Since the fortuitous discovery of carbon dots (CDs) in 2004, the interest in these luminescent nanomaterials has been increasing exponentially [1,2]. The CDs are zero-dimensional carbon nanoparticles with a size of less than 10 nm. Compared to the different types of carbon nanomaterials, the CDs have gained enormous attention due to its certain advantages such as inexpensive and easy synthesis, facile surface functionalization, low toxicity, biocompatibility, high water-solubility, tunable luminescence property, and stability at room temperature [3]. Consequently, their applications are explored in bioimaging, drug delivery, and chemical/biological sensing [4]. Additionally, carbon dot's enzyme-like activity has also attracted wide interest because of their potential to replace the naturally occurring enzymes, as the latter is ordinarily unstable, expensive, and challenging to synthesize on a large scale [5].

At present, the concept of employing CDs as smart material is of great interest in material and analytical sciences. A material is termed "smart" when it experiences variation in response to a significant external physical or chemical stimulus that includes light, temperature, pH, solvent, stress, and electric and magnetic field [6]. The synthesis and applications of these smart material or stimulus-responsive materials have been among the principal focus of research in recent times. Conventionally, the smart materials that belong to metal alloys, semiconducting materials, and inorganic compounds are widely used in smart technology such as strain sensors, actuators, and robots [7]. Such materials can change the outlook of modern science and technology and engineering at large. However, the traditional smart materials have limitations ranging from harsh synthesis/preparation conditions to high cost. Therefore, biomaterials and polymers have gradually replaced conventional smart materials in various modern technological fields and applications due to

7 Nanozymes as Potential Catalysts for Sensing and Analytical Applications

Smita Das and Pranab Goswami
Indian Institute of Technology Guwahati, Assam, India

CONTENTS

Optical Materials 115 (2021) 111017

Contents lists available at ScienceDirect

Optical Materials

journal homepage: http://www.elsevier.com/locate/optmat

An insight into the mechanism of peroxidase-like activity of carbon dots

Smita Das, Lightson Ngashangva, Hritushree Mog, Sudarshan Gogoi, Pranab Goswami *

Department of Biosciences and Bioengineering, Indian Institute of Technology Guwahati, Guwahati, 781039, Assam, India

ARTICLE INFO

Keywords:
Carbon dot
Peroxidase
Hydrogen peroxide
L-glutamic acid
Carboxylic acid group

ABSTRACT

The interest in carbon dots (CDs) as peroxidase-mimics has urged to understand the mechanism for this reaction of commercial importance. Firstly, using a theoretical-cum-experimental approach, the –COOH group was identified as an active moiety for strongly binding and degrading H_2O_2 in the presence of a reducing equivalent. Next, the stringency of different compounds containing the –COOH group was examined and identified L-glutamic acid with higher peroxidase-like activity. The $–NH_2$ group present in the vicinity of the –COOH group increased the activity of L-glutamic acid. Following a pyrolysis method, L-glutamic acid was transformed into CDs having a diameter of 3.18 ± 0.53 nm with its core made of pyroglutamic acid. The CD exhibited thermostability (~90 °C) and higher peroxidase-like activity than the L-glutamic acid. The higher activity of the CD was attributed to its binding affinity with ABTS and H_2O_2. The K_m and K_{cat} of the CD for H_2O_2 were 5.85 mM and 0.011 s^{-1}, respectively. Based on spectroscopic investigations, we confirmed the peroxidase-like activity is a surface phenomenon that did not have a significant link to the photophysical property of the CD and proposed a mechanism for the reaction. The colorimetric reaction could be reproduced on a paper platform, confirming the application potential of the CD for developing a low-cost peroxide sensor.

1. Introduction

Since the discovery of carbon dots (CDs) in 2004, the research on this 0-D carbon nanomaterial has been taken up to address the critical issues related to their preparations, properties, and applications [1]. The primary motivation for this research is the potential advantages of the CDs over the conventional quantum dots such as their biocompatibility, low toxicity, tunable luminescent properties, high water solubility, and inexpensive synthesis process [2]. The studies have also demonstrated that many CDs exhibit nanozyme properties [3]. Nanozymes are nanomaterials with intrinsic enzyme-like activity [4,5]. The interest in nanozymes has been stimulated by their several advantages over the natural protein-based enzymes, such as resistance to proteolysis, high stability, and simple and less expensive production and purification steps [6].

The research on nanomaterials as peroxidase-mimic is growing impressively [7]. It is worth mentioning that among the various redox enzymes, the peroxidases find significant interest in industrial, environmental, and analytical applications [8]. The ability of peroxidases to yield chromogenic products at low substrate concentrations makes them well-suited enzymes for various analytical applications. Ever since the discovery of Fe_3O_4 nanoparticles with peroxidase-like activity [4], considerable effort has been made to find nanomaterials that could replace peroxidase enzymes, such as the widely used horseradish peroxidase (HRP). The HRP catalyses the oxidation of various organic substrates by hydrogen peroxide, which has high importance as a synthetic reagent, biological oxidant, and intermediate in the formation and decay of reactive oxygen species [9].

A significant amount of work on the CDs acting as peroxidase mimics is known. Most of these studies are related to their synthesis [10,11], and different applications such as detection of glucose [12], cholesterol [13], bioimaging [14], and immunosorbent assay [15]. Besides, CDs are also doped or composed of different materials to enhance their peroxidase-like properties [16,17]. However, a systematic investigation to understand the detailed mechanism of CD-led peroxidase-like activity is limited. There are some efforts highlighting the mechanism for graphene oxide nanomaterials [18], metal-doped carbon QDs [13,17,19], oxygenated carbon nanotubes [20], and carbon nanodots prepared from candle soots [12]. The identification of the catalytically active and substrate-binding sites on graphene QDs following selective deactivation of the functional groups have also been reported [21]. A broad consensus of oxygen-based functional groups responsible for the CD's peroxidase-like activity is visible from these reports. In contrast, a certain amount of variations among them on the involvement of specific

* Corresponding author.
E-mail address: pgoswami@iitg.ac.in (P. Goswami).

https://doi.org/10.1016/j.optmat.2021.111017
Received 9 December 2020; Received in revised form 24 February 2021; Accepted 11 March 2021
Available online 25 March 2021

ACS APPLIED BIO MATERIALS

www.acsabm.org Article

Multifaceted Interaction Studies between Carbon Dots and Proteins of Clinical Importance for Optical Sensing Signals

Smita Das, Roshika Kaushik, and Pranab Goswami*

Cite This: ACS Appl. Bio Mater. 2022, 5, 889−896 Read Online

ACCESS | Metrics & More | Article Recommendations | Supporting Information

ABSTRACT: Carbon dots (CDs) are emerging as efficient optical probes. However, their application potential for clinical diagnosis has not been adequately explored. Herein, we examined the suitability of pyroglutamate CDs for detecting glucose, cholesterol, and alcohol in blood serum through their peroxidative activity in the respective enzyme-catalyzed reactions following fluorometric and colorimetric approaches. In buffer, the CD's fluorescence intensity ($\lambda_{ex\ 354nm}$) enhanced over 115% after interaction with the enzyme proteins due to different lifetime components on its surface. The enhancement was also linked to FRET with the proteins ($\lambda_{ex\ 274nm}$ for TRP/TYR). The electrostatic interactions, as revealed from the zeta potential study, generated binding energy (ΔG, kcal/mol) in the range of −5.8 to −6.3 and greatly shifted the protein's secondary structure to β-strand contents. The CD's fluorescence in the blood serum medium was also enhanced where serum's particulate components contributed to the emission. All these subvert fluorescence emissions could be substantially cleaned for detection of peroxide generated in the enzymatic reaction by filtering the serum particulates and redox proteins prior to the addition of CDs to the reaction systems. The CD, however, could complement well in ABTS-based (absorbance at $\lambda_{max\ 414nm}$) colorimetric reaction in blood serum without introducing protein or particle separation steps for sensitive detection of peroxide. The limit of detection, dynamic range, and sensitivity discerned for peroxide in the glucose oxidase-catalyzed reaction system were 183 μM, 0.02−0.10 mM (R^2 = 0.98), and 0.2482 AU mM^{-1}, respectively. Overall, these findings will guide clinical application of the peroxidatic CDs to detect various analytes in blood serum following fluorometric- and colorimetric-based principles.

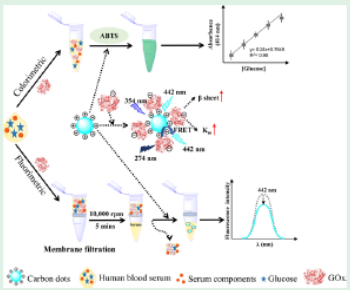

KEYWORDS: *carbon dots, peroxidase, hydrogen peroxide, fluorescence, colorimetric, blood serum*

1. INTRODUCTION

Over the last few years, carbon dots (CDs) have received wide attention due to their high-water solubility, good biocompatibility, low toxicity, high optical stability, easy surface functionalization, tunable fluorescence property, and inexpensive and straightforward synthesis protocols.[1] These properties have prompted the exploration of these zero-dimensional nanomaterials for diverse applications such as bioimaging, sensing, catalysis, dye-sensitized solar cells, drug delivery, and light-emitting devices.[2] Among these applications, CDs have been more aggressively studied in the analytical fields due to their tunable and stable fluorescence properties and high peroxidatic activities.[3−5] However, these analytical applications urge more in-depth investigations on these sensitive optical materials for their applications in biological samples where a complex cohort of diverse molecular entities is present. Again, within these entities, the molecules and materials bestowed upon with intrinsic fluorescence properties such as proteins need more attention to avoid any fluorescence cross-talk during the analytical applications.

A plethora of reports on the peroxidatic properties of CDs that address both basic as well as application facets of these nanomaterials are available.[3,6−11] These properties of CDs could provide qualitative or quantitative information on the peroxides present in the sample following both fluorometric and colorimetric principles. These peroxidatic functions of CDs could also be coupled with various peroxide-producing enzymatic reactions to indirectly determine the secondary analytes, which is the primary substrate for the redox enzyme catalysis, the way peroxidases are used in a bienzyme colorimetric system to extract analytical information for various analytes.[12−14] The current bienzyme systems for detecting these analytes have primarily relied upon horseradish peroxidase (HRP) that catalyzes the degradation of H_2O_2. However, using multiple enzymes in a single detection platform increases the cost and complexity of the analytical devices or methods. In order to reduce these drawbacks, CDs

Received: December 19, 2021
Accepted: January 24, 2022
Published: February 3, 2022

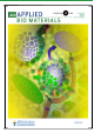

IOP Publishing Nano Express 2 (2021) 040003 https://doi.org/10.1088/2632-959X/ac3389

NANO EXPRESS

PAPER

Analytical application of H_2O_2-induced chiroptical graphitic carbon dots

Smita Das[1], **Sudarshan Gogoi**[2], **Naveen Kumar Singh**[3] **and Pranab Goswami**[1]

[1] Department of Biosciences and Bioengineering, Indian Institute of Technology Guwahati, Guwahati 781039, Assam, India
[2] Department of Chemistry, Sadiya College, Chapakhowa 786157, Assam, India
[3] Biosensors and Bioelectronics lab, Department of Electrical and Computer Engineering, University of California San Diego, California, 92037, United States of America

E-mail: pgoswami@iitg.ac.in

Keywords: carbon dots, chiroptical, hydrogen peroxide, D-(+)-Glucose, peroxidase

Supplementary material for this article is available online

OPEN ACCESS

RECEIVED
20 August 2021

REVISED
17 September 2021

ACCEPTED FOR PUBLICATION
26 October 2021

PUBLISHED
8 November 2021

Abstract

Carbon dots (CDs) have emerged as efficient peroxidase mimics in recent years. However, to further increase its efficiency as peroxidase-mimic, it is also desirable to understand the modification of CD's geometry during the catalytic reaction. Herein, we focused on the change in material property of the CDs upon their reaction with H_2O_2 during the peroxidase reaction. D-(+)-glucose was transformed into chiroptical CDs bearing peroxidase-like activity and can be used to detect H_2O_2 with a limit of detection of 630 μM. The addition of H_2O_2 to the CDs resulted in its increased molecular orderliness leading to the introduction of polycrystallinity without affecting its peroxidase-like activity.

1. Introduction

The zero-dimensional carbon dots (CDs) have recently attracted much attention because of their potential optical properties, excellent photostability, and biocompatibility [1]. These properties have stimulated its applications in diverse areas, including biochemical sensing, photocatalysis, drug delivery, biolabeling, and optoelectronic devices [1, 2]. Recent studies have also demonstrated the intrinsic peroxidase-like activity of CDs as another promising property [3–15]. The significant advantage of using CDs as peroxidase mimic is their facile synthesis, low cost, long-term storage, and resistance to proteolysis, unlike the natural peroxidase enzymes [16]. Previous work has demonstrated that the peroxidase-like activity of graphene quantum dots (GQDs) emanates from their ability to decompose H_2O_2 to $OH^{\cdot}$ [17]. Notably, the functional groups on the surface of the CDs play a prominent role in the binding of the H_2O_2 during the catalytic activity [4, 18, 19].

In recent years, CDs are also attracting more interest because of their chiroptical features [20]. Chirality constitutes a vital aspect of optically-active nanostructures and has not been focussed much. With enormous advancement to understand chirality at the molecular scale and its influence on the structural property, it also becomes crucial to study chirality at the nanoscale for its possible applications [21]. The introduction of chirality into CDs can augment remarkable properties to develop prospects for connecting material science, biology, and medicine [22]. The synthesis of chiral CDs involves covalent modification or capping with chiral moieties or synthesis with chiral molecules; the latter has advantages as it does not involve the additional step of functionalization with chiral molecules [23].

The evolution of CD's geometry during the various interaction processes is a less studied area. Previous studies have reported the importance of agglomeration of the CDs by the substrates during the peroxidase-like reaction [4]. With distinct geometry and material properties, the CDs can also serve as sensing agents for analytical applications. In this context, an in-depth mechanistic knowledge of the modification of CD's material property during the catalytic activity also becomes essential. Herein, we report the synthesis of chiroptical CDs from D-(+)-glucose using a single-step pyrolysis method. The as-prepared CDs exhibited blue photoluminescence under a single excitation wavelength and demonstrated intrinsic peroxidase-like activity.

Copyright Permissions

Chemical design of nanozymes for biomedical applications

Author: Min Wei,Jiyoung Lee,Fan Xia,Peihua Lin,Xi Hu,Fangyuan Li,Daishun Ling
Publication: Acta Biomaterialia
Publisher: Elsevier
Date: May 2021

Order Completed

Thank you for your order.

This Agreement between B-220, Subansiri Hostel, IIT Guwahati, Guwahati:781039, Assam ("You") and Elsevier ("Elsevier") consists of your license details and the terms and conditions provided by Elsevier and Copyright Clearance Center.

Your confirmation email will contain your order number for future reference.

License Number	5226430291460
License date	Jan 12, 2022

Printable Details

Licensed Content

Licensed Content Publisher	Elsevier
Licensed Content Publication	Acta Biomaterialia
Licensed Content Title	Chemical design of nanozymes for biomedical applications
Licensed Content Author	Min Wei,Jiyoung Lee,Fan Xia,Peihua Lin,Xi Hu,Fangyuan Li,Daishun Ling
Licensed Content Date	May 1, 2021
Licensed Content Volume	126
Licensed Content Issue	n/a
Licensed Content Pages	16

Order Details

Type of Use	reuse in a thesis/dissertation
Portion	figures/tables/illustrations
Number of figures/tables/illustrations	1
Format	both print and electronic
Are you the author of this Elsevier article?	No
Will you be translating?	No

About Your Work

Title	Studies on the synthesis, characterization, mechanism of peroxidase-like activity, and the application potential of carbon dots prepared from L-glutamic acid and D-(+)-glucose
Institution name	IIT Guwahati
Expected presentation date	May 2022

Additional Data

Portions	Graphical abstract

Requestor Location

Smita Das, B-220, Subansiri Hostel
IIT Guwahati

Requestor Location

Guwahati, Assam 781039
India
Attn: Smita Das

Price

Total	0.00 USD

Tax Details

Publisher Tax ID	GB 494 6272 12

Total: 0.00 USD

CLOSE WINDOW ORDER MORE

CCC | Marketplace™

Order Number: 1176900
Order Date: 12 Jan 2022

Payment Information

Smita Das
smita@iitg.ac.in
Payment method: Invoice

Billing Address:
Ms. Smita Das
Smita Das, B-220, Subansiri Hostel, IIT Guwahati
Guwahati, Assam
Guwahati, 781039
India

+91 8876996270
smita@iitg.ac.in

Customer Location:
Ms. Smita Das
Smita Das, B-220, Subansiri Hostel, IIT Guwahati
Guwahati, Assam
Guwahati, 781039
India

Order Details

1. Food & function

Billing Status: Open

Article: Protein corona formation of human serum albumin with carbon quantum dots from roast salmon.

Order License ID	1176900-1	**Type of use**	Republish in a thesis/dissertation
Order detail status	Completed		
ISSN	2042-650X	**Publisher**	Royal Society of Chemistry
		Portion	Chart/graph/table/figure

0.00 USD
Republication Permission

LICENSED CONTENT

Publication Title	Food & function	**Publication Type**	e-Journal
Article Title	Protein corona formation of human serum albumin with carbon quantum dots from roast salmon.	**Start Page**	2358
		End Page	2367
		Issue	3
		Volume	11
Author/Editor	Royal Society of Chemistry (Great Britain)	**URL**	http://pubs.rsc.org/en/Journals/JournalIssues/FO
Date	01/01/2010		
Language	English		

Country	United Kingdom of Great Britain and Northern Ireland
Rightsholder	Royal Society of Chemistry

REQUEST DETAILS

Portion Type	Chart/graph/table/figure	**Distribution**	Worldwide
		Translation	Original language of publication
Number of charts / graphs / tables / figures requested	1		
		Copies for the disabled?	No
Format (select all that apply)	Print,Electronic	**Minor editing privileges?**	No
Who will republish the content?	Author of requested content	**Incidental promotional use?**	No
Duration of Use	Current edition and up to 5 years	**Currency**	USD
Lifetime Unit Quantity	Up to 499		
Rights Requested	Main product		

NEW WORK DETAILS

Title	Studies on the synthesis, characterization, mechanism of peroxidase-like activity, and the application potential of carbon dots prepared from L-glutamic acid and D-(+)-glucose	**Institution name**	IIT Guwahati
		Expected presentation date	2022-05-31
Instructor name	Prof. Pranab Goswami		

ADDITIONAL DETAILS

The requesting person / organization to appear on the license	Smita Das

REUSE CONTENT DETAILS

Title, description or numeric reference of the portion(s)	Scheme 1	**Title of the article/chapter the portion is from**	Protein corona formation of human serum albumin with carbon quantum dots from roast salmon.
Editor of portion(s)	Song, Yukun; Wang, Haitao; Zhang, Lijuan; Lai, Bin; Liu, Kangjing; Tan, Mingqian	**Author of portion(s)**	Song, Yukun; Wang, Haitao; Zhang, Lijuan; Lai, Bin; Liu, Kangjing; Tan, Mingqian
Volume of serial or monograph	11		

Page or page range of portion	2358-2367	**Issue, if republishing an article from a serial**	3
		Publication date of portion	2022-05-31

Total Items: 1

Subtotal: 0.00 USD

Order Total: 0.00 USD

Tuning the Aggregation/Disaggregation Behavior of Graphene Quantum Dots by Structure-Switching Aptamer for High-Sensitivity Fluorescent Ochratoxin A Sensor

Author: Song Wang, Yajun Zhang, Guangsheng Pang, et al
Publication: Analytical Chemistry
Publisher: American Chemical Society
Date: Feb 1, 2017

PERMISSION/LICENSE IS GRANTED FOR YOUR ORDER AT NO CHARGE

This type of permission/license, instead of the standard Terms and Conditions, is sent to you because no fee is being charged for your order. Please note the following:

- Permission is granted for your request in both print and electronic formats, and translations.
- If figures and/or tables were requested, they may be adapted or used in part.
- Please print this page for your records and send a copy of it to your publisher/graduate school.
- Appropriate credit for the requested material should be given as follows: "Reprinted (adapted) with permission from {COMPLETE REFERENCE CITATION}. Copyright {YEAR} American Chemical Society." Insert appropriate information in place of the capitalized words.
- One-time permission is granted only for the use specified in your RightsLink request. No additional uses are granted (such as derivative works or other editions). For any uses, please submit a new request.

If credit is given to another source for the material you requested from RightsLink, permission must be obtained from that source.

BACK CLOSE WINDOW